

RICE UNIVERSITY

MODELING WIDE-ANGLE SEISMIC DATA
FROM THE CENTRAL CALIFORNIA MARGIN

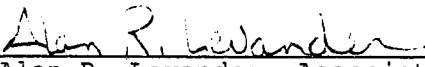
by

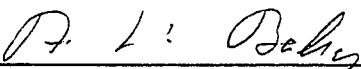
NATHANIEL E. PUTZIG

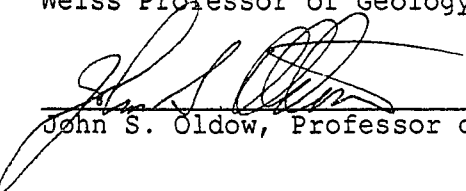
A THESIS SUBMITTED
IN PARTIAL FULFILLMENT OF THE
REQUIREMENTS FOR THE DEGREE

MASTER OF ARTS

APPROVED, THESIS COMMITTEE:


Alan R. Levander, Associate
Professor of Geophysics, Director


Albert W. Bally, Harry Carothers
Weiss Professor of Geology


John S. Oldow, Professor of Geology

Houston, Texas

April, 1988

MODELING WIDE-ANGLE SEISMIC DATA
FROM THE CENTRAL CALIFORNIA MARGIN

Nathaniel E. Putzig

ABSTRACT

Rice conducted an onshore-offshore seismic survey across the central California transform margin. Refraction velocity modeling of shot and receiver gathers has generated two models with similar near surface features. Model synthetics produce excellent fits to first arrivals and good matches for later arrivals in the data. CMP stacking of nearer offset traces imaged an event interpreted as reflections from the top of a dipping lower crustal layer. Model raytracing indicates layer flattening landward and seaward of the coast. High amplitude late arrivals seen at long offset on receiver gathers are modeled by imbricating the lower crust beneath the coast. This feature is interpreted as a result of overthrusting of the continental and Farallon plates onto the Pacific plate. The models differ in the middle crust, where one includes a laterally discontinuous low velocity zone. No direct indication of this LVZ exists in the data or in offshore reflection profiles.

ACKNOWLEDGEMENTS

I would like to thank Alan Levander for providing me the opportunity to work on this project and for his unflagging support, advice, and encouragement throughout its development. I also deeply appreciate the constructive and enlightening comments of Albert Bally, Manik Talwani, and John Oldow with regards to this manuscript and the project in general. Anne Meltzer generously provided reflection data, software, literature, and sharp insight into Californian geology and tectonics. Lorraine Wolf smoothed the way for me with her careful instruction in the use of the raytracing software, and Claude Lafond's graphics program PLOTIT spared me vast amounts of time and effort. I also thank: all the members of the Rice Geophysics group who's efforts in the field helped make the experiment a great success; Pacific Gas and Electric company for allowing us to "piggyback" on their crustal geophysical investigation project and for a line drawing of some of their offshore reflection data; and Amoco for providing the SGR III recorders and for transcribing the field data to SEG-Y format on 9-track tape. I would like to express my gratitude to my sister Clara and her husband Glen Mizenko who's constructive comments and moral support carried me through some trying times. Finally, I dedicate this thesis to my mother Frances and to the memory of my father Albert Frederick Putzig. None of this would have been possible without the strength of their love, faith, and guidance.

TABLE OF CONTENTS

ABSTRACT		page	i
ACKNOWLEDGEMENTS			ii
CHAPTER 1	INTRODUCTION		1
CHAPTER 2	RECENT TECTONICS AND GEOLOGY		5
CHAPTER 3	EXPERIMENT GEOMETRY		20
CHAPTER 4	THE CONTINUOUS OFFSET DATA		23
CHAPTER 5	REFRACTION DATA MODELING		34
CHAPTER 6	DISCUSSION		66
CHAPTER 7	CONCLUSION		77
REFERENCES			79
APPENDIX A	RAY DIAGRAMS - MODEL 1		83
APPENDIX B	RAY DIAGRAMS - MODEL 2		116

CHAPTER 1:
INTRODUCTION

The Rice Geophysics group conducted a seismic experiment in the fall of 1986 across the transform margin in west central California. The purpose of the experiment was to delineate major crustal features, particularly in the lower crust, and to test hypothesized extensive lower-crustal low velocity zones in the lower crust proposed by previous workers (Trehu and Wheeler, 1987; Blumling and Prodehl, 1983). This work provides general insight into the crustal structure of transform margins. Because of the experiment's unusual geometry, we have been able to use both reflection and refraction processing and interpretation to model the structure along a 120 km seismic line which covers the transition zone. A secondary objective of the experiment was to test the feasibility of using seismic group recorders on land to detect signals generated by a marine airgun source from a seismic vessel at sea. This has proven to be a workable system, providing an inexpensive and efficient means of acquiring wide-angle crustal data in various transitional and coastal regions throughout the world.

I have used this unique data set to produce two different models of the region's velocity and structure (Figures 14 and 24). The models are generally the same, but differ in some details of the lower crust. The upper crust (depths to about 10 km) of both models contains the same

gross features which reflect the surface geology and the major faults which the seismic line crossed. The greatest amount of lateral velocity variation in the models occurs in association with the known faults. The velocity structure observed beneath the Salinian and Sur Obispo terranes is compatible with the velocities known to be typical of granitic and Franciscan rocks, respectively. At greater depths, the models differ, where one model (Figure 24) has a slightly shallower lower crust (varying in depth from 12.5 km seaward to 22.5 km landward) with oceanic velocities beneath a thick (up to 6.5 km), laterally discontinuous low velocity zone. Other workers (Walter and Sharpless, 1987, Trehu and Wheeler, 1987; Blumling and Prodehl, 1983) have interpreted low velocity zones in the lower crust of the California transform margin, and the model I produced was used to examine whether our data supports such interpretations. While the data does not entirely exclude low velocity zones, alternative models without extensive low velocity zones match the data equally well or better. My preferred model (Figure 14) contains a slightly deeper lower crustal layer (from 13.5 to 22 km in depth) with oceanic velocities. In both models, this layer is imbricated beneath the coast. It is my interpretation that this feature developed after the subduction of the Pacific-Farallon spreading ridge, which is thought to have occurred in the Late Oligocene at this latitude. I suggest that the upper section of lower crust is

a remnant of the Farallon plate which has been thrust onto the underlying Pacific plate. A gravity profile (Figure 34) taken from a Bouguer anomaly map (Burch et al, 1968) shows a gravity high at the coast as might be expected over an area with a thick lower crust of dense oceanic material.

Although the term "transition crust" is often used, this phrase is vague and imprecise in reference to the California margin, where extensive right-lateral strike-slip deformation has juxtaposed entirely different geologic units. We propose discarding "transition crust," when one refers to the California transform margin, in favor of an accretionary transform crust with recognizable fragments from the subduction model (see Chapter 2).

The subject of this thesis has been interpretation of both reversed land shot gathers and unreversed receiver gathers from the 120 km seismic profile. Also, we have produced an image from reflection processing of the same data (Figure 10). The combination of the velocity models with the reflection image has helped provide a better understanding of the present structure of the crust in this transition zone. Other seismic surveys offshore and onshore have also contributed to the present work.

In the next chapter, I will discuss the recent tectonic history and present geology of west central California and the issues concerning the current state of structure and active tectonism in the study area. Then I will describe the

experiment geometry we used in collecting the seismic data, and will follow that with an in-depth look at the data itself. After that, I will give an overview of the final models and a more detailed discussion of the modeling process and the model synthetics produced. I will then provide a discussion of my preferred models and some of the geologic problems that remain unresolved.

CHAPTER 2:

RECENT TECTONICS AND GEOLOGY

During the latter part of the Mesozoic and much of the Cenozoic eras, California was the site of a convergent margin along which the oceanic Farallon plate was being subducted beneath the North American craton (Dickinson, 1981). The basement geology of California is composed of units which formed as a result of this activity. However, the latter part of Cenozoic time saw a change from a convergent to a transform margin due to the total subduction of the Farallon plate beneath central California and the juxtaposition of the Pacific and North American plates (Page, 1981). This recent change introduced complications in the geologic record by displacing large blocks of crustal material along numerous right-lateral faults (Figure 1), some with offsets of 550 km or more (Ross, 1978).

Subduction model

In general, any subduction zone will have a specific set of rock assemblages associated with it, and each of these will in turn contain a distinct package of rock types depending on its environment and proximity to the subduction zone (Figure 2). In Uyeda's (1984) model for high-stress subduction zones, an accretionary prism attaches to the leading edge of the continent. The accretionary prism is composed of oceanic basalts and pelagic sediments scraped from the downgoing plate and mixed with turbidity flow

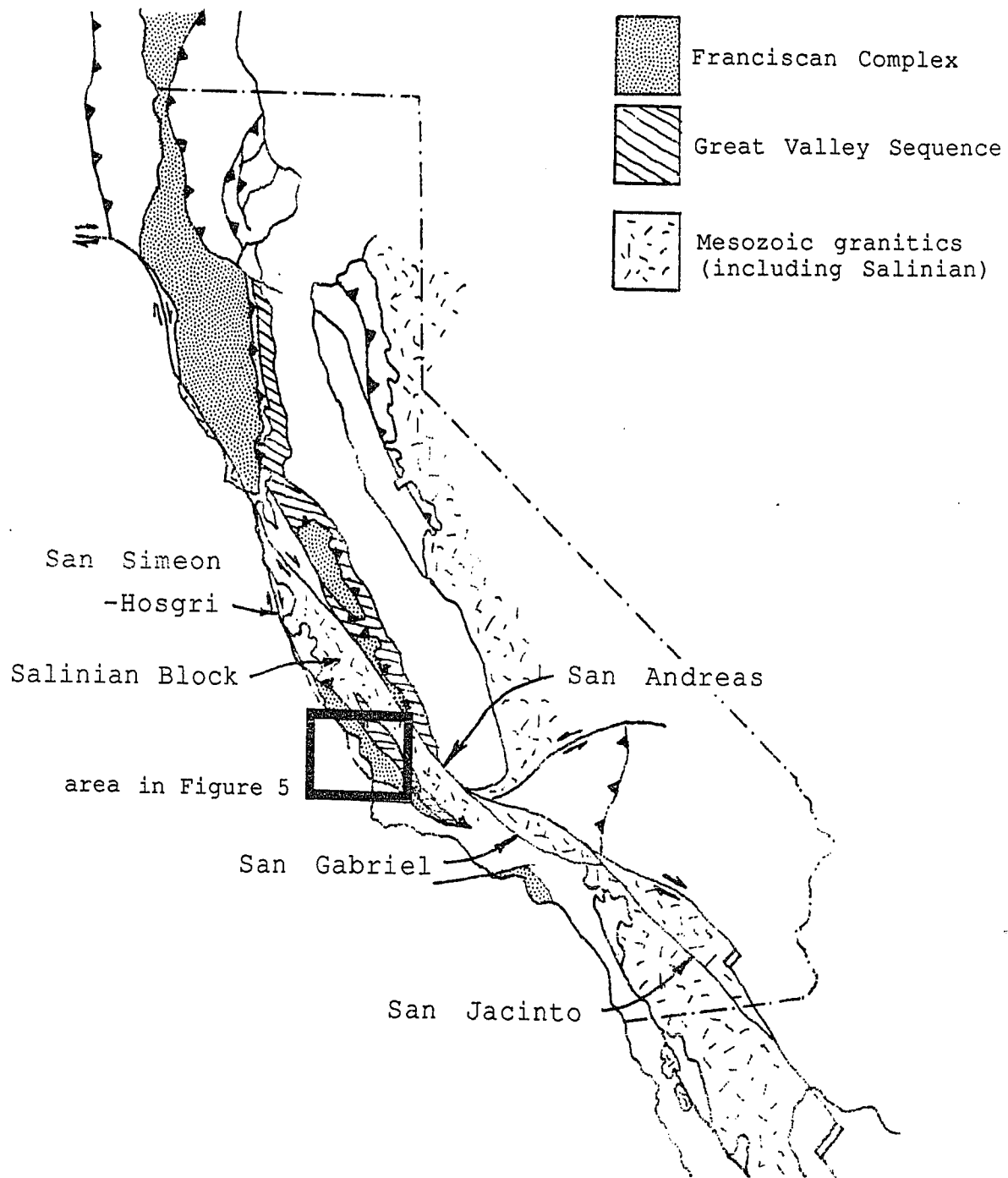


Figure 1: Generalized geology map of California. Map shows effect of faulting on basement rocks (from Ernst, 1981, fig. 1).

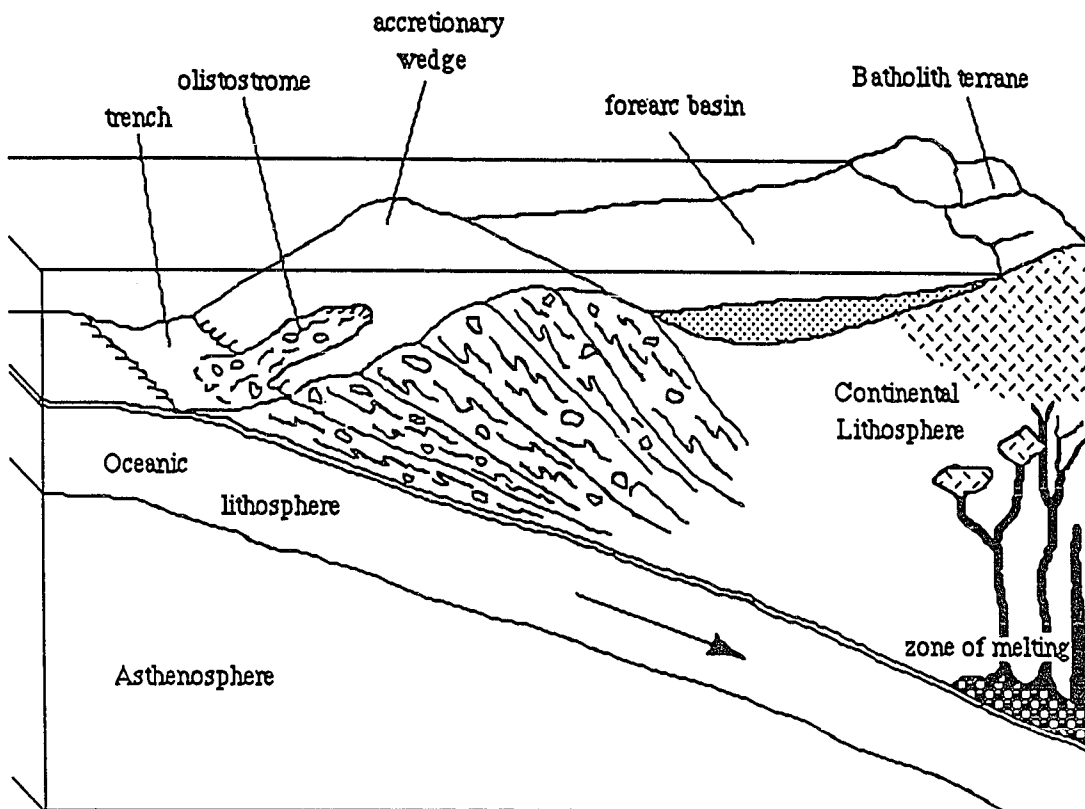


Figure 2: Schematic diagram of the subduction zone along the California margin during Jurassic to Tertiary time (adapted from Page, 1981).

sediments and shelf carbonates introduced at the trench. Further inland, an arc of volcanism and igneous intrusion is emplaced within the continental plate above a melting zone at the top of the subducted oceanic plate, thereby producing the granitic batholiths and possibly a mountain range. A forearc basin collects clastic terrigenous sediments within the gap between the accretionary wedge and the magmatic arc. Along our seismic line, the rock types of each of these zones can be found, although they have been displaced by the more recent transform motion.

The units produced during the convergence of the Farallon and North American Plates consist of 1) the Franciscan Complex of deformed sediments, volcanics, and minor carbonates, 2) the Great Valley Sequence of terrigenous sediments, and 3) the Sierran-Salinian-Peninsular Range of granitic batholiths in older metasedimentary rocks. These units correspond respectively to the accretionary wedge, forearc basin, and magmatic arc units of the plate subduction model. During subsequent transform motion, the Salinian block was separated from the Sierran-Peninsular range batholiths and displaced to its present location along the Central California margin (Figure 1).

Tectonic activity

In west central California, subduction-related tectonism during the Cretaceous emplaced some ophiolites as well as Upper Jurassic to Lower Cretaceous sediments resembling the

Great Valley Sequence over the Franciscan basement, forming the Sur-Obispo belt (Page, 1981). Stratigraphic relationships with overlying sediments demonstrate that displacements along the Sur-Nacimiento fault zone brought Sur-Obispo belt rocks into contact with those of the Salinian sometime in the Late Cretaceous (Dickinson, 1983; Nilsen and Clarke, 1975). The processes which caused the juxtaposition of these terranes is still unclear. Several mechanisms have been proposed, the three most prominent as follows: tectonic erosion with right-lateral strike-slip; left-lateral strike-slip followed by right-lateral strike-slip; and major overthrust in Southern California followed by right-lateral strike-slip (Page, 1981; Dickinson, 1983). The only characteristics common to all of the proposed mechanisms are right-lateral strike-slip along the San Andreas fault to achieve the present geologic configuration of west central California, and the requirement of a horizontal decollement at depth.

As the Pacific-Farallon ridge encountered the North American plate in the Late Oligocene, the Mendocino and Rivera triple junctions formed. As the Mendocino junction passed up the coast, subduction ceased to the south, giving way to transform motion (Atwater, 1970). This motion caused a complex system of right-lateral strike-slip faults to develop, resulting in the broad transform zone between the base of the continental slope and the modern San Andreas fault (Crowell, 1979). The exact nature of movement along

these faults is debated. The oblique relative motion between the Pacific and North American plates since the opening of the Gulf of California at the close of the Miocene has been estimated as being 15% compressional (Minster and Jordan, 1984). Contention exists over the mode of compression. Some favor local wrench faulting within a regional strike-slip zone (cf. Graham and Dickinson, 1978), while others suggest a regional thrust fault system over a midcrustal decollement (cf. Crouch et al, 1984).

Much of the structure formed by the pre-Miocene subduction activity has been overprinted by Neogene and Quaternary deformation and faulting associated with the transform zone. This activity displaced west central California from the Sierra Nevada-Peninsular Range lineament along the San Andreas fault and caused concurrent deformation, producing features such as the Transverse Ranges (Dickinson, 1981). Additional displacements along the Sur-Nacimiento, Rinconada, Hosgri, and other subsidiary faults caused further offsets within the Salinian, Sur-Obispo, and offshore terranes (Graham and Dickinson, 1978; Larson et al, 1968). Some of the subsidiary faults on land show primarily strike-slip motion, but others exhibit significant thrust components. These latter faults along with structural evidence of NE-SW shortening since the Late Miocene have led some to believe there has been recent thrusting in west central California (Crouch et al, 1984).

Franciscan Complex

Page (1981) has described the significant features of Franciscan Complex which are seen in the Sur Obispo belt, and the following is a summary of those features relevant to this study. He divides the Franciscan into two units, one of which is a melange mixture of terrigenous sediments and oceanic material forming blocks of different age and degree of metamorphism. Alternating with the melange are semiparallel units of coherent sandstones which have been described as turbidites and channel conglomerates possibly deposited in subsea midfan environments. In many places, these sandstones have undergone metamorphism anywhere from the incipient to the blueschist stage. Although the bedding is fairly continuous within them, the sandstone units have very erratic orientations and are disturbed along their contacts with the melanges. These melanges are highly variable, containing blocks of graywacke, basaltic greenstone, radiolarian chert, serpentinite, conglomerate, high grade blueschist, minor limestones and various other rocks. The stratification, bedding, graywacke source material, and degree of metamorphism within the melange are also highly variable. On the regional scale, the prevalence of the coherent sandstone units varies as well. In the area of our seismic line, the coherent sandstone units are not as common, nor are there large blocks of schist as are found further north. In the Sur Obispo belt, the melanges consist

of graywacke, greenstone, chert and blueschist blocks while other typical Franciscan components are less prevalent. Several anomalous sedimentary units of unknown origin have been indentified within the Franciscan of this area, most notably the Cambria slab, which is a 16 km long turbidite-facies sandstone. Studies by numerous authors have supported several different interpretations of this unit, some of which claim it is not even part of the Franciscan but rather a tectonically displaced portion of the Great Valley Sequence.

The blueschist blocks found in the Franciscan imply that the rocks were carried down into the subduction zone, metamorphosed, and then returned to the surface without encountering high temperatures. This idea is supported by the experimental data such as that of Bostick (1974), who examined samples of Franciscan graywacke and metagraywacke from the Diablo range. Based on altered grains of organic matter (phytoclasts), he estimates past confining pressures of approximately 4.5 to 6.5 kbar and low temperatures of 120° to 150°C the samples, some of them containing jadeitic pyroxene. Continual underthrusting of these rocks by cooler material may have sheilded them from the heat of the mantle below.

Great Valley Sequence

The forearc basin deposits of the Great Valley Sequence are primarily stratified terrigenous clastic sediments

derived from the former magmatic arc (the Sierran-Salinian-Peninsular Range batholiths). The majority of the Great Valley Sequence deposits are deep sea fan turbidites. The older (Late Jurassic to Early Cretaceous) units within the sequence are inferred to overlie the Coast Range ophiolite basement which contains volcanic and ultramafic rocks, diabase, and gabbro (Blake and Jones, 1978). Outside the Great Valley proper, other lithologically correlative units such as those in the Sur Obispo belt have been identified and are interpreted to have been deposited in similar environments to the south before being displaced northward.

Salinian Block

The Salinian Block is composed of Mesozoic and older Sur Series metamorphosed sediments intruded by felsic plutons of Cretaceous age (Ross, 1978). The geographic source of the metasedimentary host rocks is unknown, and the rocks have not been definitively correlated with any other sequence. The plutonic rocks are predominantly granodiorite and quartz monzonite, with some quartz diorite, and have been described by Ross (1978) and numerous other authors.

Current configuration

The portion of the Franciscan crossed by the wide angle seismic line is located southwest of the Salinian block (Figure 1). Collectively with other rocks located west of the Sur-Nacimiento fault zone (such as ophiolites and

terrigenous sedimentary rocks similar to those of the Great Valley Sequence), this part of the Franciscan is known as the Sur-Obispo belt (Page, 1981). Paleomagnetic studies indicate that the Sur-Obispo belt has been displaced over 2500 km northward since the Cretaceous (Champion et al, 1984). Despite this large displacement, the Sur-Obispo Franciscan rocks appear very similar both petrologically and structurally to other Franciscan assemblages found in the Diablo Range and Northern Coast Ranges.

All along the California margin, the Franciscan rocks are thought to have been underthrust beneath Great Valley sediments and a basal ophiolite, but in west central California and many other locations this contact has been disturbed by subsequent thrusting, folding and faulting, and is often buried by subsequent deposition (Page, 1981). In a refraction study by Holbrook and Mooney (1987), a discontinuous fragment of ophiolite was interpreted to lie beneath the Great Valley Sequence in the San Joaquin Valley, implying that some tectonic disturbance had affected the ophiolite before the Great Valley sediments were deposited.

Page (1981) finds that the Salinian plutons compare quite closely with those of the Sierra Nevada batholith. He therefore concludes that the plutons of the Salinian Block were emplaced in a line with intrusives of the Sierra Nevada and Peninsular Ranges (Figure 3) during the late Mesozoic, and subsequent motion beginning in the Paleocene along the ancestral San Andreas and other faults brought the Salinian

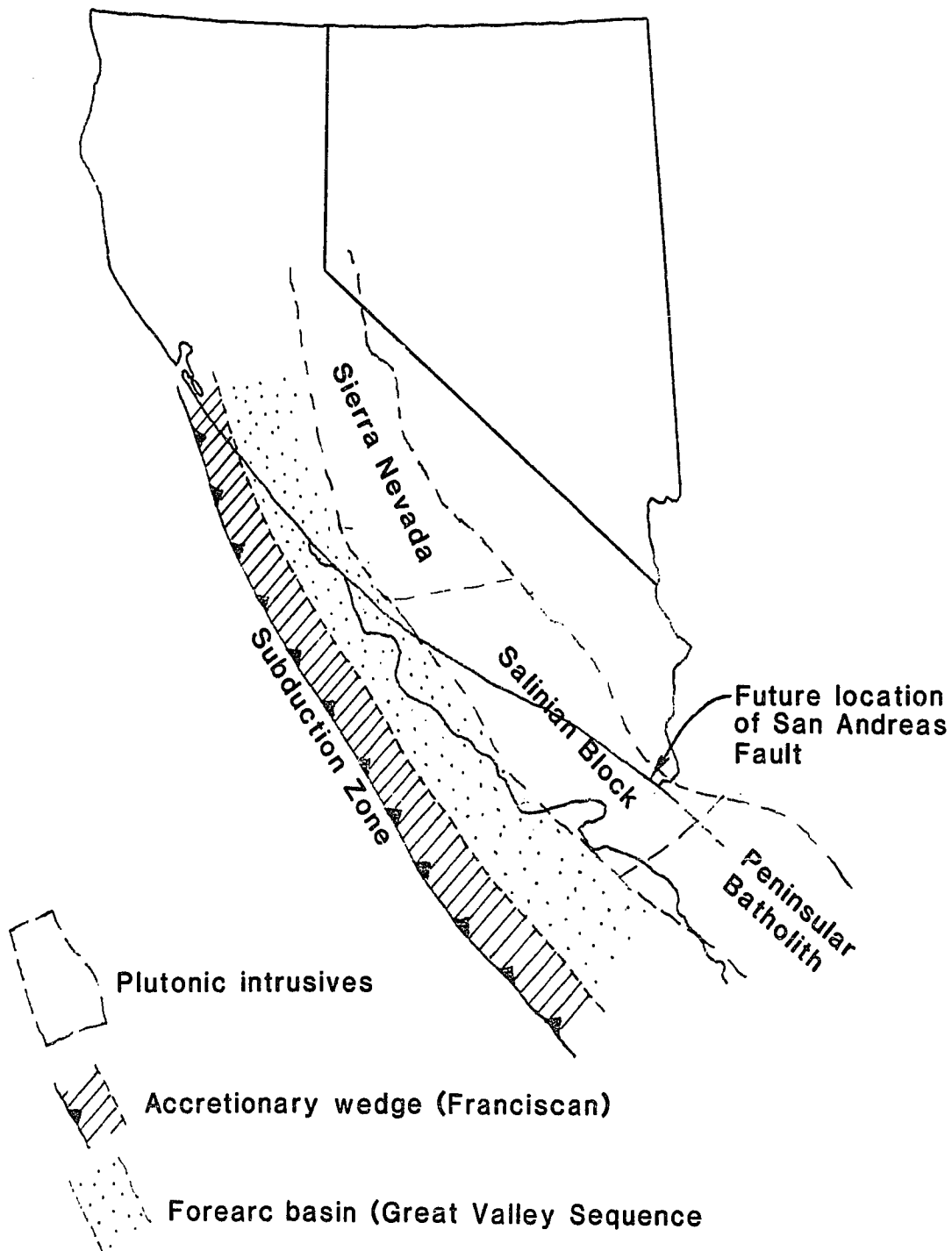


Figure 3: Late Cretaceous plutonic belt of western North America. Figure shows suggested location of Salinian Block between Sierra Nevadan and Peninsular batholiths, previous to Cenozoic faulting (after Page, 1981, fig. 13-13a).

to its present location. The vertical extent of the Salinian Block is unclear. A seismic refraction study by Stewart (1968) provided indirect evidence of either elevated temperatures or the presence of Franciscan material beneath the Salinian basement. Healy and Peake (1975) produced a velocity model with a primary-wave velocity of 6.8 km/s below 12 km depth, which is probably too high for both granite and Franciscan rocks unless the latter have been highly metamorphosed. The modeling herein and that of another recent study (Trehu and Wheeler, 1987) have found somewhat lower velocities (6.3-6.5 km/s), more consistent with either Franciscan or granitic materials, at these depths.

Offshore geology

The offshore portion of our seismic line extended over the upper Tertiary Santa Maria basin to the Santa Lucia High. Like the onshore terranes, the Santa Maria basin is also bounded by faults; the Hosgri fault, located approximately 15 km from the coast, separates the basin from uplifted basement rocks to the east, and the Santa Lucia Bank fault marks the basin's westward edge where the Santa Lucia High begins at about 65 km offshore. The basement is further offset by faulting within the basin itself. None of these faults is well understood, although seismic evidence indicates that they have very steep dips and long linear traces (McCulloch, 1987) which suggests strike-slip motion. Some authors (cf. Hoskins and Griffiths, 1971) suggest that the basement

beneath the basin is granitic, a theory which is in contrast with existing tectonic models restricting the westward extent of granitic basement to the Salinian Block. Metasediments and altered igneous rocks dredged from the Santa Lucia High and intrabasin seismic reflectors lead others to favor Franciscan basement beneath the offshore basin (McCulloch, 1987; Page et al, 1979).

Previous seismic investigations

A number of refraction data sets have been collected in central California, some of which have been interpreted to include low velocity zones in the lower crust (Blumling and Prodehl, 1983; Walter and Sharpless, 1987; Trehu and Wheeler, 1987). These zones have been attributed to the presence of sedimentary material at depths of 20 km or more. In a study including USGS reflection data, Trehu and Wheeler (1987) proposed a subduction mechanism for the emplacement of such sediments. The USGS purchased a Western Geophysical Company reflection line across central California from the coast at Morro Bay to the San Andreas Fault near Cholame. The southwest end of this line was located in approximately the same location as our receiver spread. The following year, the USGS collected refraction data along this same line, but extending east of the San Andreas fault, using large (about 1000 kg) land shots and a receiver spacing much wider than we employed in our profile (1000 vs. 300 m). The reflection data showed a landward dipping reflector at 6 to 9 s twt and

35 to 55 km inland from the coast. They modeled this event on the refraction data with a thick low velocity (5.0 km/s) wedge at 15 to 22 km depth, and interpreted it as a sedimentary package which had been emplaced during the Tertiary between the Franciscan above and the Moho and mantle below (Figure 4). Because of the wide spacing used and the lack of offshore sources, the deep part of their model was not well constrained. We repeated the survey, using a denser spacing and offshore as well as onshore sources, to see whether such an extensive low velocity zone exists by providing a clearer seismic picture of the lower crust.

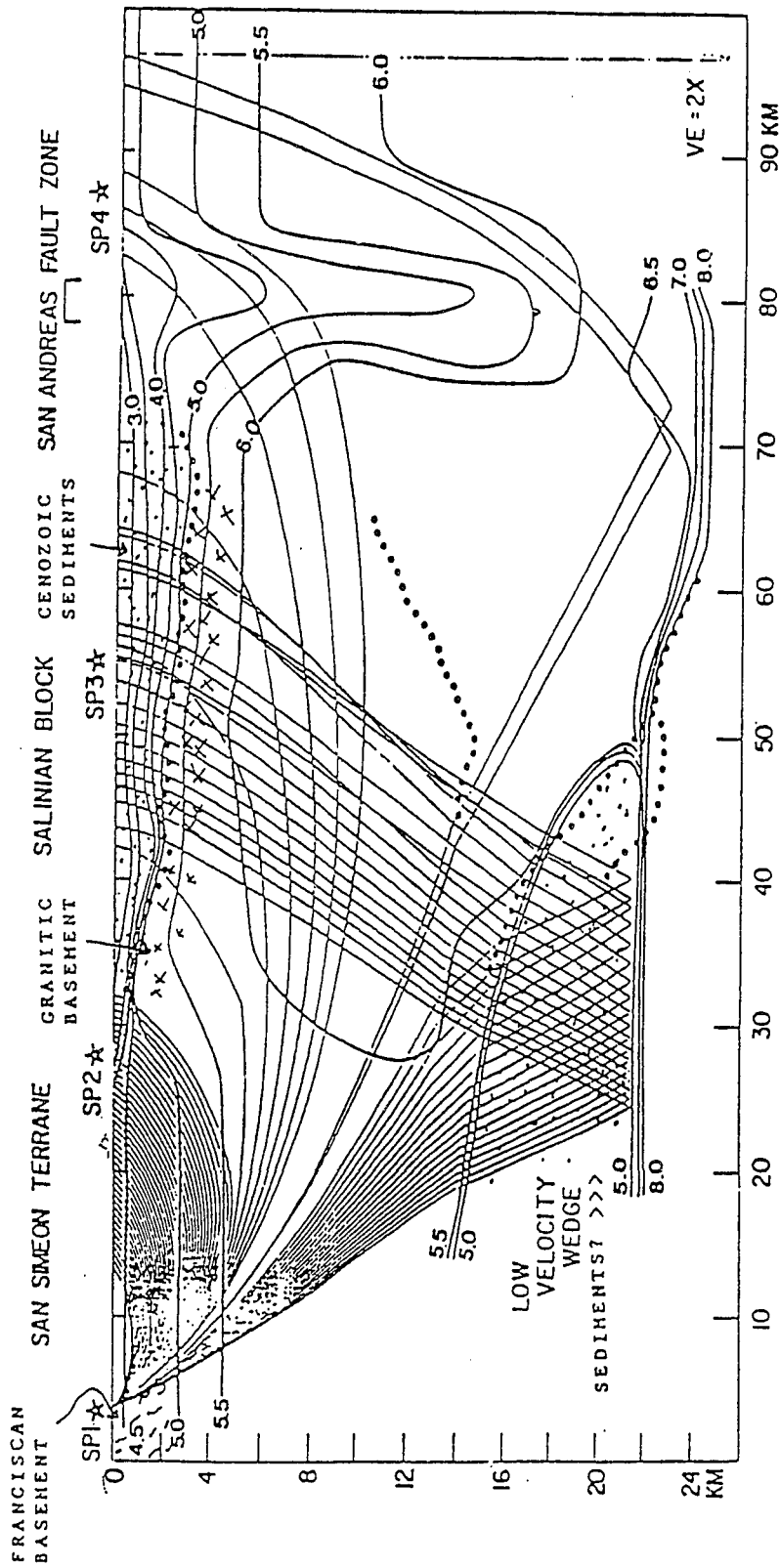


Figure 4: Model produced by Trehu and Wheeler from USGS data. Shot point 3 of this figure corresponds (approximately) to Land Shot 2. Shot point 1 was located about midway between Land Shot 1 and Airgun Shot 1.

CHAPTER 3:
EXPERIMENT GEOMETRY

The continuous offset experiment was conducted by members of the Rice Geophysics group and Digicon, Inc. on October 31 and November 1, 1986. A diagram of the experiment geometry is shown in Figure 5. The receiver array consisted of 154 SGR III seismic group recorders placed at 350 m intervals along State Route 41. At each station, 12 geophones were deployed, using a 1 m square array to avoid an array response, and connected to the group recorder. The experiment was conducted at night to reduce wind and cultural noise. Data was recorded on field tapes within each recorder and later transcribed to standard SEG-Y format on 9 track 6250 bpi tapes. The line of receivers extended from Morro Bay, through Atascadero, to a point 50 km inland. Energy sources consisted of three land shots and 406 marine airgun shots. The land shots, about one ton of explosive each, were located at either end and in the middle of the receiver array line. Spaced at 160 m intervals, the 10,000 cubic inch airgun array shots were fired from 2.4 to 68.5 km offshore and in line with the receivers. With this geometry, we have source-receiver offsets ranging from 2.4 to 120 km, and therefore refer to the survey as a "continuous offset profile". We set up this rather unique geometry to enable us to interpret the data in three ways: as a long offset CMP profile; as an unreversed onshore-offshore refraction

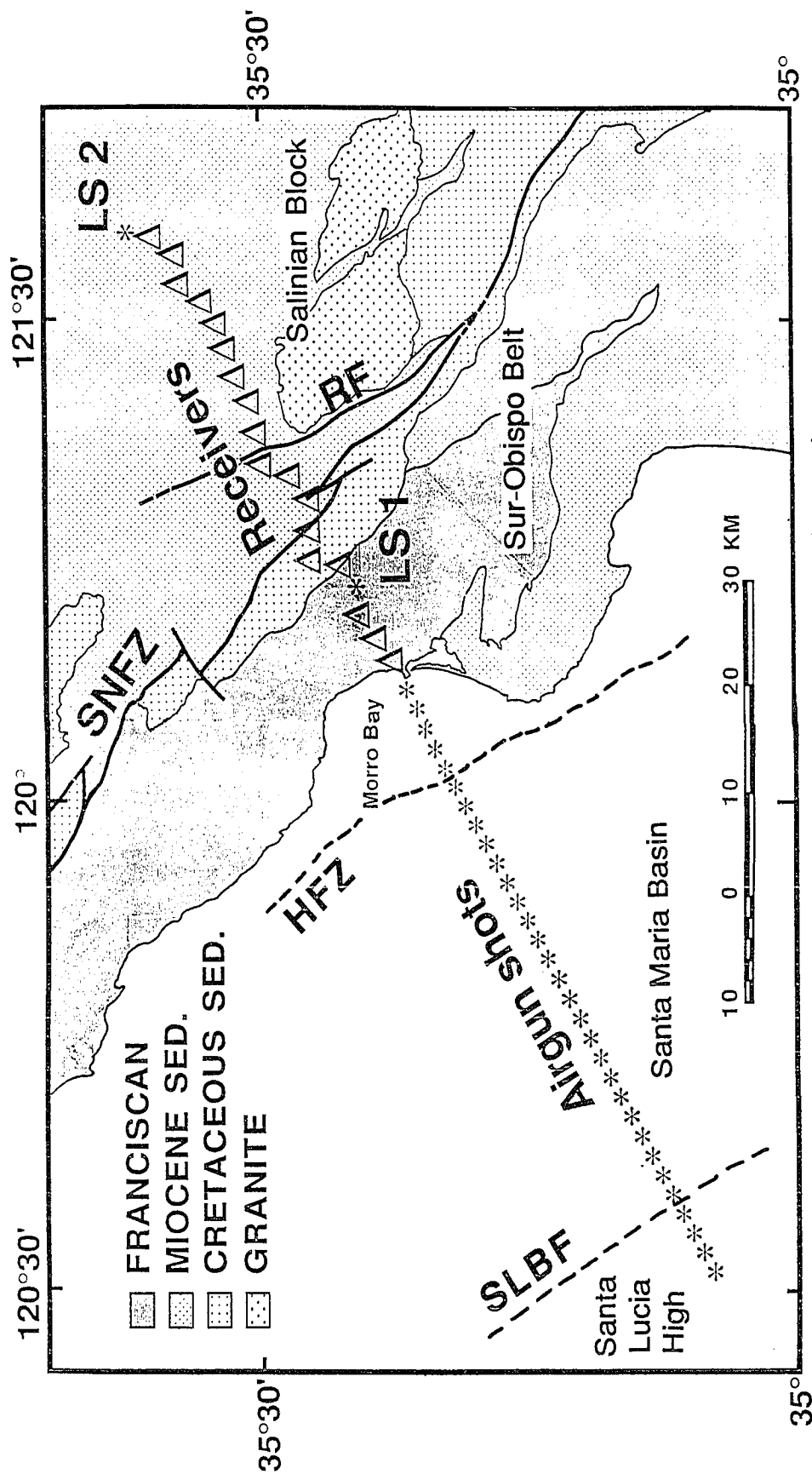


Figure 5: Location map showing surface geologic regions, faults, and the shot and receiver locations discussed in the text. Abbreviations: SNFZ-Sur Nacimiento Fault Zone; RF-Rinconada Fault; HFZ-Hosgri Fault Zone; SLBF-Santa Lucia Bank Fault; LS 1-Land Shot 1; LS 2 Land Shot 2 (geology from Burch et al, 1968).

profile; and as a reversed land refraction profile.

The receiver line crossed parts of the two major geologic regions described earlier, the Sur-Obispo belt (dominantly Franciscan), and the sediment (Miocene through Quaternary) covered Salinian Block. These units are separated by the Sur-Nacimiento and Rinconada fault zones (Figure 5). Offshore, the airgun shots were fired in a line which extended over the Santa Maria Basin to the Santa Lucia High and the bounding Hosgri and Santa Lucia Bank faults. The next chapter describes the data which we collected using this geometry.

CHAPTER 4:
THE CONTINUOUS OFFSET DATA

This study shows that the continuous offset experiment successfully produced excellent data, both from the land shots and the marine airgun source array. Only two of the land shots proved to be useful, because the shot in the middle of the line coupled poorly with the earth, and no useful information was contained in the shot record. Fortunately, the others (Land shots 1 and 2 in Figure 5), produced two very clear shot records after muting and editing a few bad traces, with strong first breaks all the way across the receiver spread (Figures 6 and 7).

The airgun shots also produced good results. The range of a marine airgun signal at offsets beyond 50 km had been in question, but we have examined receiver gathers with signals at offsets up to 95 km or more. This important result demonstrates a new method of collecting crustal seismic data in geologically complex coastal areas and provides an inexpensive means of bridging the gap between offshore and onshore data.

When comparing one of the earlier airgun shot records (Figure 8; see Airgun Shot 1 in Figure 2 for location) with Land Shot 1 (Figure 6; located 10.8 km eastward), an interesting feature becomes evident. The airgun shot shows a distinct event at reduced travel times of 4.5 to 5 seconds beginning at offsets of about 28 km. No comparable event appears on the land shot record at this or any greater

Figure 6: Shot record for western land source, Land Shot 1.

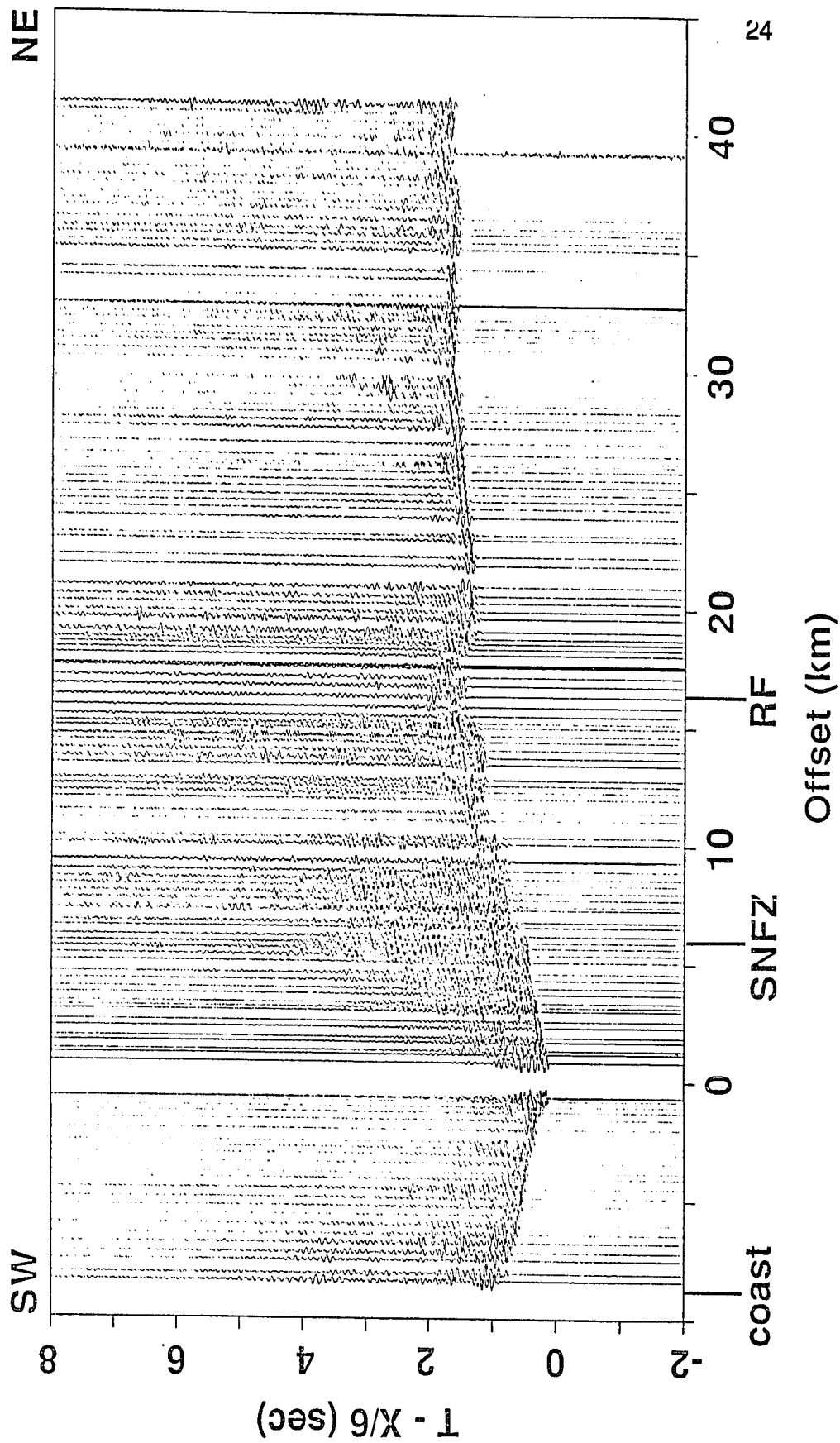
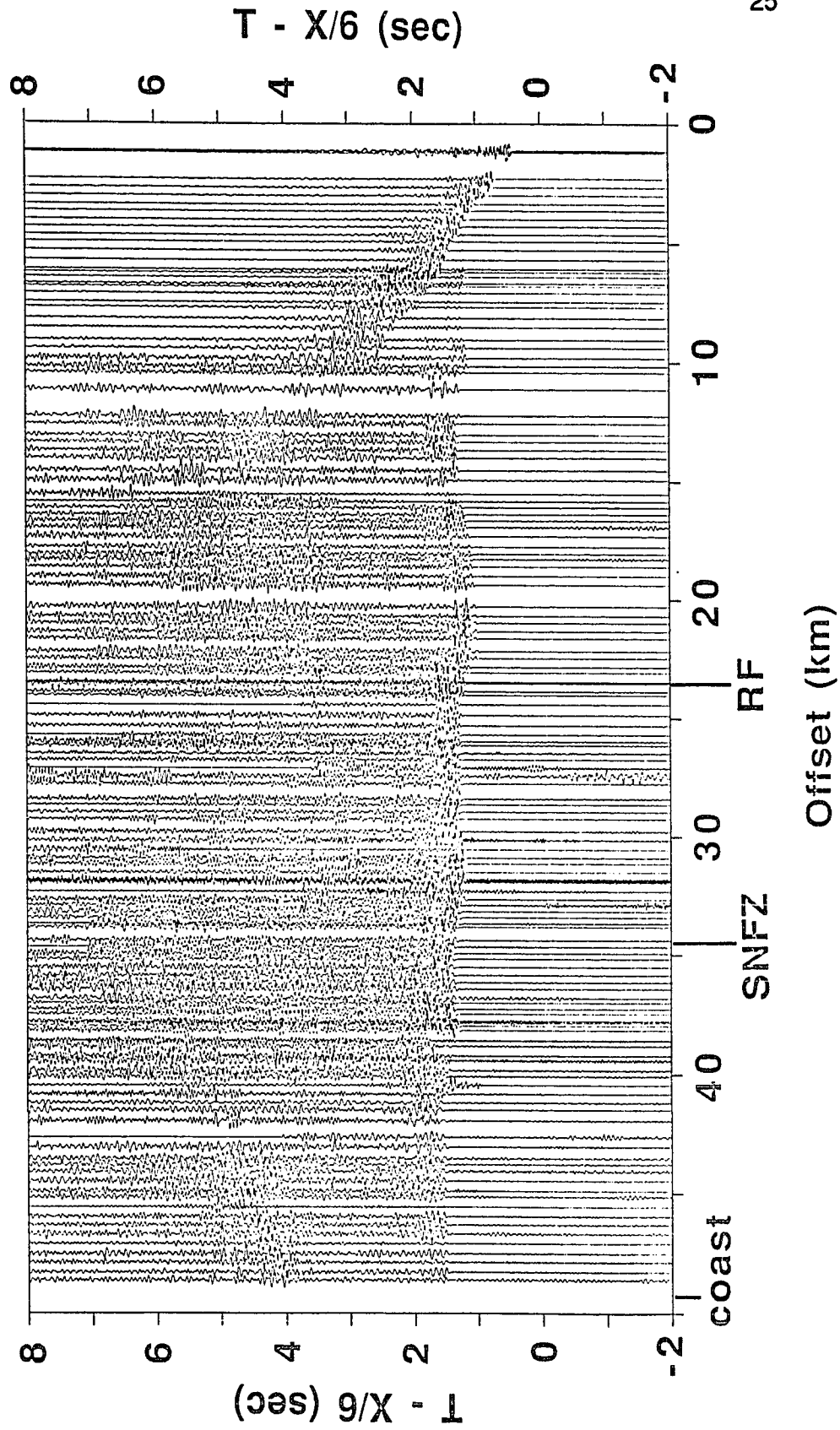
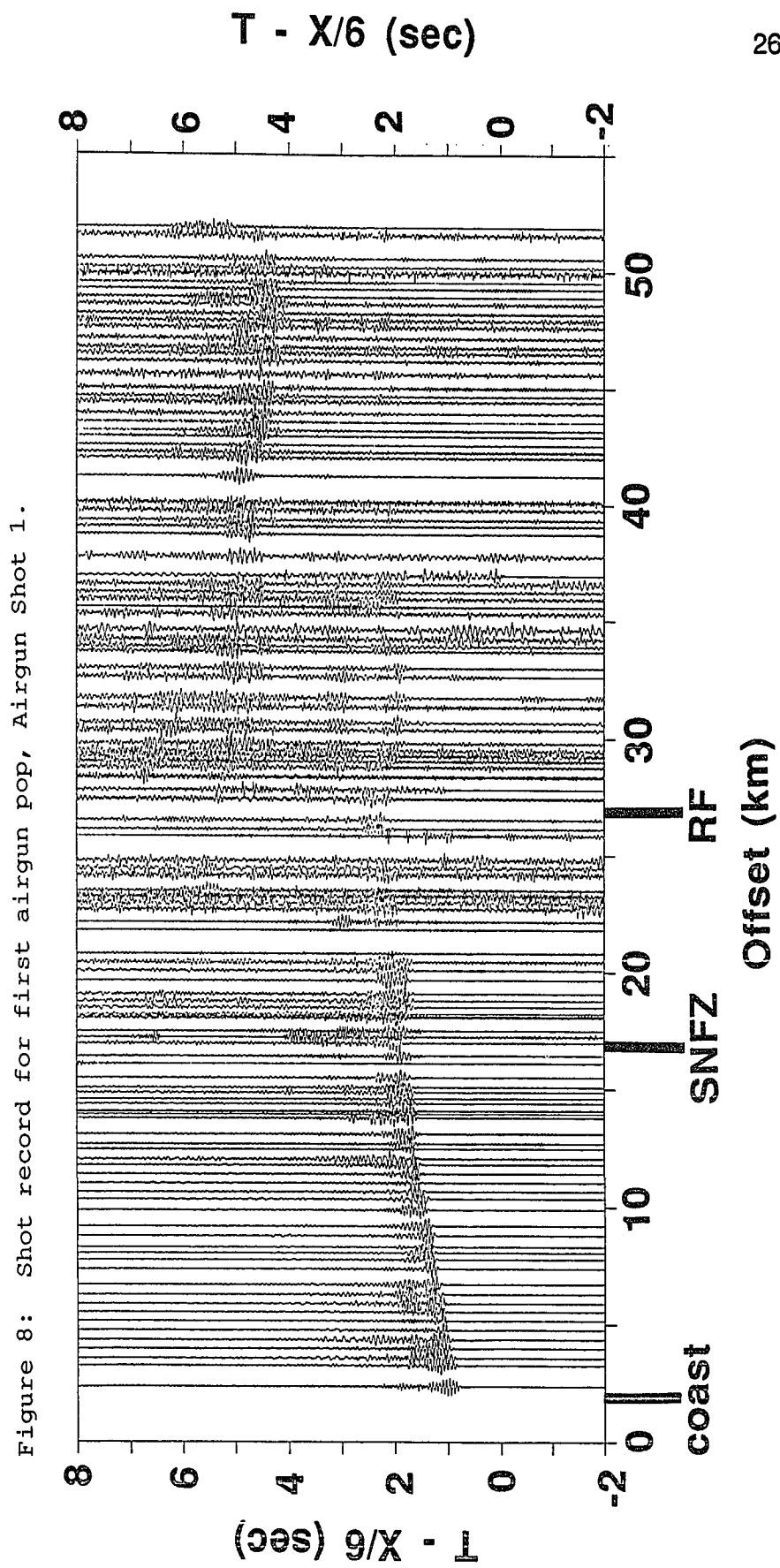
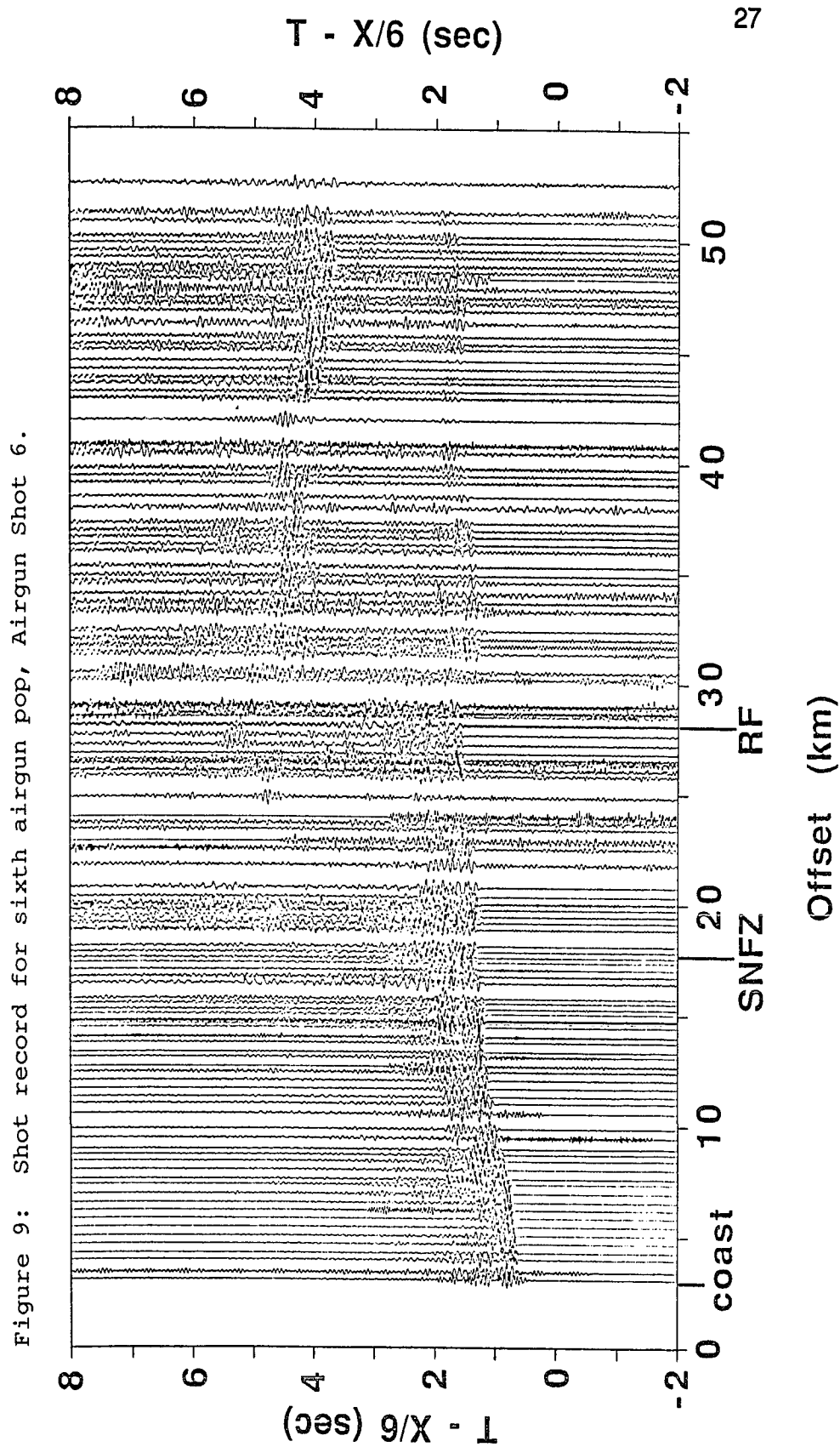


Figure 7: Shot record for eastern land source, Land Shot 2.





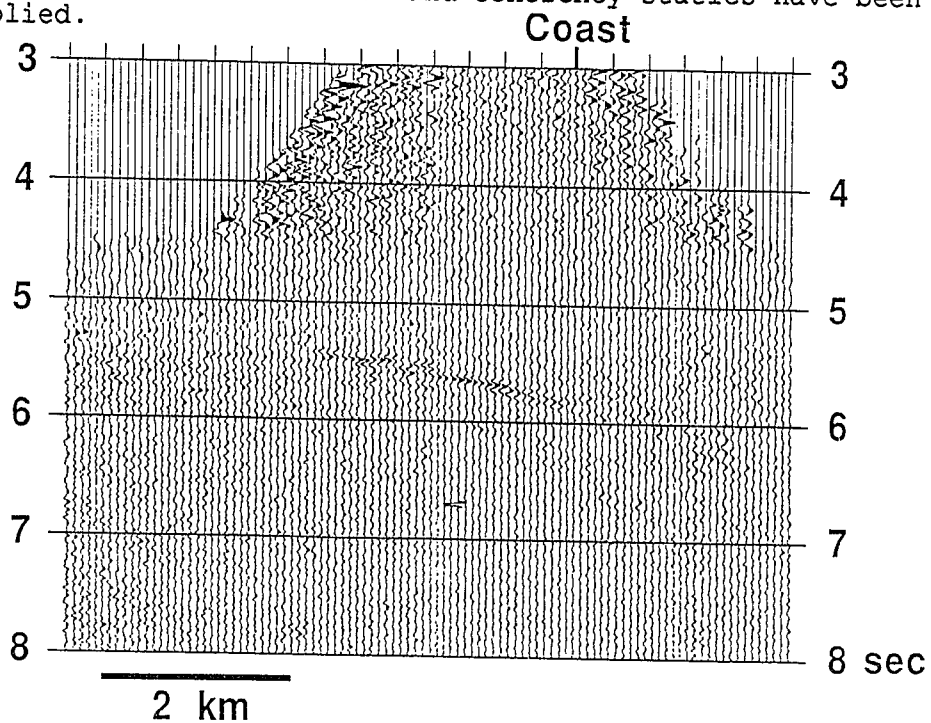


offset. However, there is a similar event on the gather for the easternmost shot (Land Shot 2; Figure 7) at reduced travel times of 4 to 4.5 seconds beginning at offsets of about 42 km. The apparent velocities of the two features from the airgun and land shot records are 7.8 km/s and 18.6 km/s, respectively. If in fact these events are caused by one interface, then this implies that it is dipping eastward, since the apparent velocity of an event from a dipping bed is greater from a shot on the down-dip side (Dobrin, 1976). A rough calculation done by approximating the feature as a dipping interface with a constant slope indicates that it is 15 to 20 km beneath the coast, and dipping about 5 or 10 degrees to the east. Reflection processing on part of the same data sorted to common midpoint has produced an image of a dipping reflector at a comparable depth. A CMP stack of traces with offsets less than 20 km shows a distinct reflection on the stack at 5.5 to 6 s twt dipping to the east (Figure 10). We believe the event is a reflection from the top of the lower crust, located at a depth of about 14 km (Levander and Putzig, 1987).

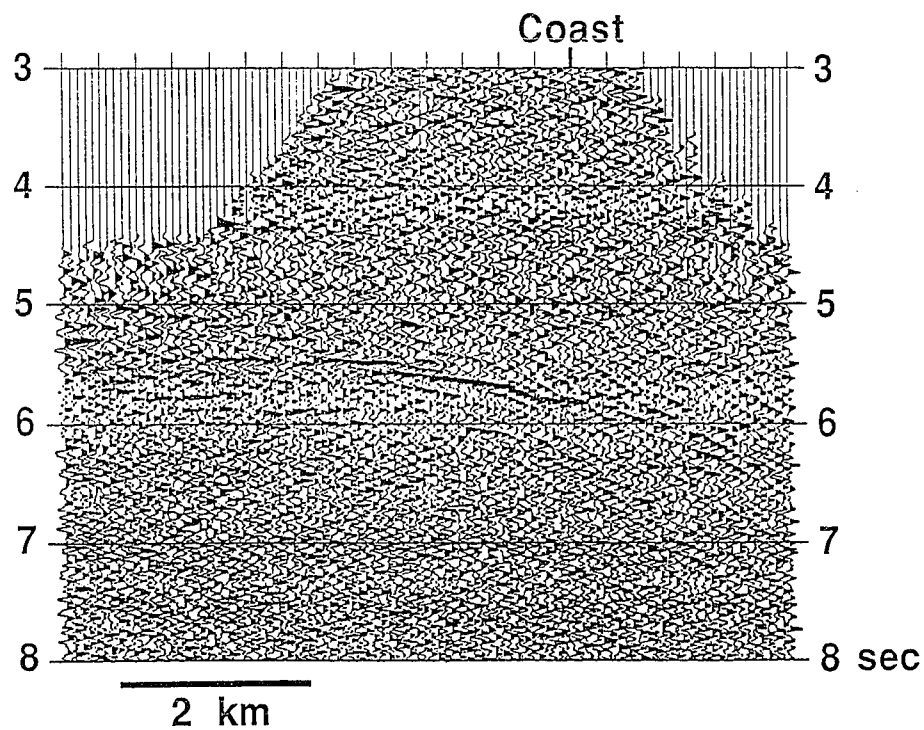
All the shot gathers have distinct first breaks in which the travel times are quite variable (for example, see Land shot gather 1 in figure 6 at offsets from 10 to 20 km). While much of this variability is due to structure at depth, the topography as well as the irregular recording geometry along the receiver spread also contribute. Even though the records are complex, the noise level is generally quite low,

Figure 10:

A) Reflection CMP stack of continuous offset data to which deconvolution before stack and coherency statics have been applied. ²⁹



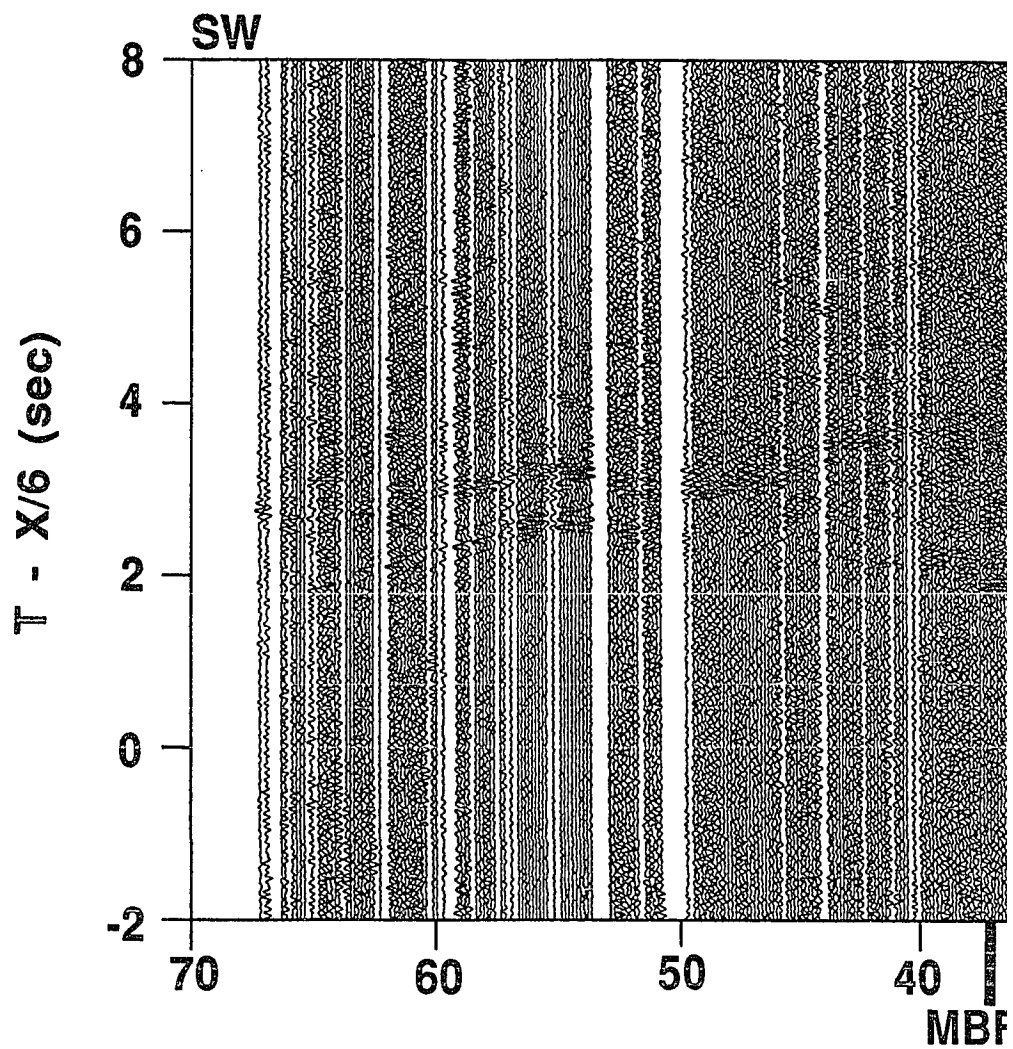
B) The same as (A) but with the addition of automatic gain control.



especially for the landshots. The most complex parts of the record are those associated with segments of the line covering the Sur-Obispo belt. This is as one might expect, considering the internal deformation of the Franciscan rocks contained therein.

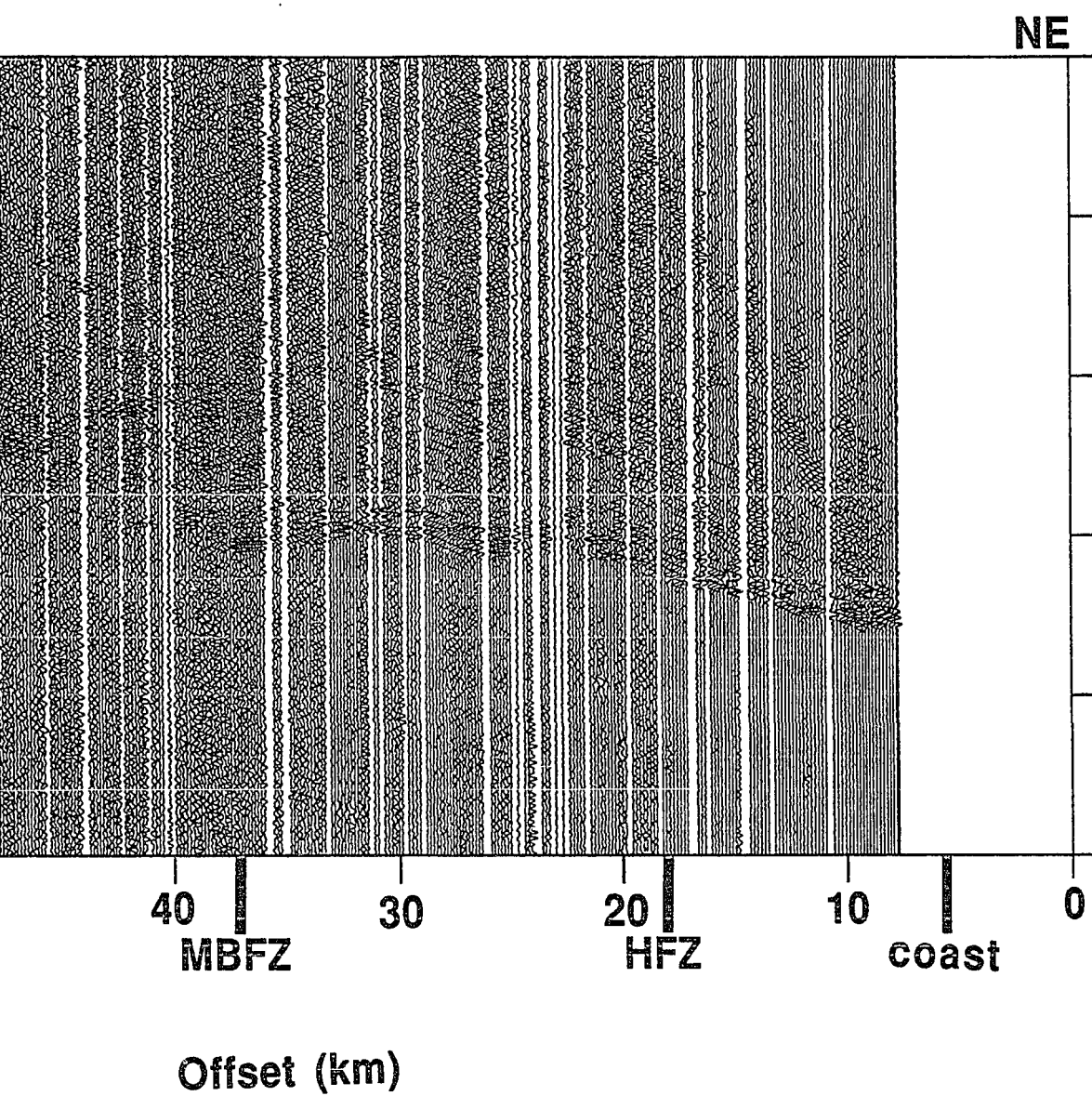
Receiver gathers of the data provide information about the offshore half of the seismic profile. Gathers for receivers 15, 29, and 49, which are spaced at approximately 5 km are shown in Figures 11, 12, and 13. Similar to the shot gathers, we see a strong reflection at long offsets, but there is also a second large amplitude arrival which is not easily seen on the shot gathers. At nearer offsets the complexity of the first arrivals once again indicates the extreme deformation which has occurred in the Franciscan, and distinct changes in travel time occur in the vicinity of the Hosgri and Mid-basin fault zones.

Receiver Gather 15



Offs

Figure 11: Receiver gather of airgun array shots 15.



irgun array shots at Receiver

Receiver Gather 29

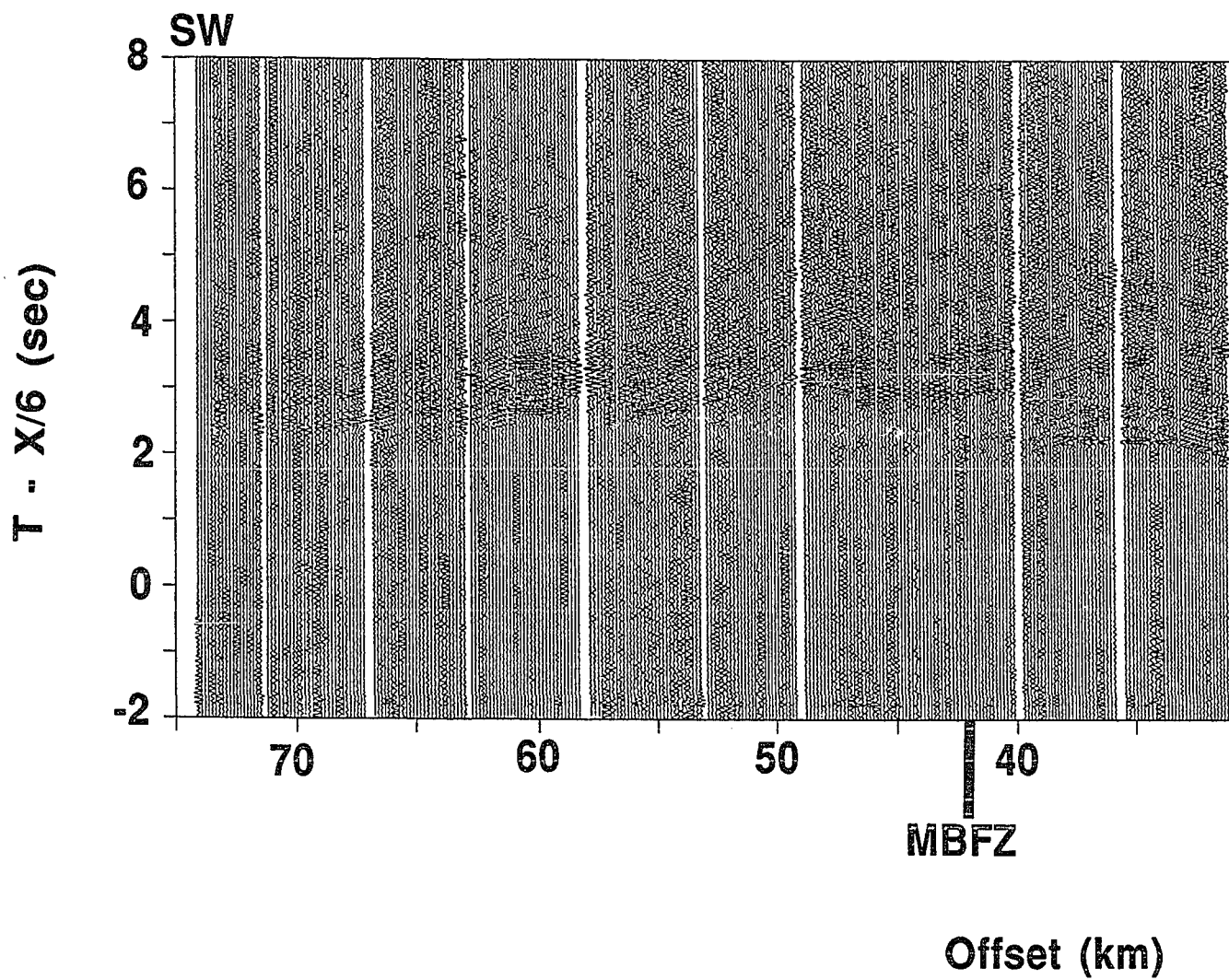
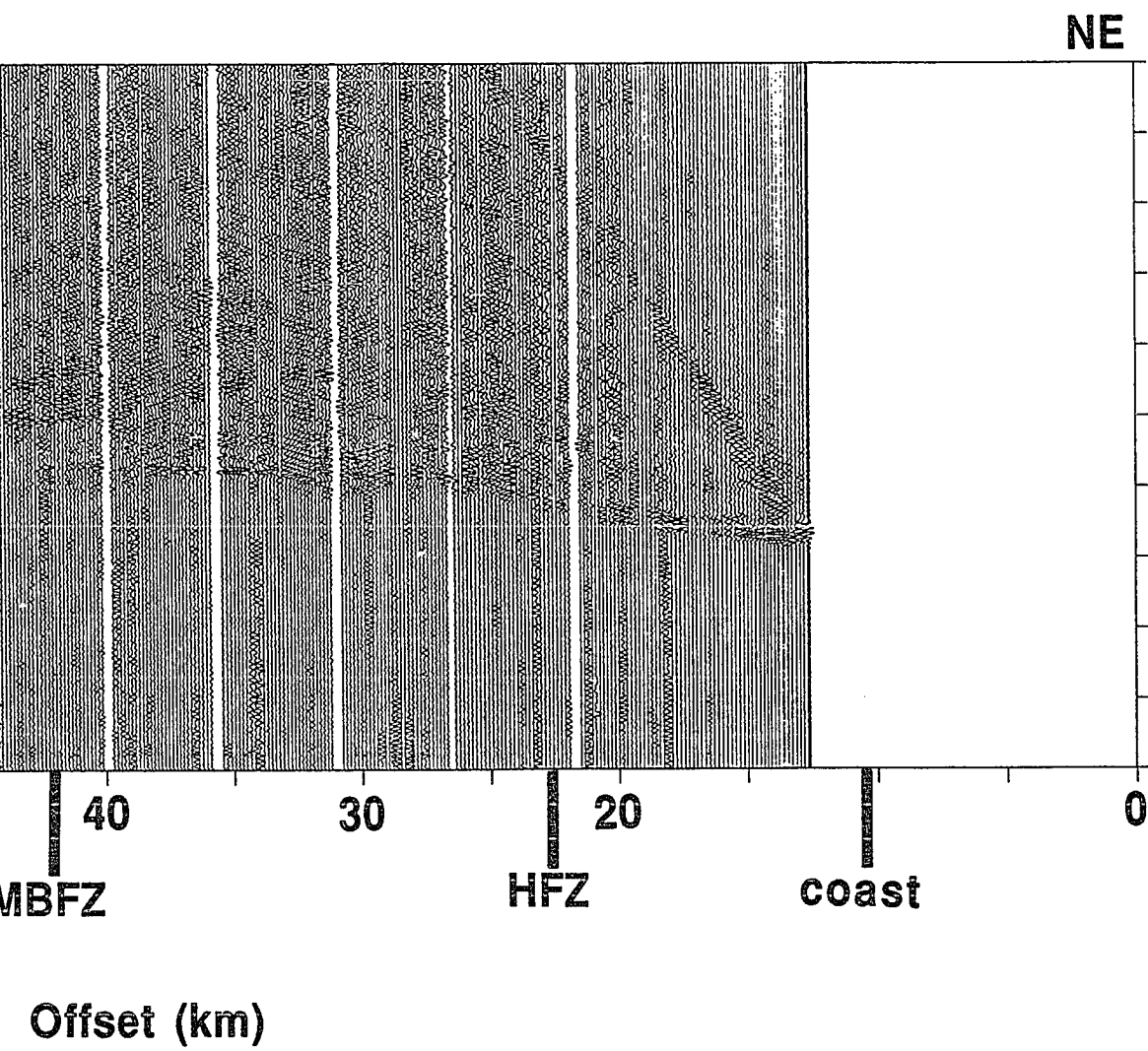


Figure 12: Receiver gather of airgun array shots at Receiver 29.



cs at Receiver

Receiver Gather 49

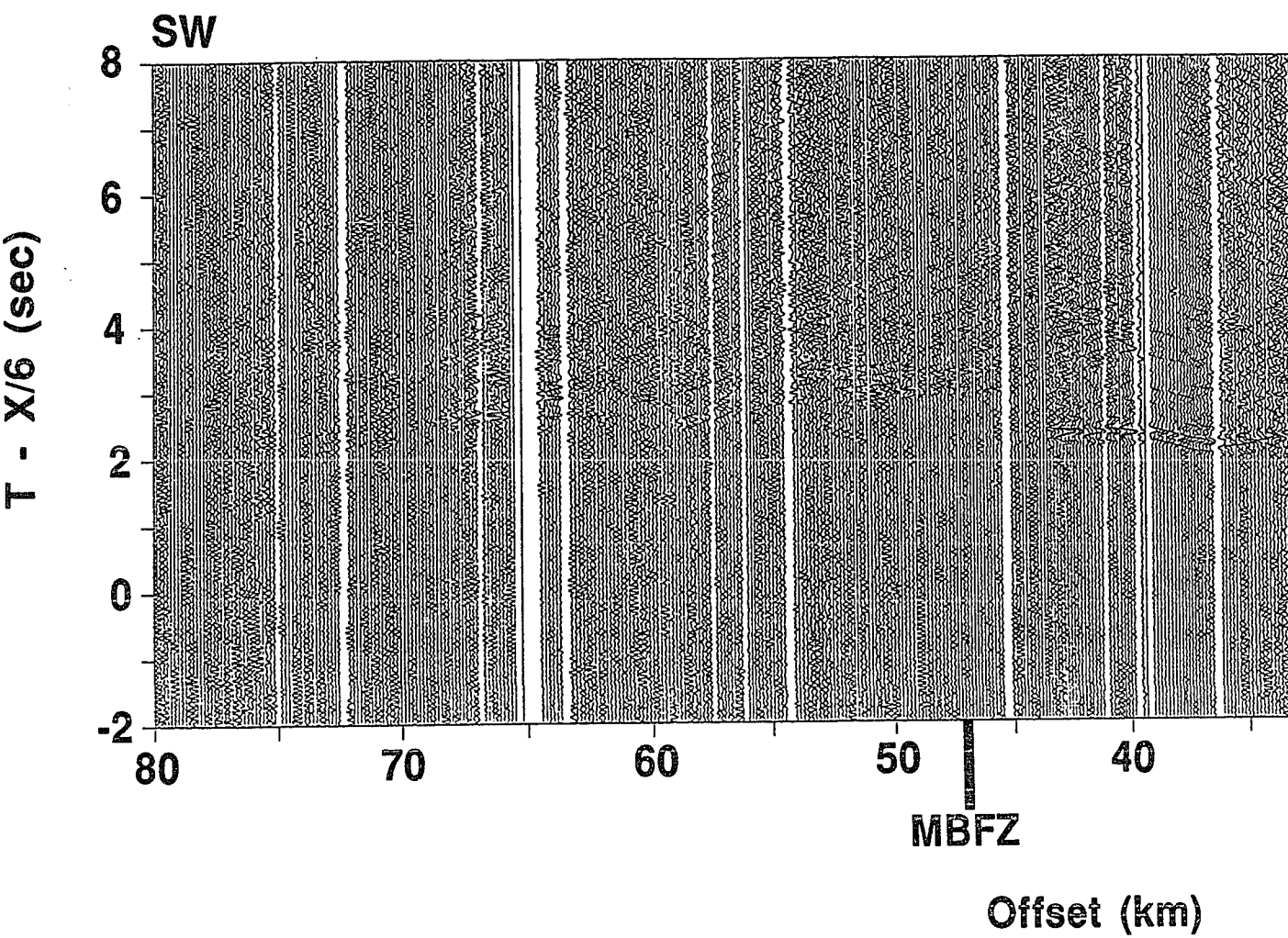
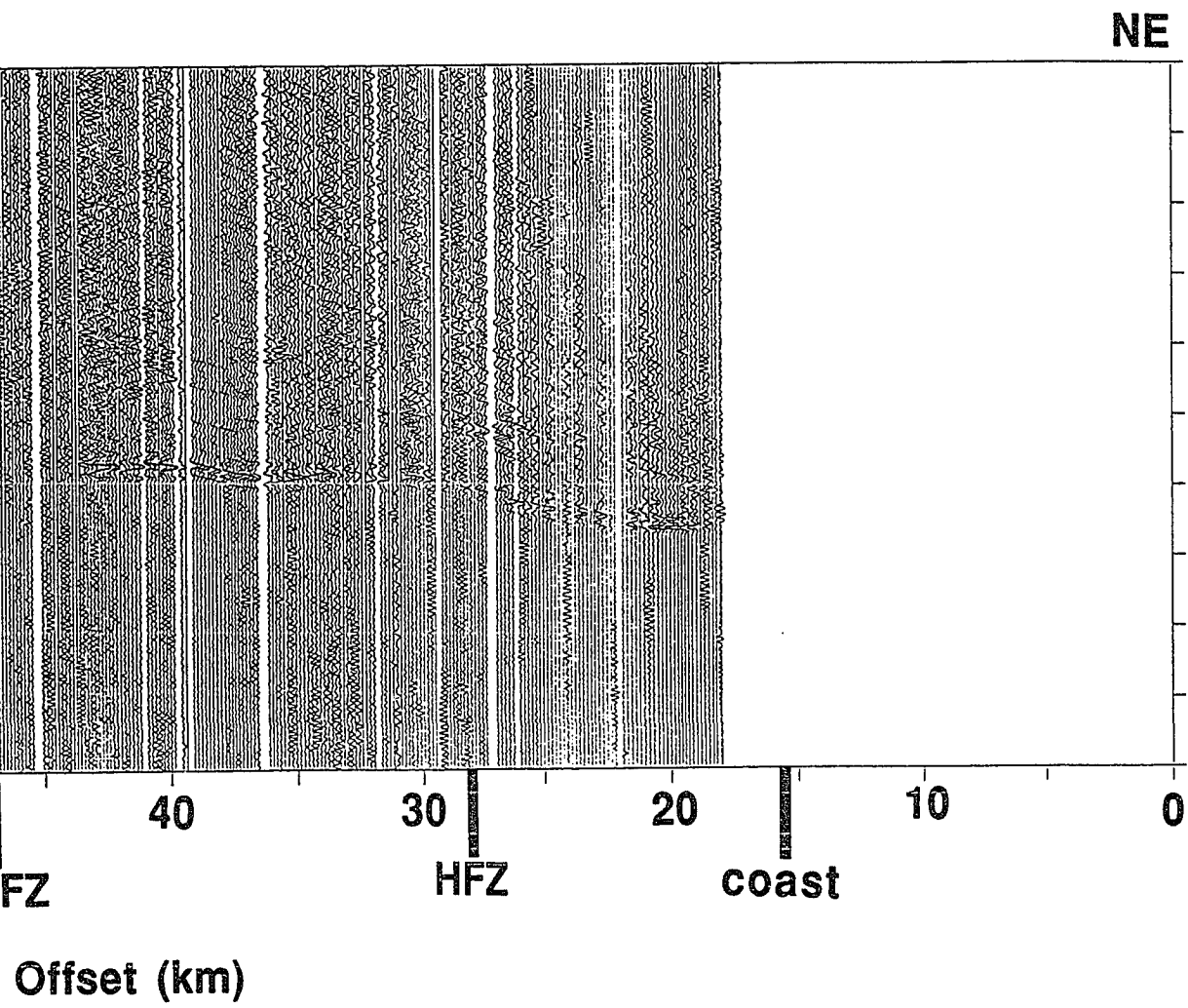


Figure 13: Receiver gather of airgun array shots at Receiver 49.

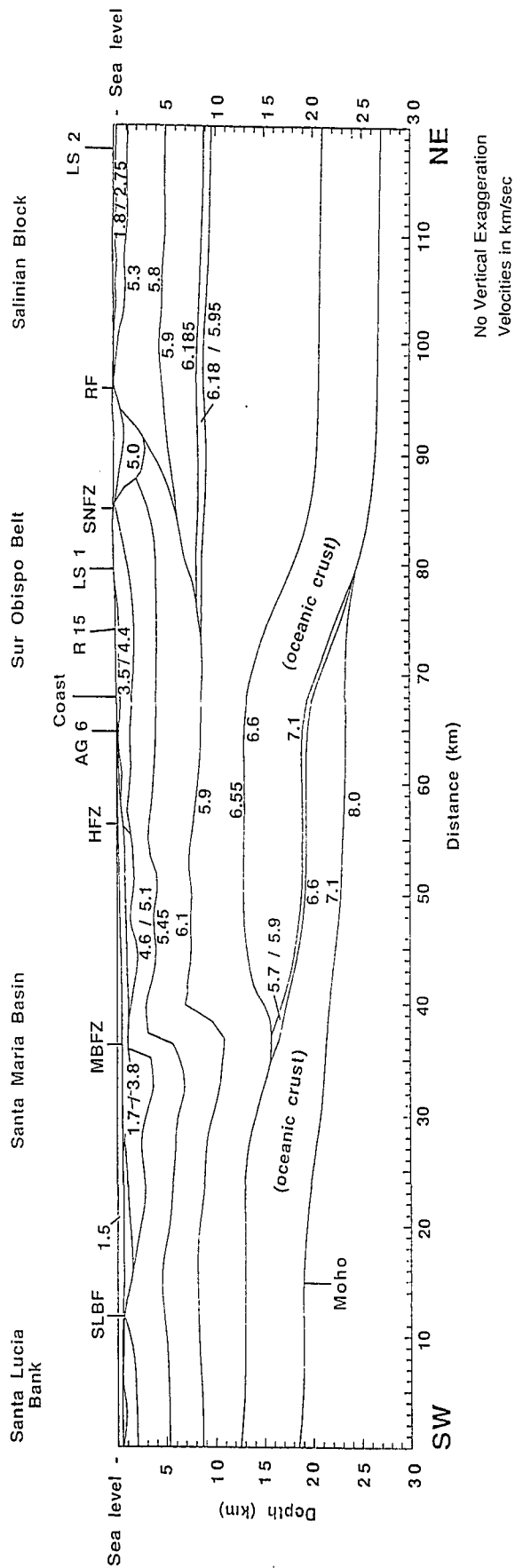


CHAPTER 5:
REFRACTION DATA MODELING

The purpose of refraction modeling is to determine gross velocity layering as a function of depth within the earth. I have used shot and receiver gathers of the data collected in California to obtain two different profiles for the velocity and structure in the transform margin crust down to depths of about 30 km (Velocity Model 1 is in Figure 14; Velocity Model 2 is in Figure 24). Both models use the same near surface layering and velocities, which were derived from line drawings of reflection data offshore and from reversed first-break travel time matches on land. Each model was constructed in two parts; one is based on receiver gather interpretations and covers the western, primarily offshore half, and the other was produced from shot gather interpretations over the eastern land-based half of the models. The model distances are given in offset from the westernmost airgun pop (Airgun Shot 425). The major difference between the two models is the velocity structure of the lower half of the crust. Above the Moho, both models have an imbricated lower crustal layer with oceanic velocities. Model 1 has a slightly positive velocity gradient in the layer above the oceanic lower crust, whereas Model 2 has a low velocity zone (LVZ) of variable thickness and limited lateral extent above a somewhat shallower lower crust. A similar LVZ had been identified by Walter and Sharpless (1987) in a USGS refraction line running parallel

Figure 14:

VELOCITY MODEL 1



Abbreviations: SNFZ-Sur Nacimiento Fault Zone; RF-Rinconada Fault; HFZ-Hosgri fault zone; MBFZ-Mid-basin fault zone; SLBF-Santa Lucia Bank fault; AG-Airgun Shot; LS-Land Shot; RG-Receiver Gather.

to the coast and crossing the Rice line at about Land Shot 1 (Figure 15). Other workers have modeled more pronounced and deeper LVZs beneath coastal California (cf. Trehu and Wheeler, 1987, figure 4; Blumling and Prodehl, 1983). We have no direct evidence for such a feature in the continuous offset data, and Meltzer and Levander (1987) do not see any reflection signature near the depth of the hypothesized LVZs in offshore reflection profiles. Model 1 therefore presents an alternative interpretation of the lower crust in which no large LVZs occur. The model does contain a thin LVZ located at the base of the upper crust beyond 73 km at 10 km depth, and both models have a thin LVZ sandwiched between the two halves of the imbricated lower crust. The thin LVZs were included to improve amplitude matches between the data and the synthetics.

Velocity Model 1

The preferred model with no thick LVZ is shown in Figure 14. Offshore, lateral velocity changes in the near surface of the model correspond to known fault traces, particularly the Hosgri, Mid-basin and Santa Lucia Bank faults of the Santa Maria Basin. Because of the geometry, no reversed coverage of the offshore was possible, and that part of the model is based on receiver gather interpretations. Primarily, Receiver Gather 15 (Figure 11) was used in constructing the offshore model. This gather shows distinct arrivals out to about Airgun Shot 340 at 60 km offset.

SUR-OBISPO VELOCITY MODEL

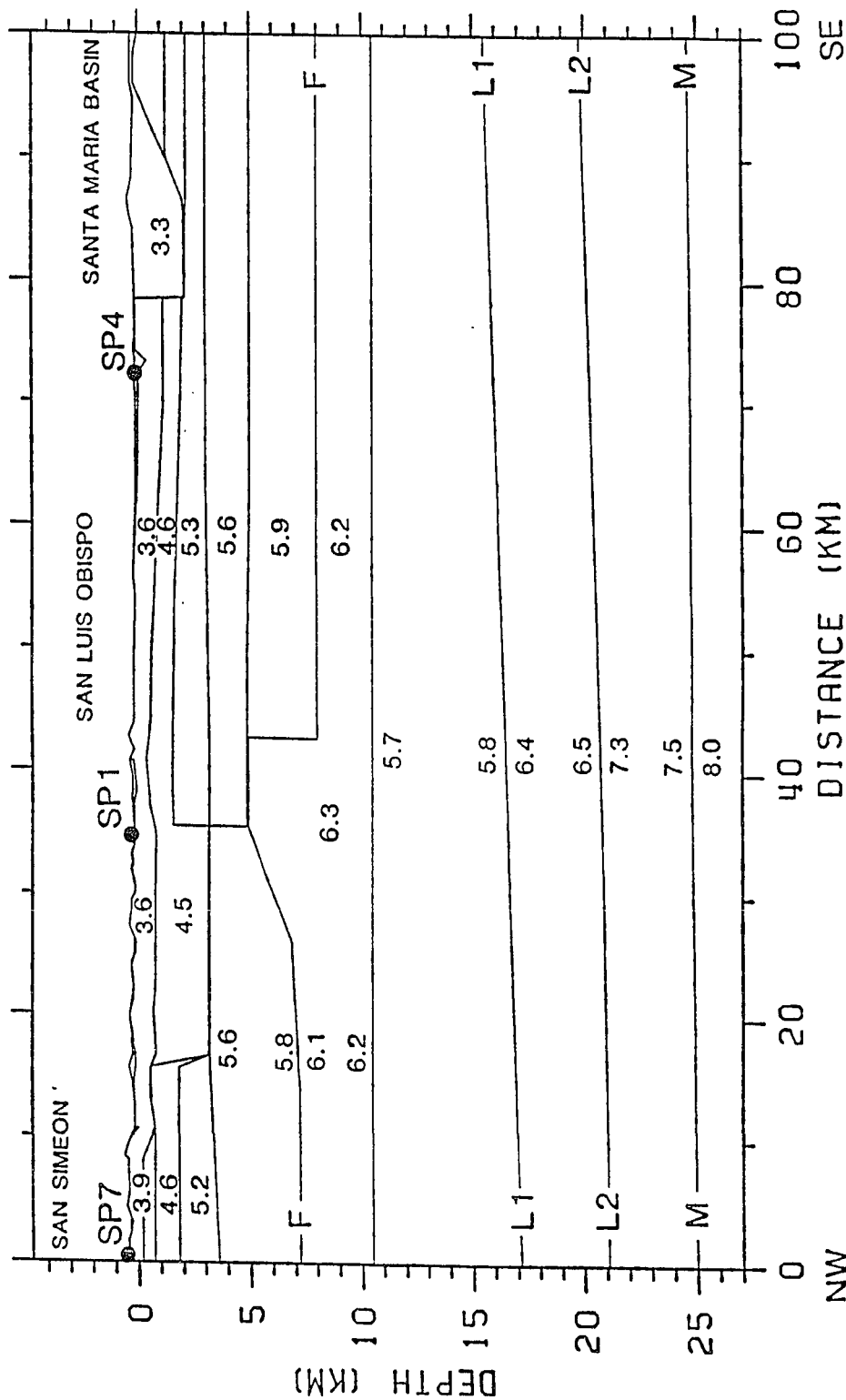


Figure 15: Preliminary velocity model produced from a USGS refraction line parallel to the coast (Walter and Sharpless, 1987). Crosses the continuous offset profile at Land Shot 1.

Synthetics generated from the model for Receiver Gather 15 are shown in Figure 16 (lines drawn on gathers in 16A represent ray-trace synthetic travel times). Waves through the upper crust produces the strong first breaks out to 38 km offset, and these arrivals are well matched both in amplitude and travel time, where the latter are matched to within less than 0.1 seconds. Between 40 and 50 km offset, crustal wave amplitudes fall off in the data. Matching this feature on the synthetics requires a decrease in velocity at the base of the upper crust, where the velocity changes from 5.9 to 6.1 km/s.

To produce the upper crustal model, I used linear approximations of first break travel times to generate a flat layered model which I then refined with iterative ray tracing. Asymptotic ray theory based programs SEIS83 and RAYPLOT (Cerveny, 1977) were used to first match travel times and then amplitudes. Pacific Gas and Electric Company collected reflection data over the same track as our airgun sources offshore (Savage et al, 1988; PG&E line FLEC1). A line drawing of FLEC1 showing near surface layering interpreted as Tertiary sediment overlying basement provided a constraint for the upper 3 km of Model 1A, and refraction-derived velocities were taken from a parallel Rice reflection line (Meltzer and Levander, 1987; line RU-13).

One of the main features that we wished to model was the deep dipping event observed on shot gathers and CMP sections. Using the depth of 15 km that we estimated from the CMP stack

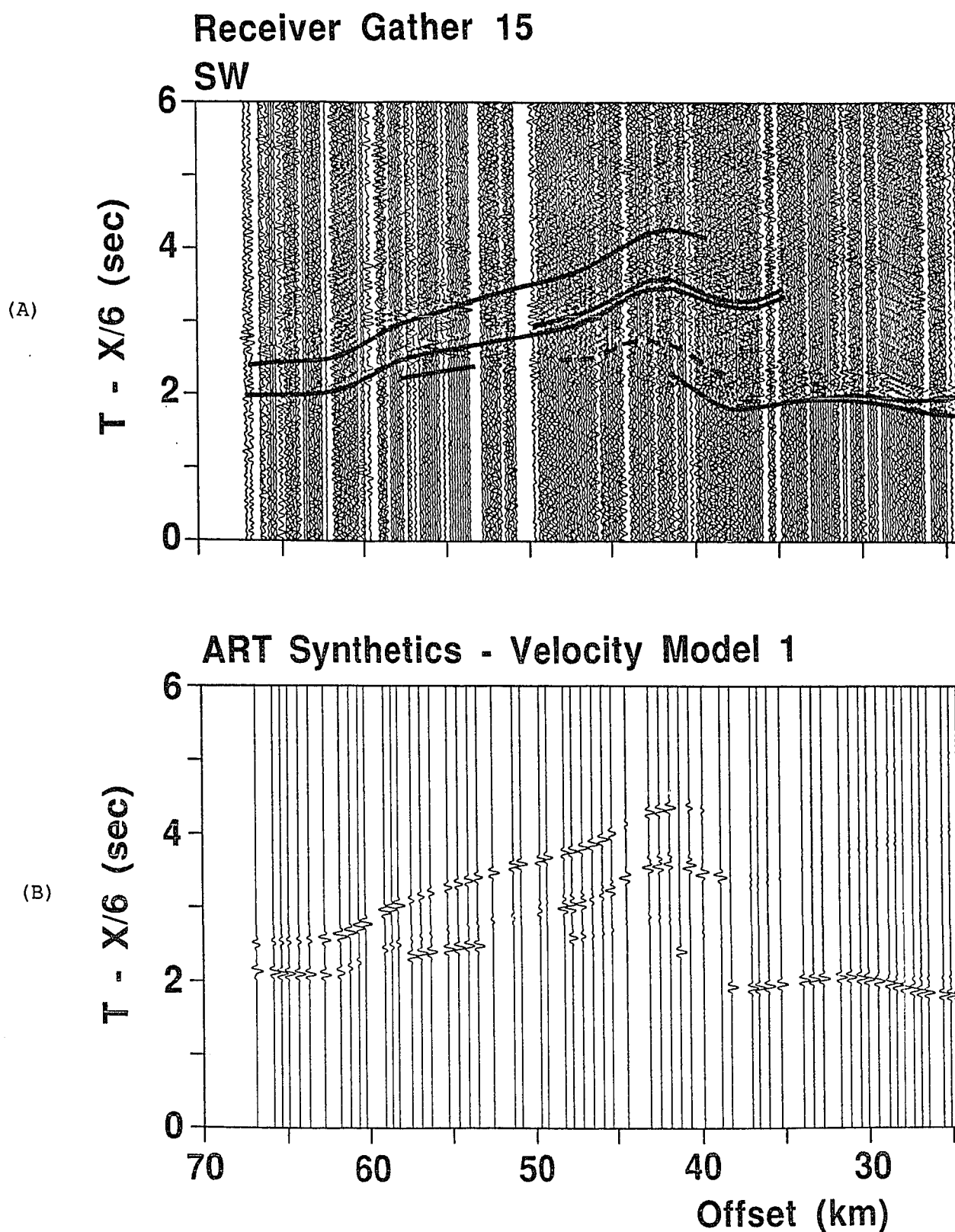
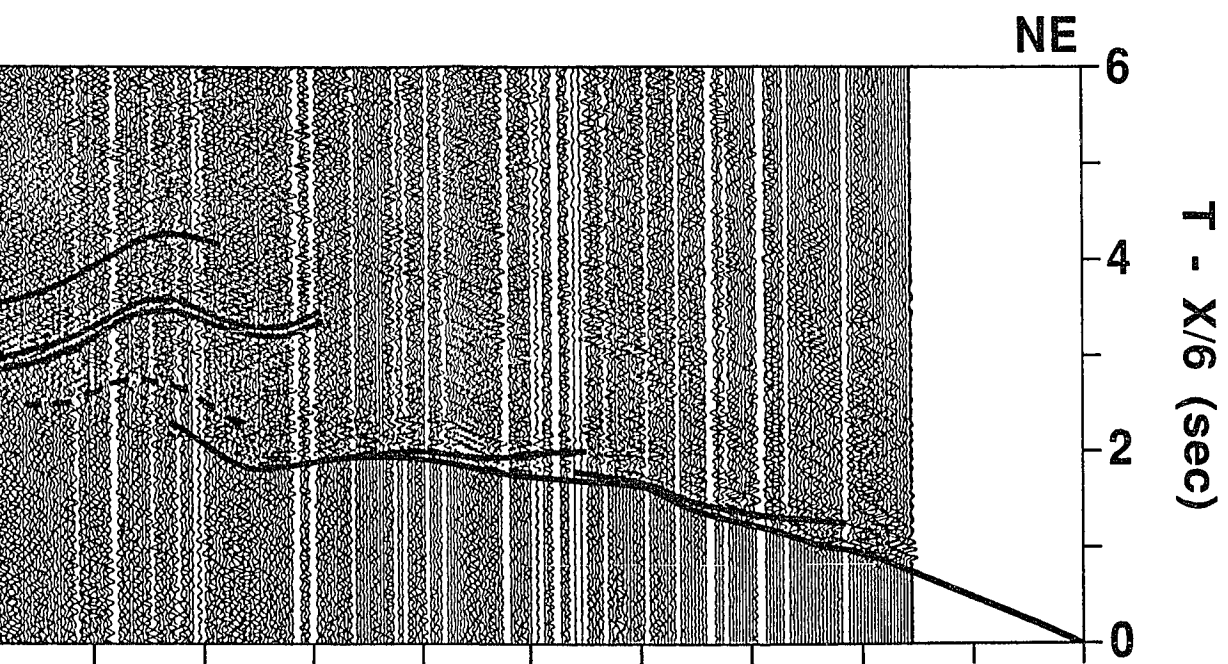
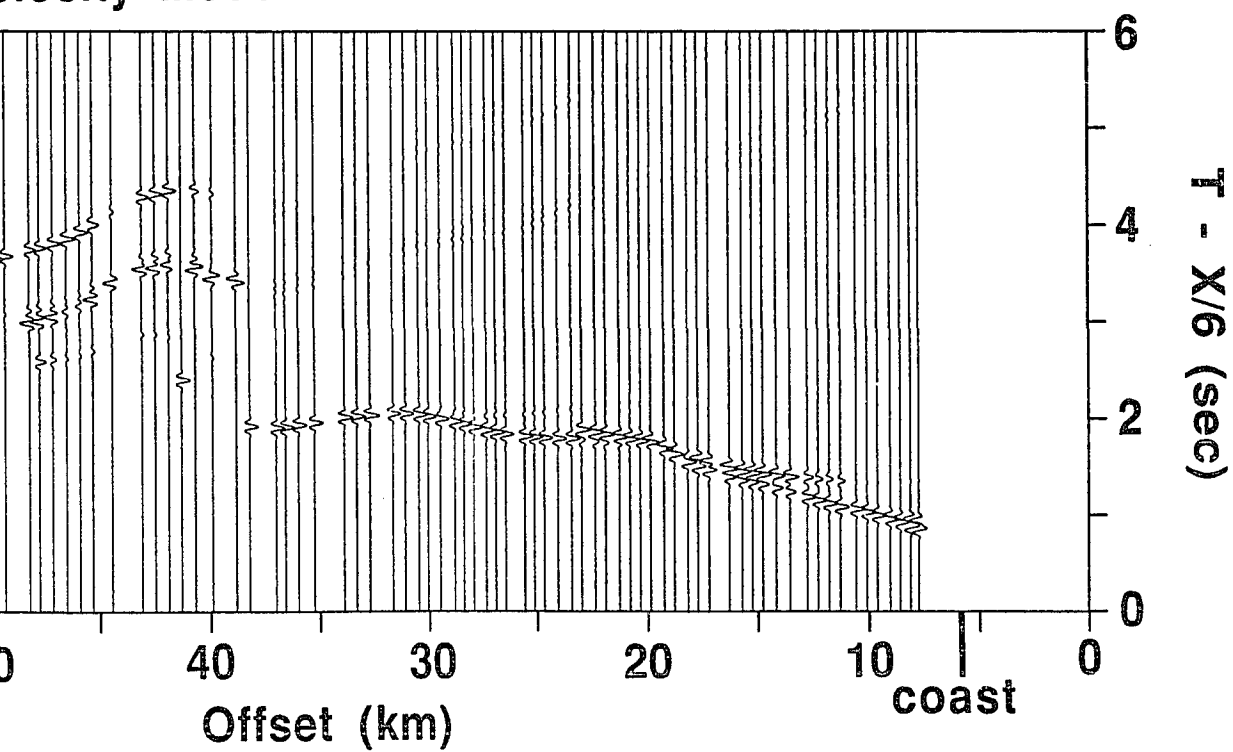


Figure 16: A) Receiver Gather 15 with travel time curves produced from the model in Figure 14. B) Synthetics produced from rays traced from airgun shots offshore to Receiver 15.



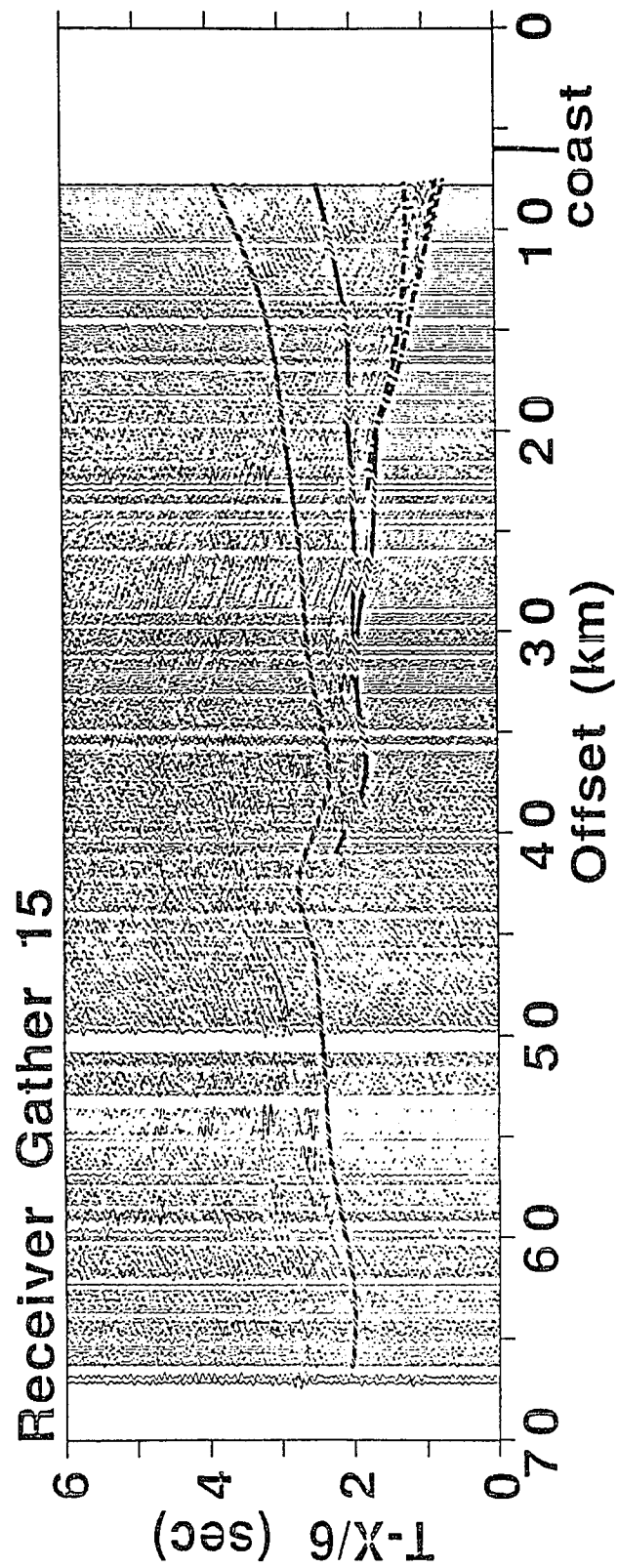
Velocity Model 1



15 with travel time curves
 Figure 14. B) Synthetics produced
 shots offshore to Receiver 15.

(Putzig and Levander, 1988), we inserted a slightly (about 15°) dipping layer with a velocity gradient typical of oceanic crust (6.6-7.1). This layer is seen on Figure 14 plunging beneath the coast between about 65 and 90 km on the model at depths of 15 to 25 km. Offshore reflection lines of Meltzer and Levander (1987) show prominent horizontal reflectors at 6 and 8 s twt. The authors suggest that the latter reflection may be from the Moho, and they estimate a lower crustal layer thickness of 6 to 7 km, assuming oceanic velocities. In our model, the lower crustal layer was extended seaward and flattened out to correspond with the reflection data interpretation. The lower crust of the model provided a match to amplitudes and travel times of Receiver Gather 15 beyond 38 km offset, with wide angle reflections from the base of the deep dipping layer corresponding to the first strong arrival on the gather (Figure 17). However, the second strong arrival (between 2.5 and 3 seconds and beyond 50 km offset) could not be matched with a single lower crustal layer, nor would a simple double-layered lower crust provide appropriate travel times or amplitudes. Modeling them as multiples also proved unsatisfactory, since the amplitudes were much too low. An imbricated layer provides a good fit both for travel times and for amplitudes of the second arrival beyond 50 km. Amplitude behavior was further improved by including the thin LVZ between the two layers. Figure 17 shows diagrams of where rays pass through the crust for Receiver Gather 15.

Figure 17A



Ray Diagrams - Velocity Model 1

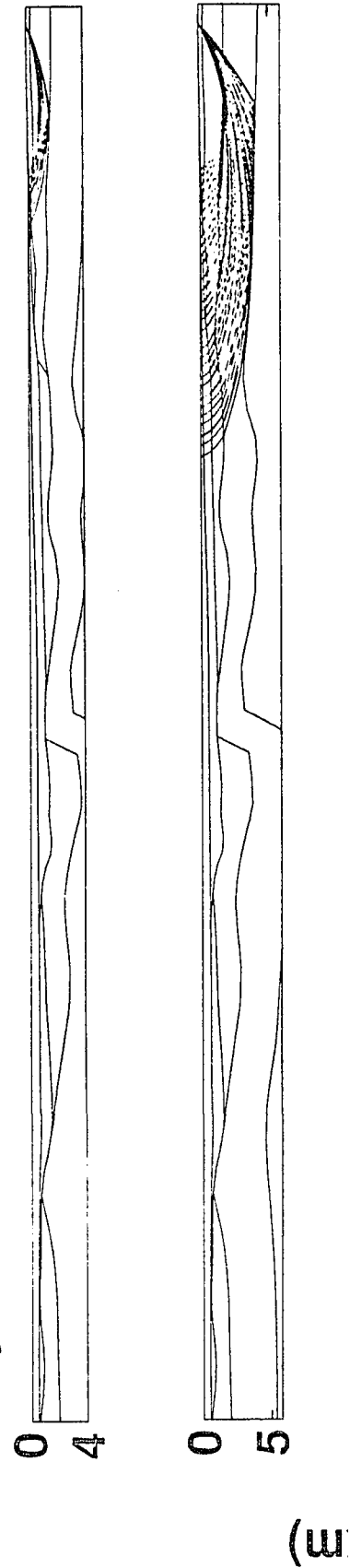
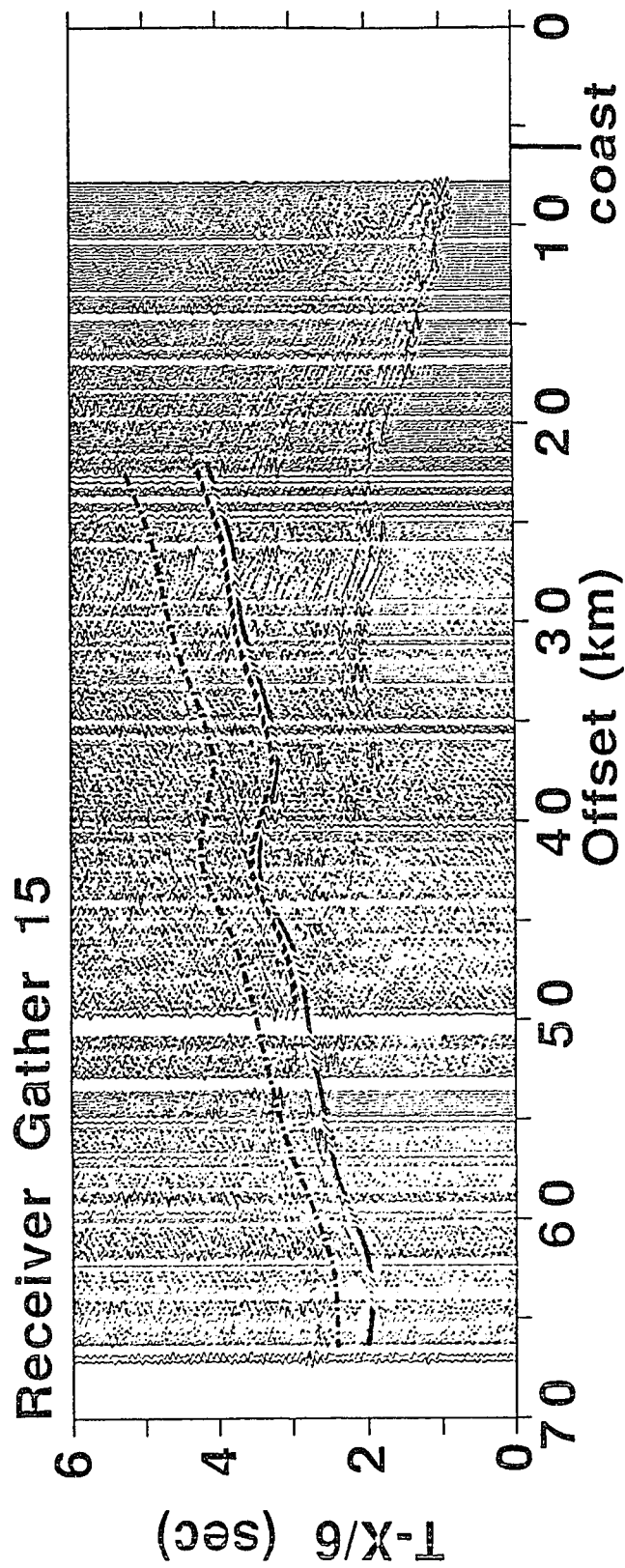




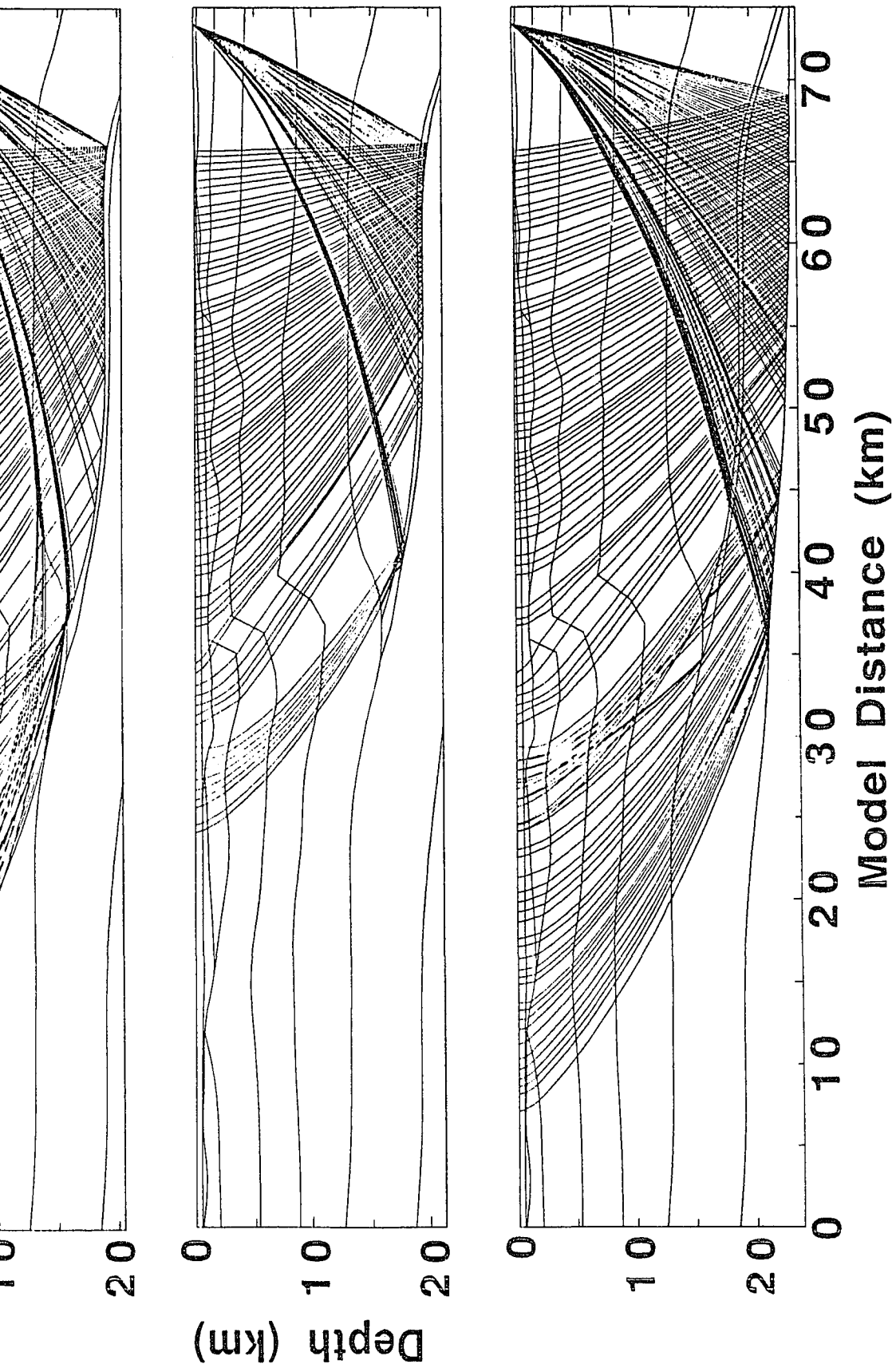
Figure 17: Ray diagrams traced through Velocity Model 1 from airgun shots to Receiver 15. A) Upper crustal rays. B) Lower crustal rays.

Figure 17B



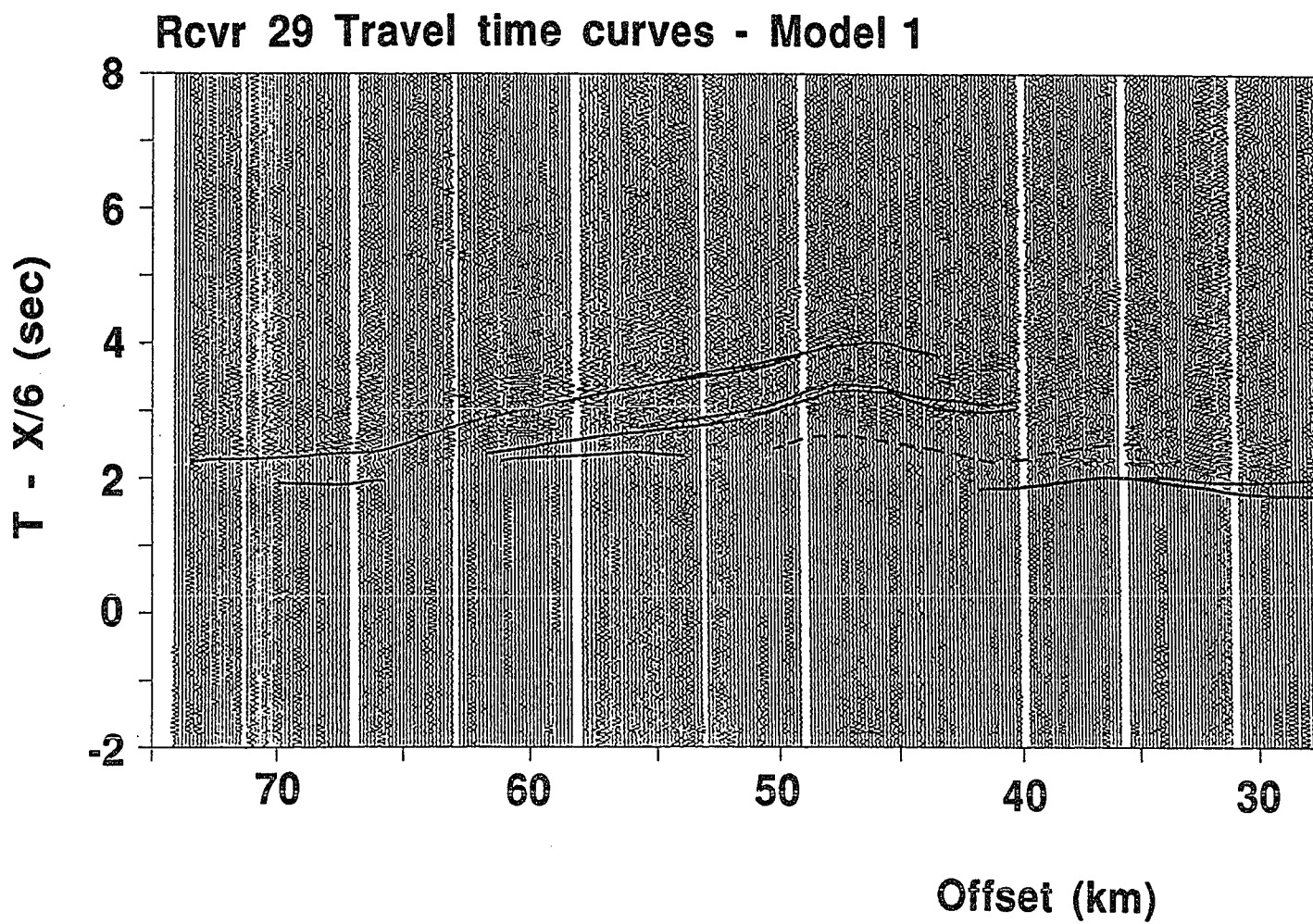
Ray Diagrams - Velocity Model 1





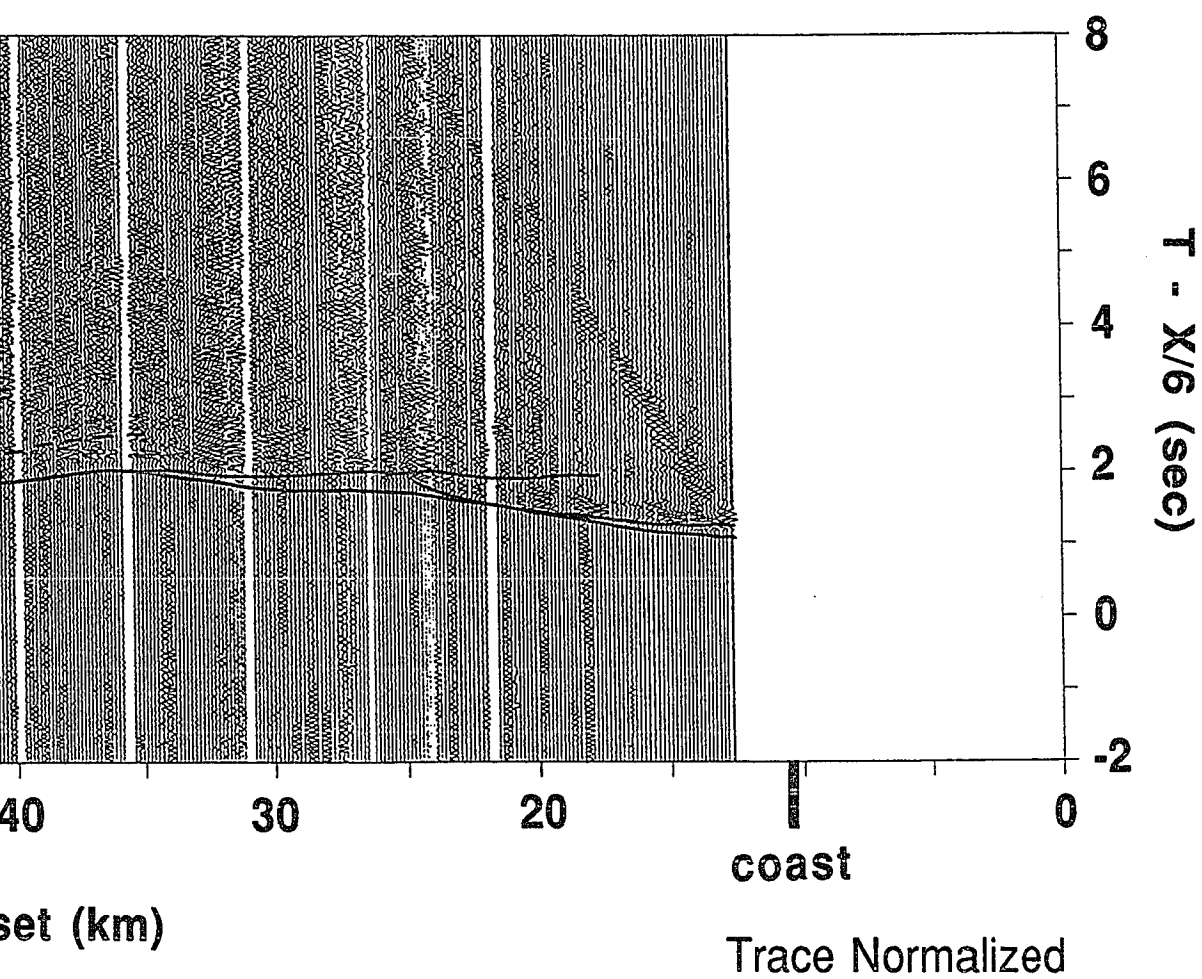
In the synthetics (Figure 16), the amplitude of the second arrival remains comparable to the first between 40 and 50 km, which is not the case in the data. This discrepancy is probably due to a more complex velocity structure in the lower half of the imbricated layer beneath the coast than I have been able to model. I also could not properly match a few other features seen on the data, such as the two arrivals with low apparent velocity between 51 and 53 km offset. One possible explanation is that these arrivals are from some feature out of plane such as a nearby fault. Another source of problems is model parameterization. The modeling program does not allow vertical boundaries and often fails when a ray encounters a steep boundary or sharp corner. In order to cause rays to turn, vertical velocity gradients are used, but where layers pinch out, such as in the imbricated zone, a physically unreasonable infinite velocity gradient results.

Further refinement of the model offshore was made upon examination of gathers from two other receivers located 5 and 10 km further east (Receiver Gathers 29 and 49; Figures 12 and 13). These gathers contain similar features to those of Receiver Gather 15, but since the offsets are greater, the signal strength has deteriorated. They were chosen so as to provide more constraint on the lower crust where it dips below the coast. Synthetics for these gathers produced from Velocity Model 1 are shown in Figures 18 and 19. For Receiver Gathers 29 and 49, the same general features have been matched as with Receiver Gather 15; a strong crustal



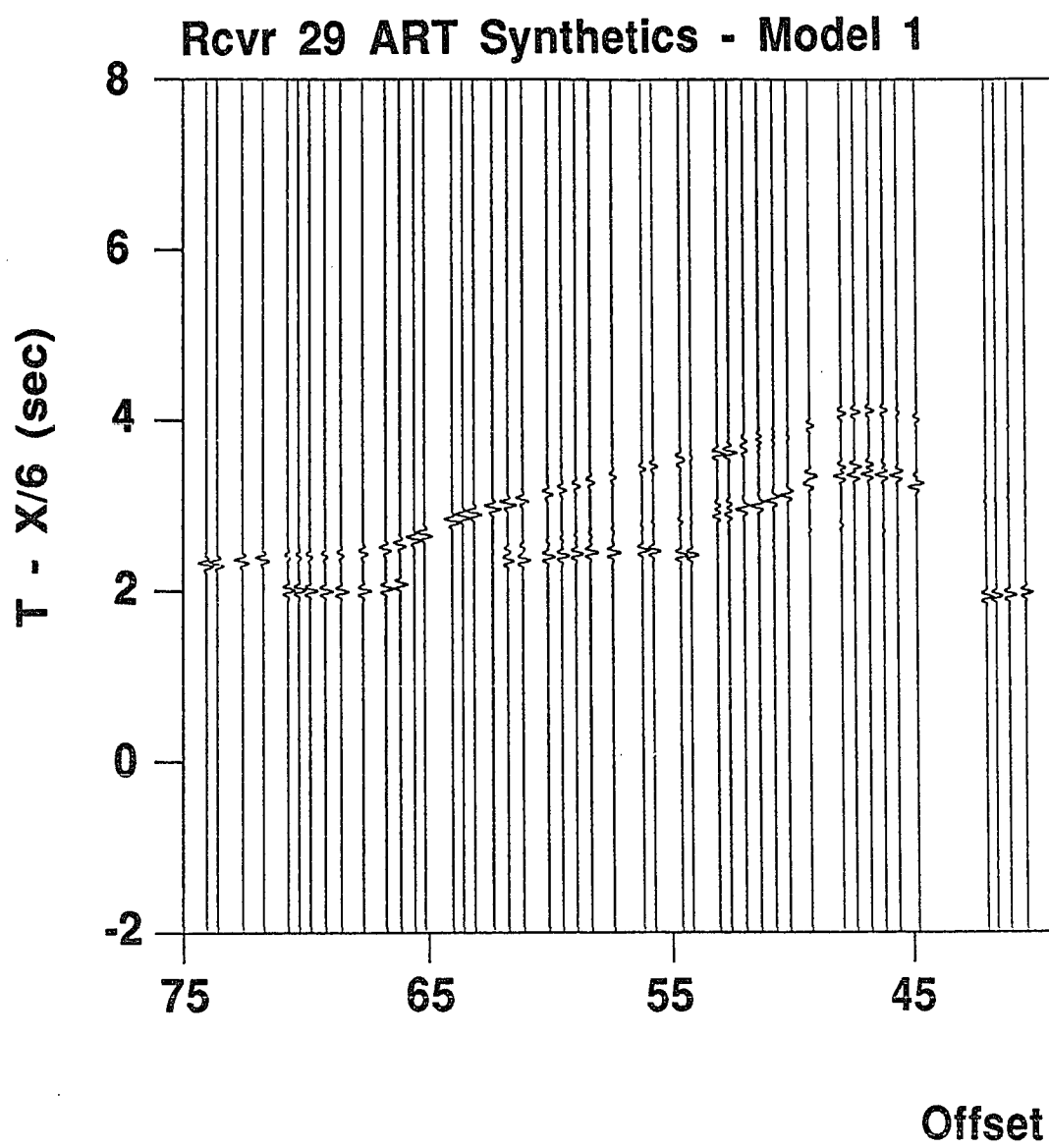
(A)

Figure 18: A) Receiver Gather 29 with travel times produced from the model in Figure 14. B) Synthetic data from rays traced from airgun shots offshore to Receiver 29.



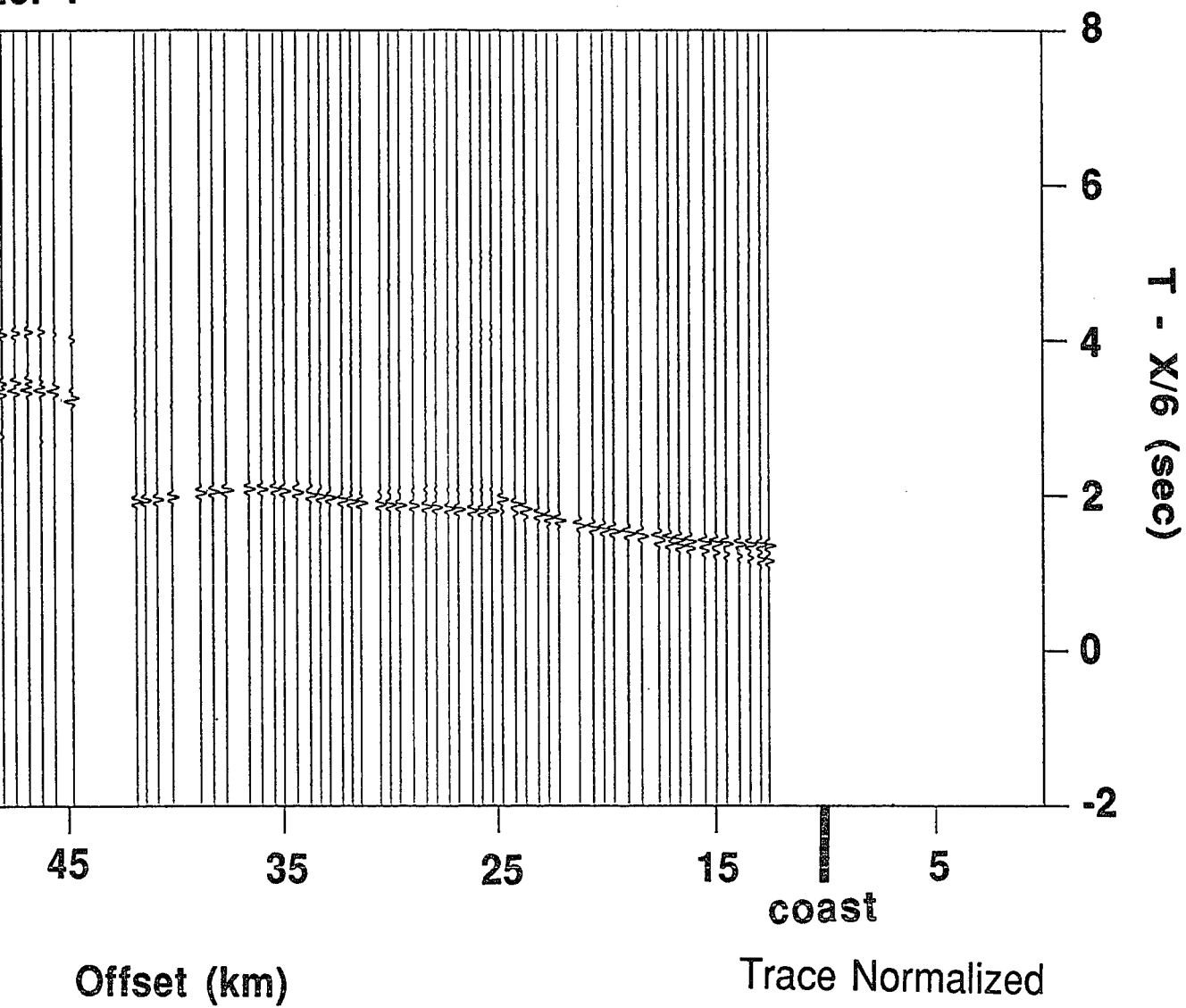
(A)

er 29 with travel time curves
 figure 14. B) Synthetics produced
 shots offshore to Receiver 29.

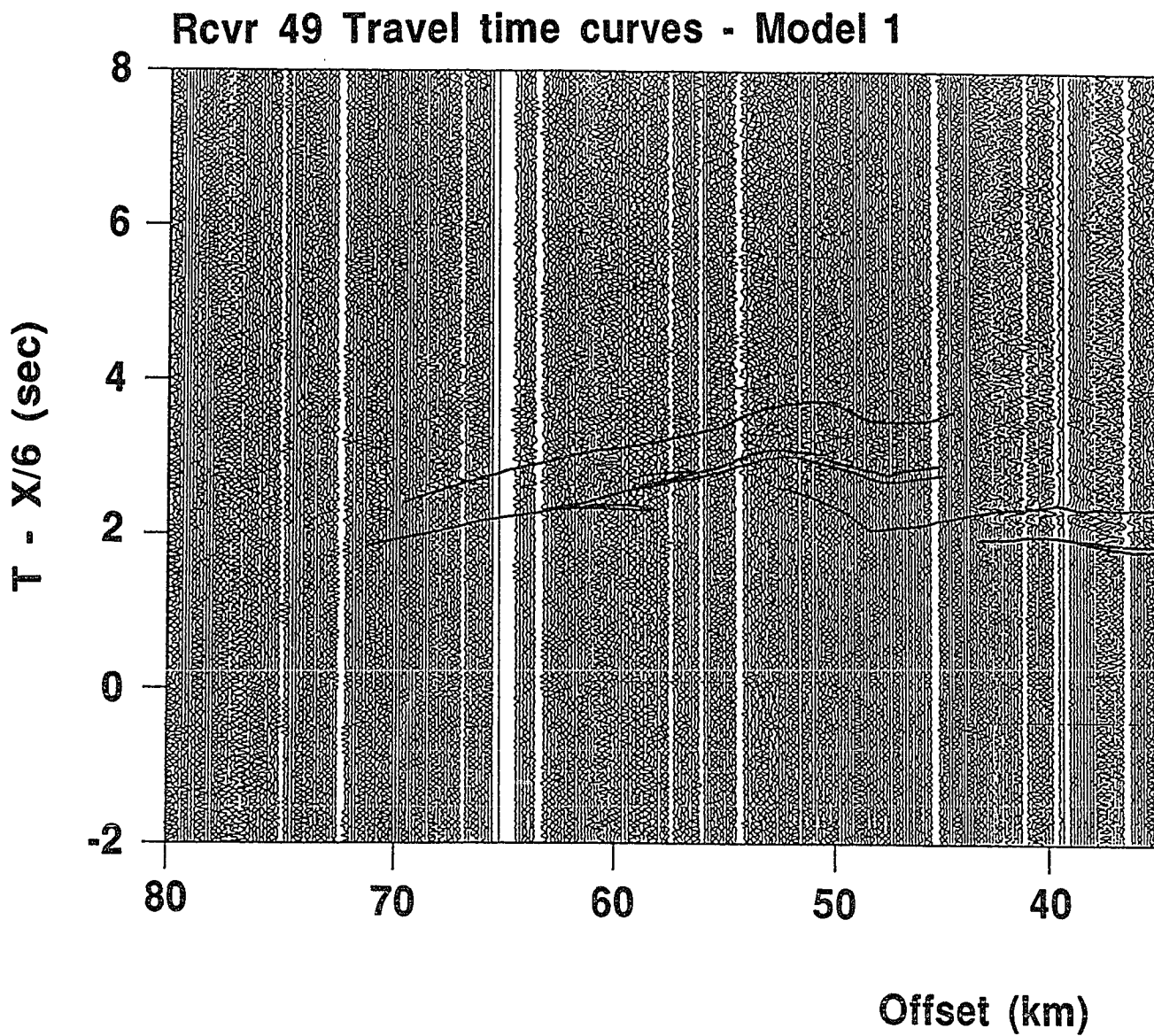


(B)

el 1

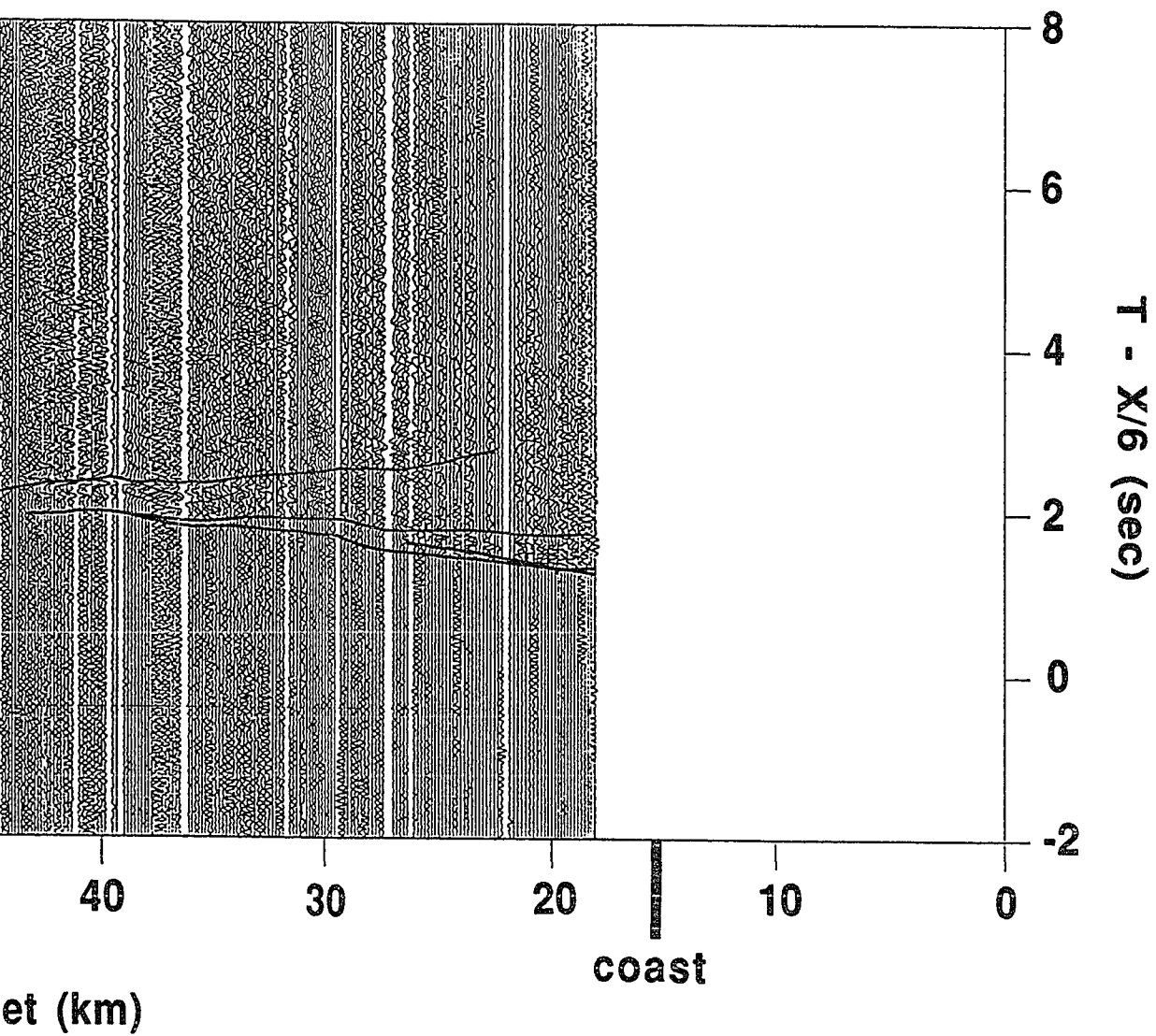


(B)



(A)

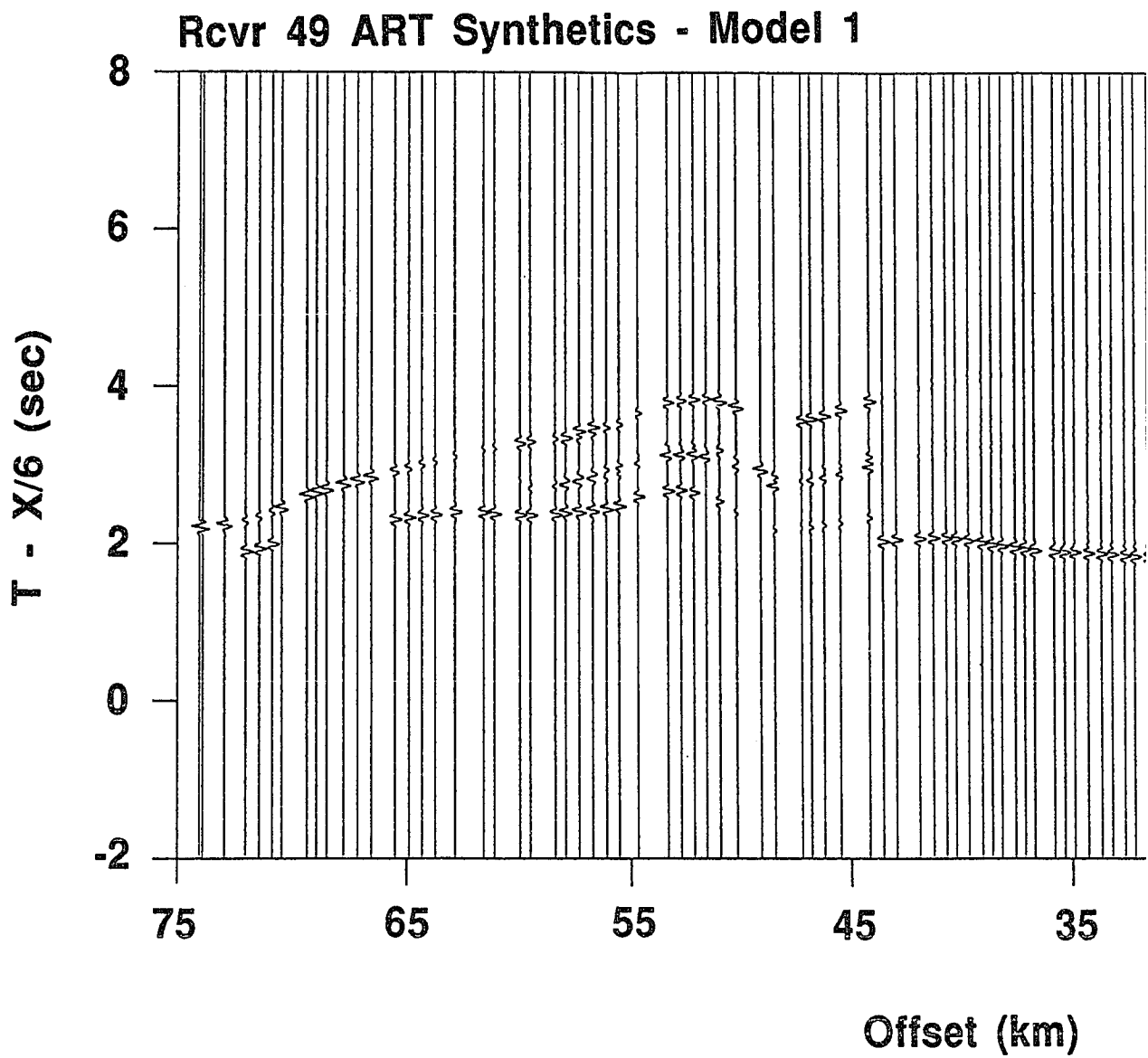
Figure 19: A) Receiver Gather 49 with travel time curves produced from the model in Figure 14. B) Synthetic seismograms from rays traced from airgun shots offshore



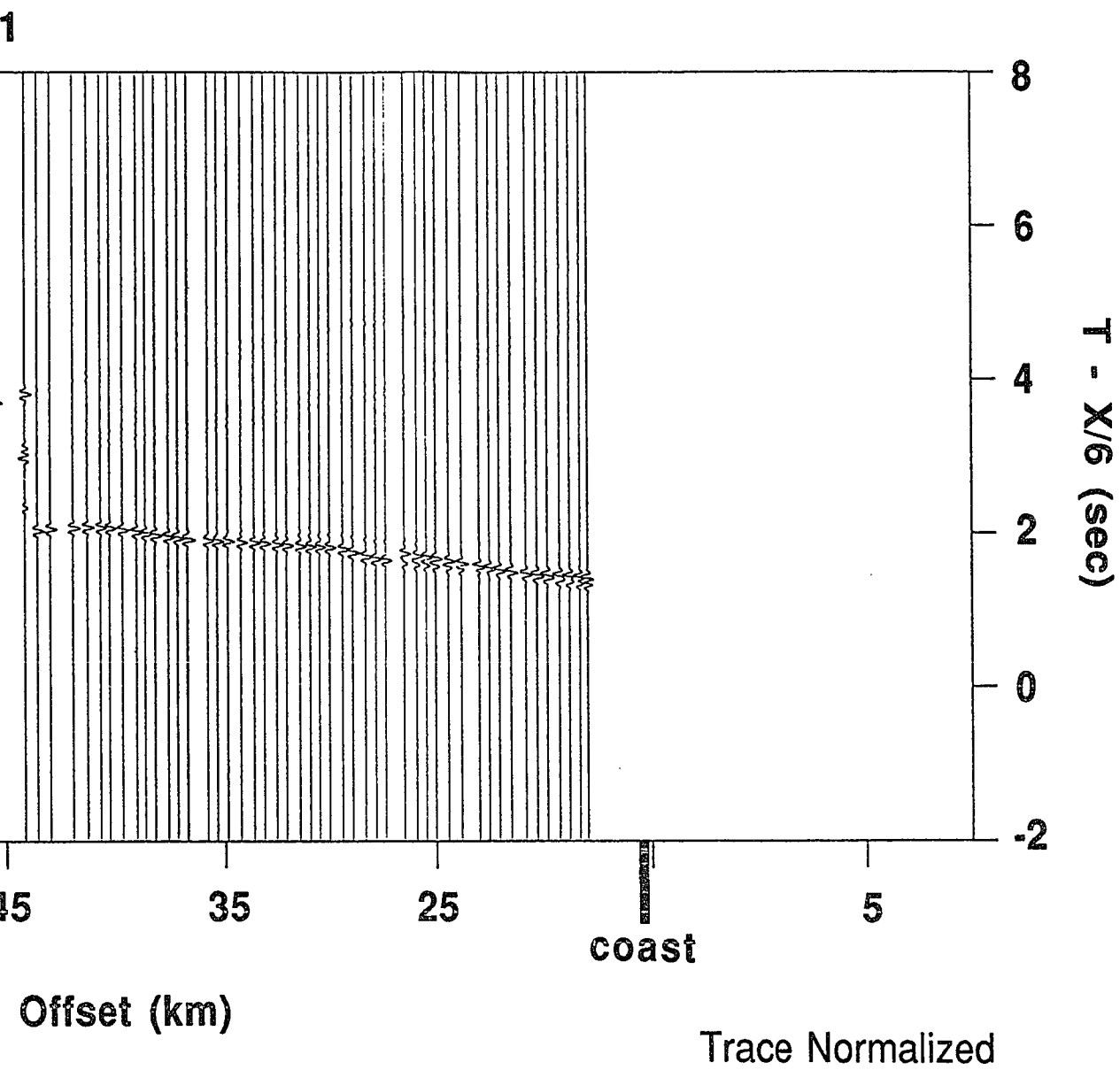
Trace Normalized

(A)

49 with travel time curves
 Figure 14. B) Synthetics produced
 shots offshore to Receiver 49.



(B)



(B)

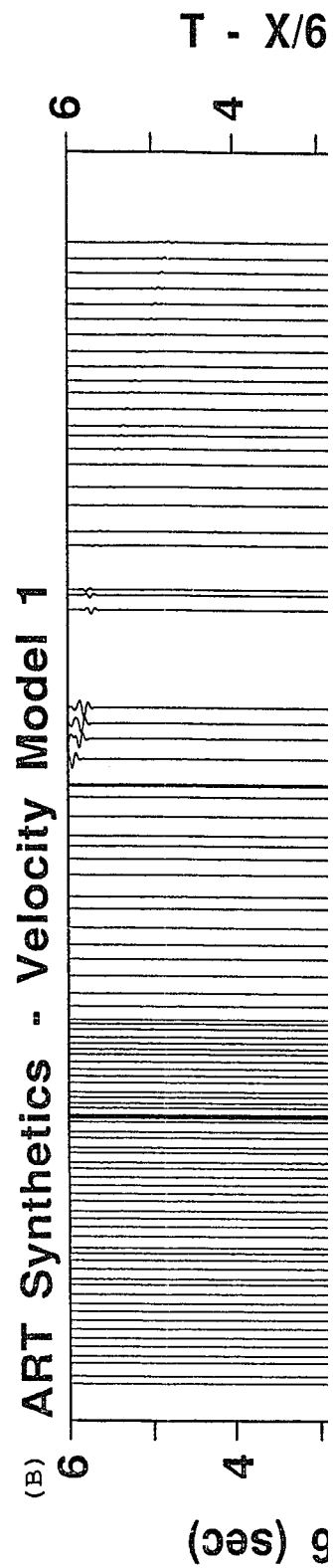
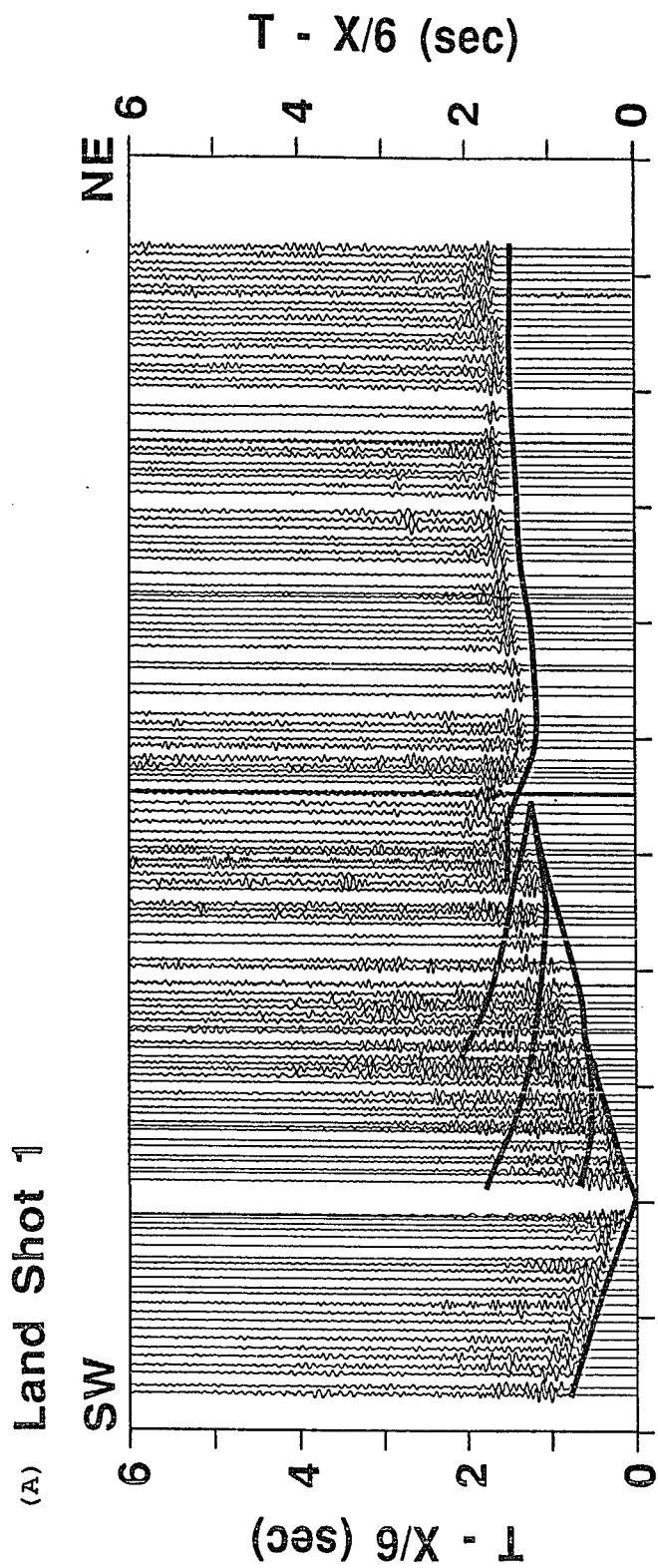
wave dies out at 40 and 45 km offset and two distinct arrivals are seen at longer offsets. There are several discrepancies which I have been unable to work out. For both gathers, the synthetic travel times for the upper crustal wave beyond 25 km offset are up to 0.25 s early and those for the two strong arrivals vary by as much as 0.3 s. These problems may be caused by some combination of out of plane arrivals and small scale lateral velocity variation, and I could not readily solve them with the available modeling software.

The landward half of the preferred model also shows regions of lateral velocity change; of particular interest is the region between about 80 and 100 km, where low velocity material near the surface overlies and is flanked by areas of velocity pull-up. This region is located directly beneath the surface trace of the Rinconada fault and Sur-Nacimiento fault zone. These faults delineate the boundary between the Sur-Obispo and Salinian terranes. The average velocities in the upper crust (to 10 km depth) west and east of the faults are about 5.5 and 6.2 km/s respectively, which correspond to mean velocity determinations for Franciscan rock assemblages and granite (cf. Stewart and Peselnick, 1978; Lin and Wang, 1980).

As with the upper crust of the offshore model, I began with plane layered interpretations of the first arrivals, using records from Airgun Shots 1 and 6 and Land Shots 1 and 2, and refined the model using iterative raytracing. A

topographic profile from receiver elevations and major lithologic boundaries from a geologic map (Burch et al, 1968) constrain the upper surface of the model, and reversed refraction modeling on land provided further constraints at depth. Previous seismic work estimating depth to Moho of about 25 km beneath the Salinian Block (cf. Healy and Peake, 1975) suggests that the oceanic lower crustal layer probably flattens out to the east, although that part of the model is not well resolved by our data.

Ray tracing through the model from the two land and two airgun shot locations produced the synthetics shown in Figures 20, 21, 22, and 23. The agreement between first break travel times from the shot gathers and those generated by model ray tracing are quite satisfactory. For the most part, they agree to within 0.1 second. The later arrivals are also well matched, particularly the prominent reflection which appears in both airgun shot gathers and Land Shot Gather 2. The travel time curves which match these reflections correspond to rays which arrive from the bottom of the deep dipping layer in the models (see Appendix A). The amplitudes of the synthetics match quite well with those of the shot gathers, with a few discrepancies. For Land Shot 1, the synthetics (Figure 20) incorrectly predict a large amplitude event at 17 to 21 km offset and 5.5 to 6.0 s reduced time from the base of the lower crust. Land Shot 2 provides what is probably the best match of the data set (Figure 21), although the complex variation of first break



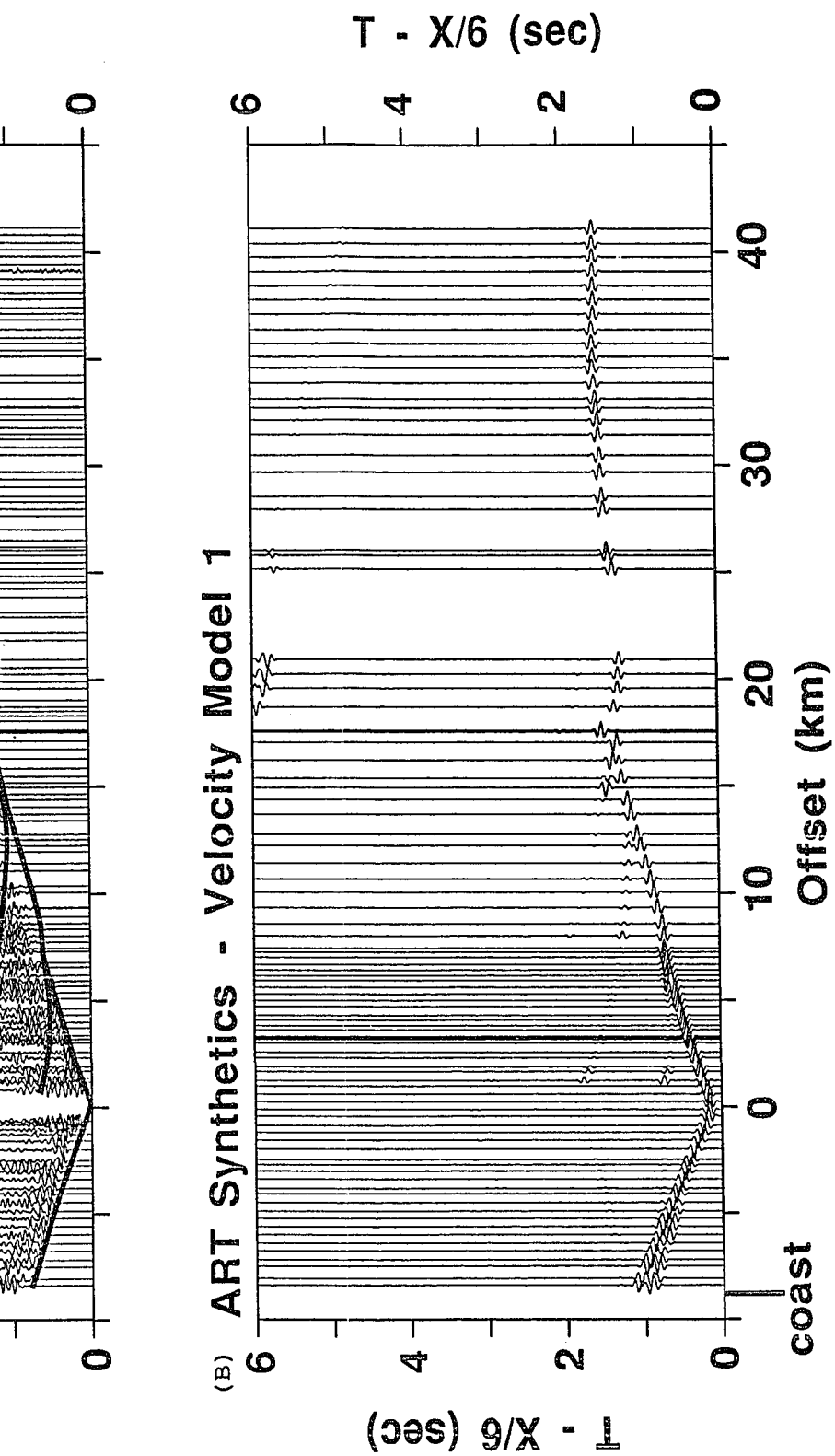
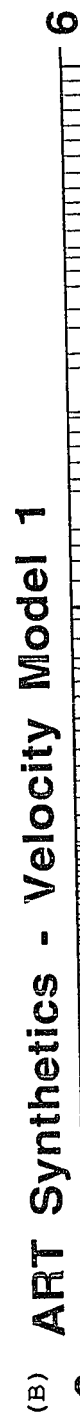
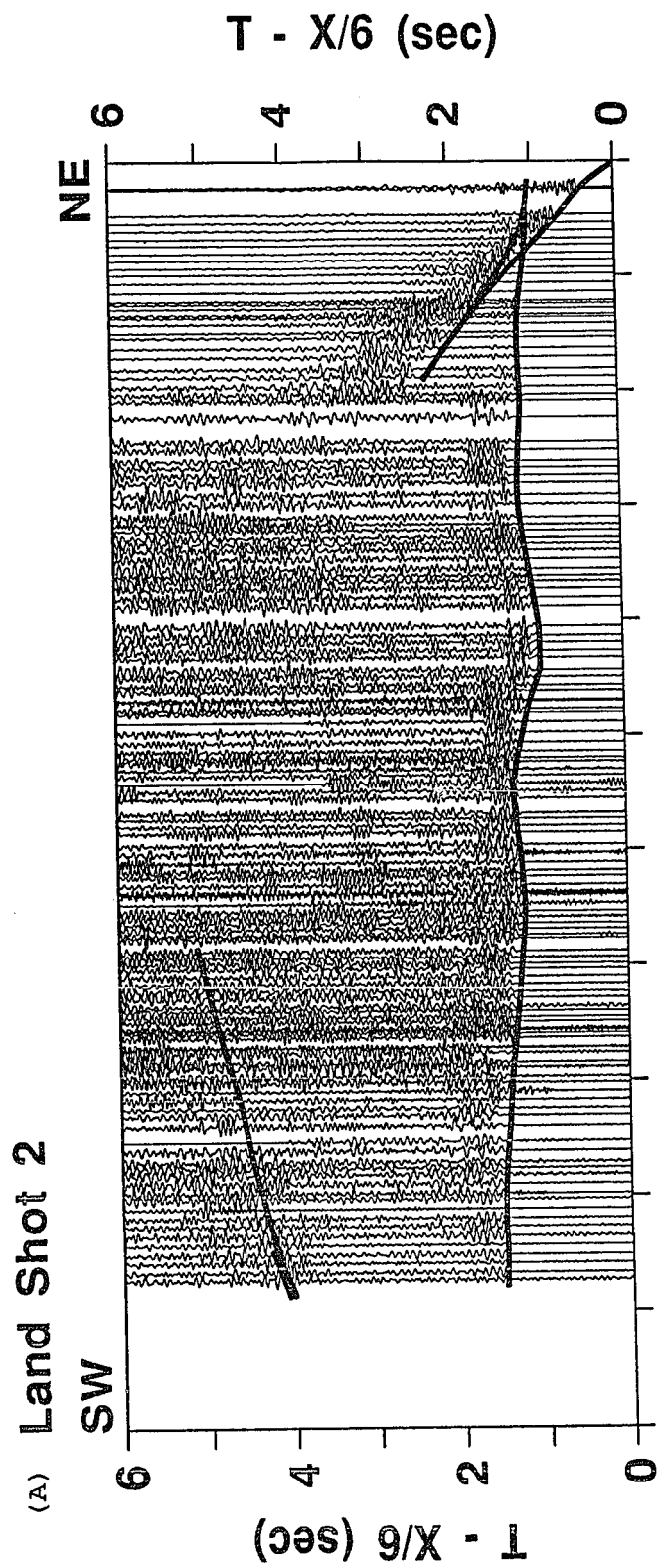


Figure 20: A) Land Shot Gather 1 with travel time curves produced from the model in Figure 14. B) Synthetics produced from rays traced from Land Shot 1.



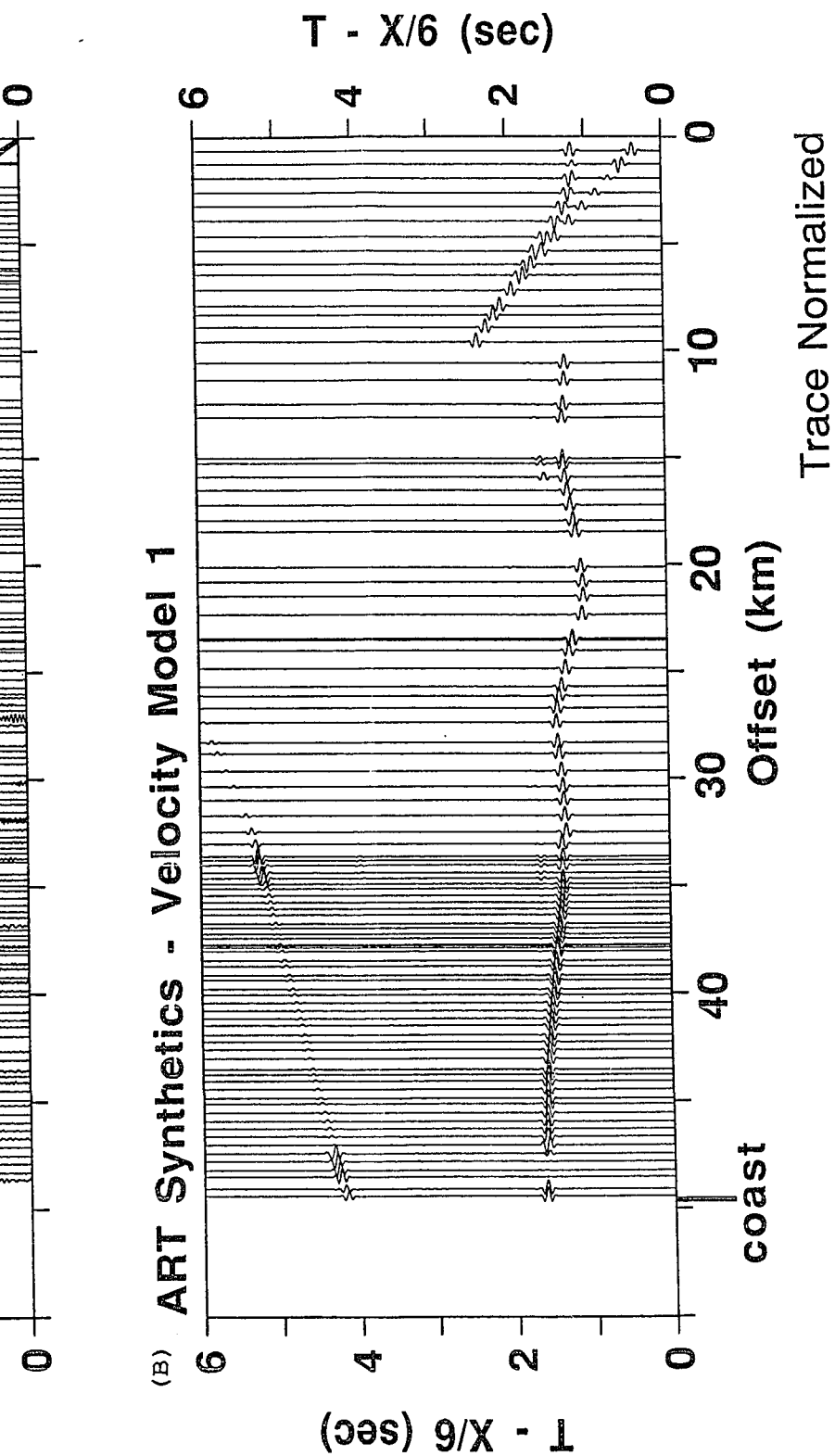
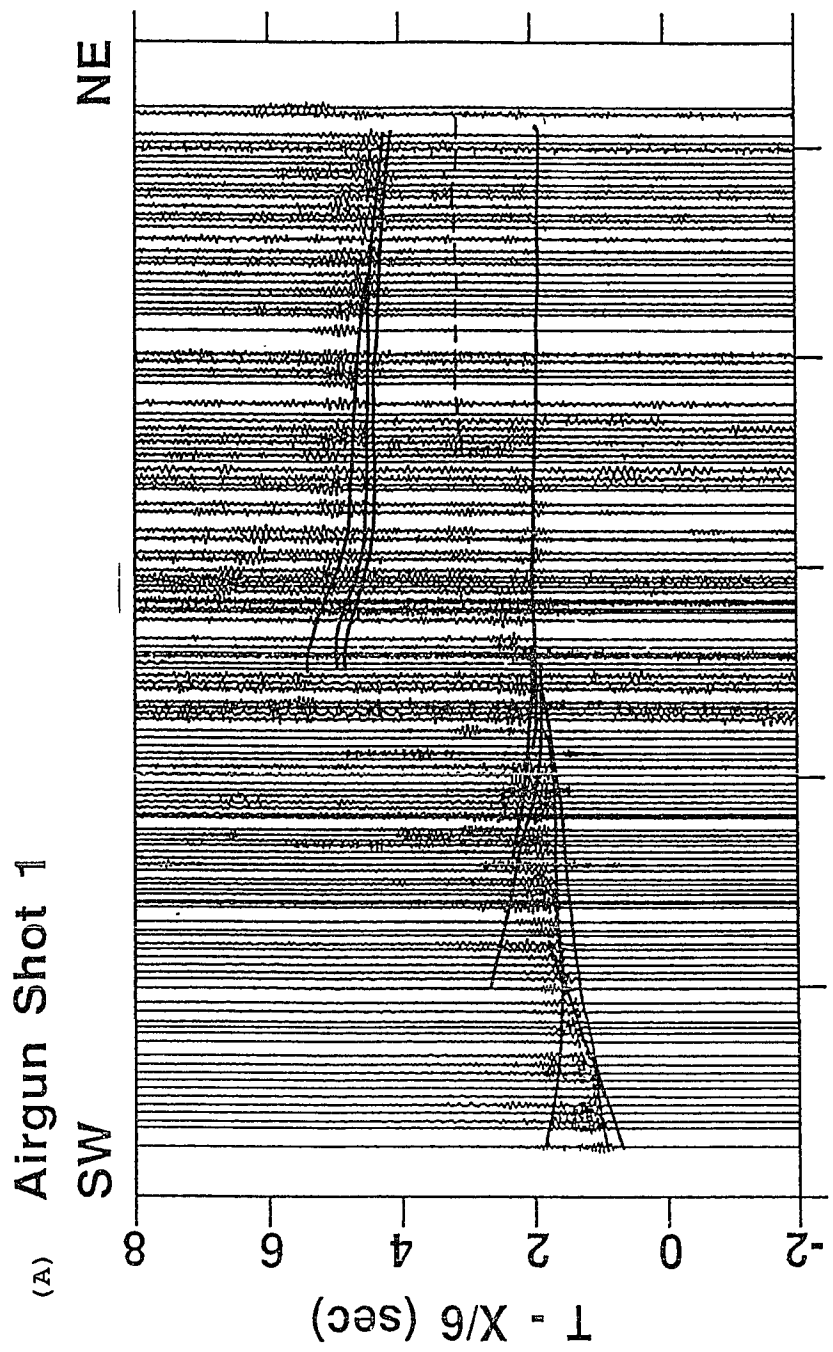


Figure 21: A) Land Shot Gather 2 with travel time curves produced from the model in Figure 14. B) Synthetics produced from rays traced from Land Shot 2.



(A) (R) 1 2 3 4 5 6 7 8 9 10 11 12 13 14 15 16 17 18 19 20 21 22 23 24 25 26 27 28 29 30 31 32 33 34 35 36 37 38 39 40 41 42 43 44 45 46 47 48 49 50 51 52 53 54 55 56 57 58 59 60 61 62 63 64 65 66 67 68 69 70 71 72 73 74 75 76 77 78 79 80 81 82 83 84 85 86 87 88 89 90 91 92 93 94 95 96 97 98 99 100

(B) ART Synthetics - Velocity Model 1

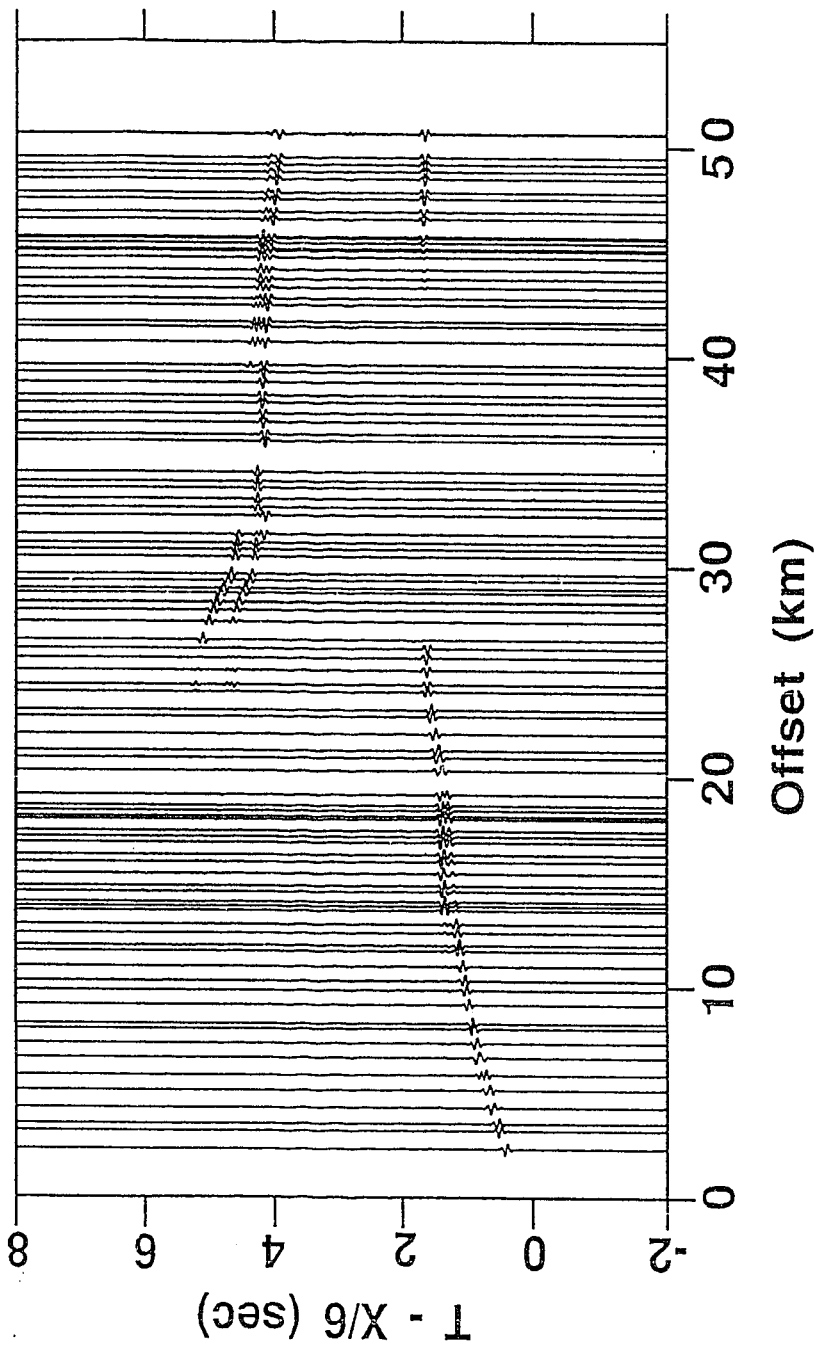
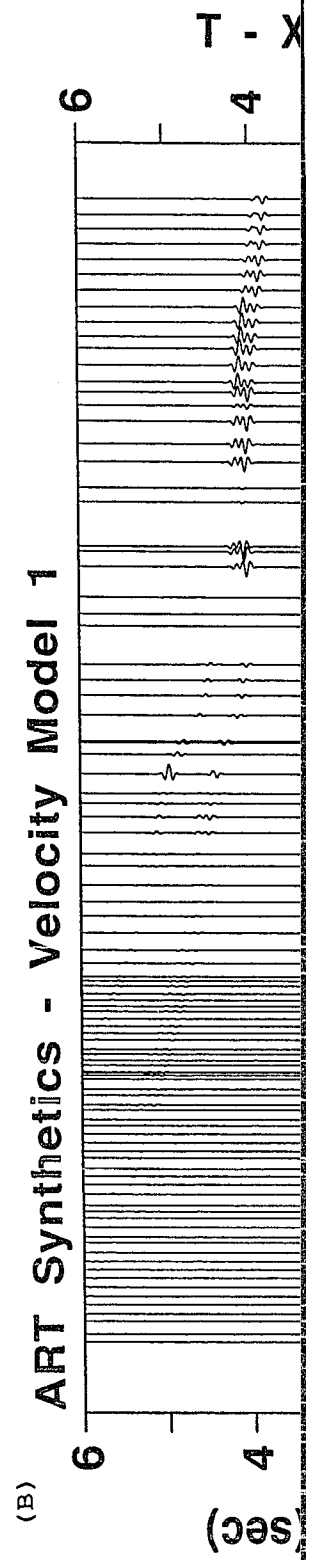
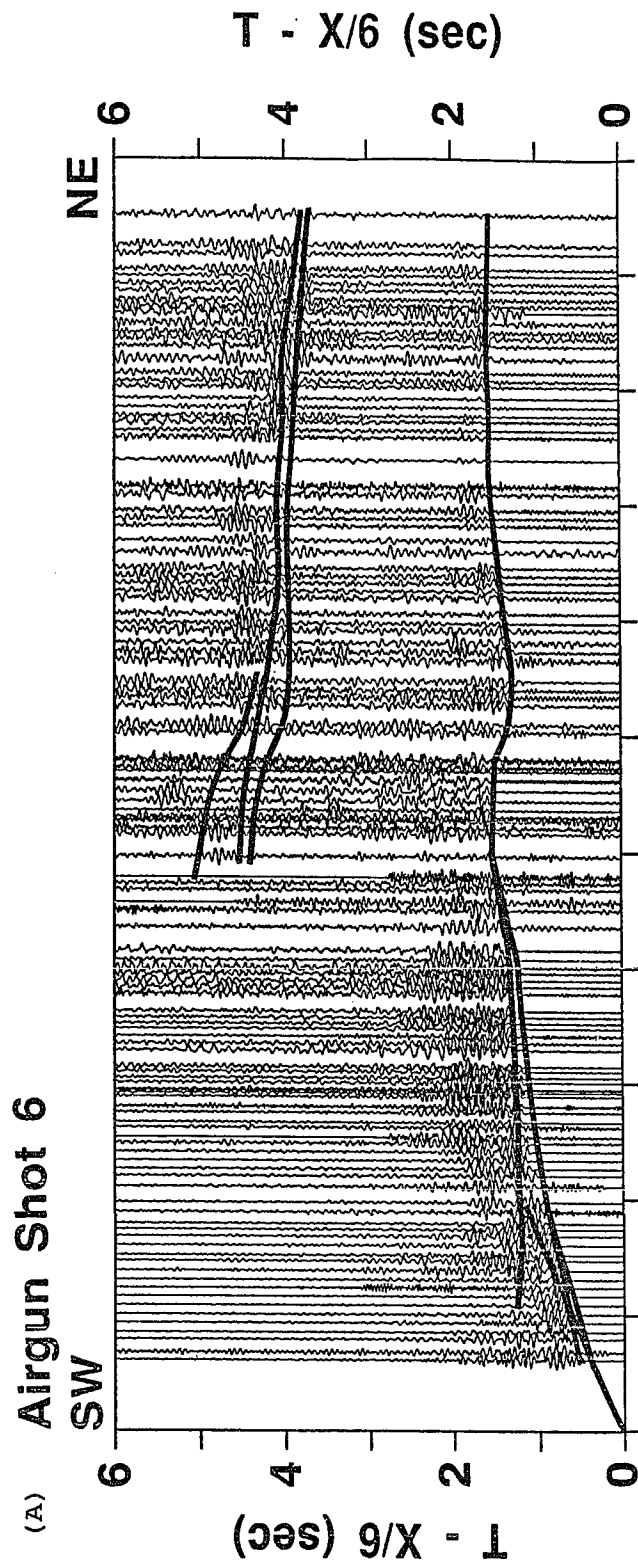


Figure 22: A) Airgun Shot Gather 1 with travel time curves produced from the model in Figure 14. B) Synthetics produced from rays traced from Airgun Shot 1.



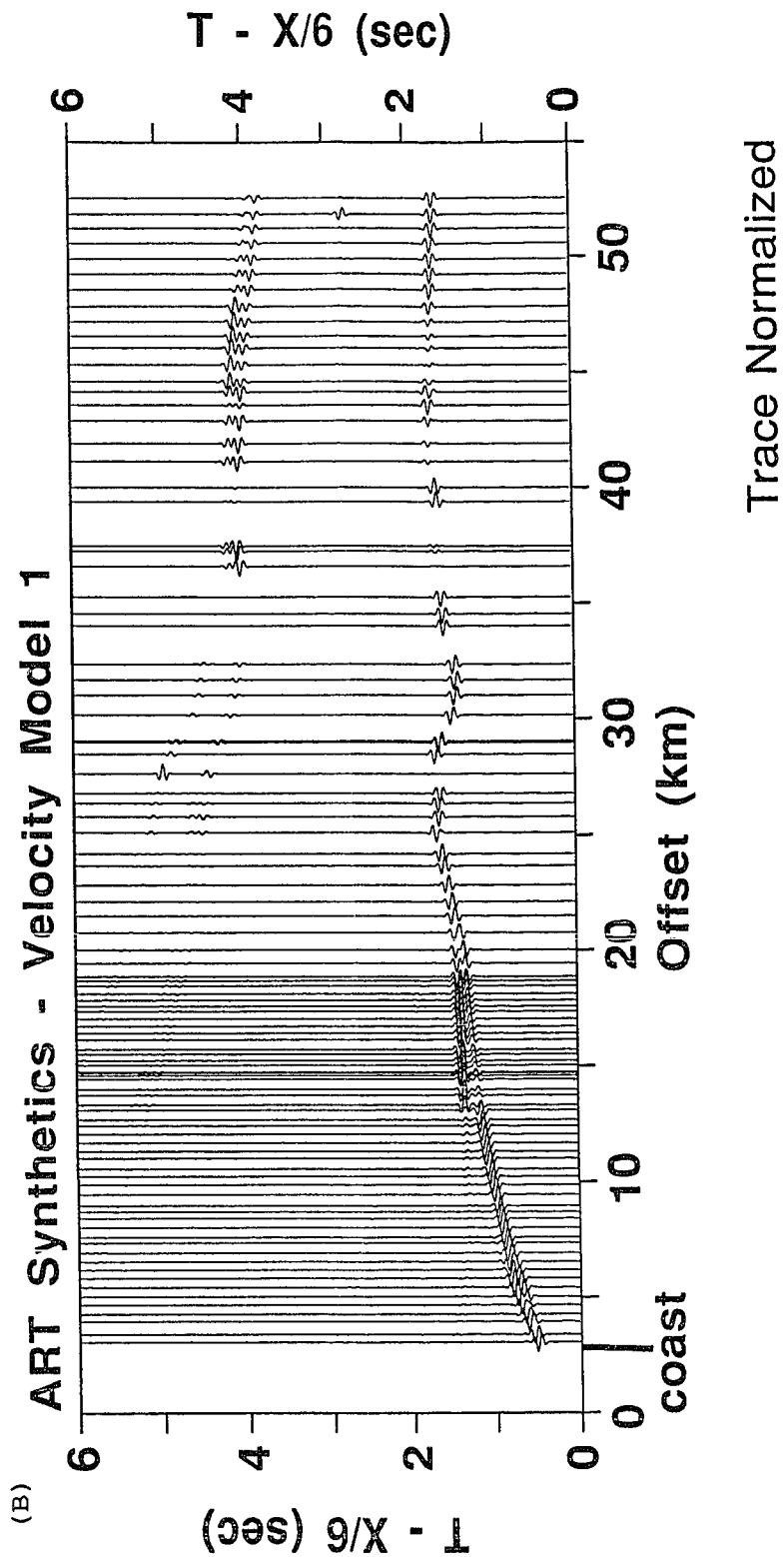


Figure 23: A) Airgun Shot Gather 6 with travel time curves produced from the model in Figure 14. B) Synthetics produced from rays traced from Airgun Shot 6.

amplitudes is not precisely matched. For Airgun Shot 1, the synthetics (Figure 22) show the upper crustal wave amplitudes dying off at 26 and reappearing beyond 44 km offset, while in the data they do not die off until 33 km offset and do not reappear. Also, the event at 3 s reduced time between 30 and 35 km offset does not appear in the synthetics. For Airgun Shot 6, the synthetics (Figure 23) produce an event from the base of the lower crust which matches the strong event on the shot record (at 3.5 to 4 s reduced time), but the amplitude relative to the first break event does not correlate precisely between the two, particularly between 30 and 35 km. It seems likely that these inconsistencies are due to small scale lateral velocity variations, out of plane arrivals, and model parameterization problems. Generally, the synthetics provide an excellent match to the data. Appendix A shows diagrams of rays passing through Velocity Model 1 from Land Shots 1 and 2, and Airgun Shot 6.

Velocity Model 2

The Walter and Sharpless (1987) preliminary velocity model of the USGS strike line (Figure 15) included a two-layer lower crust with oceanic crustal velocities, which was overlain by a 6 to 7 km thick low velocity layer (5.7-5.8 km/s.). Early versions of Velocity Model 2 contained a two-layer lower crust, but this introduced an extra arrival in the synthetics which did not correspond to any in the data. Therefore, the final version of Model 2 (Figure 24)

includes a one-layer lower crust beneath a smoothed version of the LVZ at the same depth below where the USGS line crossed. The smoothing was achieved by using gradients to reduce the velocity contrast at the top and bottom interfaces of the LVZ, and was introduced to properly match the amplitudes of the later arrivals in both shot and receiver gather models. The effect of the LVZ is to slightly shallow the lower crustal layer and the Moho, and the smoothing prevents any large amplitude arrivals off the base of the LVZ from appearing on the synthetics (Figures 25-31). Comparing these figures with the synthetics produced from Velocity Model 1 shows that virtually the same results are achieved. Only minor differences can be detected, the most prominent of which are unimportant changes in the amplitude and range of the first lower crustal event on Receiver Gathers 19 and 29 and of the event from the base of the crust on Airgun Shot 1. Appendix B shows diagrams of rays passing through the lower crust of Velocity Model 2 from Receiver 15, Land Shots 1 and 2, and Airgun Shot 6. Upper crustal rays are the same as for Velocity Model 1 (see Appendix A).

VELOCITY MODEL 2

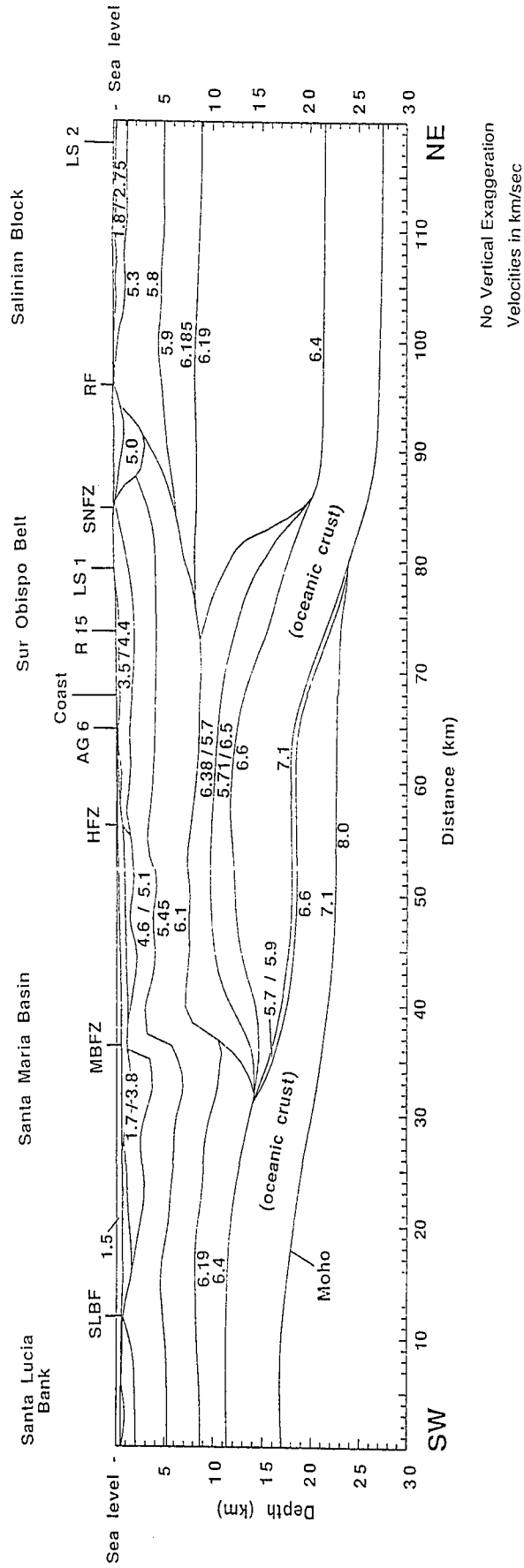


Figure 24: Velocity Model 2: With LVZ above lower crustal layer. Abbreviations as in Figure 14.

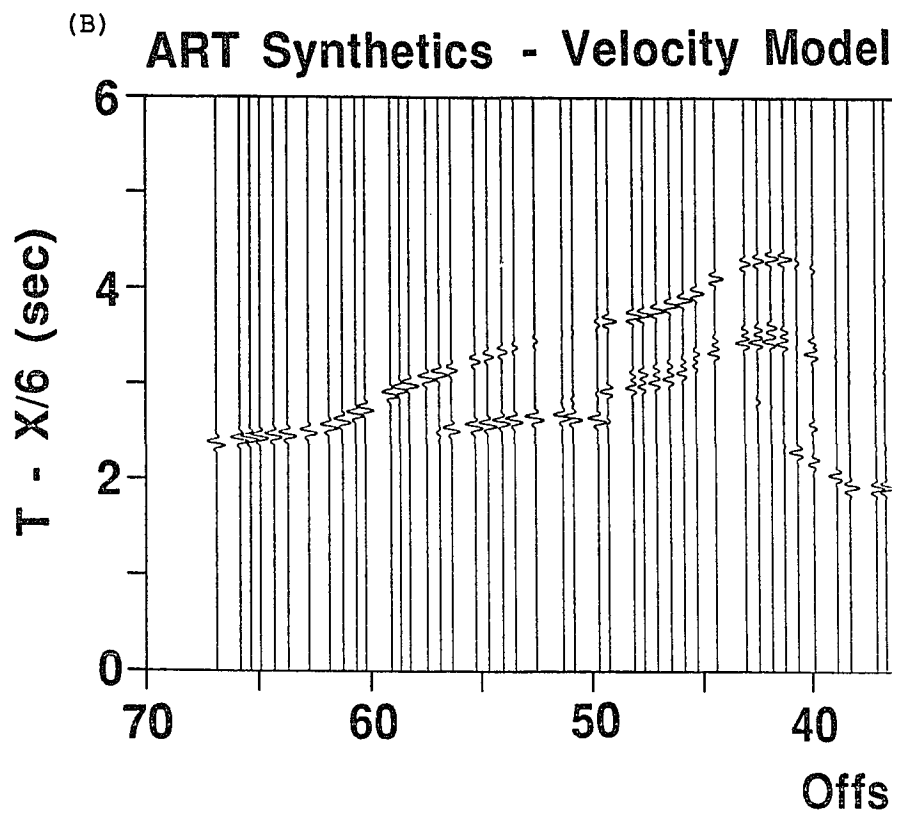
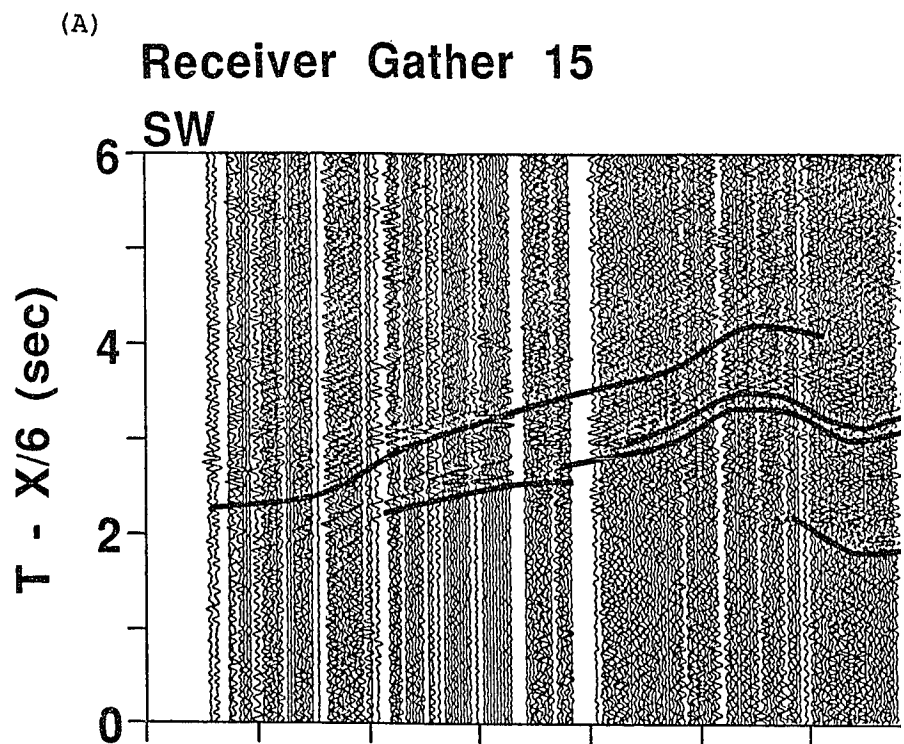
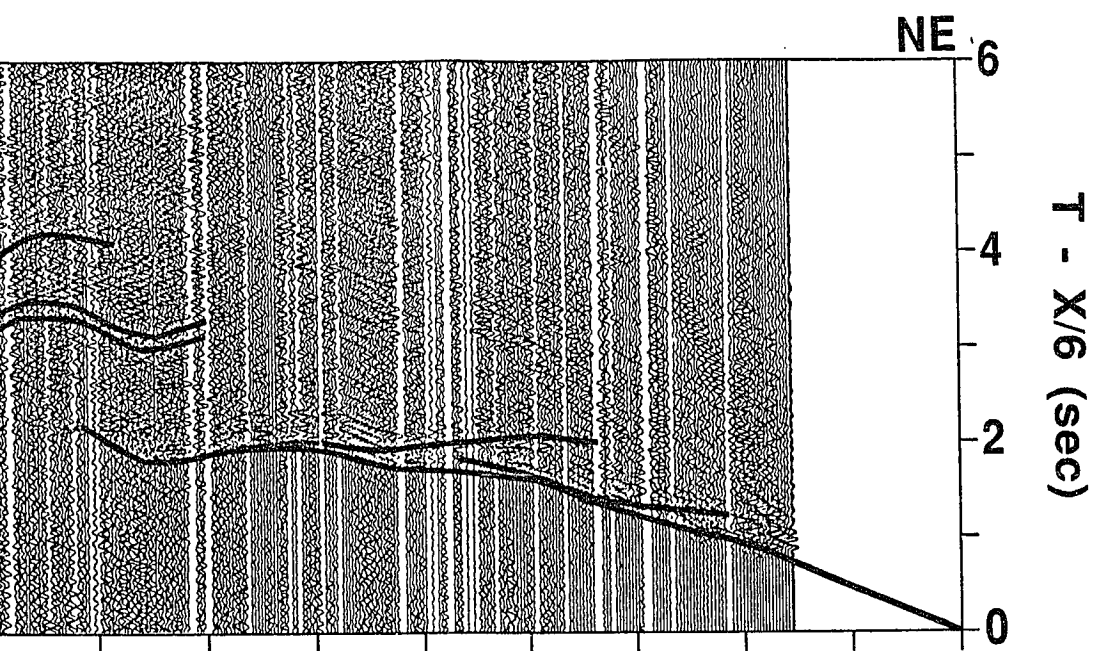
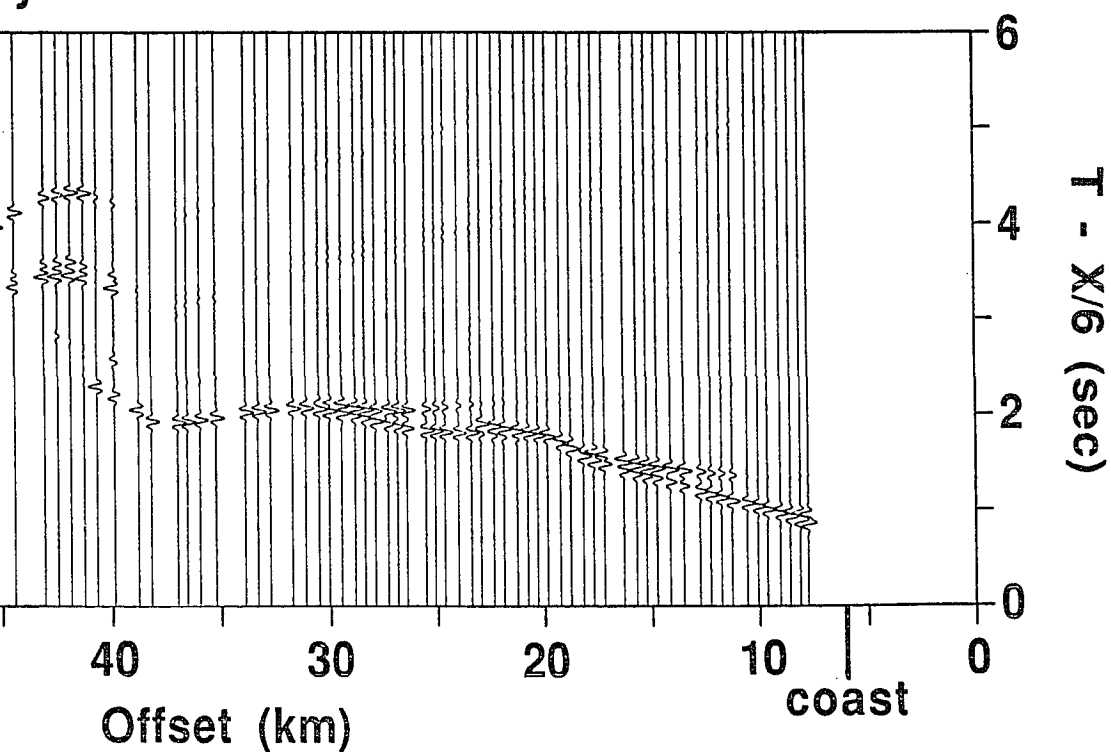


Figure 25: A) Receiver Gather 15 with travel time curves produced from the model in Figure 24. B) Synthetic seismic data from rays traced from airgun shots offshore



Model 2



5 with travel time curves
e 24. B) Synthetics produced
ts offshore to Receiver 15.

Trace Normalized

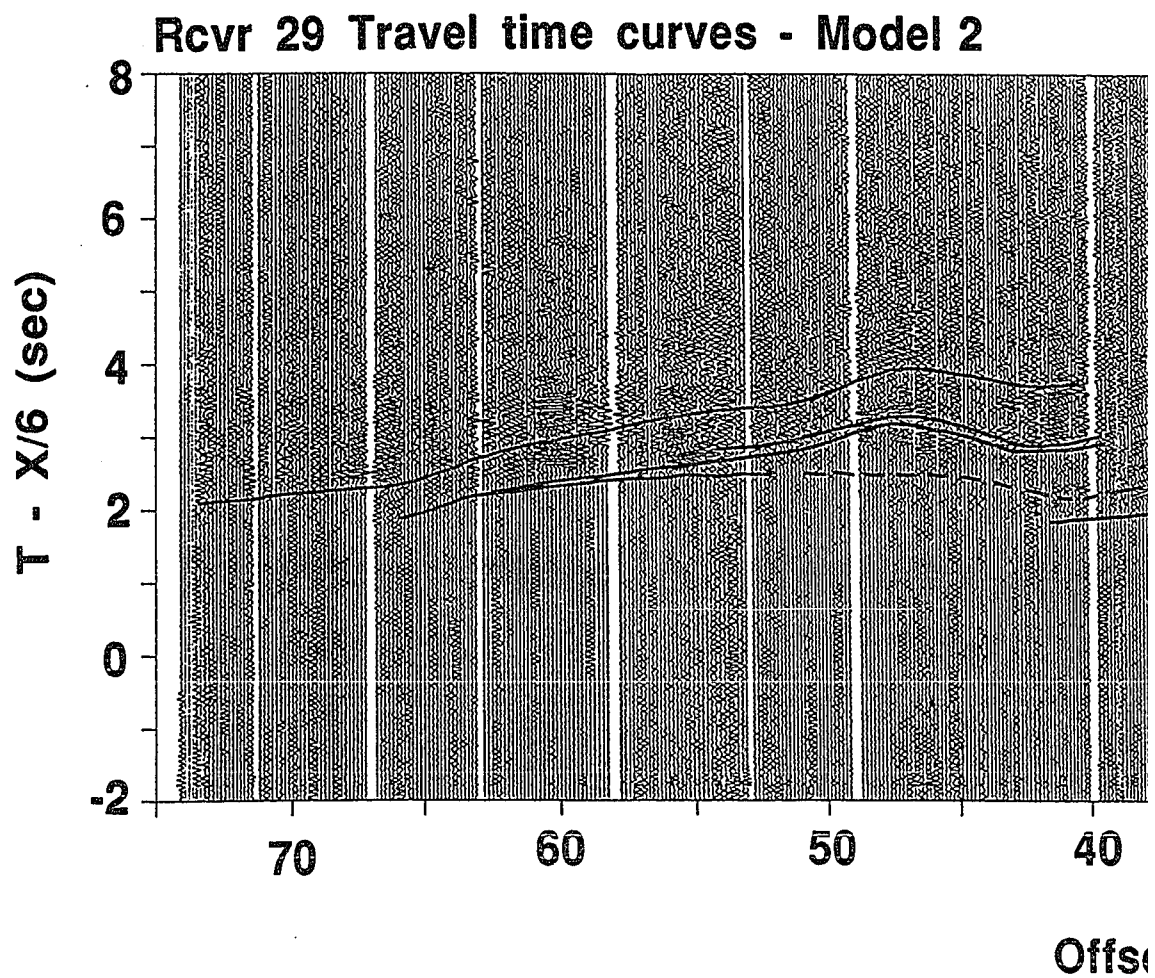
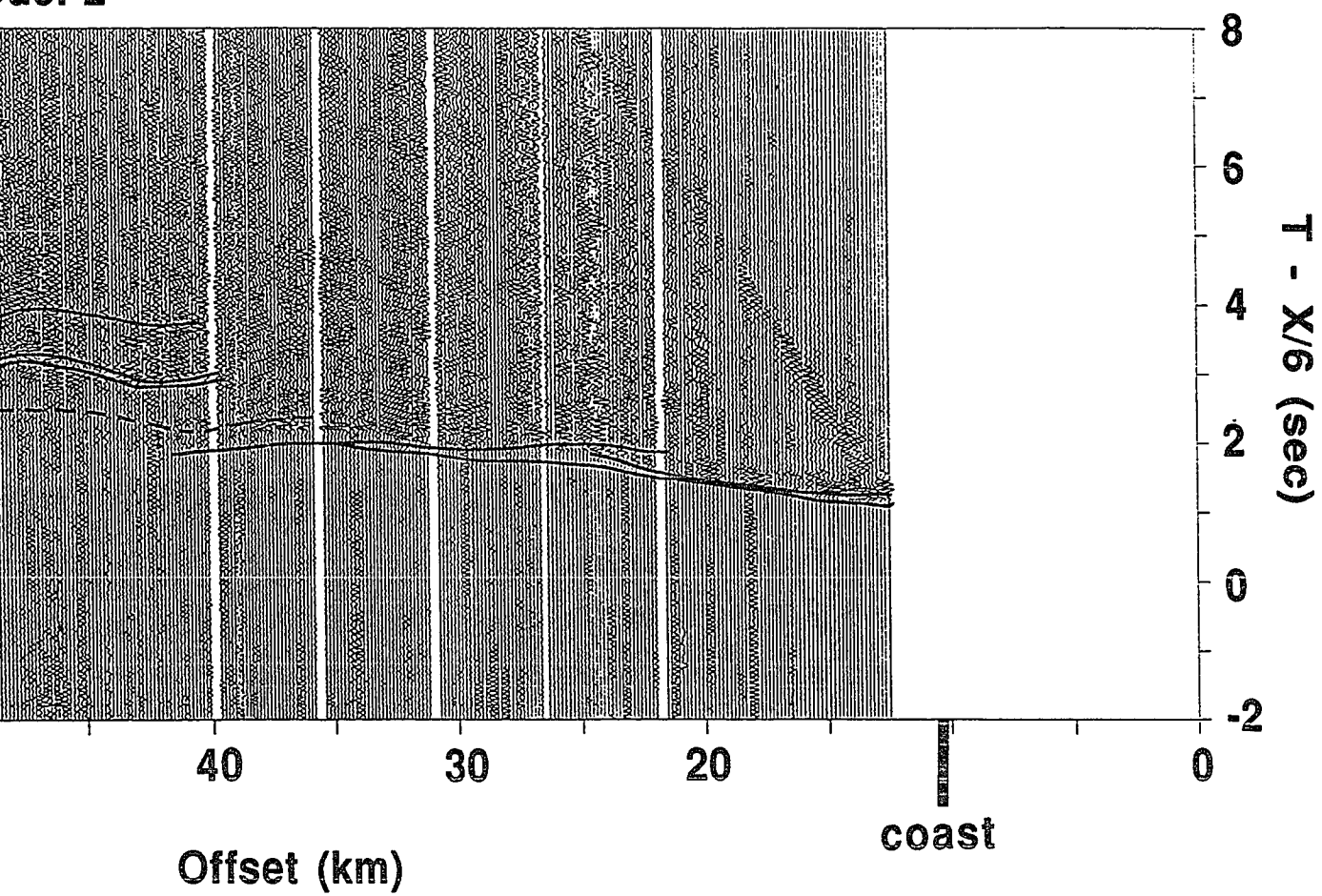


Figure 26: A) Receiver Gather 29
produced from the model in Figure
from rays traced from airgun shots

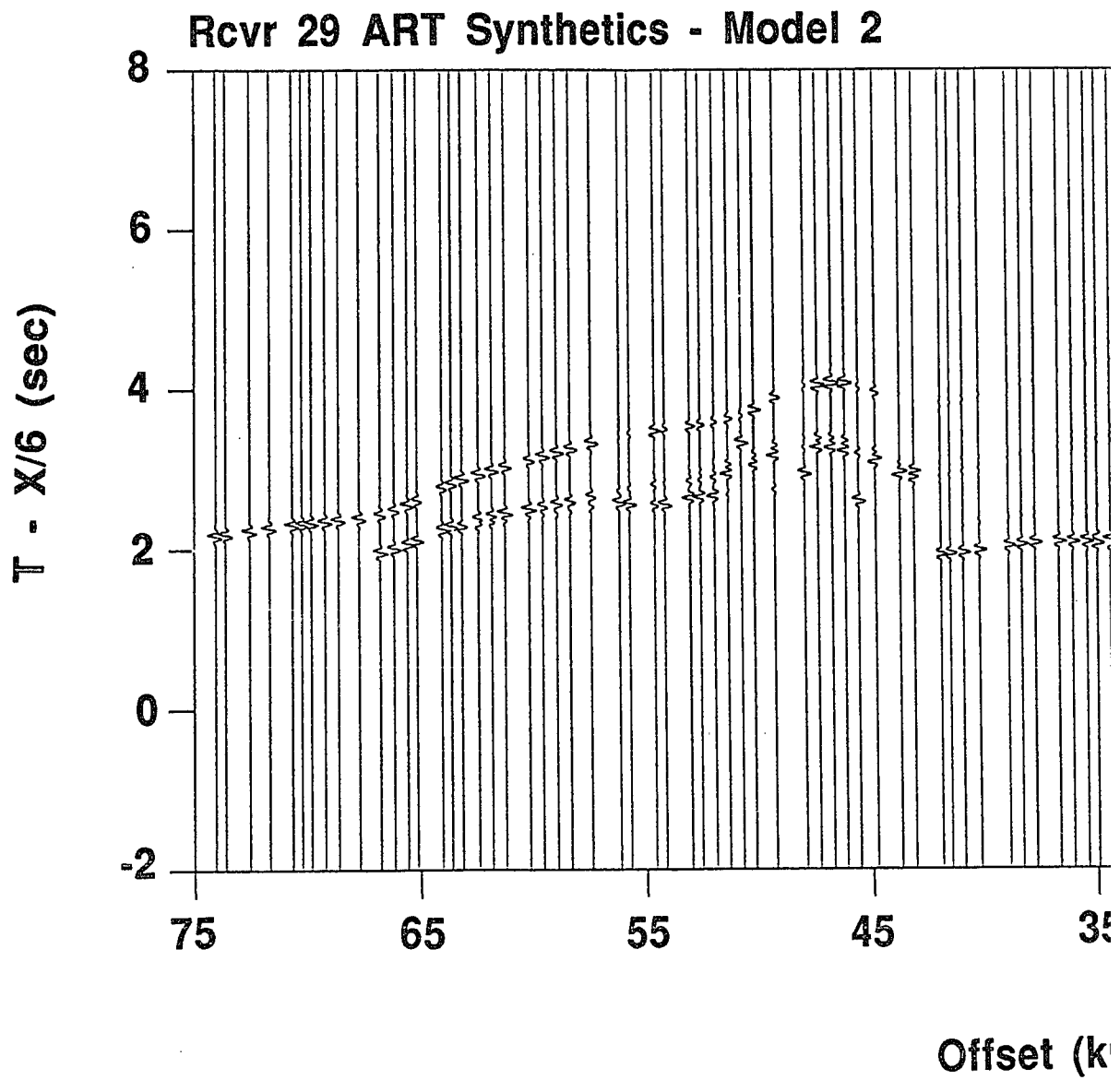
Model 2



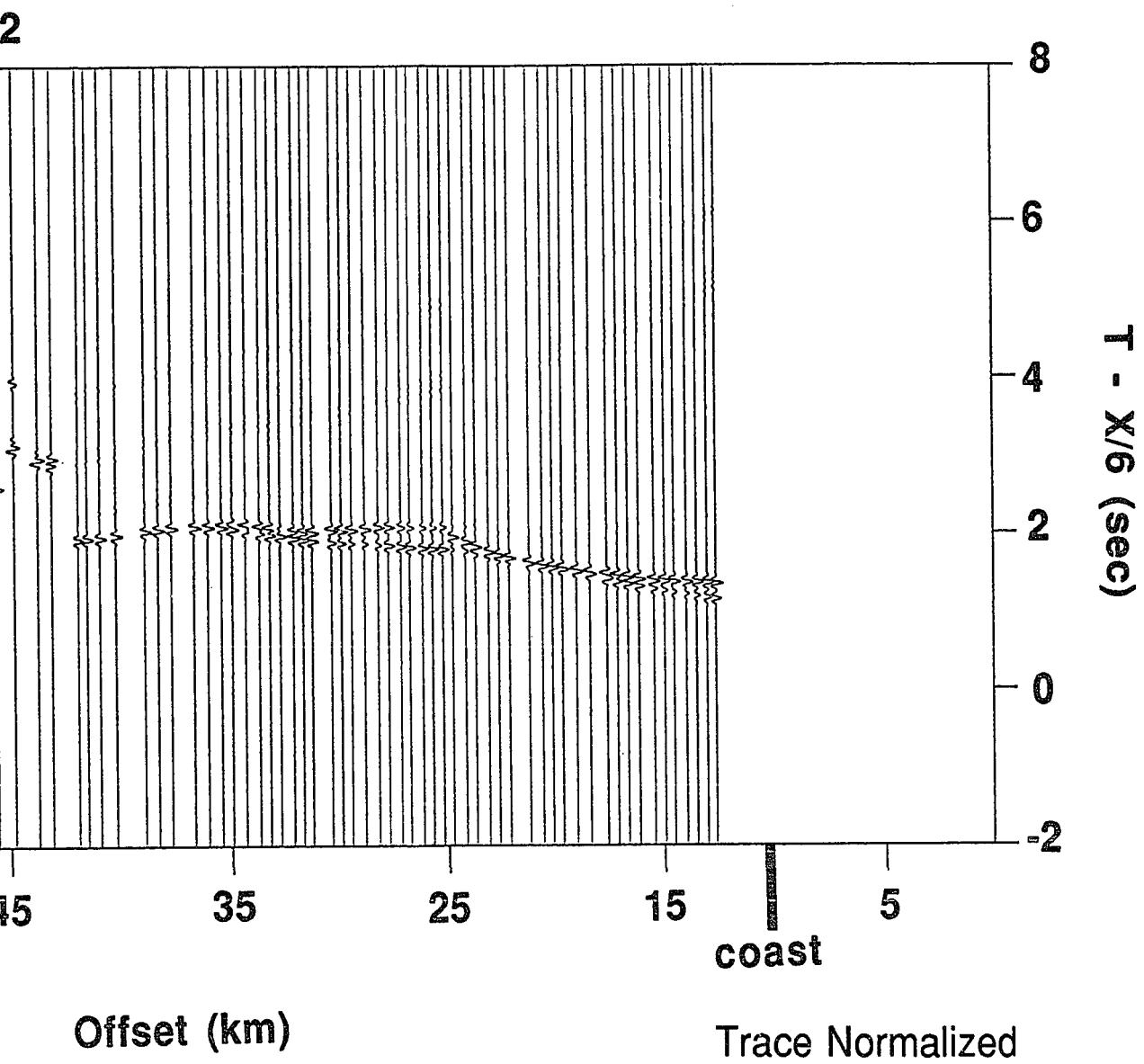
(A)

Trace Normalized

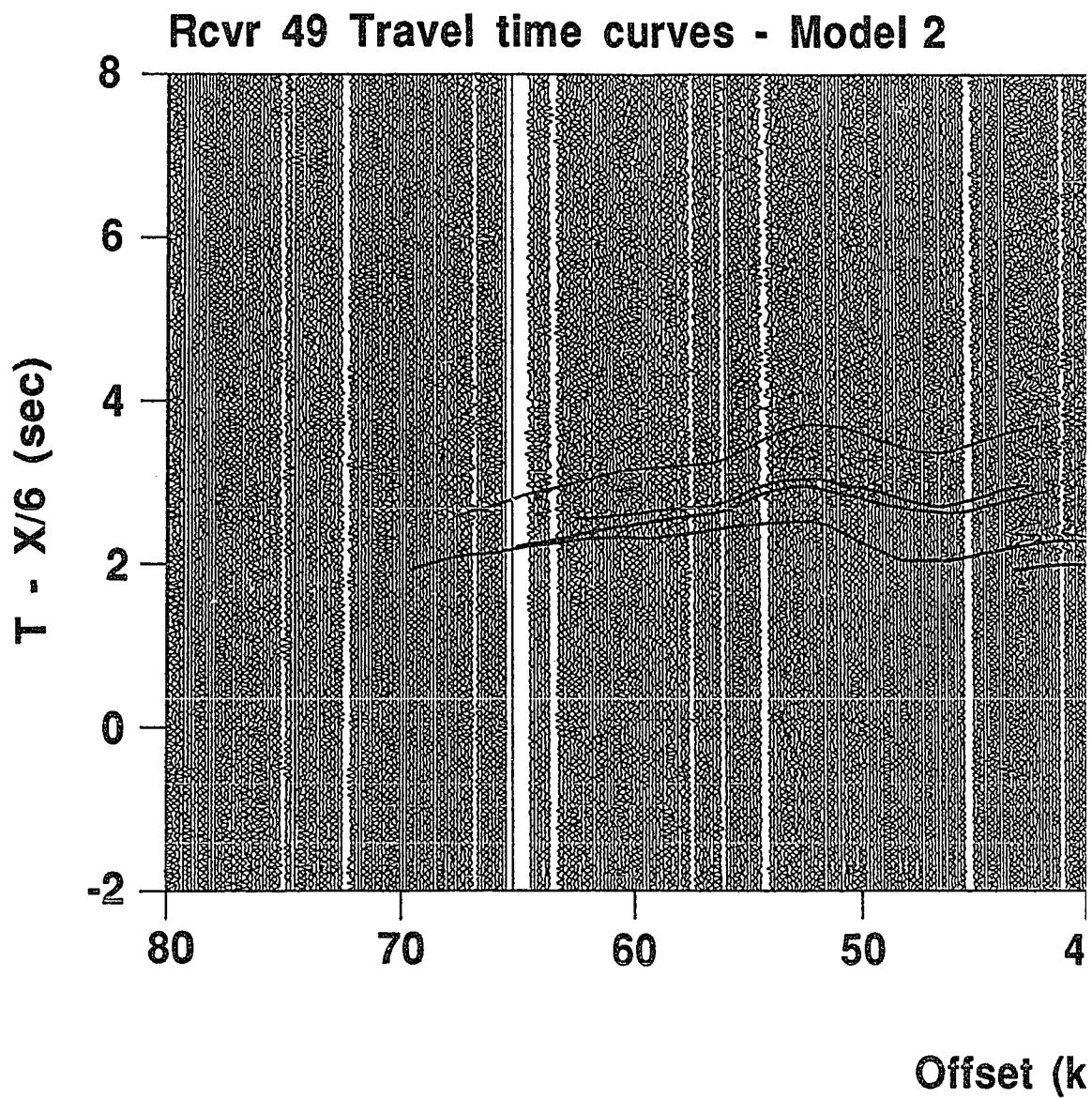
Receiver Gather 29 with travel time curves
 e model in Figure 24. B) Synthetics produced
 from airgun shots offshore to Receiver 29.



(B)

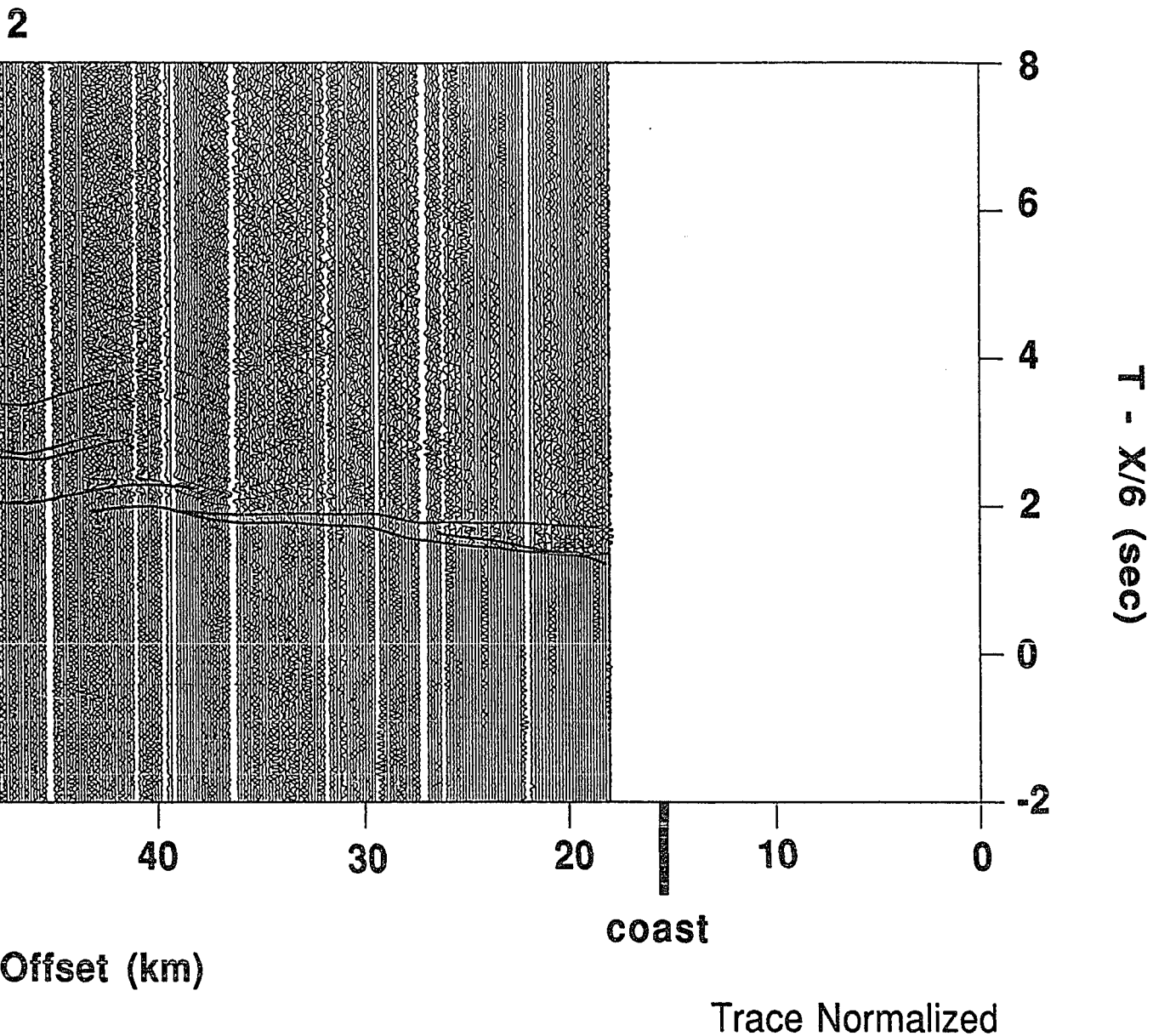


(B)



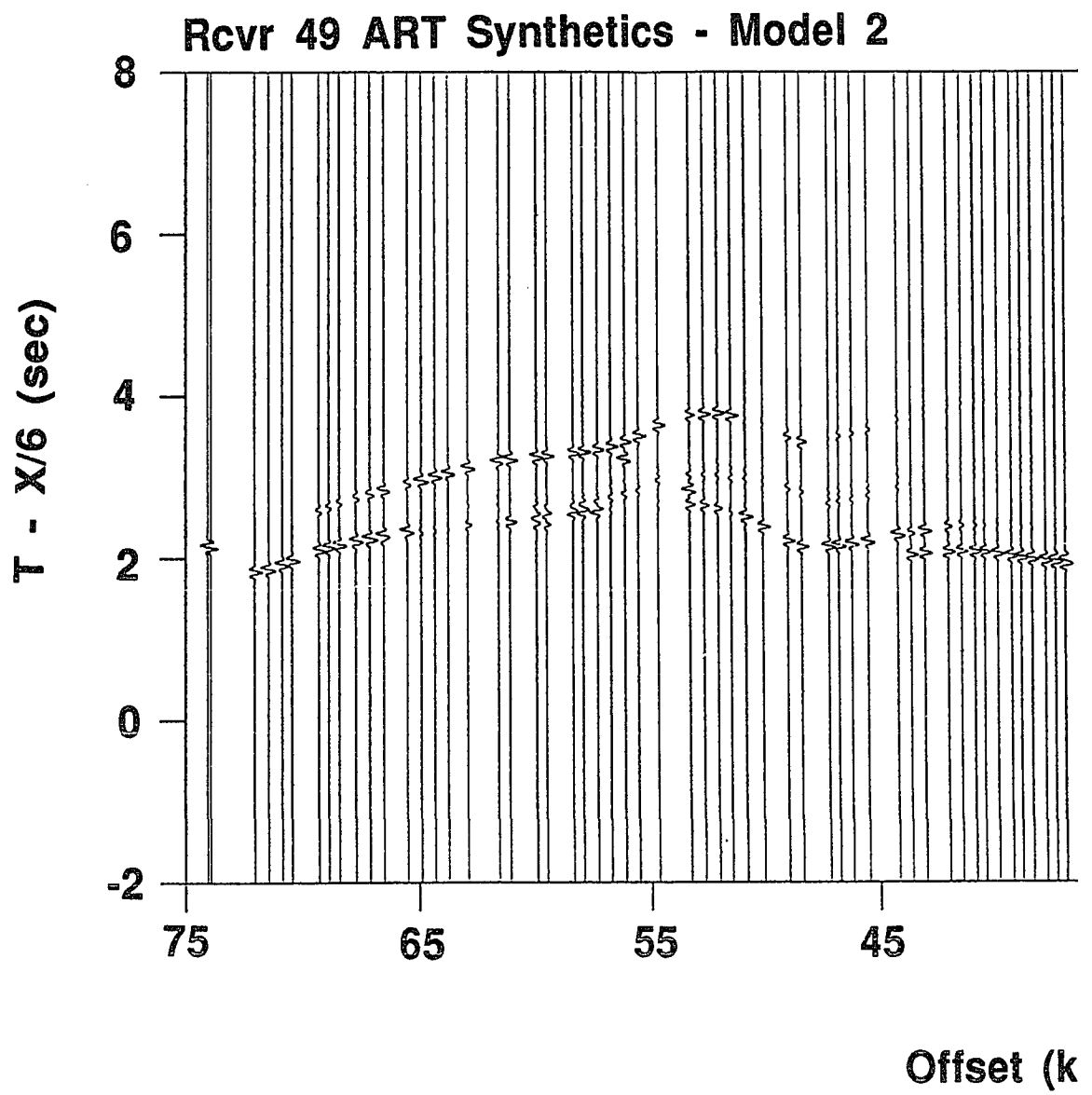
(A)

Figure 27: A) Receiver Gather 49 wi
produced from the model in Figure 24
from rays traced from airgun shots o



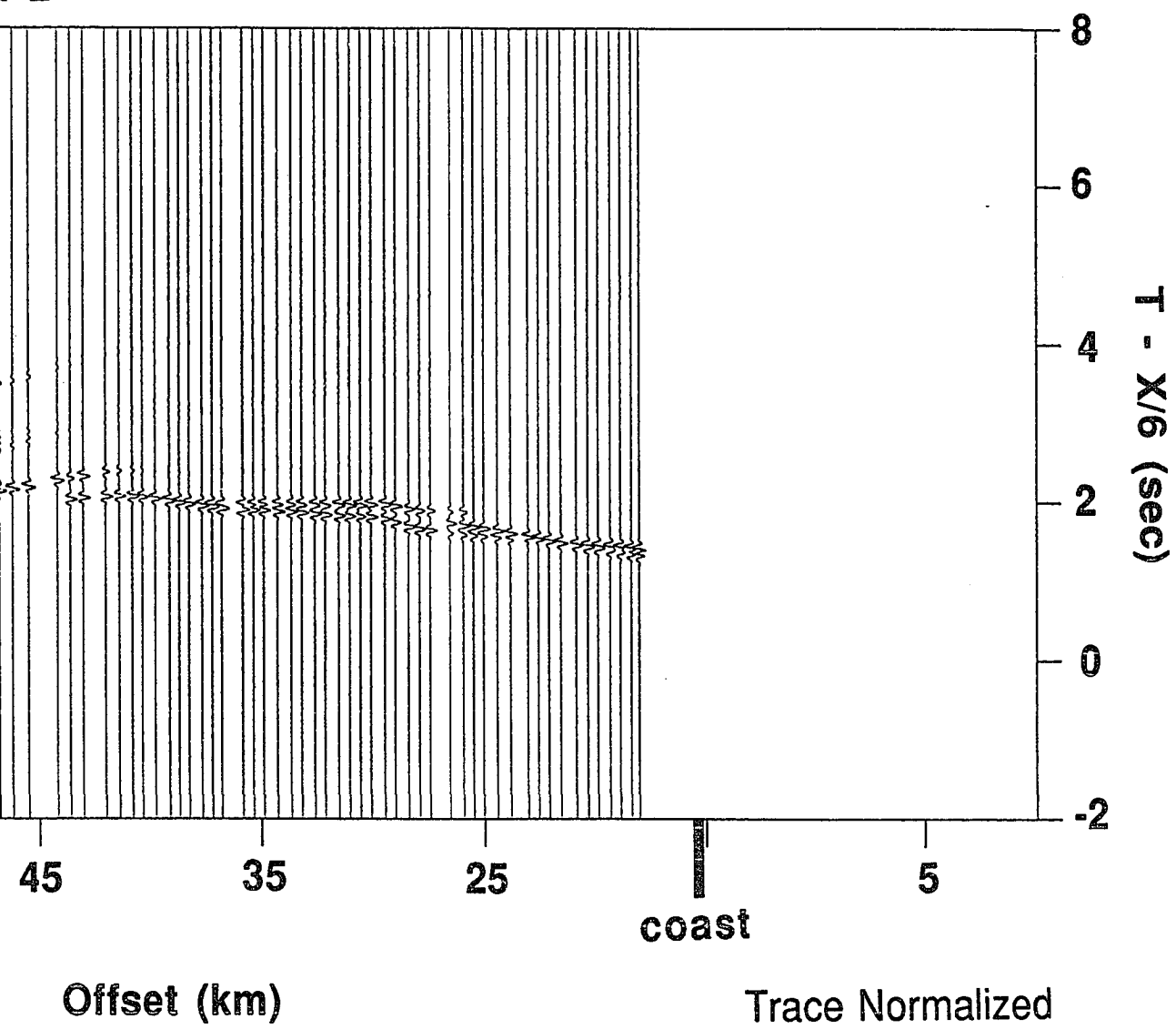
(A)

Gather 49 with travel time curves
 in Figure 24. B) Synthetics produced
 by gun shots offshore to Receiver 49.

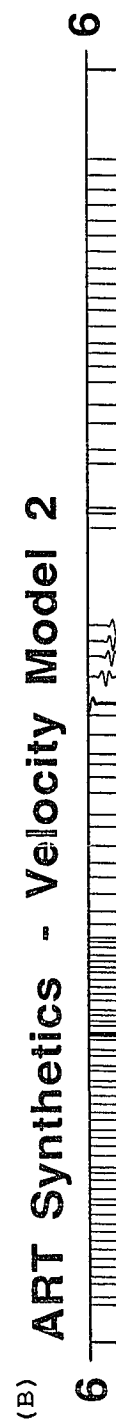
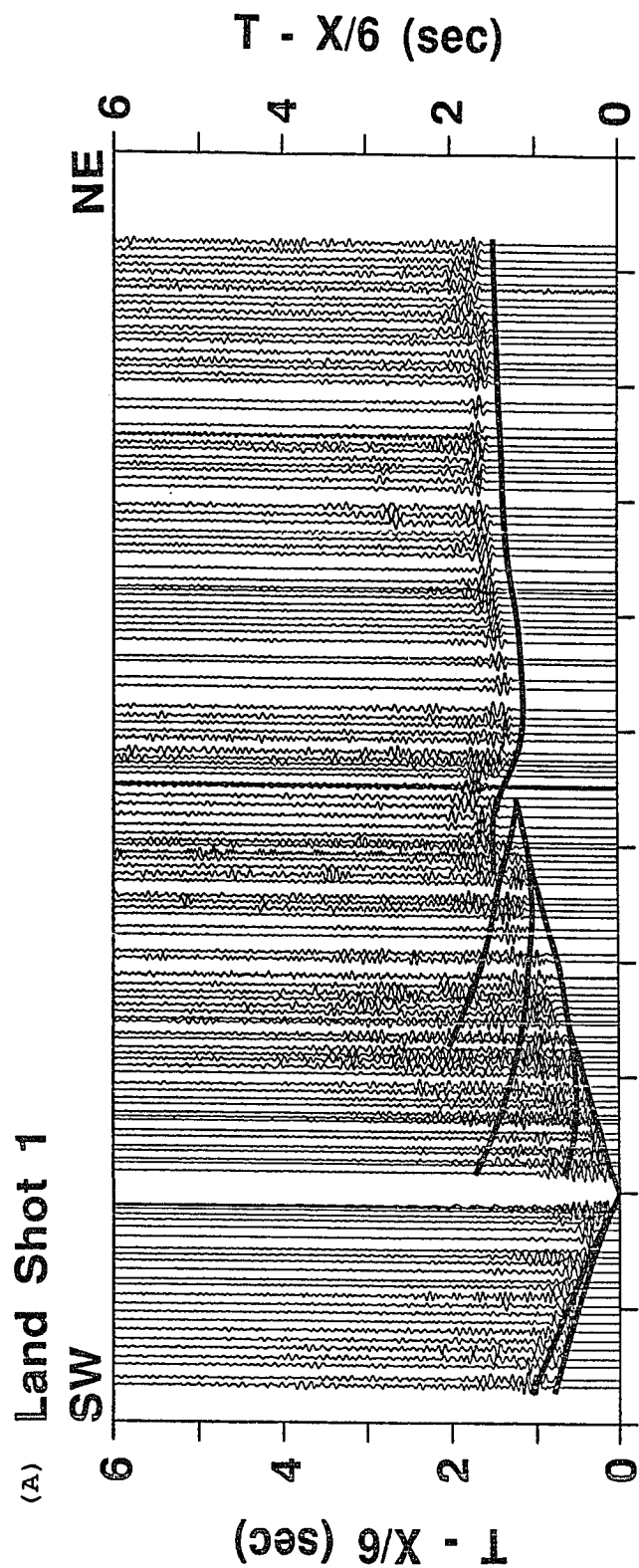


(B)

1 2



(B)



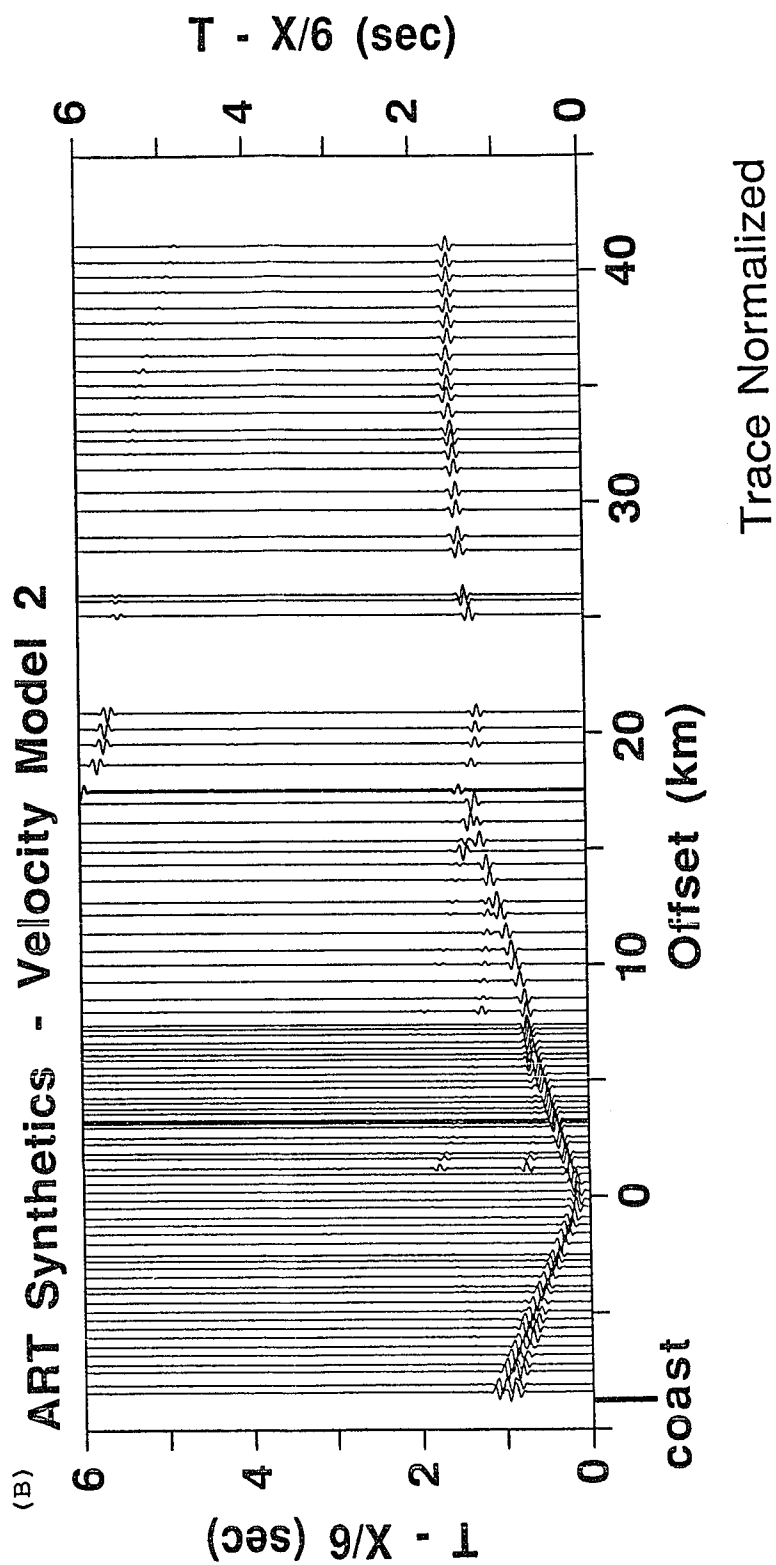
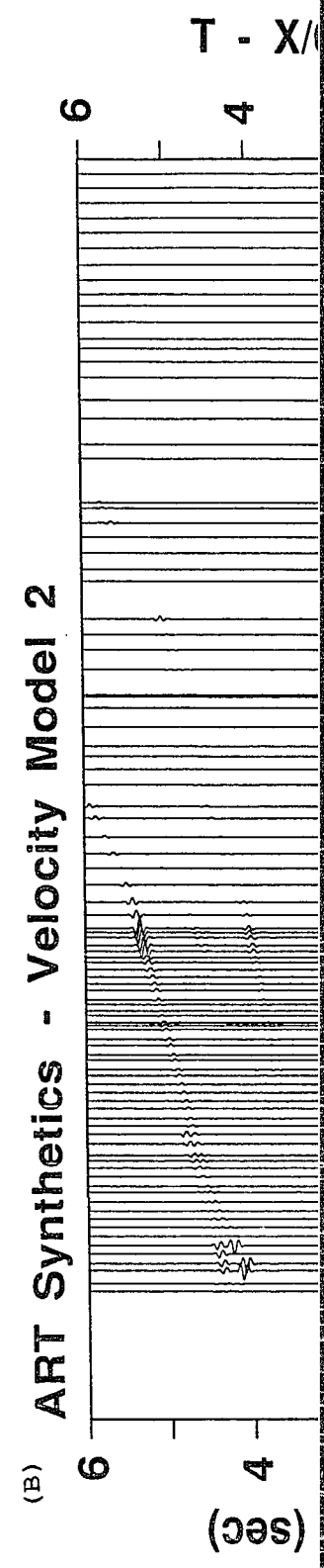
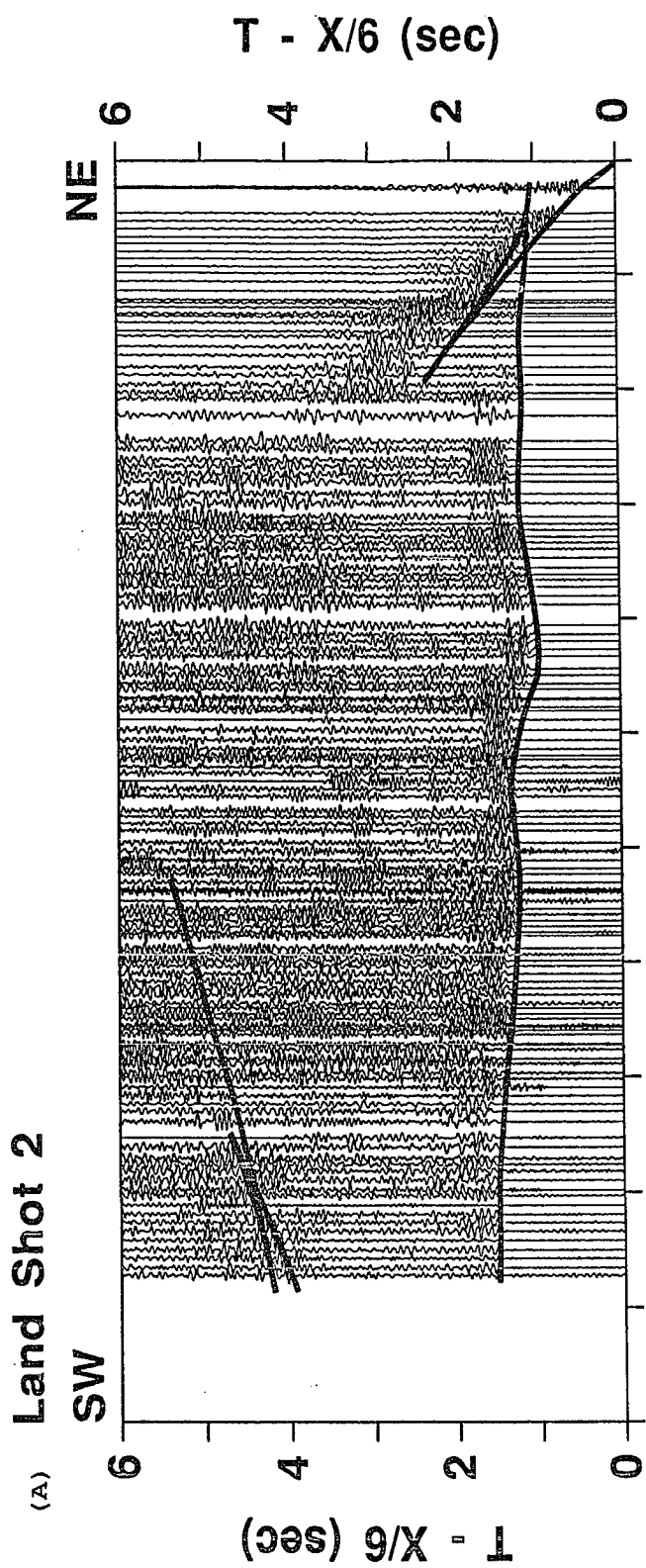


Figure 28: A) Land Shot Gather 1 with travel time curves produced from the model in Figure 24. B) Synthetics produced from rays traced from Land Shot 1.



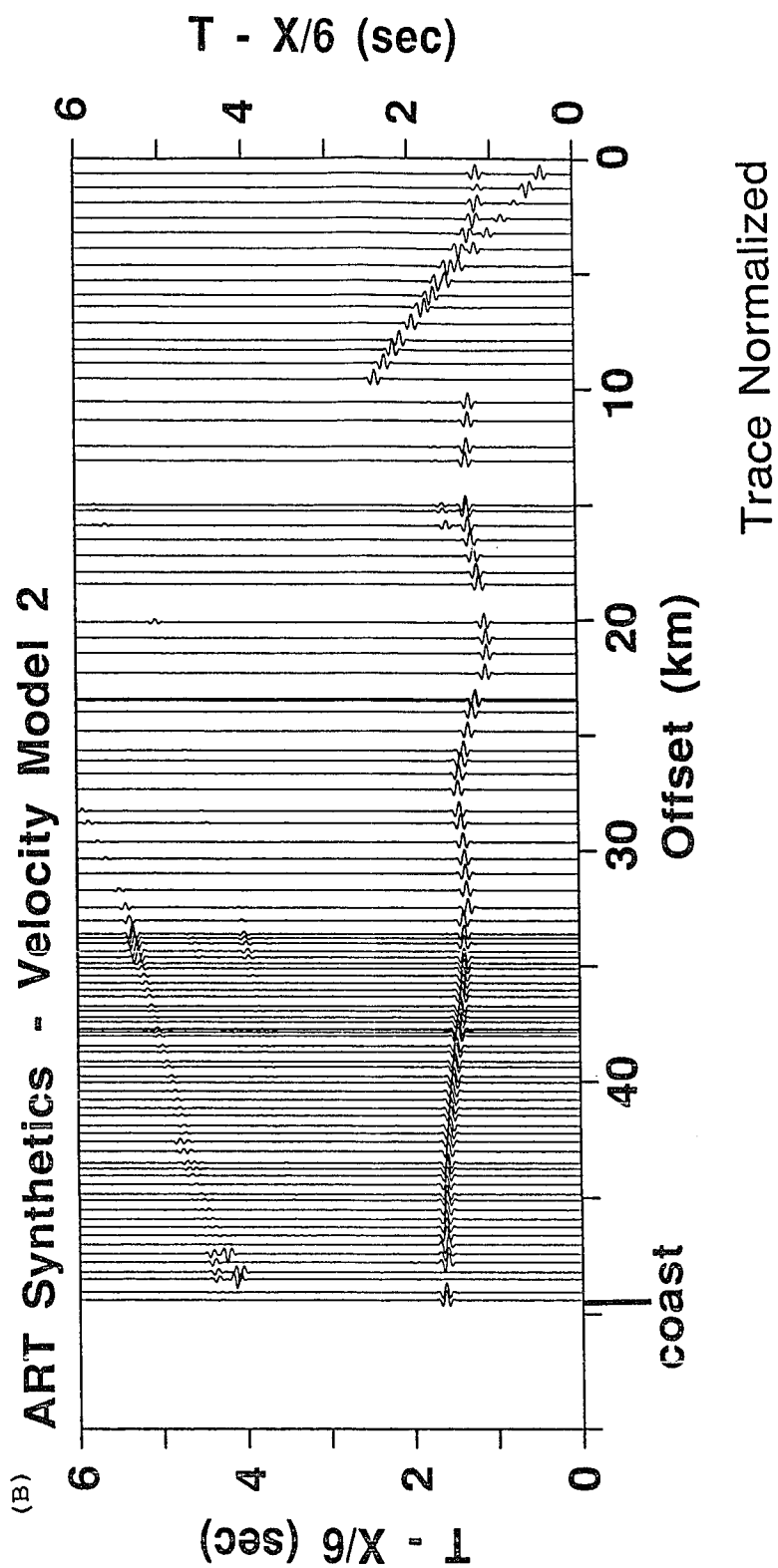
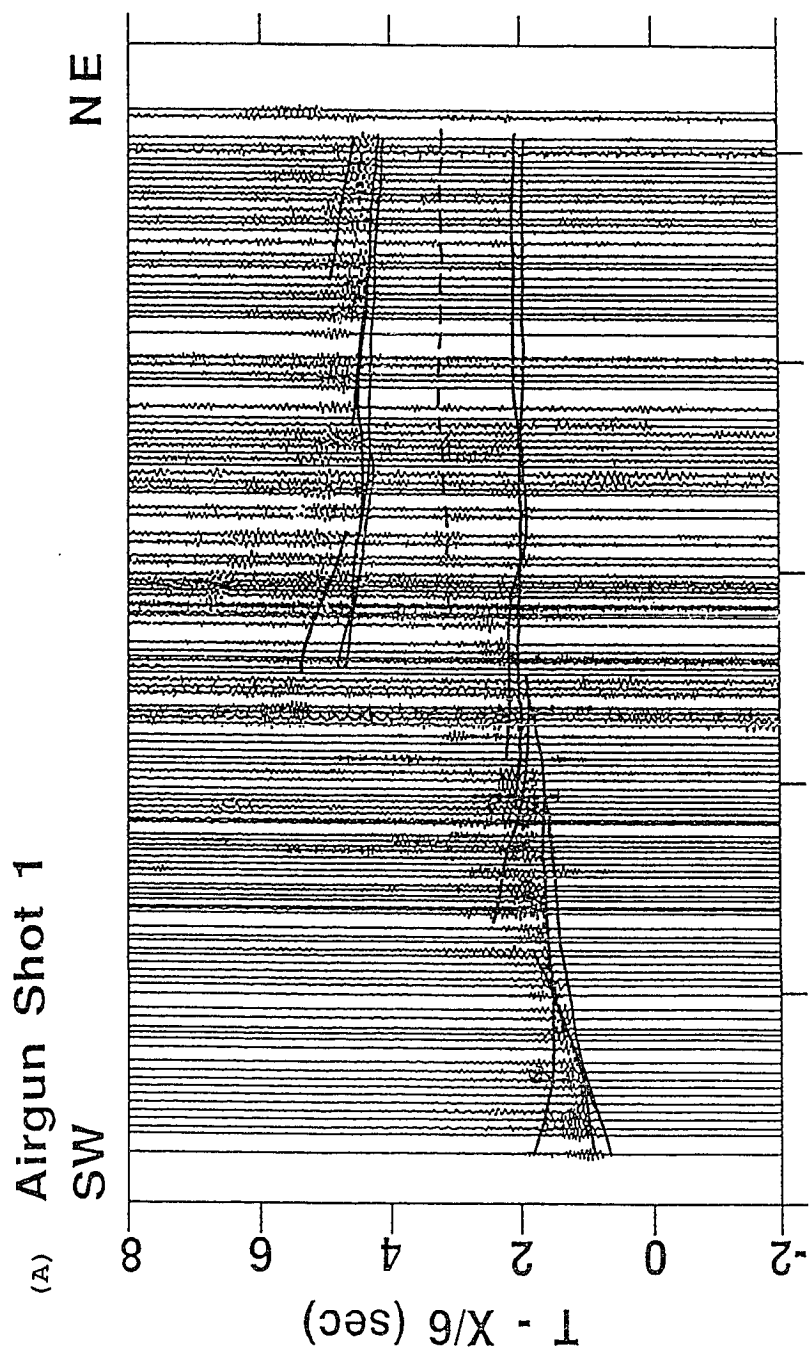


Figure 29: A) Land Shot Gather 2 with travel time curves produced from the model in Figure 24. B) Synthetics produced from rays traced from Land Shot 2.



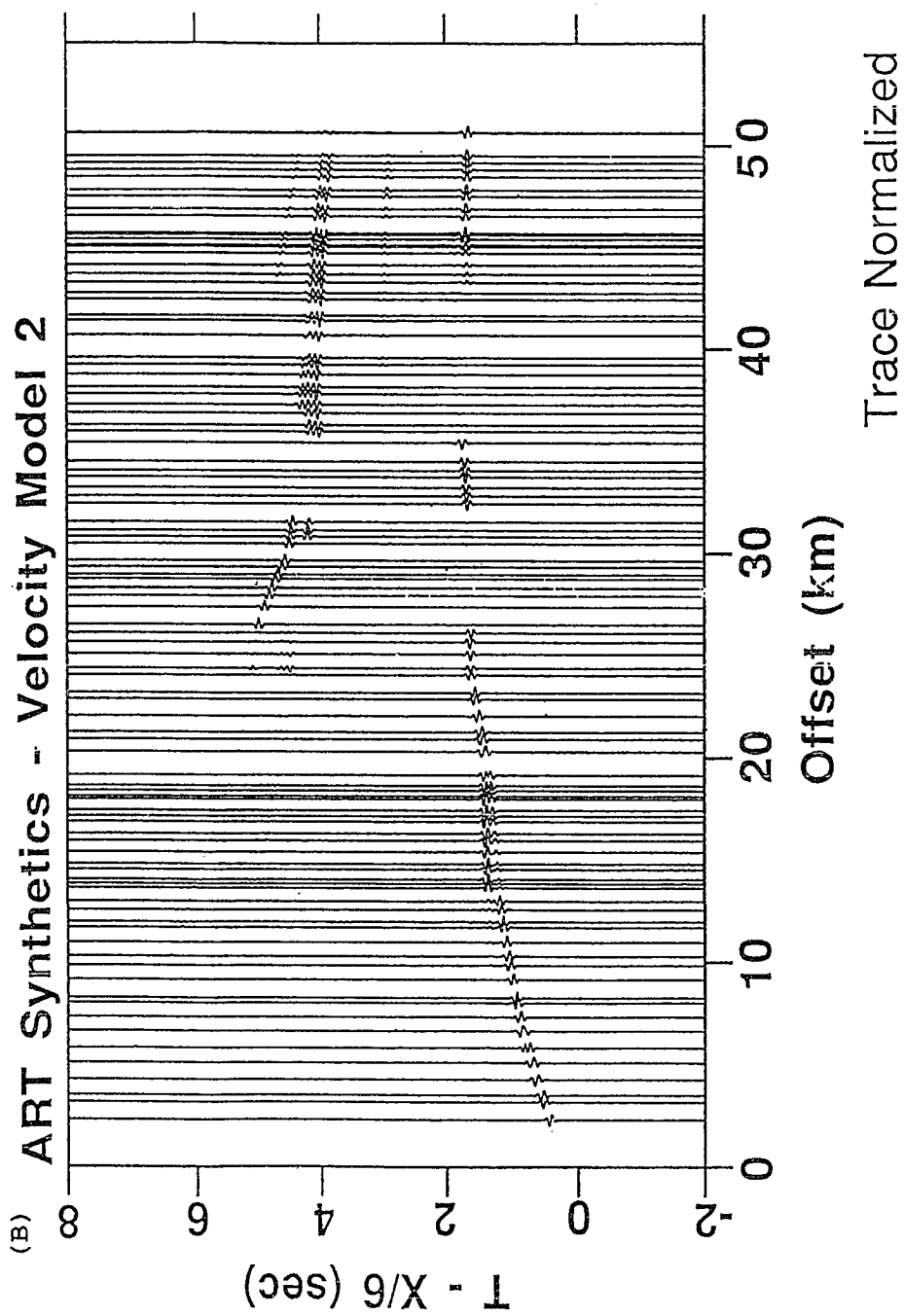
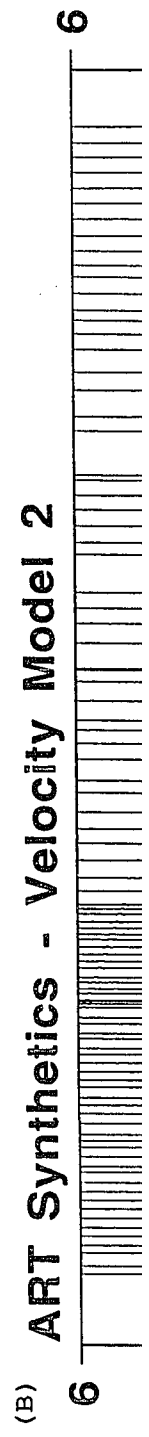
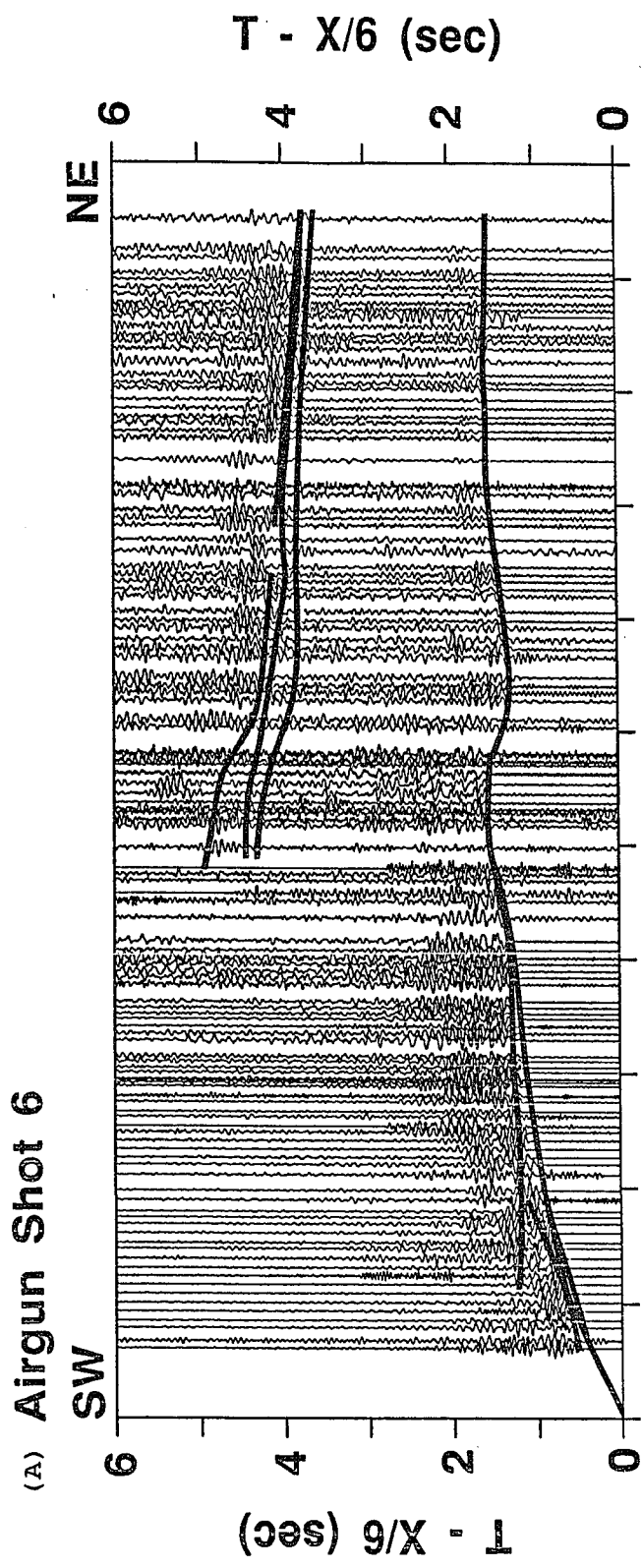


Figure 30: A) Airgun Shot Gather 1 with travel time curves produced from the model in Figure 24. B) Synthetics produced from rays traced from Airgun Shot 1.



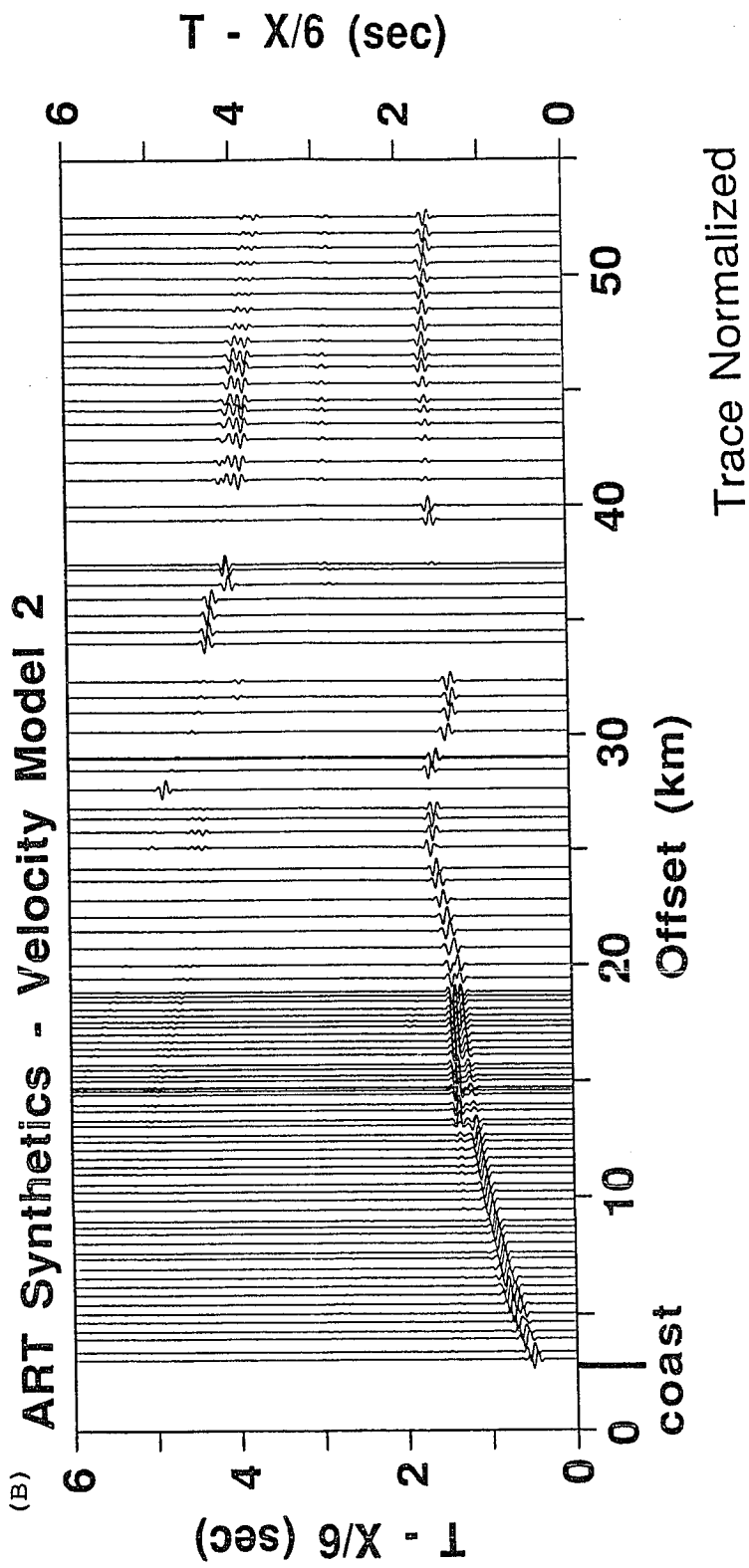


Figure 31: A) Airgun Shot Gather 6 with travel time curves produced from the model in Figure 24. B) Synthetics produced from rays traced from Airgun Shot 6.

CHAPTER 6:

DISCUSSION

As mentioned earlier, the receiver array crosses the Rinconada and Sur-Nacimiento faults, and these features are correlated with a change in the first break travel times seen on the shot records. In the model, velocity pull-ups flank a region of low near-surface velocities beneath the surface location of the faults. Although the boundaries in the velocity field do not necessarily represent lithologic or structural boundaries, the region beneath the faults does resemble thrust layering. This is likely to be the nature of the subsurface in the area, since such a features will probably be associated with a subduction zone, as was present along the central California margin until the Late Oligocene. Whether the faults continue to have thrust motions is a question of major importance for structural engineers and geoscientists alike. This problem remains unresolved by the continuous offset data which does not have the resolution necessary to directly image the steep fault planes in the subsurface; the lack of receivers offshore and the long offsets onshore disallow imaging of shallow features.

A comparison between Velocity Model 1 and models produced by previous workers for the California crust demonstrates a general similarity. Figures 32A, B, and C compare one-dimensional velocity models of California crust derived from experimental petrological data with that of Velocity Model 1 at 65 and 105 km. The experimental data is

Figure 32A

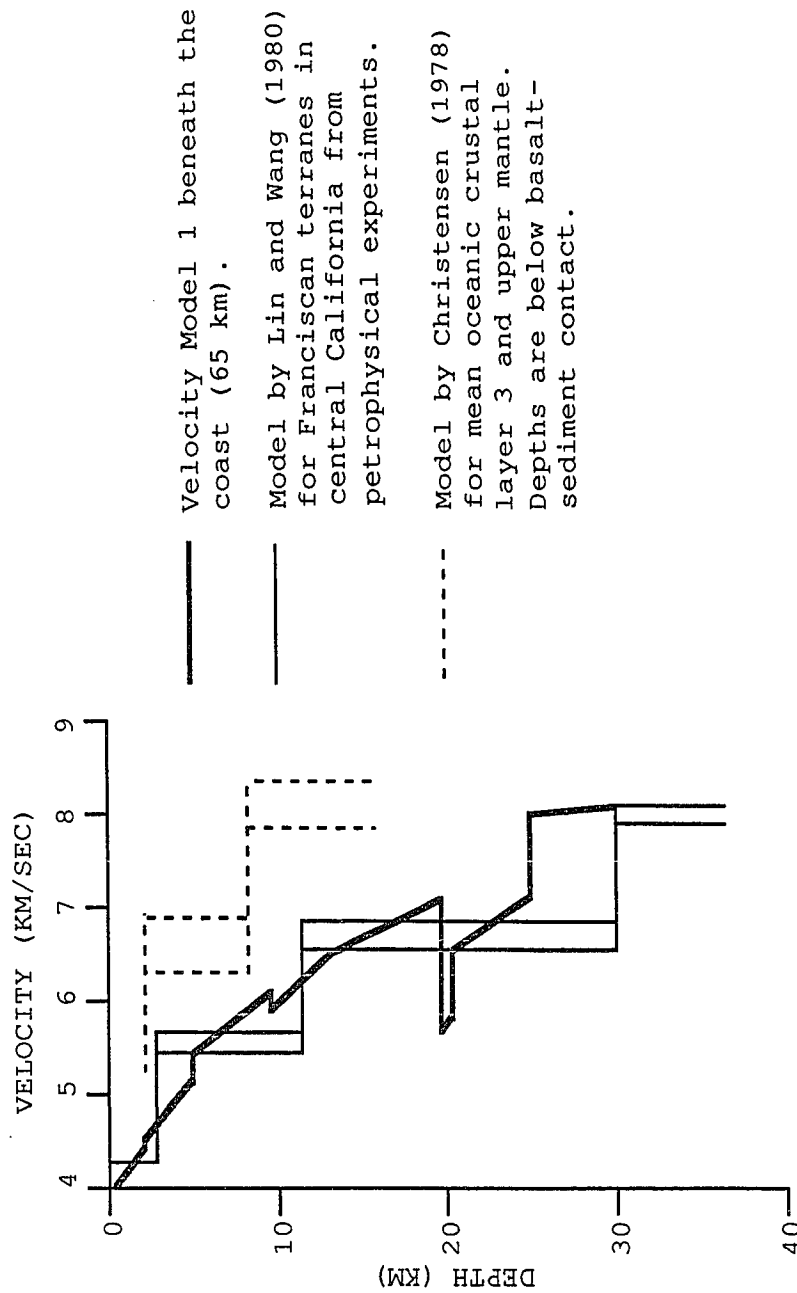


Figure 32: Comparison of one-dimensional models and petrological studies from various authors with Velocity Model 1 at 65 km (Franciscan rocks) and 105 km (Salinian Rocks).

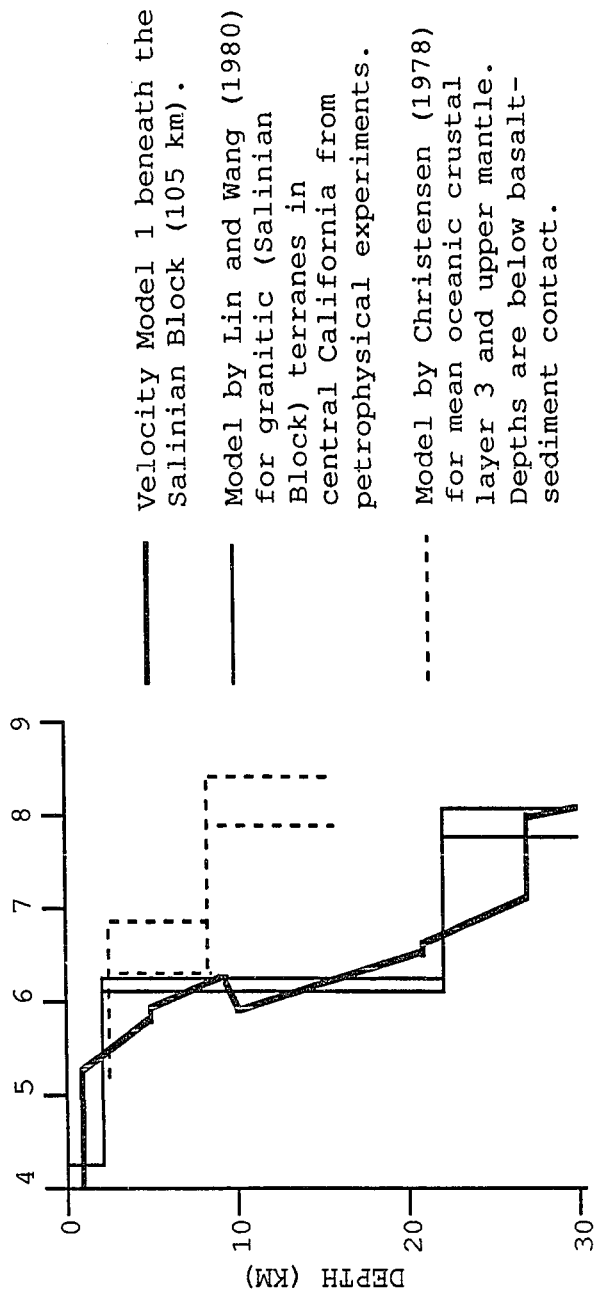


Figure 32B

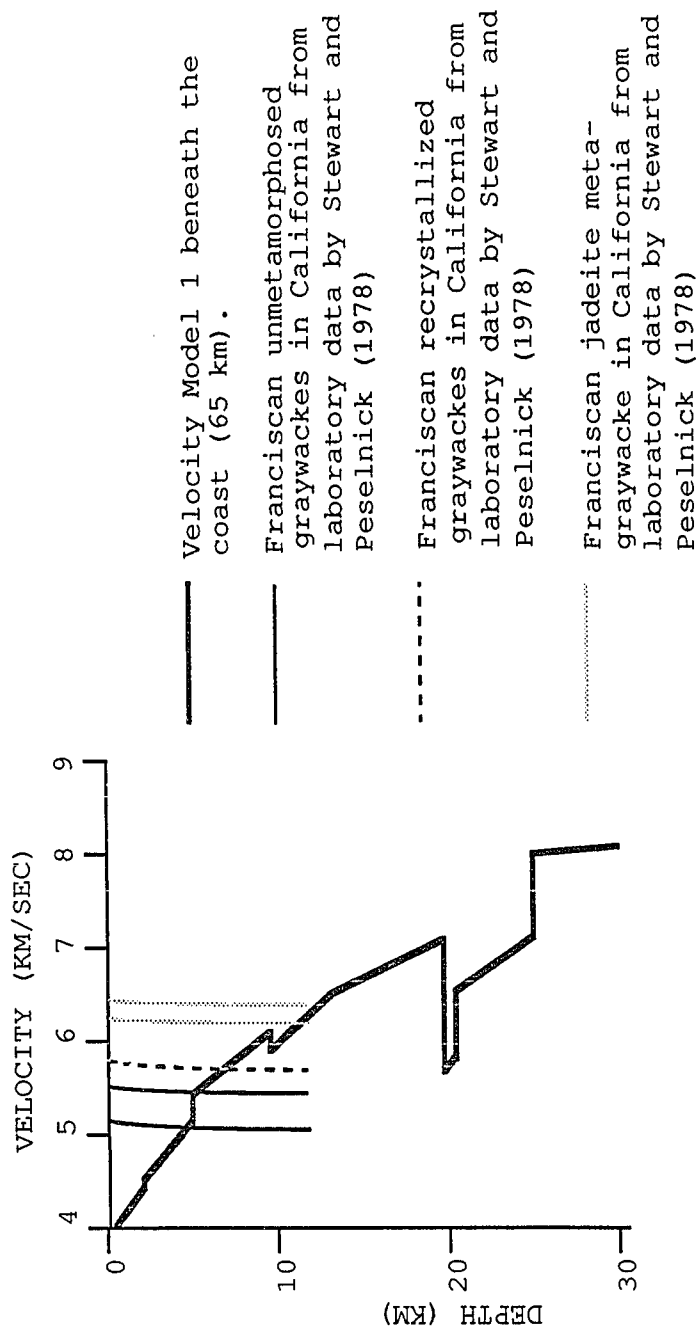


Figure 32C

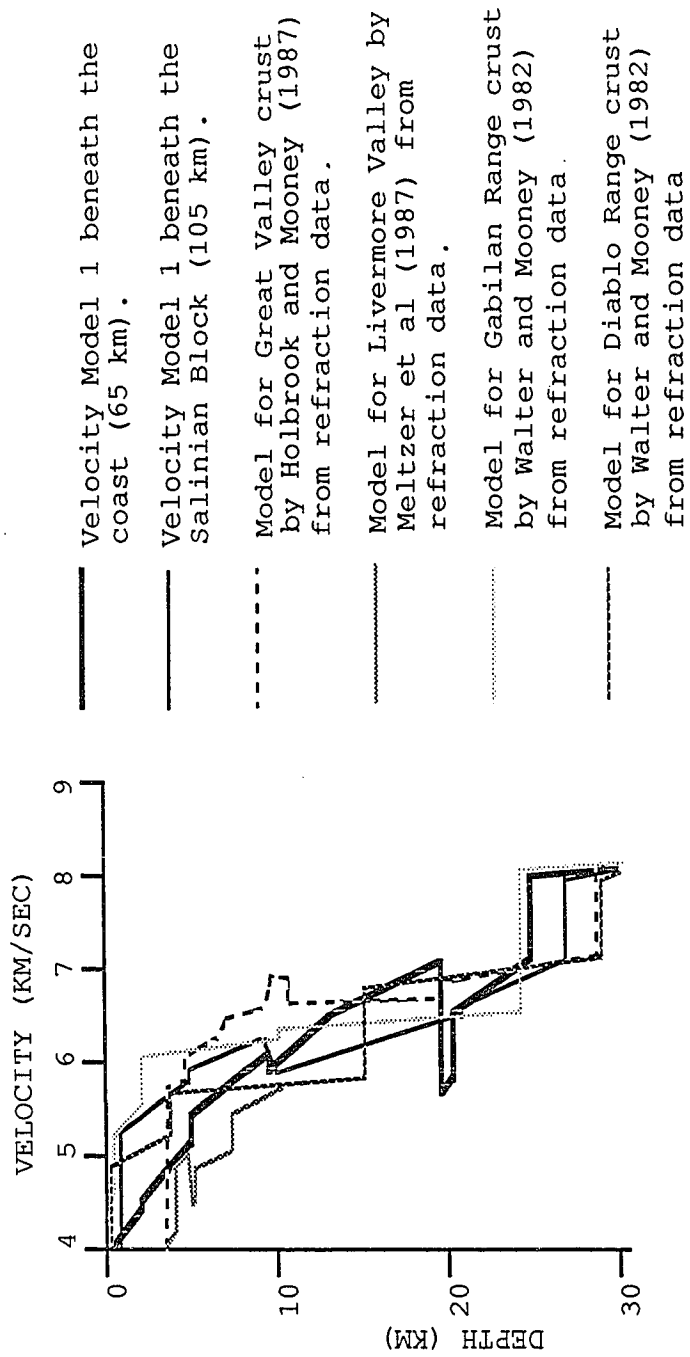


Figure 32D

plotted with a range of velocities for any given depth, that range depending on differences in pressure and temperature at depth. Figure 32D compares Velocity Model 1 with several other models of the California crust based on ray trace modeling of refraction data.

In the lower crust, the prominent reflector observed on shot and receiver gathers has been modeled with rays traced from the base of a dipping layer. With its oceanic velocities, it is quite possible that this feature is either an extension of the Pacific plate which has been partially subducted beneath North America, or a remnant of the Farallon plate which is thought to have been completely subducted beneath North America during Miocene time (Dickinson, 1981). A second reflection seen primarily on the receiver gathers has been modeled with an imbrication of the dipping layer beneath the coast. We suggest that the upper layer could be Farallon plate material which was trapped beneath the leading edge of North America after it ceased spreading from the Pacific plate. With the opening of the Gulf of California, the compressional component of North American-Pacific plate relative motion may have caused the continental and Farallon plate package to overthrust the Pacific plate material found in the lower layer.

In the modeling, I have included a second velocity model with a smoothed LVZ above the lower crustal layers with oceanic velocities. The LVZ only serves to shallow the lower crust slightly and does not produce significant arrivals,

because the velocity contrast at the base of the zone is small. The two models are very similar, even with this relatively minor LVZ. This is best demonstrated by the series of one-dimensional velocity functions shown in Figure 33. The figure compares velocities in the two models at 10 km intervals from 20 to 110 km. Also, I have compared the velocity functions at Land Shot 1 (77 km) from my models with that from the same location on the USGS strike line model in Figure 15.

Both of my models provide a good match to the data, but I prefer the model without the LVZ because it is simpler. However, if stronger evidence for the LVZ can be produced, perhaps with the USGS strike line data (Walter and Sharpless, 1987), then the second model may prove to be a more reasonable one.

One explanation for LVZs in the lower crust was put forward by Trehu and Wheeler (1987). They produced a model from older USGS data of the same area (Figure 4). A comparison of the continuous offset shot gather models (Figures 14 and 25) with theirs shows that we have modeled the same gross features in the upper crust, most notably the horizontal change in velocity at 30 to 35 km (Figure 4) and depths of 1 to 10 km beneath the Nacimiento and Rinconada faults. At depth, they included a low velocity wedge below 12 km on the western side of the model which was interpreted as subducted sedimentary material. Because the continuous offset experiment used greater receiver and shot density and

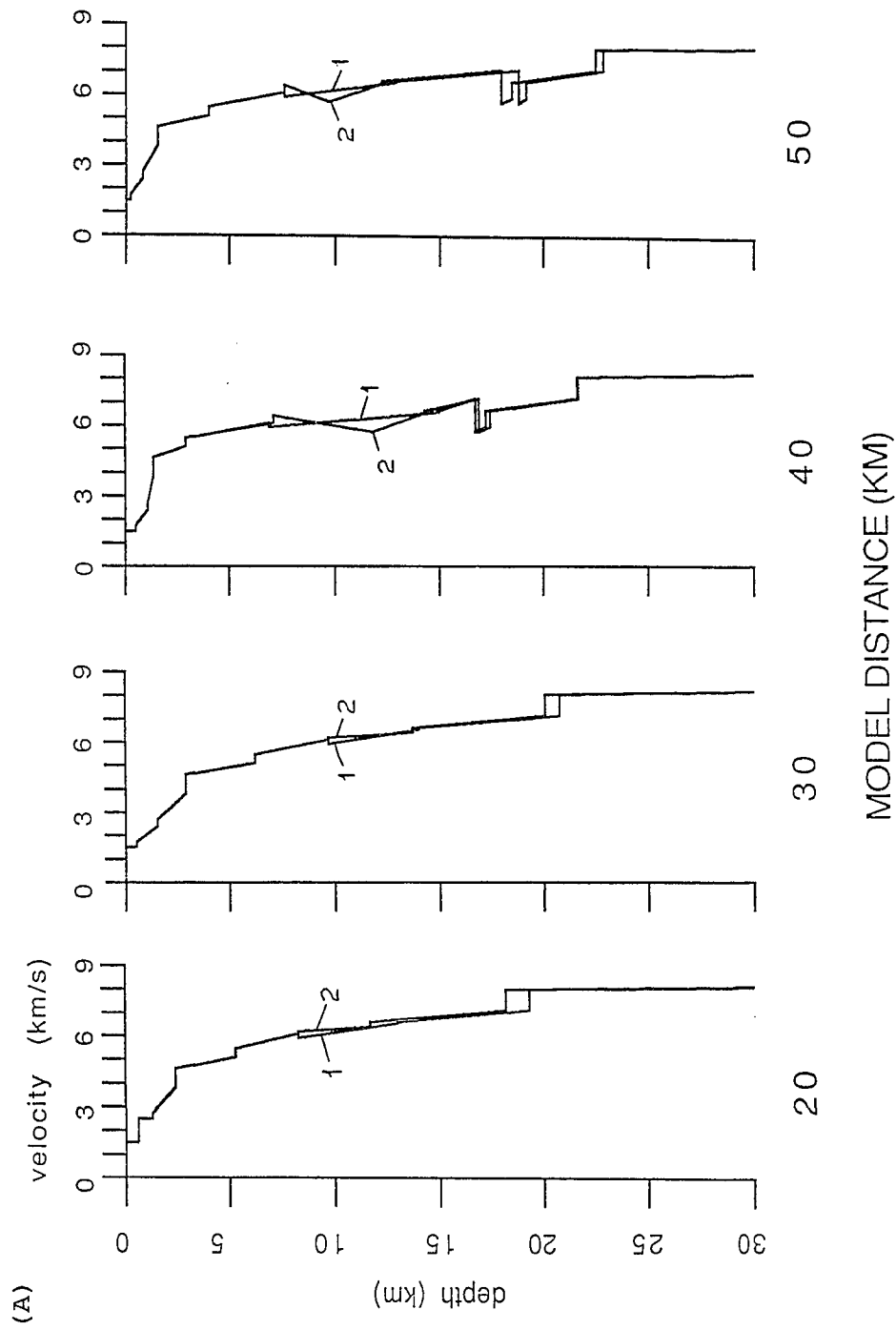
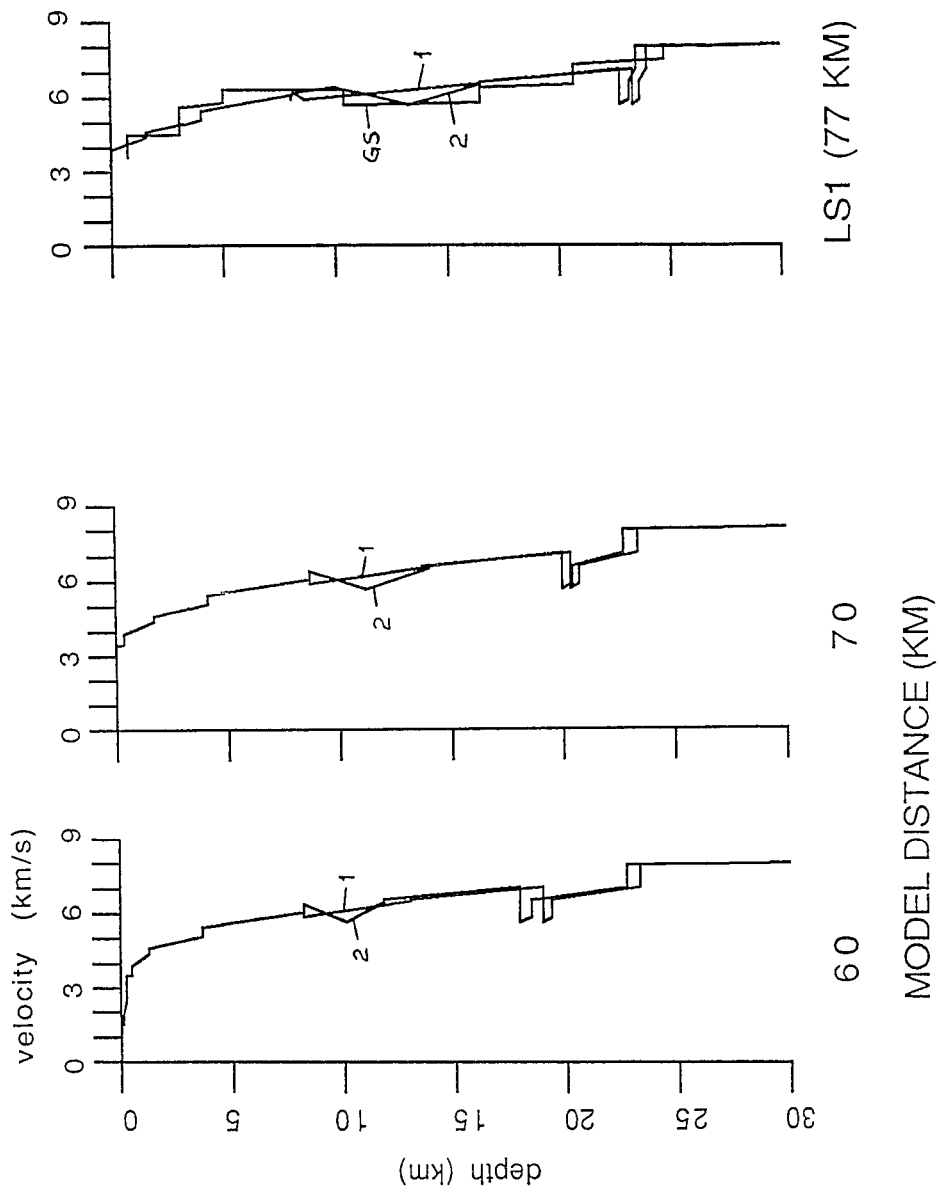
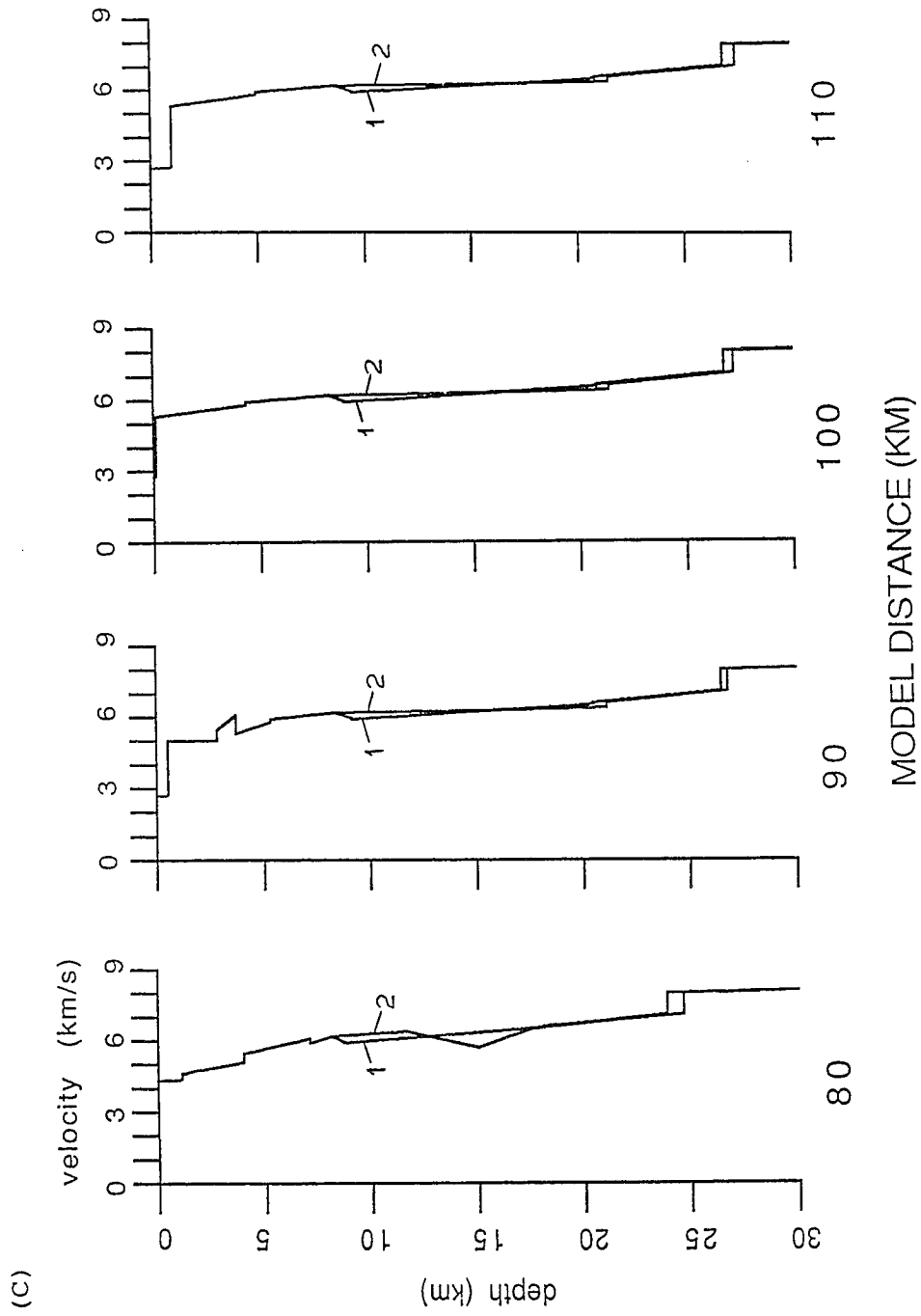


Figure 33: One dimensional velocity functions taken every 10 km across models.

(B)





longer offsets extending offshore, a more precise model is possible than with the USGS data, particularly beneath the coast. I have tested a model very similar to this USGS model with rays traced from both land shots and Airgun Shot 6, and while some of the amplitude and travel time synthetics showed a general resemblance to the data, many features were not well matched and the travel time for the deep reflection off the base of the LVZ from the airgun shot was over 0.5 s slower than the arrival in the data. Arrivals from this zone had been the basis for including the LVZ in the USGS model, and the travel time discrepancy provides a good argument against including such a feature.

I have constructed synthetic seismograms using an asymptotic ray theory algorithm (McMechan and Mooney, 1980). While the method is theoretically capable of dealing with vertical or nearly vertical boundaries, the program seems to have some difficulty handling them, due to model parameterization. It is possible that a finite difference based algorithm (cf. Wolf et al, 1986) could provide a more precise match to the data, particularly in the region beneath the Rinconada and Sur-Nacimiento fault zones where the model becomes quite complex. Because of time constraints, I have not attempted a finite difference model, but future work with the continuous offset data may help to further refine the models presented herein. These models will also provide a basis for migration of CMP gathers from the same data.

CHAPTER 7:

CONCLUSION

I have produced a 120 km wide velocity and structure profile across the transform margin in central California, extending 25 to 30 km below the surface to Moho depths. Together with the reflection processing of the same data, the refraction velocity modeling provides the most complete image of a crustal transition zone ever obtained anywhere. The near surface of the models made here produces excellent matches to the first breaks of the field data and shows a strong correlation with the surface geology. At depth, two different models have been proposed. Both provide an imbricated lower crust which has oceanic crustal velocities and is interpreted as Pacific plate beneath Farallon plate material. One model shows a laterally discontinuous LVZ above the lower crust, demonstrating the feasibility of including such a feature at depth as has been done by other authors. The other model contains no such LVZ but rather a slightly deeper lower crust. I prefer this simpler model because I have not seen direct indication of any extensive low velocity zones in either the continuous offset data or in offshore reflection profiles.

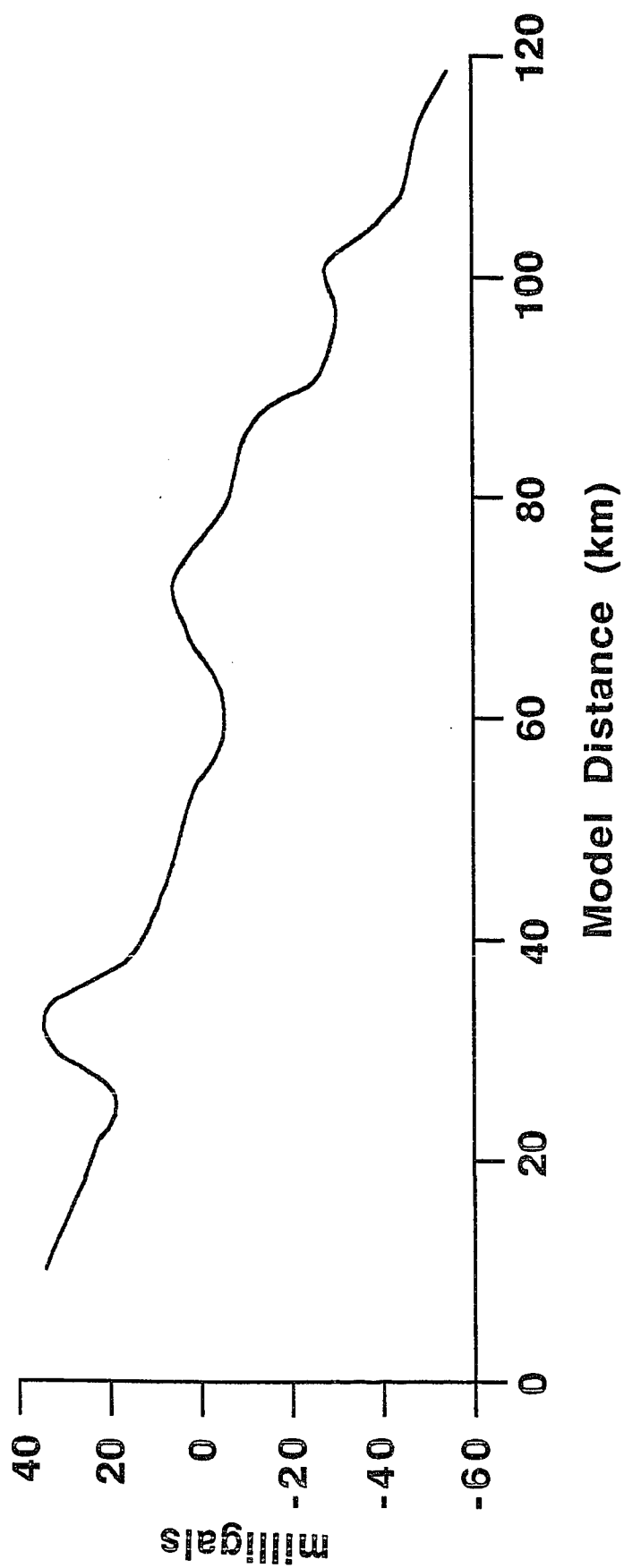


Figure 34: Bouguer gravity profile taken from a map by Burch et al (1968).

REFERENCES

- Atwater, Tanya, 1970, Implications of plate tectonics for the Cenozoic tectonic evolution of western North America: Geol. Soc. America Bull., v. 81, p.3513-3536.
- Blake, M.C., Jr., and Jones, D.L., 1974, Origin of Franciscan melanges in northern California, in Dott, R.H., Jr., and Shaver, R.H., eds., Modern and ancient geosynclinal sedimentation: Soc. Econ. Paleontologists and Mineralogists Spec. Pub. 19, p. 345-357.
- Blumling, P., and Prodehl, C., 1983, Crustal structure beneath the eastern part of the Coast Ranges (Diablo Range) of central California from explosion seismic and near earthquake data: Phys. Earth Planet. Inter., v. 31, p. 313-326.
- Bostick, N.H., 1974, Phytoclasts as indicators of thermal metamorphism, Franciscan assemblage and Great Valley Sequence (Upper Mesozoic), California: Geol. Soc. America Spec. Paper 153, p. 1-17.
- Burch, S.H., Grannell, R.B., and Hanna, W.F., 1968, Bouguer gravity map of California, San Luis Obispo sheet (Geology from the Geologic map of California, Olaf P. Jenkins edition, San Luis Obispo sheet, 1968), California Division of Mines and Geology.
- Cerveny, V., Moltokov, I.A., and Psencik, I., 1977, Ray method in seismology: University of Karlova, Prague, Czechoslovakia, 214 p.
- Champion, D.E., D.G. Howell, and Gromme, C.S., 1984, Paleomagnetic and geologic data indicating 2500 km of northward displacement for the Salinian and related terranes, California: J. Geoph. Research, v.89, no.B9, p. 7736-7752.
- Christensen, N.I., 1978, Ophiolites, seismic velocities and oceanic crustal structure: Tectonophysics, v.47, p. 131-157.
- Crouch, J.K., Bachman, S.B., and Shay, J.T., 1984, Post Miocene compressional tectonics along the central California margin, in Crouch, J.K., and Bachman, S.B., eds., Tectonics and sedimentation along the California Margin: Pacific Section of the SEPM, v. 38, p. 37-54.
- Crowell, J.C., 1979, The San Andreas fault system through time: Geol. Soc. London, v. 136, p. 293-302.

- Dickinson, W.R., 1983, Cretaceous sinistral strike-slip along the Nacimiento fault in coastal California: AAPG Bull., v. 67, p. 624-645.
- Dickinson, W.R., 1981, Plate tectonics and the continental margin of California: in Ernst, W.G., ed., The Geotectonic Development of California, v. 1, p. 1-28.
- Dobrin, M.B., 1976, Introduction To Geophysical Prospecting: McGraw Hill, Inc., New York, NY, 630 p.
- Ernst, W.G., 1981, ed., The Geotectonic Development of California: Prentice Hall Inc., 706 pp.
- Graham, S. A. , and Dickinson, W.R., 1978, Apparent offsets of on-land geologic features across the San Gregorio-Hosgri fault trend: Calif. div of Mines and Geol., Spec. Report 137, p 13-24.
- Healy, J.H., and Peake, L.G., 1975, Seismic velocity structure along a section of the San Andreas fault near Bear Valley, California: Seismol. Soc. America Bull., v.65, p. 1177-1197.
- Holbrook, W.S., and Mooney, W.D., 1987, The crustal structure of the axis of the Great Valley, California, from seismic refraction measurements: Tectonophysics
- Hoskins, E.G., and Griffiths, J.R., 1971, Hydrocarbon potential of northern and central California offshore: AAPG Mem. 15, p.212-228.
- Larson, R.L., and others, 1968, Gulf of California: A result of ocean floor spreading and transform faulting: Science, v.161, p. 781-784.
- Levander, A.R., Putzig, N.E., Gibson, B.S., 1987, A continuous-offset seismic experiment in the central California margin, abs., EOS, v.68, no. 16, p.348.
- Levander, A.R., and Putzig, N.E., 1987, Interpretation of a continuous-offset seismic profile in the central California margin, abs., EOS, v.68, no. 44, p.1366.
- Lin, W., and Wang, C., 1980, P-wave velocities in rocks at high pressure and temperature and the constitution of the central California crust: Geophys. J. R. astr. Soc., v.61, p.379-400.
- McCulloch, D.S., 1987, Regional geology and hydrocarbon potential of offshore central California: in Scholl, D.W., Grantz, A., and Vedder, J.G., eds., Geology and resource potential of the continental margin of western North America and adjacent ocean basins-Beaufort Sea to

Baja California: Circum-Pacific Council for Energy and Mineral Resources, Earth Science Series, Houston, Texas, Chapt. 15B.

- McMechan, G.A., and Mooney, W.D., 1980, Asymptotic ray theory and synthetic seismograms for laterally varying structures: theory and application to the Imperial Valley, California: Bull. Seismological Soc. America, v. 70, p. 2021-2035.
- Meltzer, A.S., and Levander, A.R., 1987, Interpretation of deep crustal reflection profiles offshore southern central California, abs., EOS, v. 68, no. 44, p. 1365.
- Meltzer, A.S., Levander, A.R., and Mooney, W.D., 1987, Upper crustal structure, Livermore Valley and vicinity, California Coast Ranges: Bull. Seismological Soc. America, v. 77, no. 5, p. 1655-1673.
- Minster, J.B., and Jordan, T.H., 1984, Vector constraints on Quaternary deformation of the western United States east and west of the San Andreas fault, in Crouch, J.K., and S. B. Bachman, eds., Tectonics and sedimentation along the California margin: Pacific Section Soc. Econ. Mineralogists and Paleontologists, v. 38, p. 1-16.
- Nilsen, T.H., and Clarke, S.H., Jr., 1975, Sedimentation and tectonics in the early Tertiary continental borderland of central California: U.S. Geol. Survey Prof. Paper 925, 64 pp.
- Page, B.M., 1981, The Southern Coast Ranges, in Ernst, ed., The Geotectonic development of California, v. 1, p. 329-417.
- Page, B.M., Wagner, H.C., Mc Culloch, D.S., Silver, E.A., and Spotts, J.H., 1979, Geologic cross section of the continental margin off San Luis Obispo, the Southern Coast Ranges, and the San Joaquin Valley, California: Geol. Soc. America map and chart series MC-28G.
- Press, F., 1966, Seismic Velocities: in Clark, S.P., Jr., ed., Handbook of physical constants, revised edition, Mem. Geol. Soc. Am. 97, sec. 9, p.195-218.
- Putzig, N.E., and Levander, A.R., 1988, Interpretation of continuous-offset seismic data in the central California Margin, abs., Pacific sections AAPG, SEG, SEPM, SPWLA annual meeting, to be presented on April 18 in Santa Barbara, CA.

- Ross, D.C., 1978, The Salinian block-a Mesozoic granitic orphan in the Californian Coast Ranges, in Howell, D.G., and McDougall, K.A., eds., Mesozoic Paleogeography of the Western United States: Pacific Coast Paleogeography Symp. 2, Pacific Coast, S.E.P.M., p.509-522
- Howie, J.M., and Savage, W.U., 1988, Initial crustal velocity model for south central California coastal margin, abs., EOS, v.68, no. 44, p.1366.
- Stewart, R., and Peselnick, L., 1978, Systematic behavior of compressional velocity in Franciscan rocks at high pressure and temperature: JGR v.83, no.B2, p.831-839.
- Stewart, S.W., 1968, Preliminary comparison of seismic travel times and inferred crustal structure adjacent to the San Andreas fault in the Diablo and Gavilan Ranges of central California, in Dickinson, W.R., and Grantz, A., eds., Proceedings of conference on geologic problems of San Andreas fault system: Stanford Univ. Pub. Geol. Sci., v.11, p. 218-230.
- Trehu, A.M., and W.H. Wheeler IV, 1987, Possible evidence for subducted sedimentary materials beneath central California, Geology, v.15, p. 254-258.
- Uyeda, S., 1984, Subduction zones: their diversity, mechanism and human impacts, GeoJournal, v. 8.4, p.381-406.
- Walter, A., and Sharpless, S., 1987, Crustal velocity structure of the Sur-Obispo (Franciscan) terrane between San Simeon and Santa Maria, California: abs., EOS, v.68, no. 44, p.1366. Presented at the AGU Fall Meeting, December 7-10, 1987, San Francisco, CA.
- Walter, A.W., and Mooney, W.D., 1982, Crustal structure of the Diablo and Gabilan Ranges, central California: Bull. Seismological Soc. America, v. 72, p. 1255-1275.
- Wolf, L.W., Levander, A.R., and Fuis, G.S., 1986, Upper crustal velocity structure of the accreted Chugach terrane, Alaska, abs., EOS, v. 67, p. 1195.

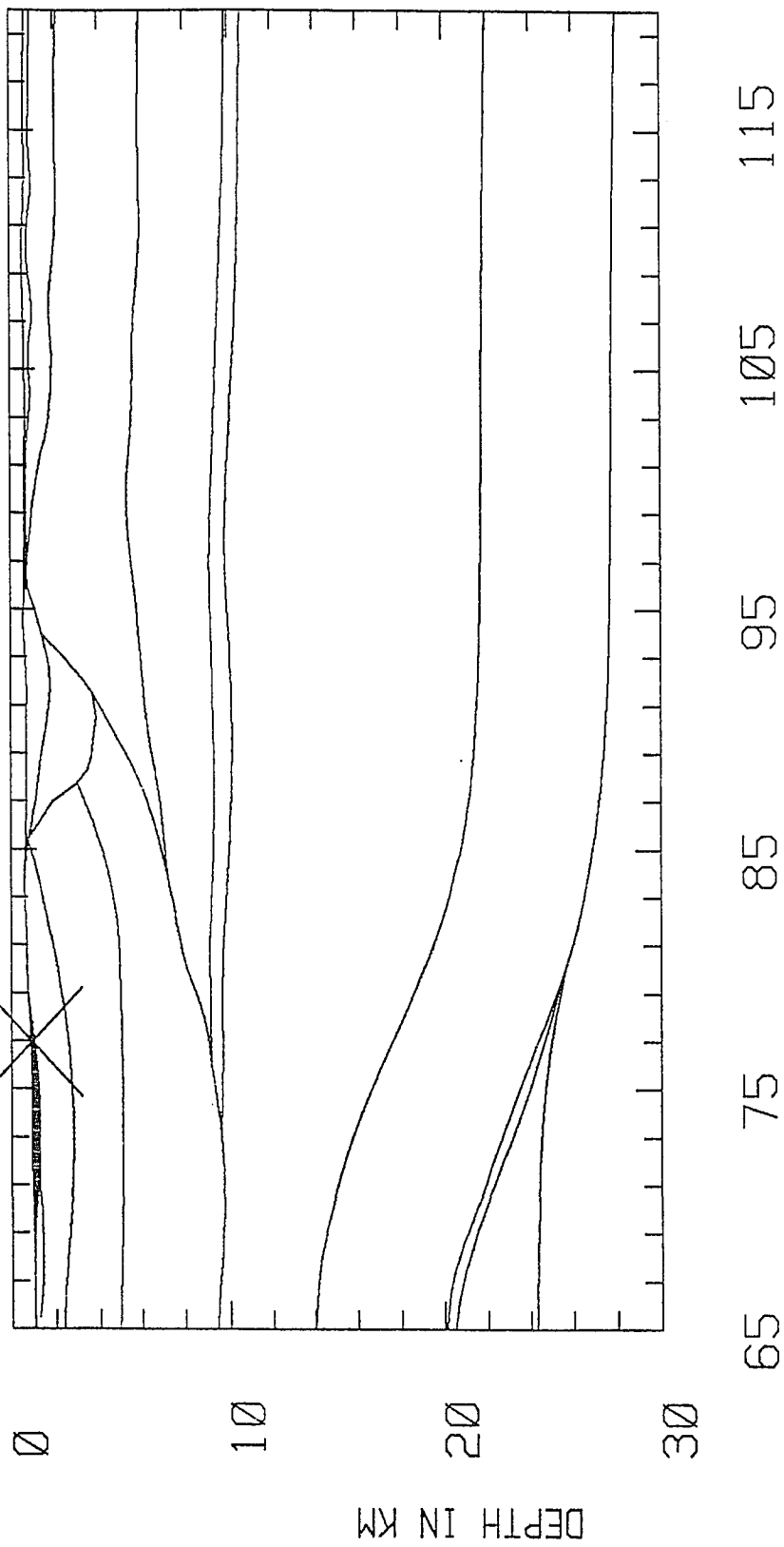
Appendix A

Ray diagrams for Velocity Model 1 (Figure 14) from:

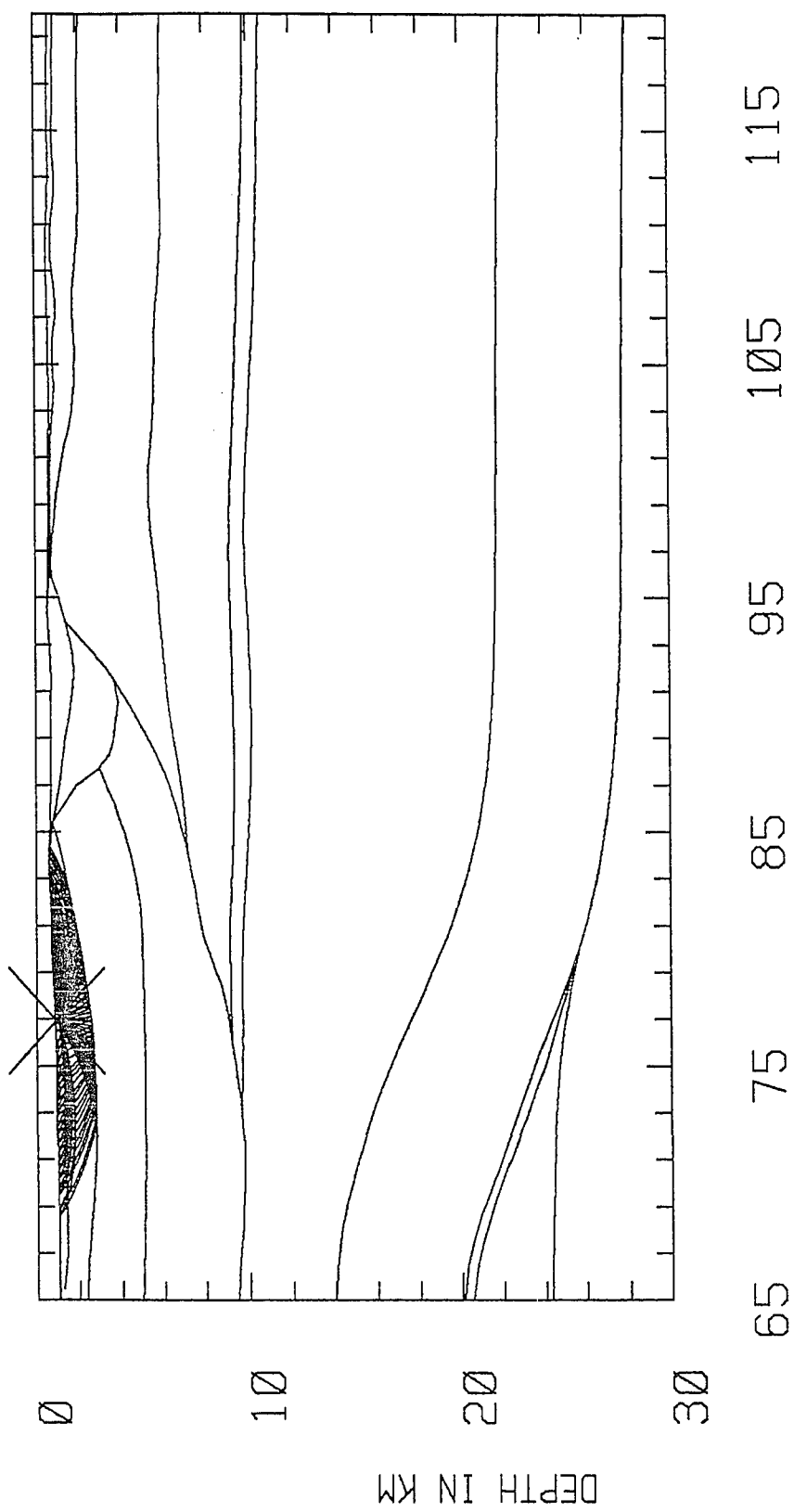
- A) Land Shot 1
- B) Land Shot 2
- C) Airgun Shot 6

Travel time curves are included at the end of each section of ray diagrams, along with first break picks from the gathers.

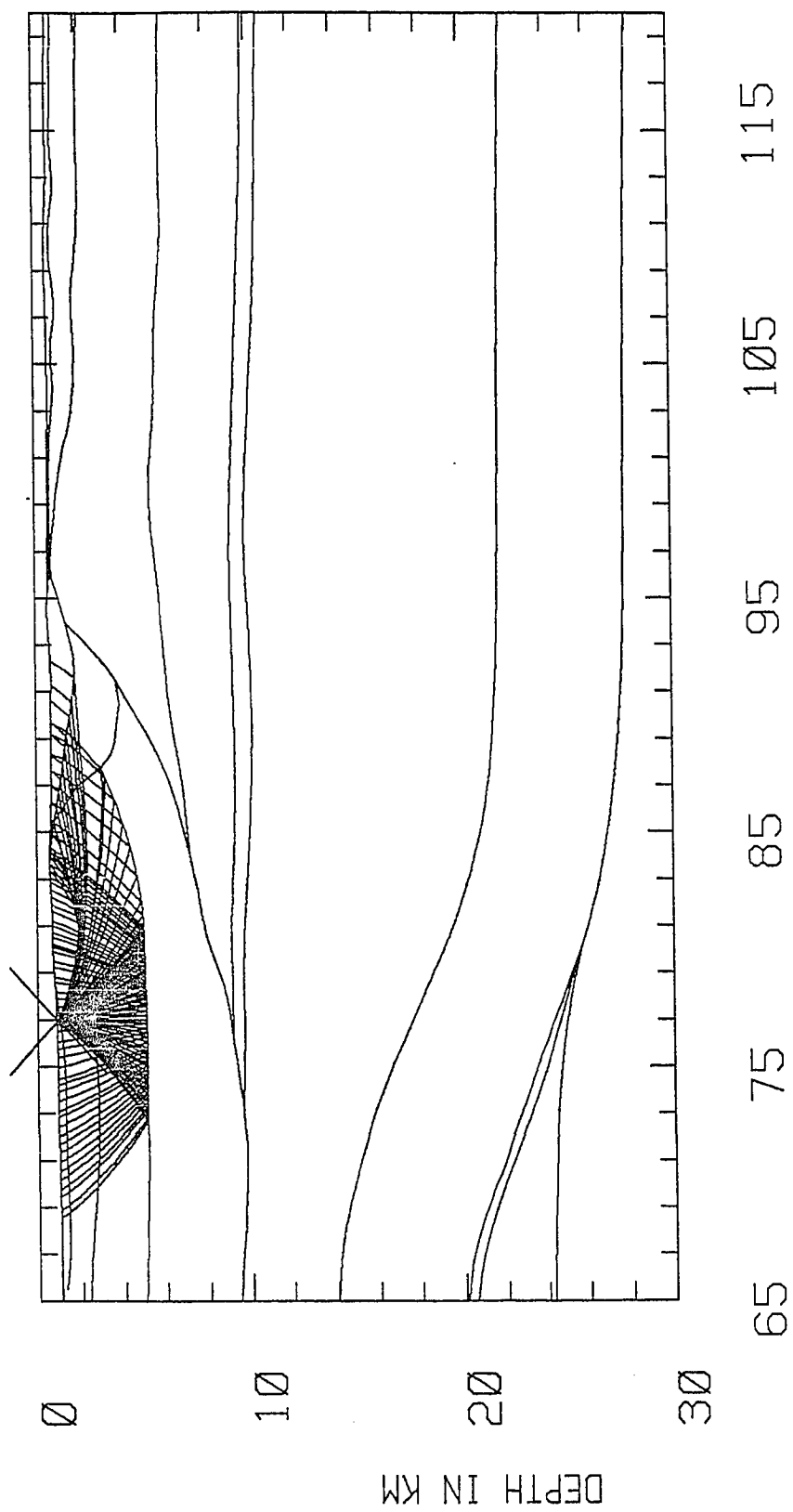
LS1

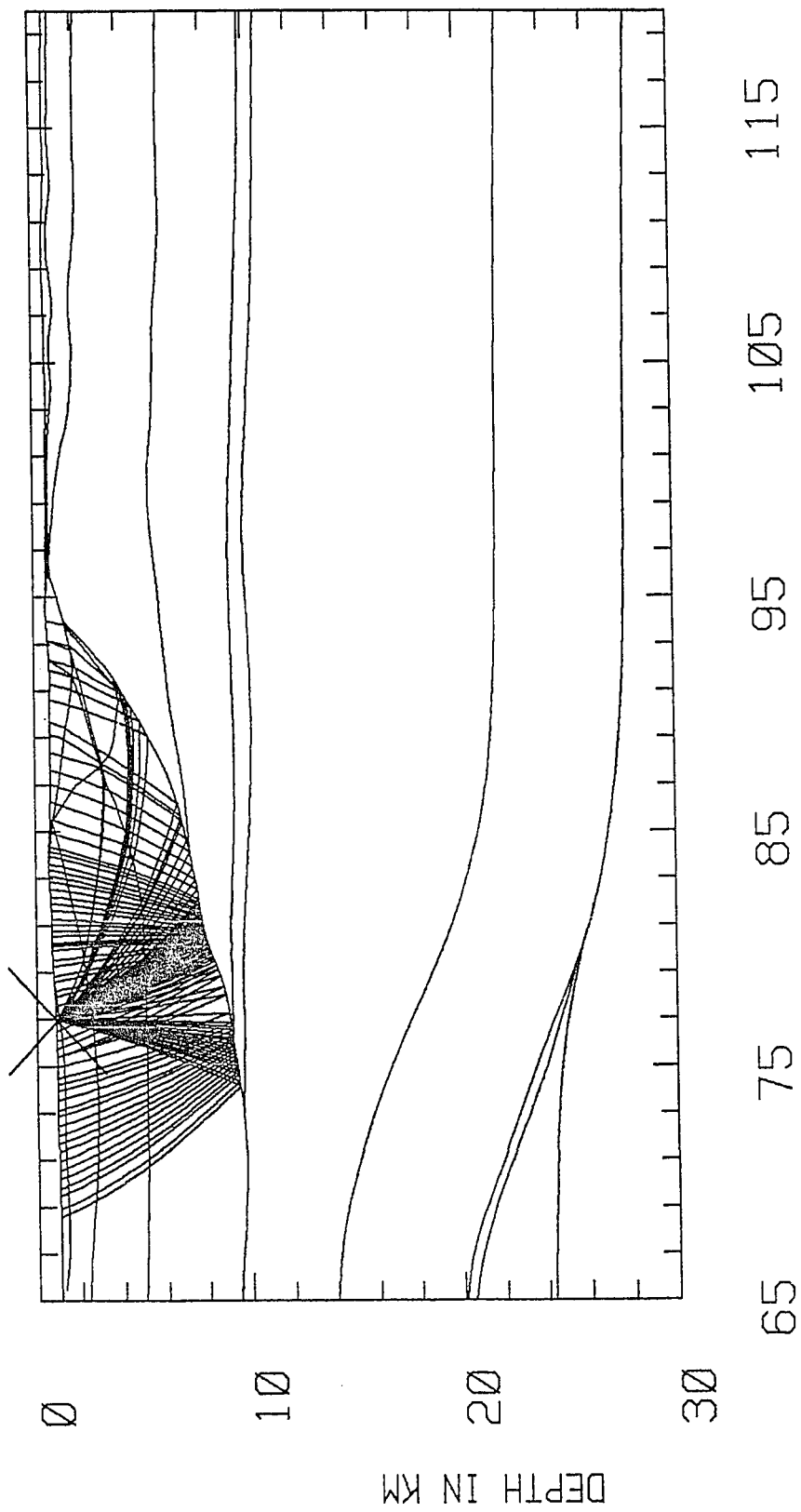


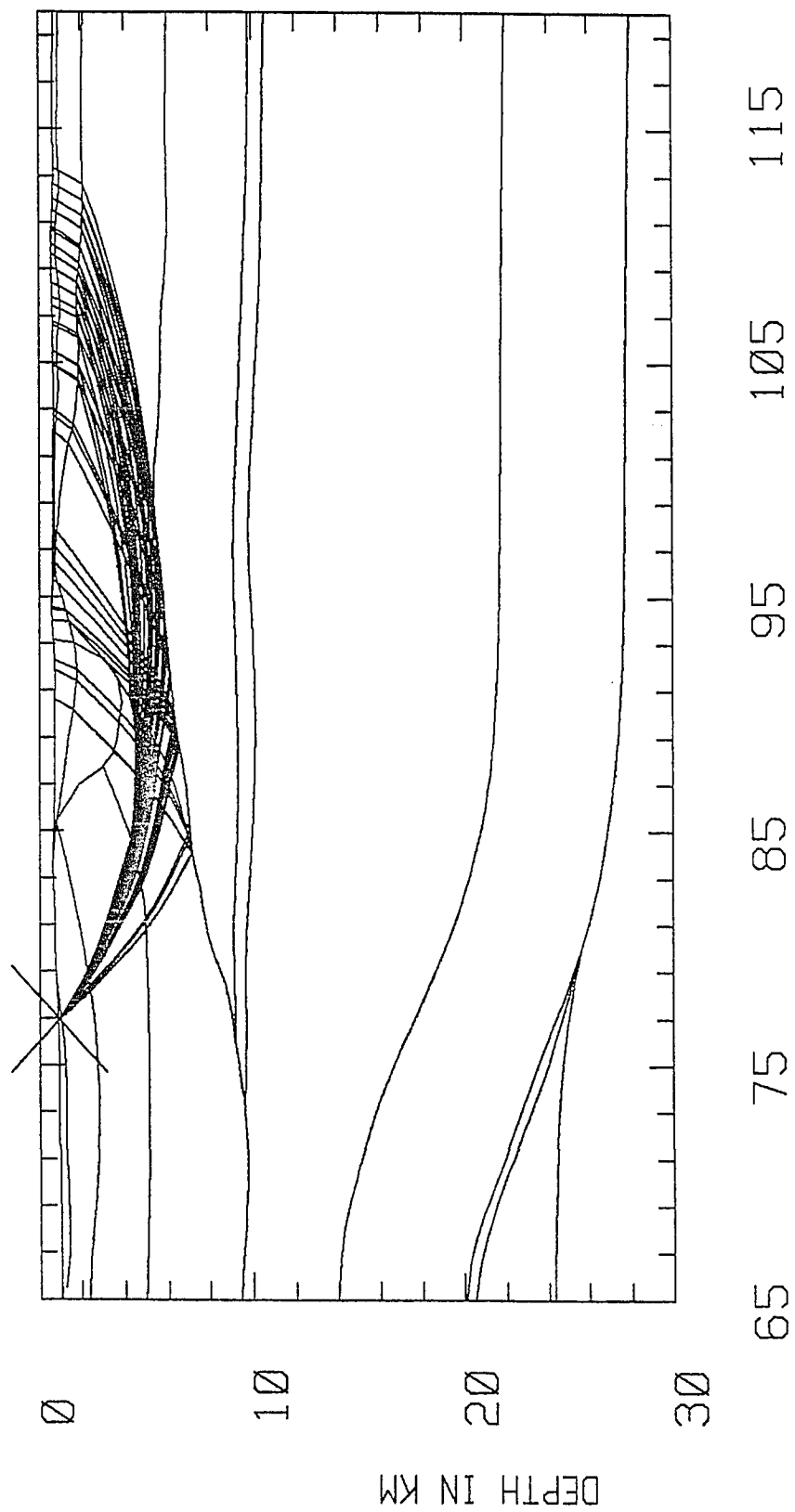
DISTANCE IN KM

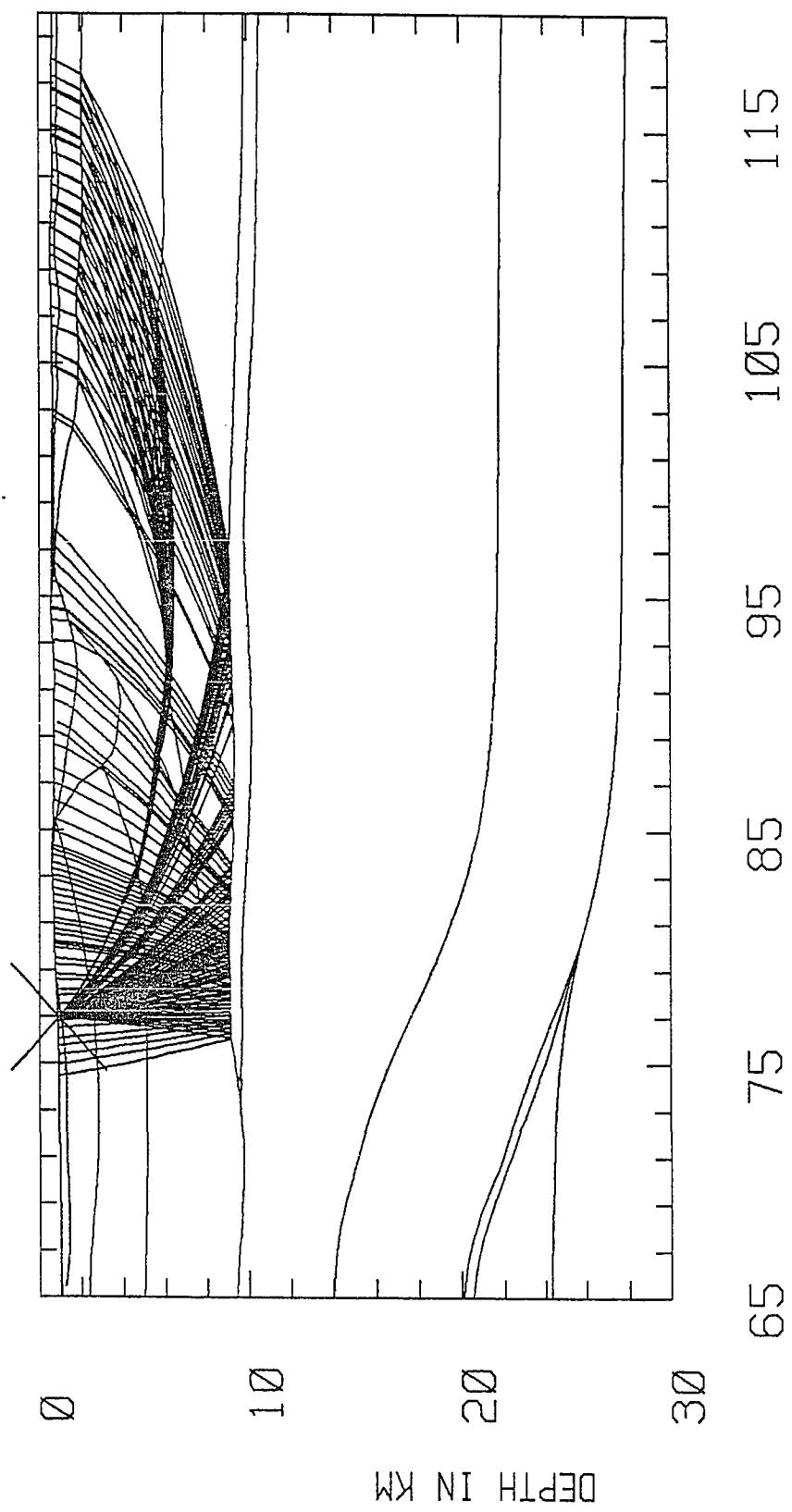


DISTANCE IN KM

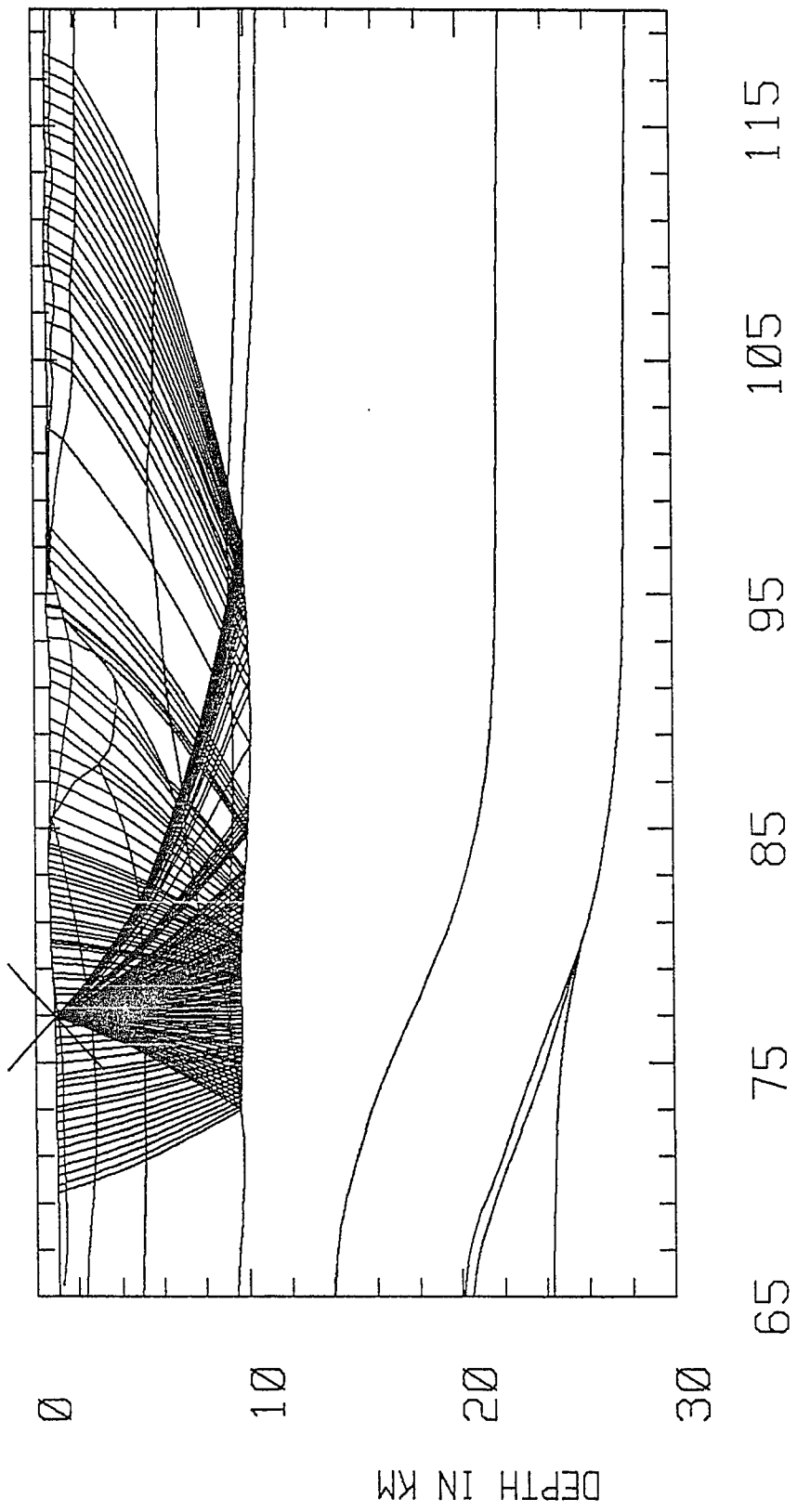




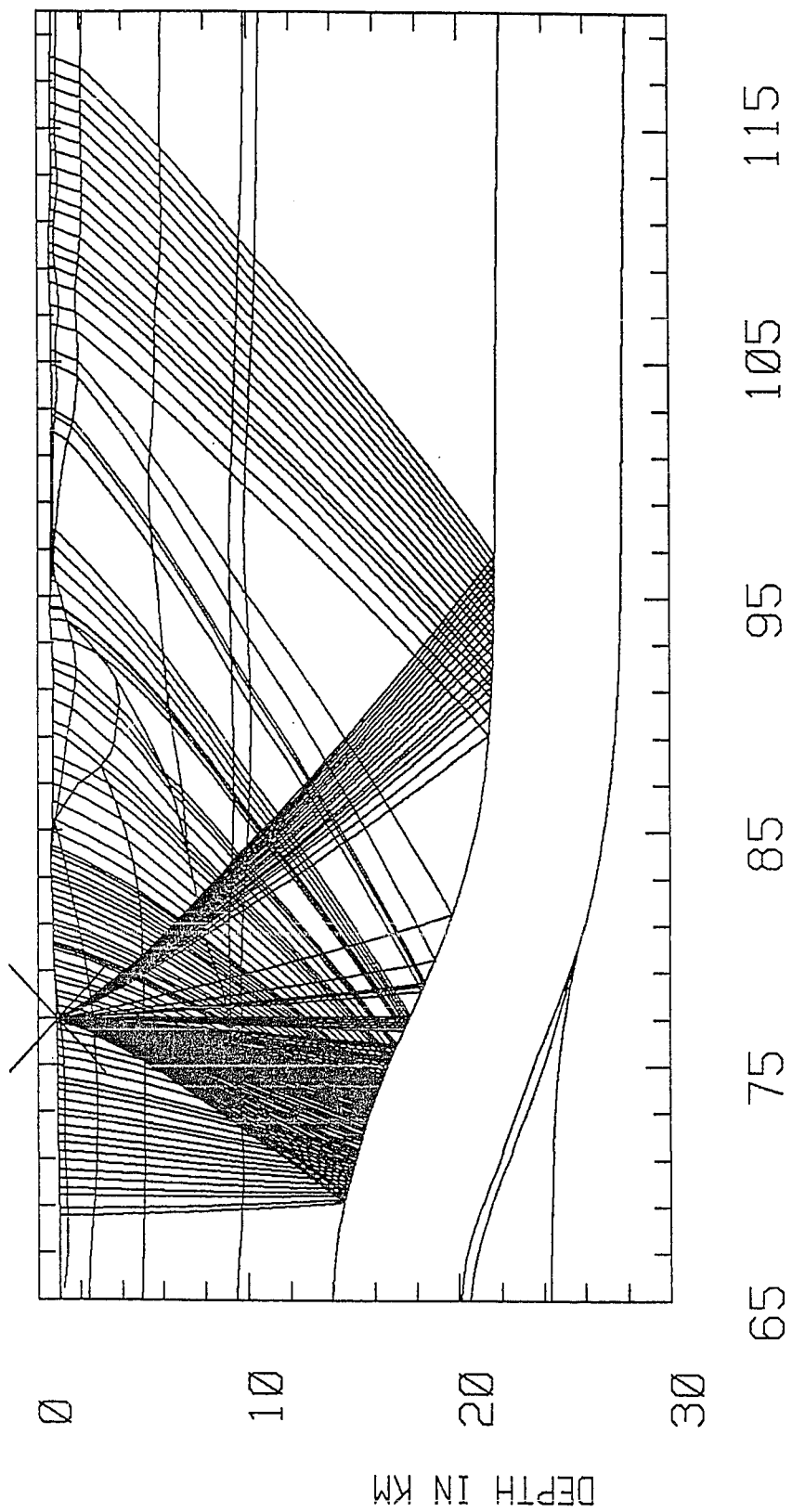




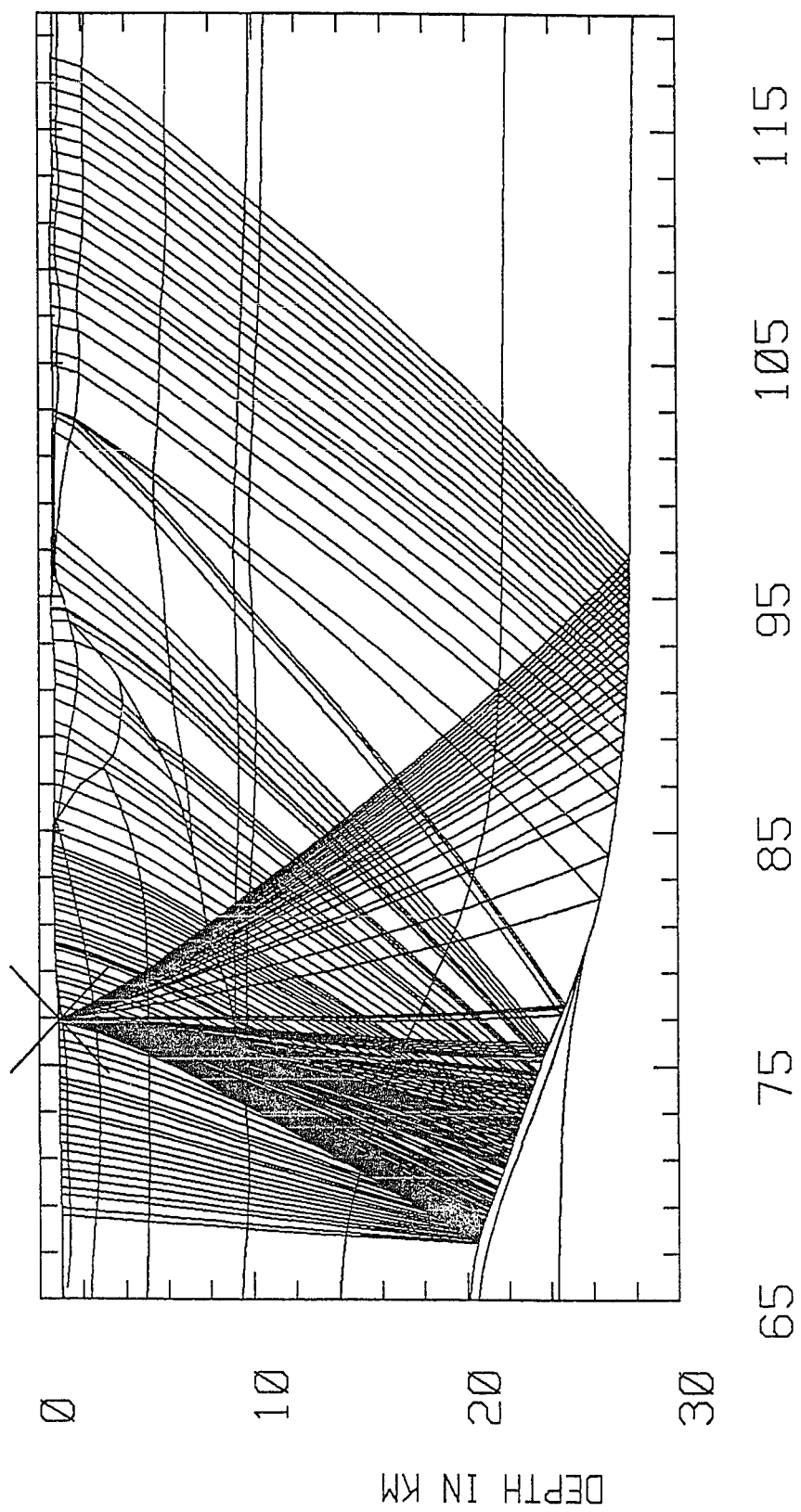
DISTANCE IN KM

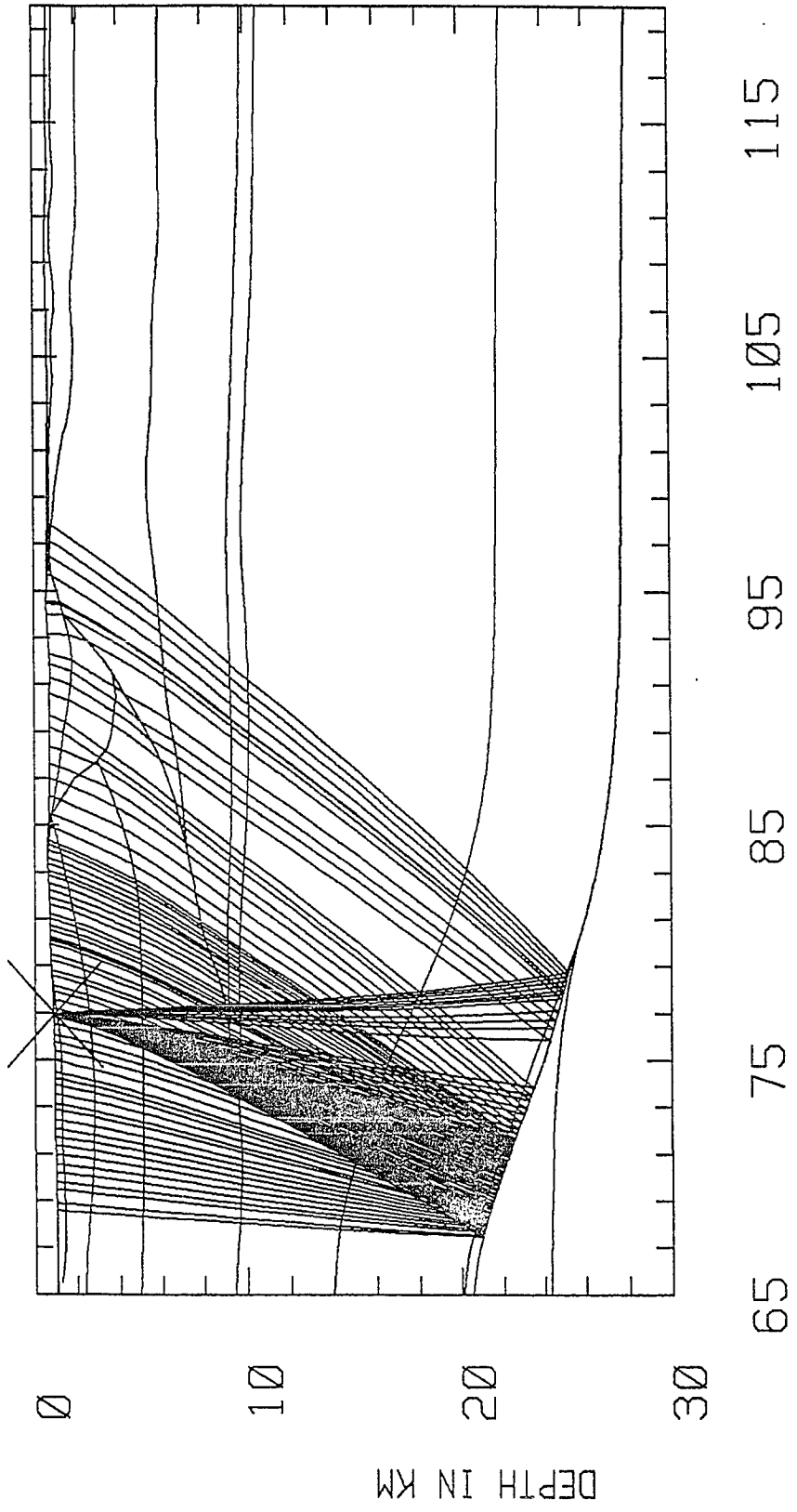


DISTANCE IN KM

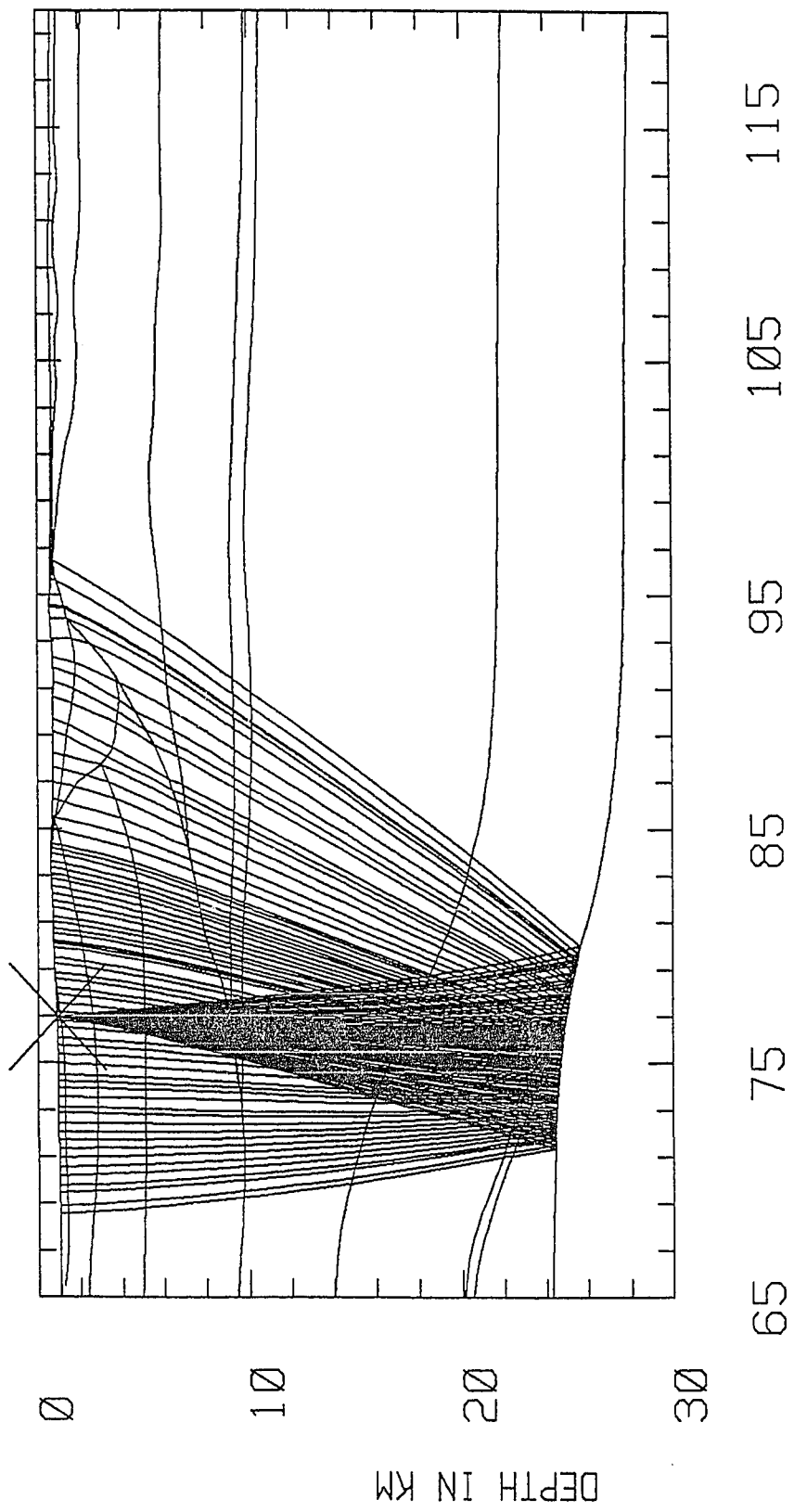


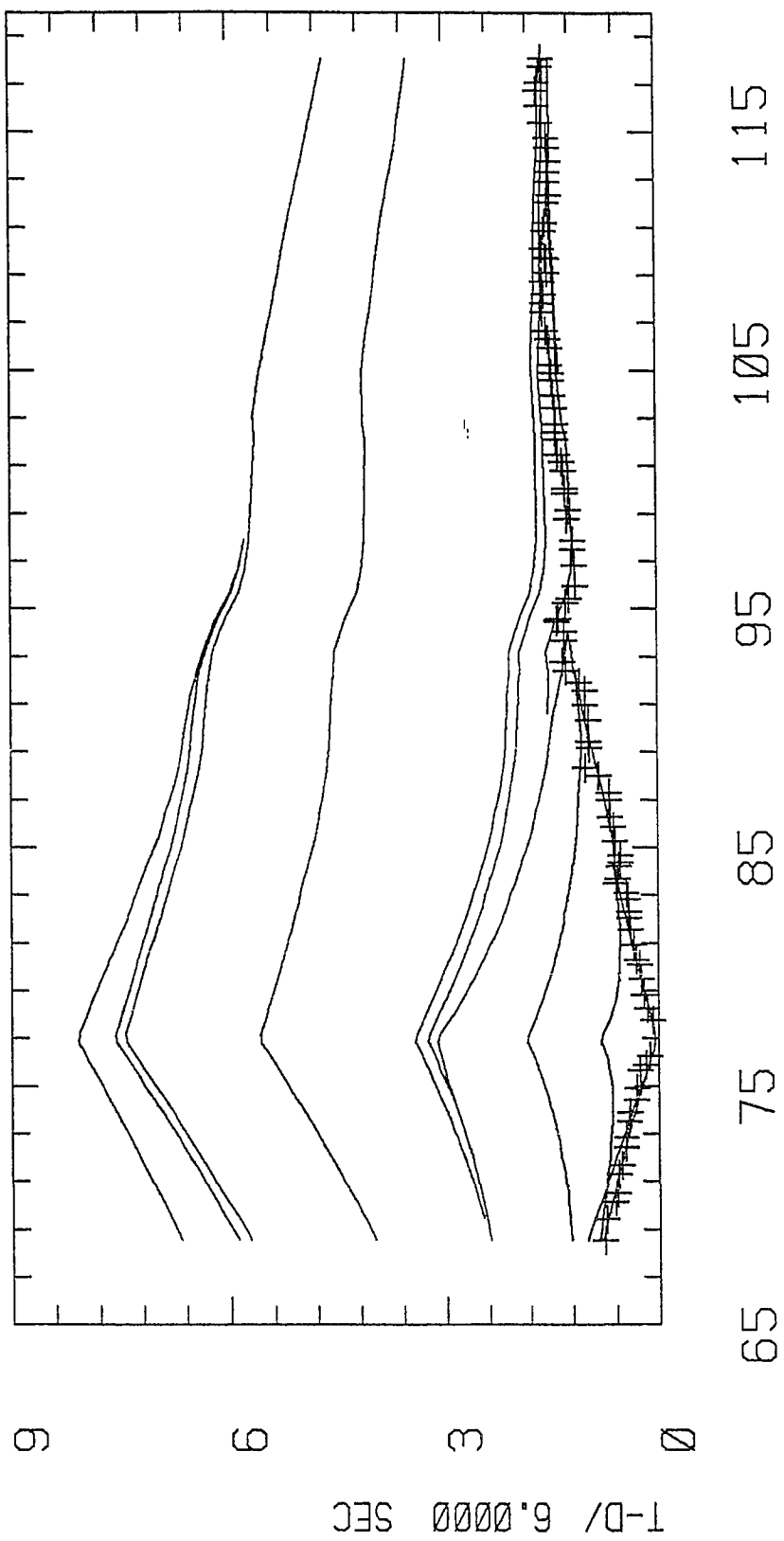
DISTANCE IN KM



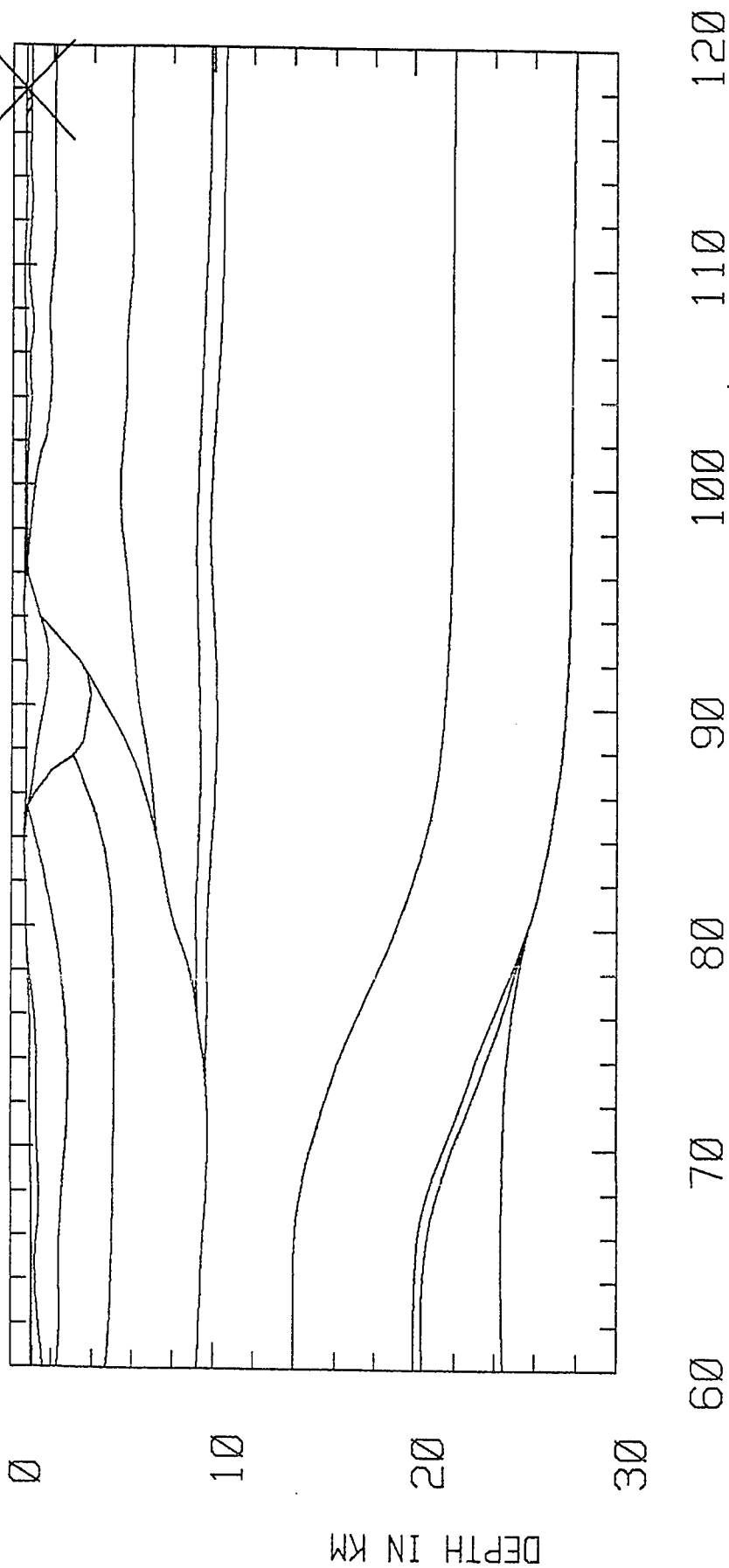


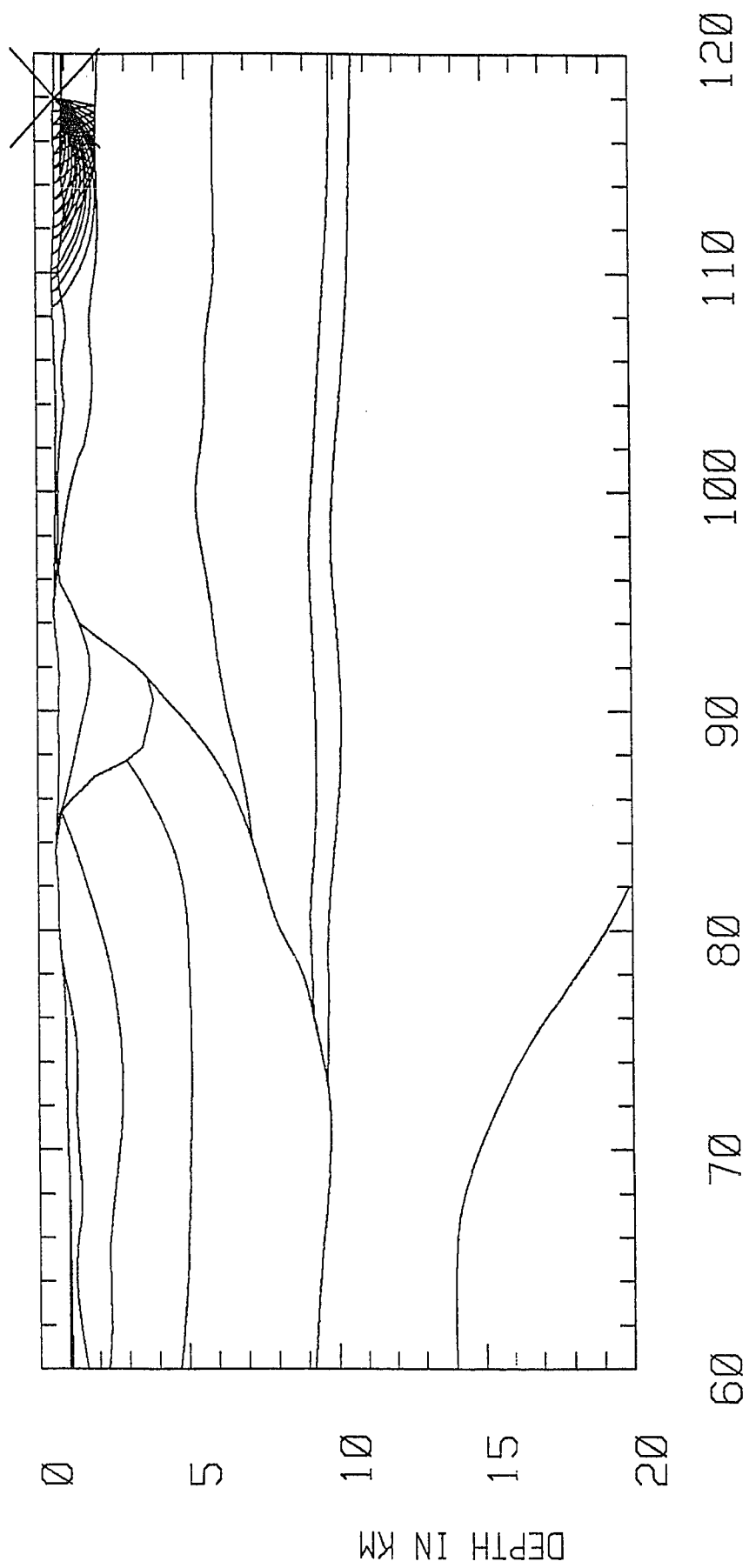
DISTANCE IN KM

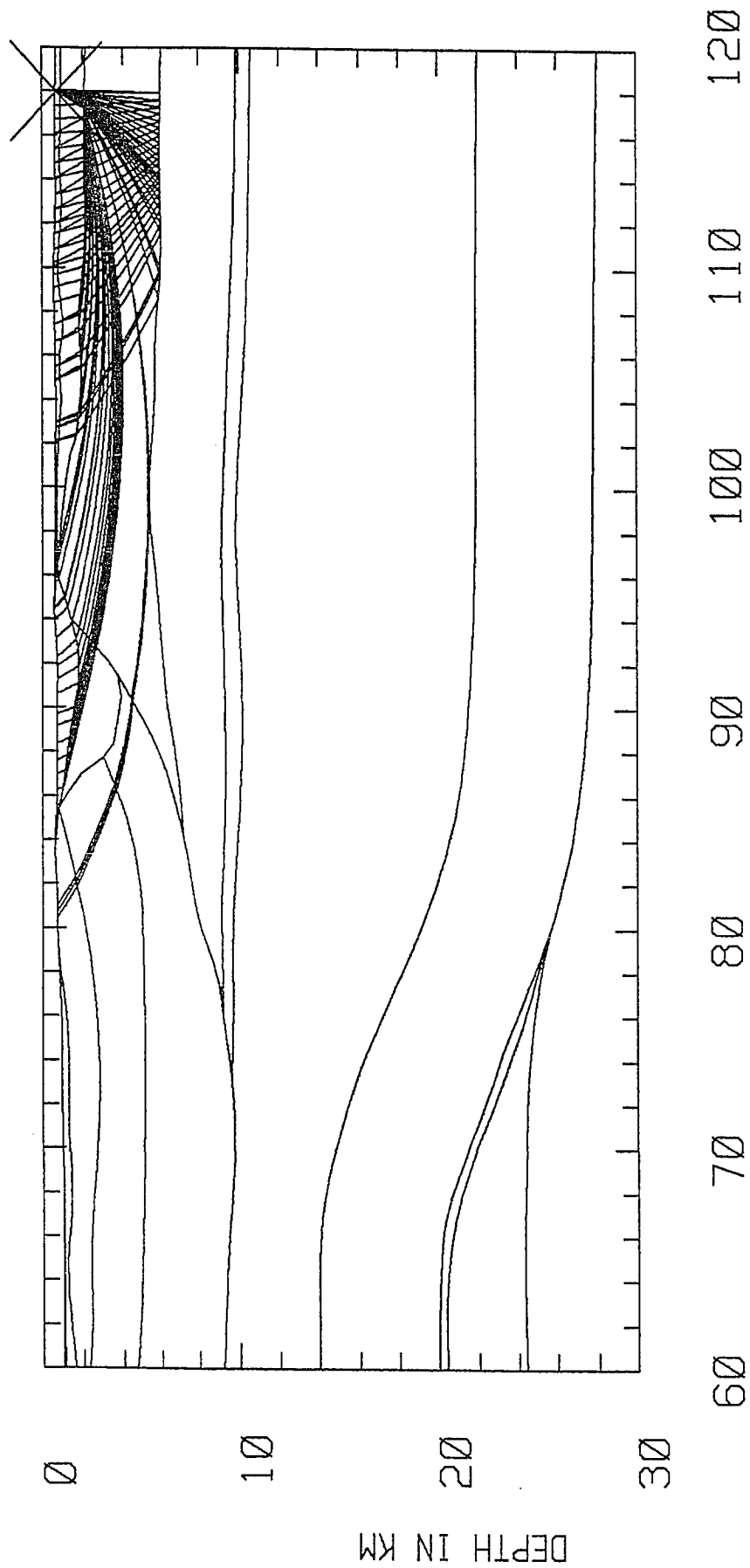




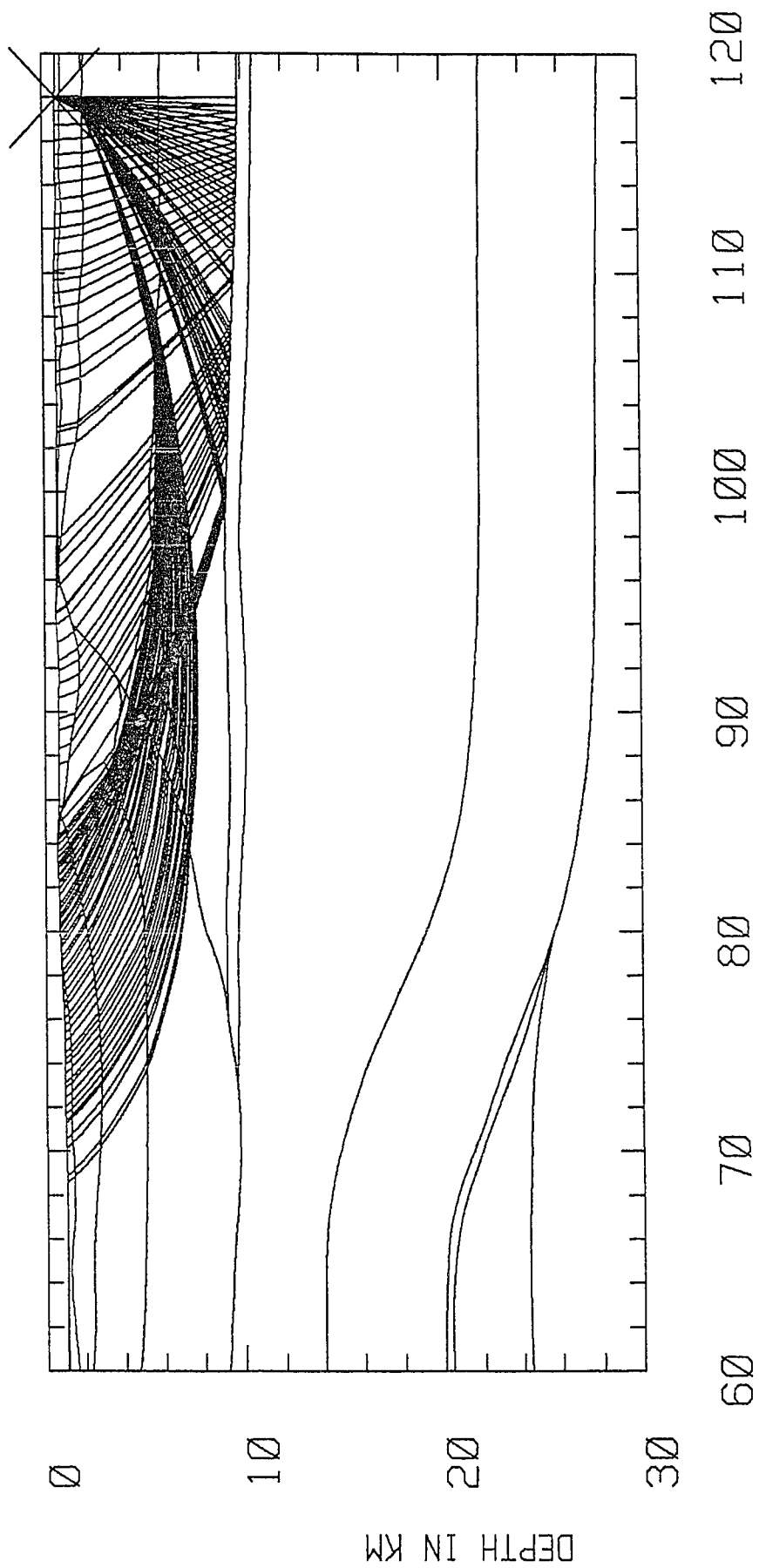
~~LS 2~~



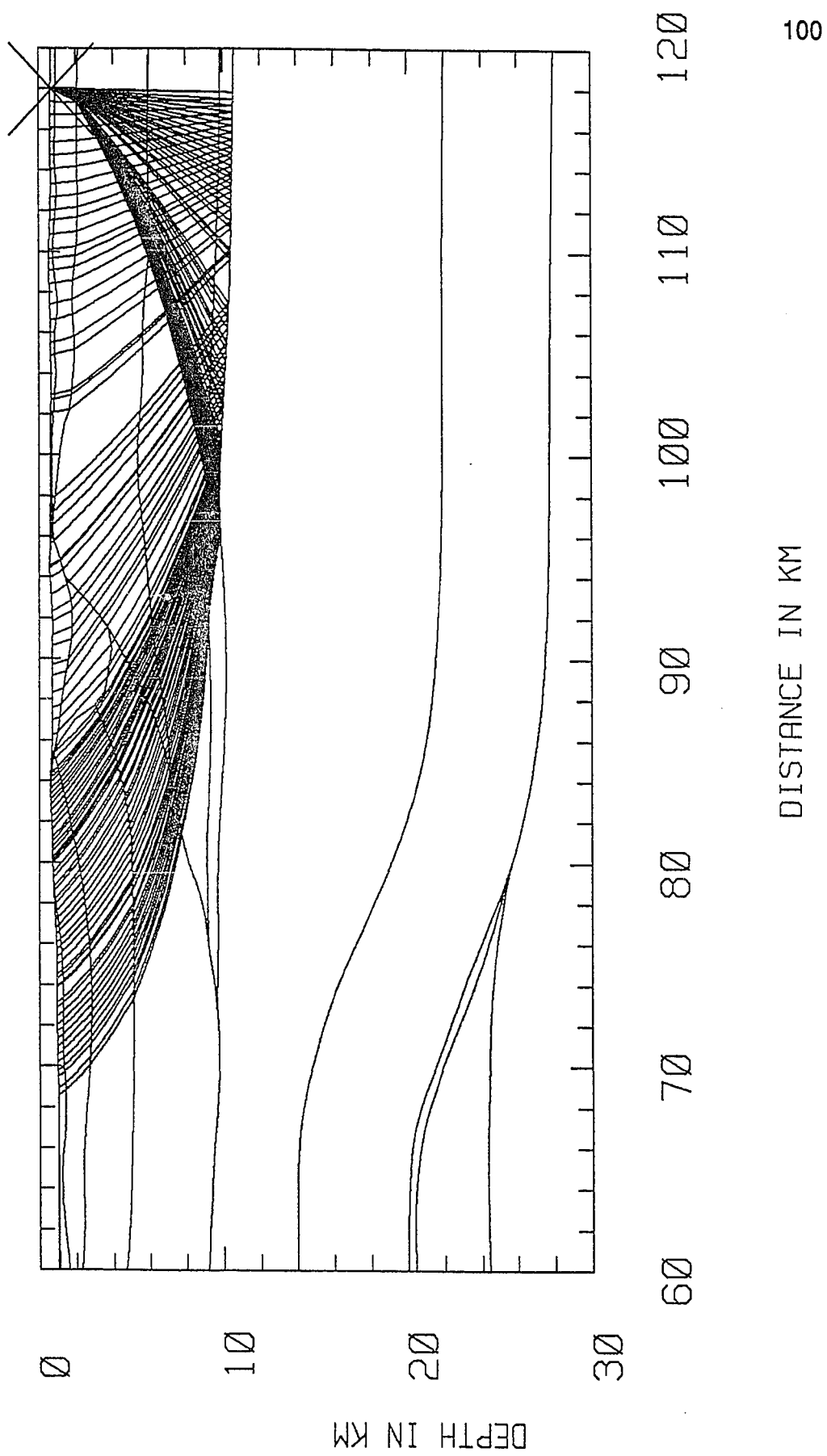


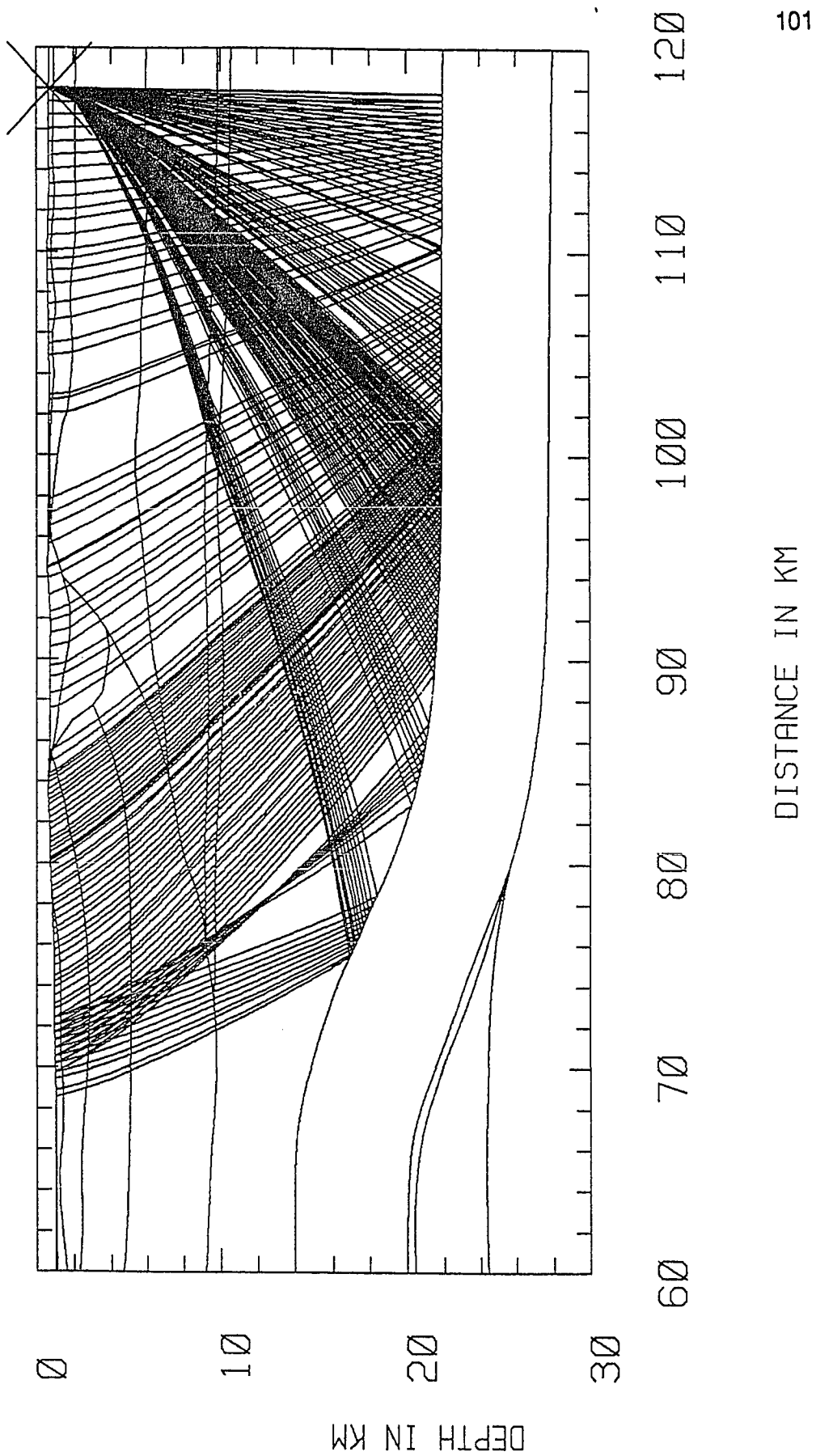


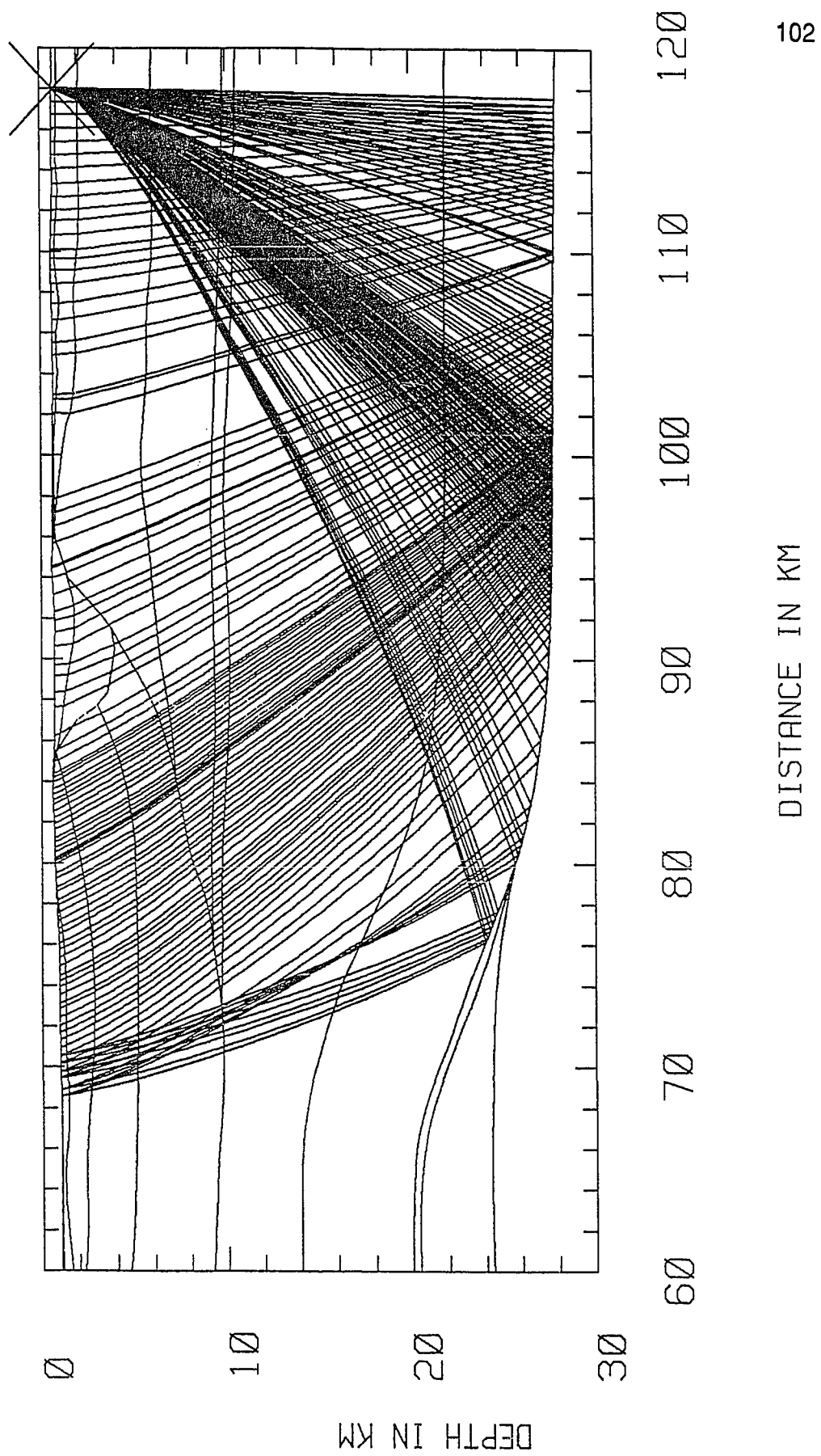
DISTANCE IN KM

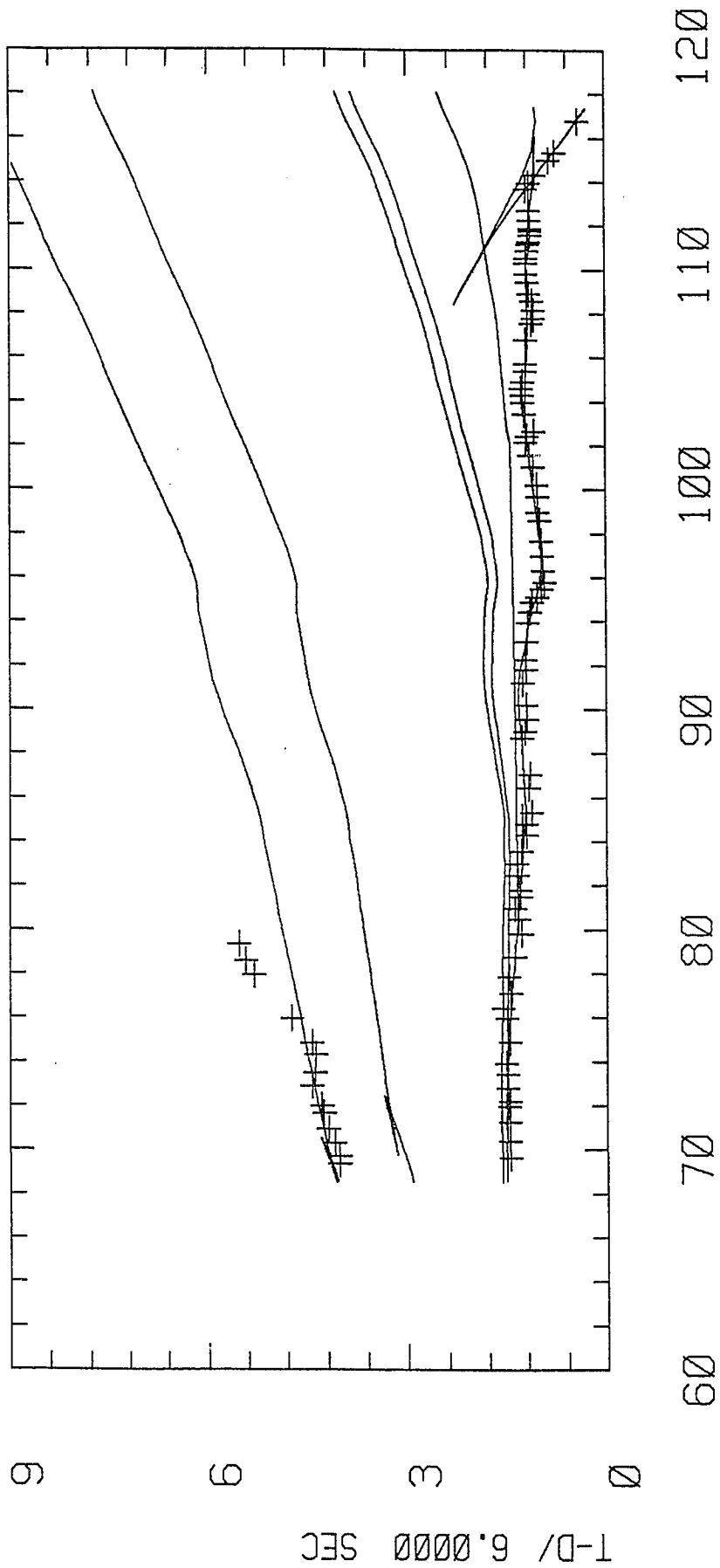


DISTANCE IN KM

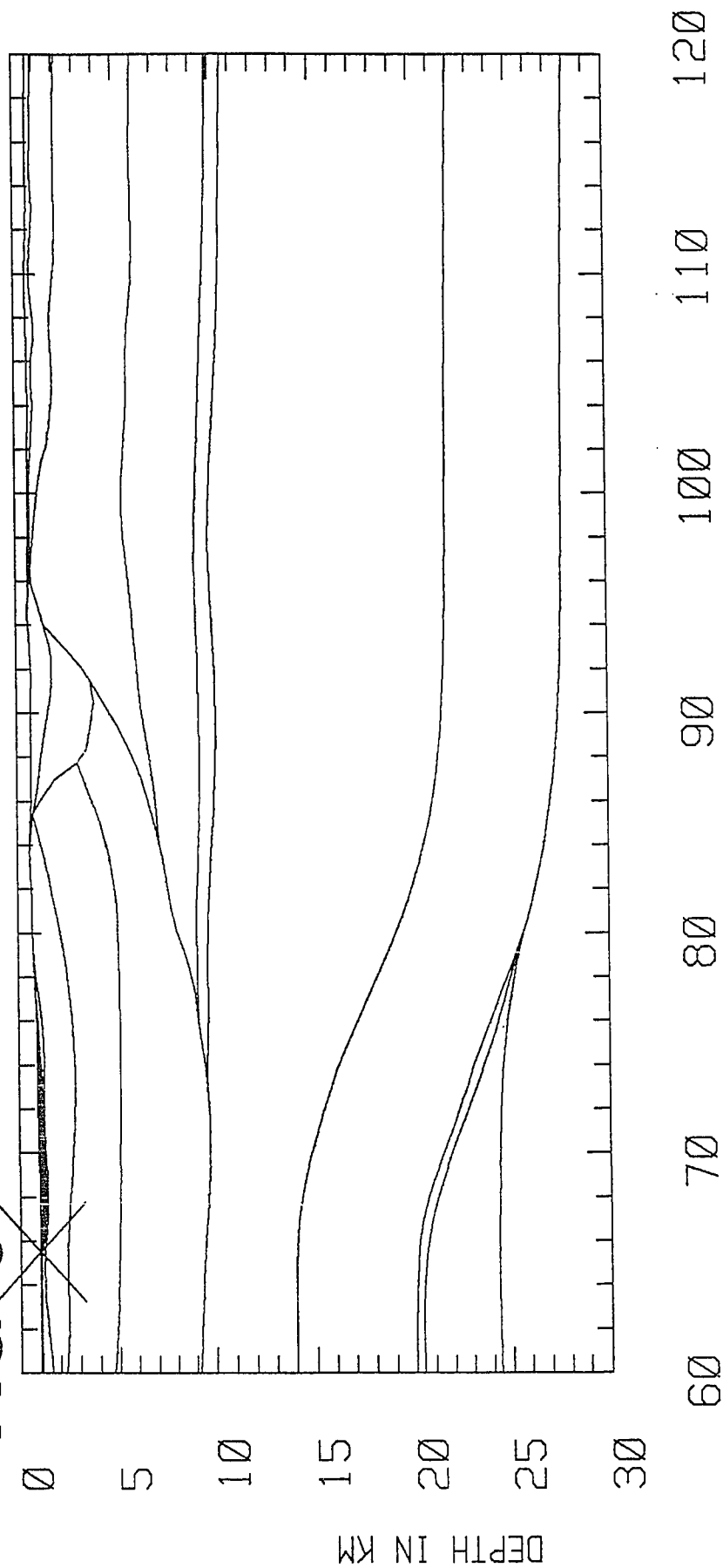


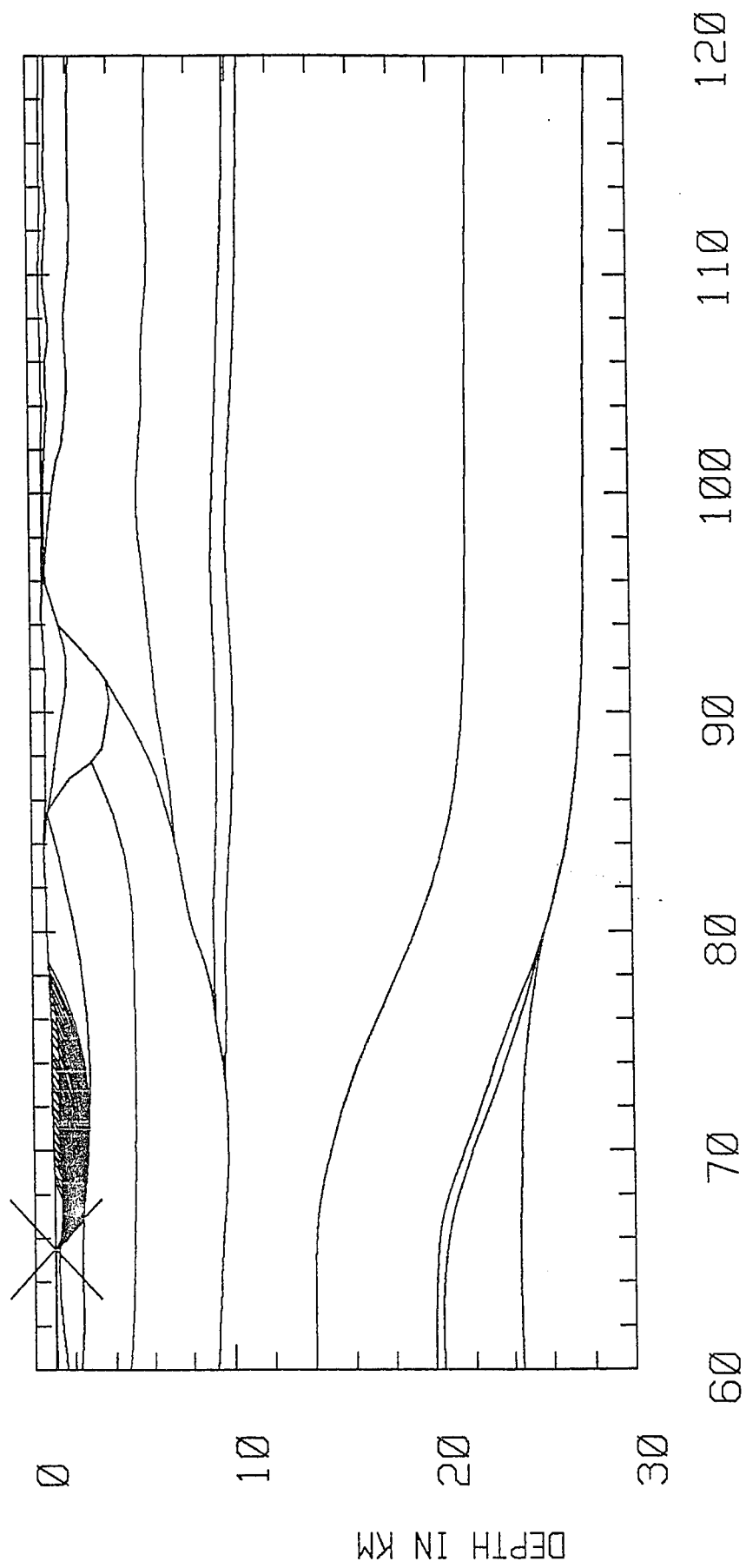


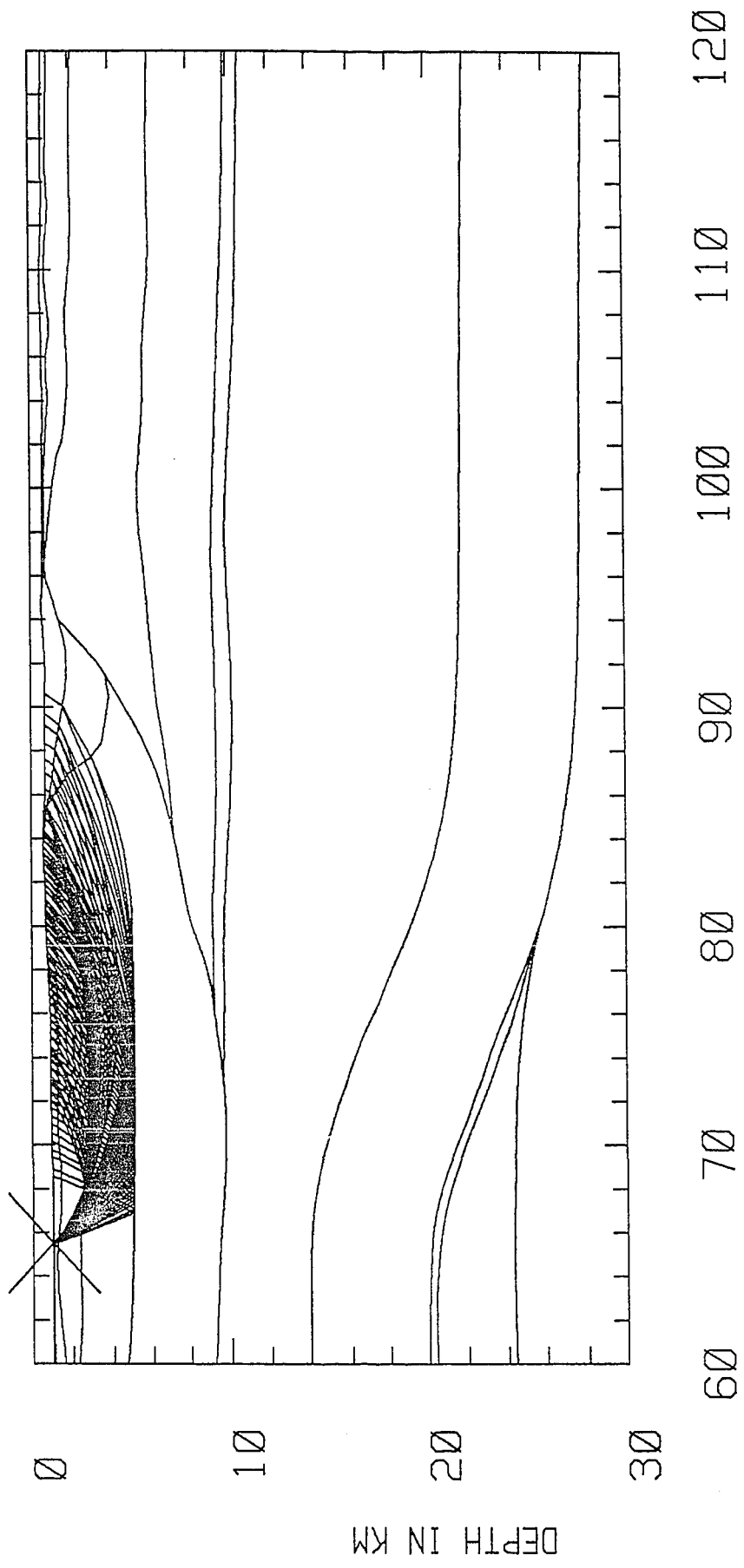


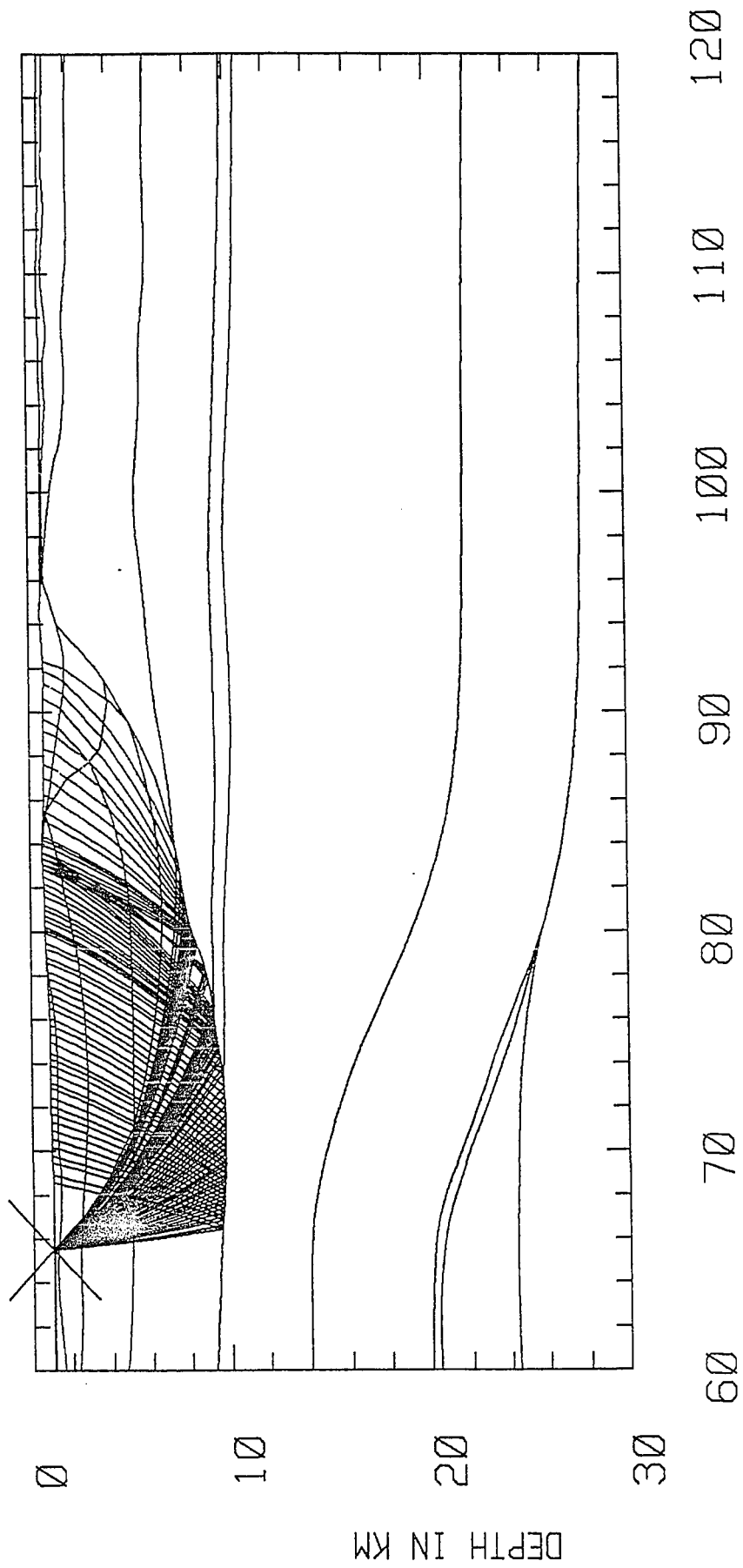


AG 6

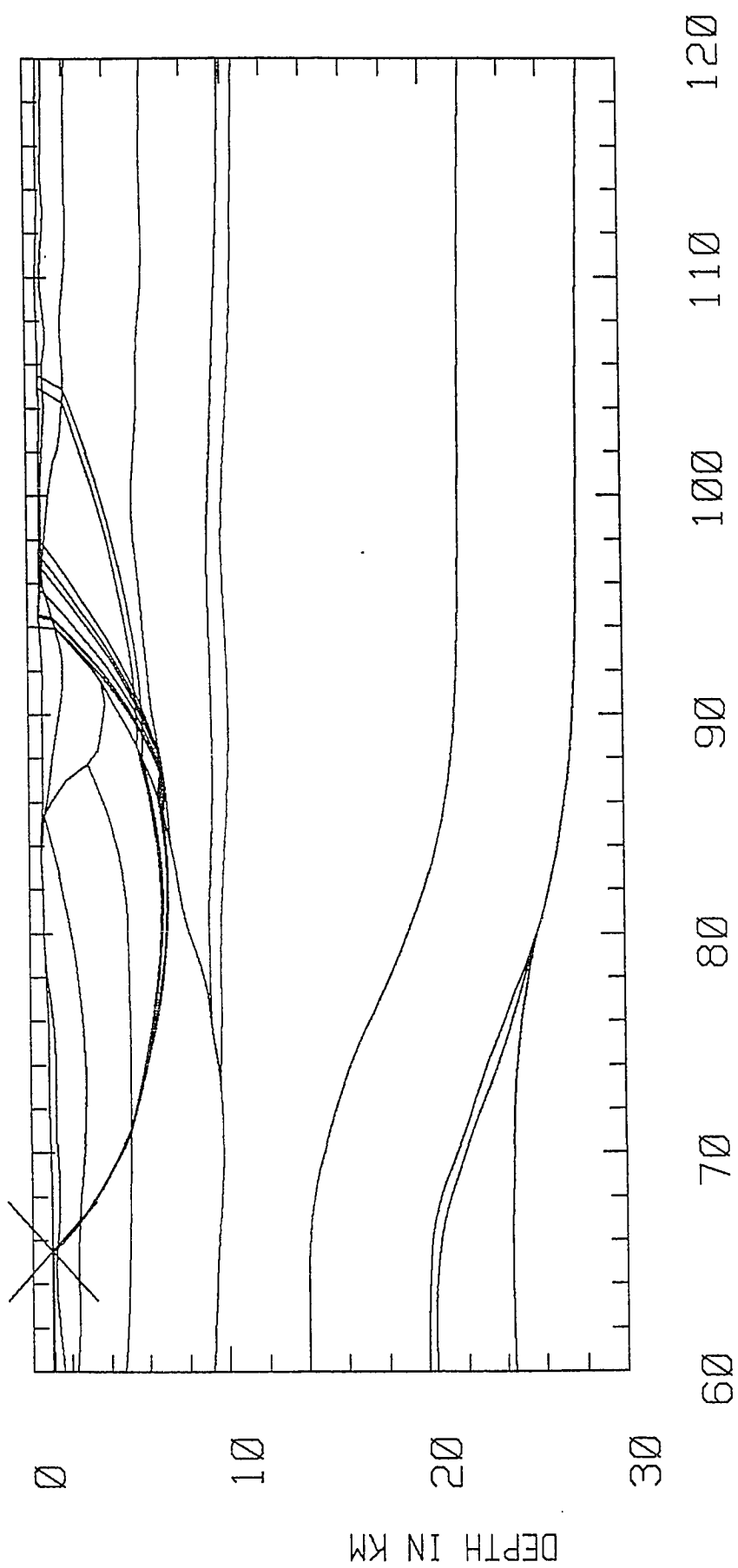


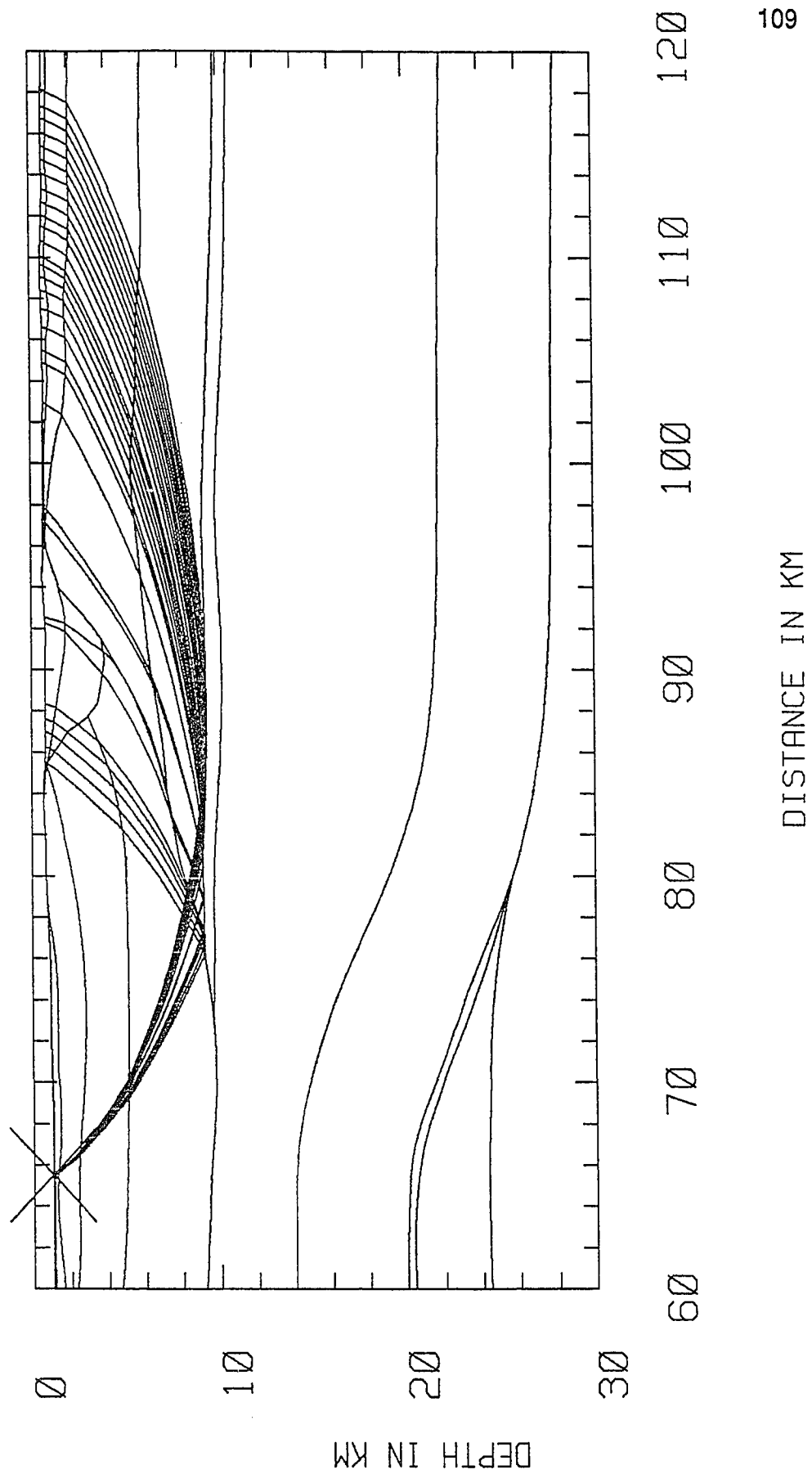


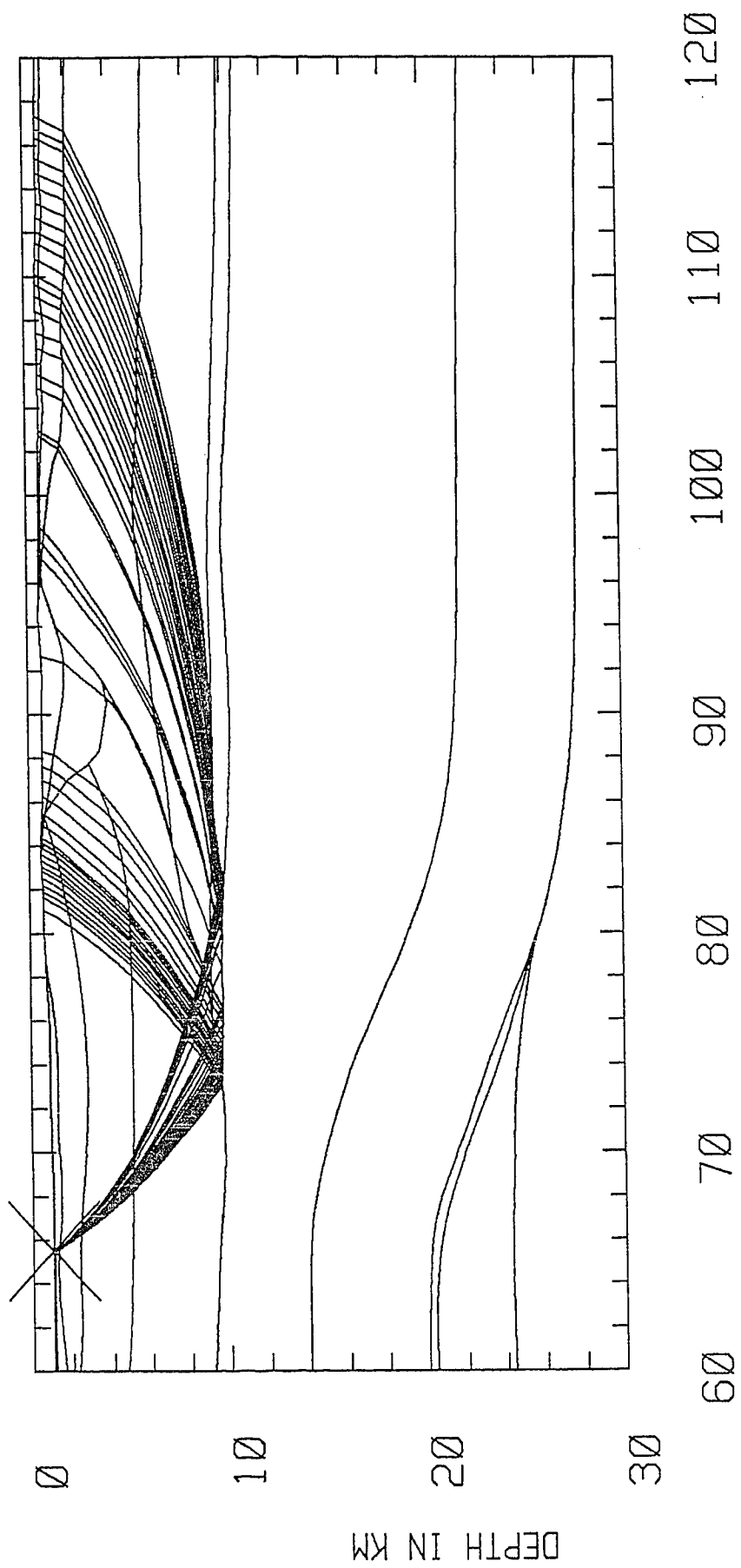


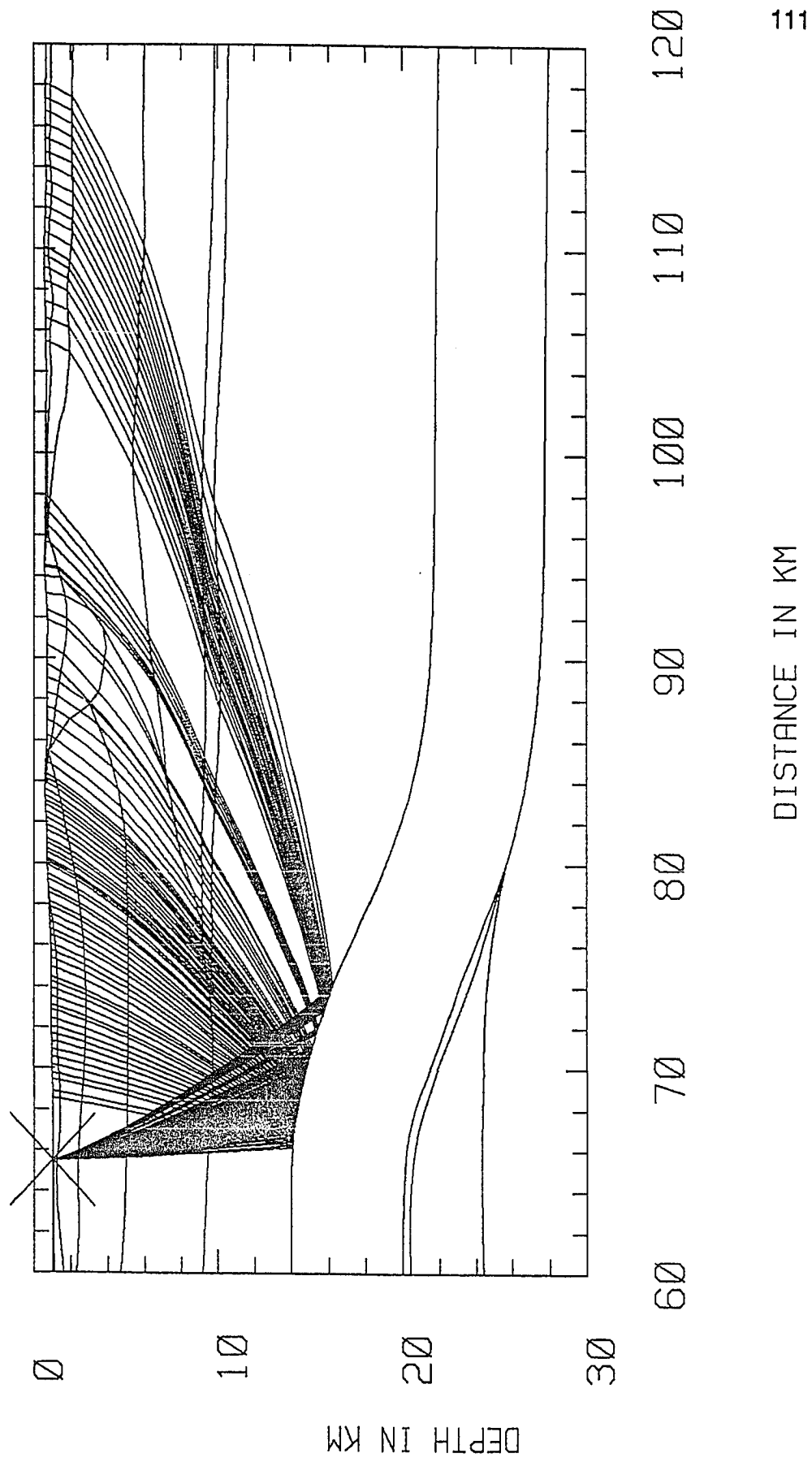


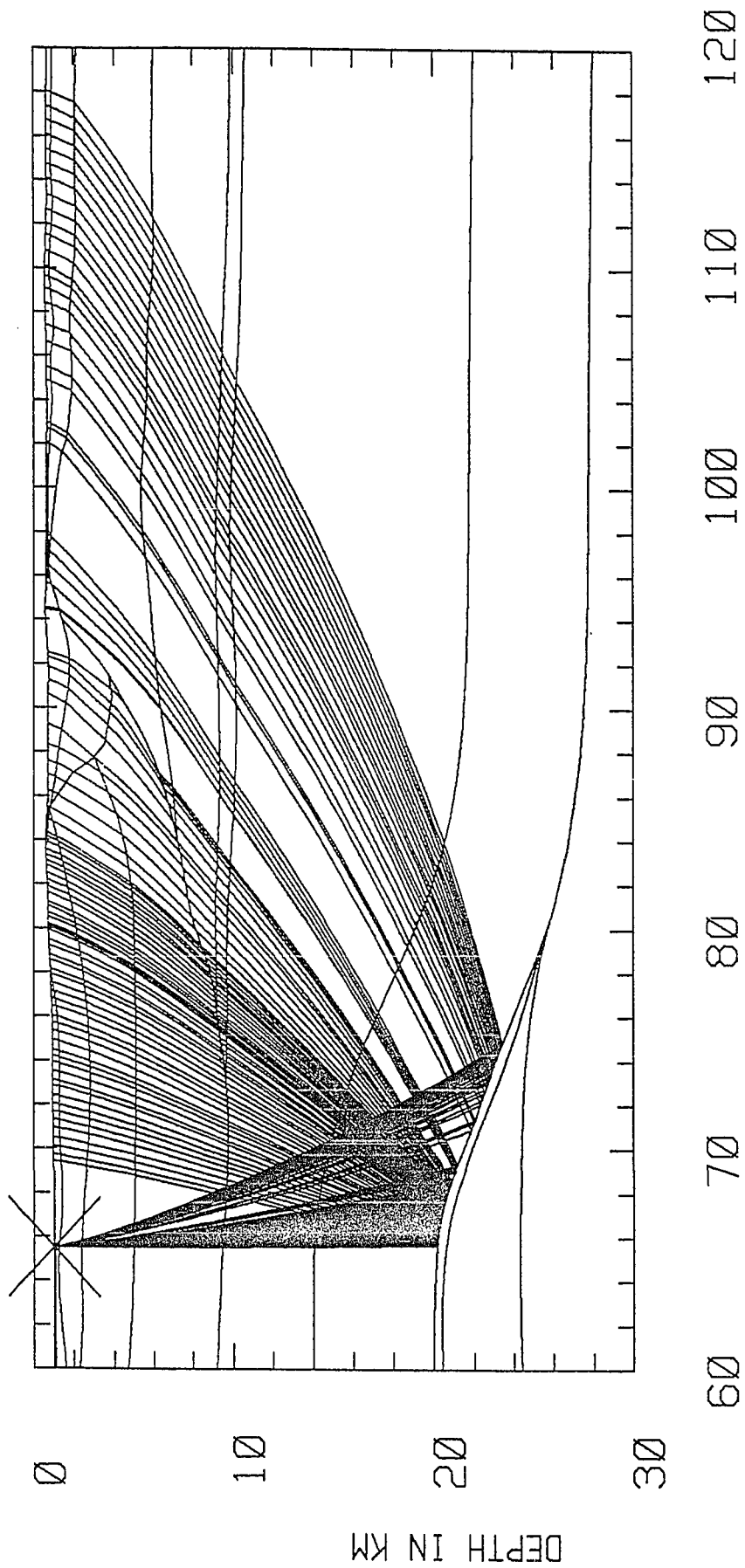
DISTANCE IN KM

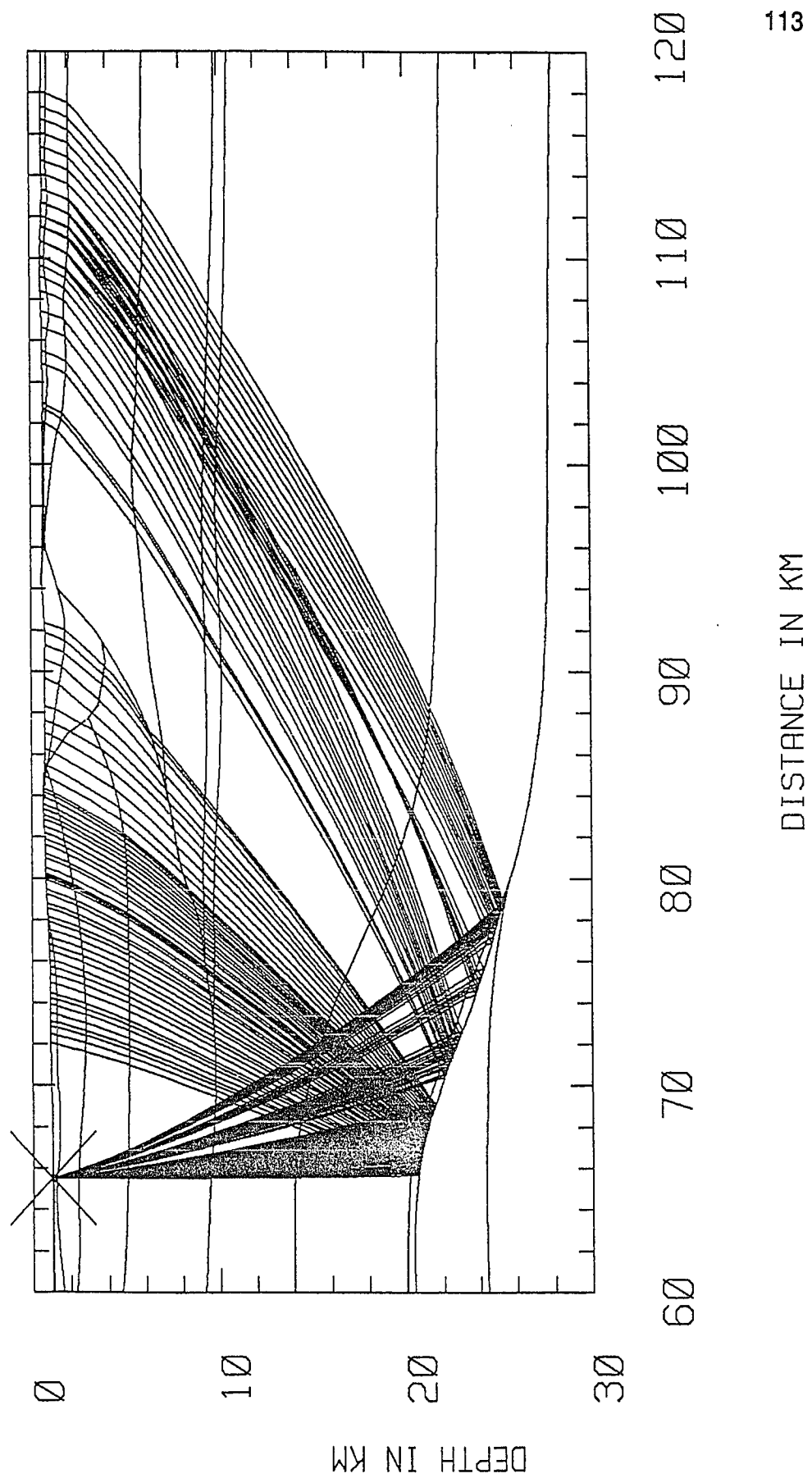


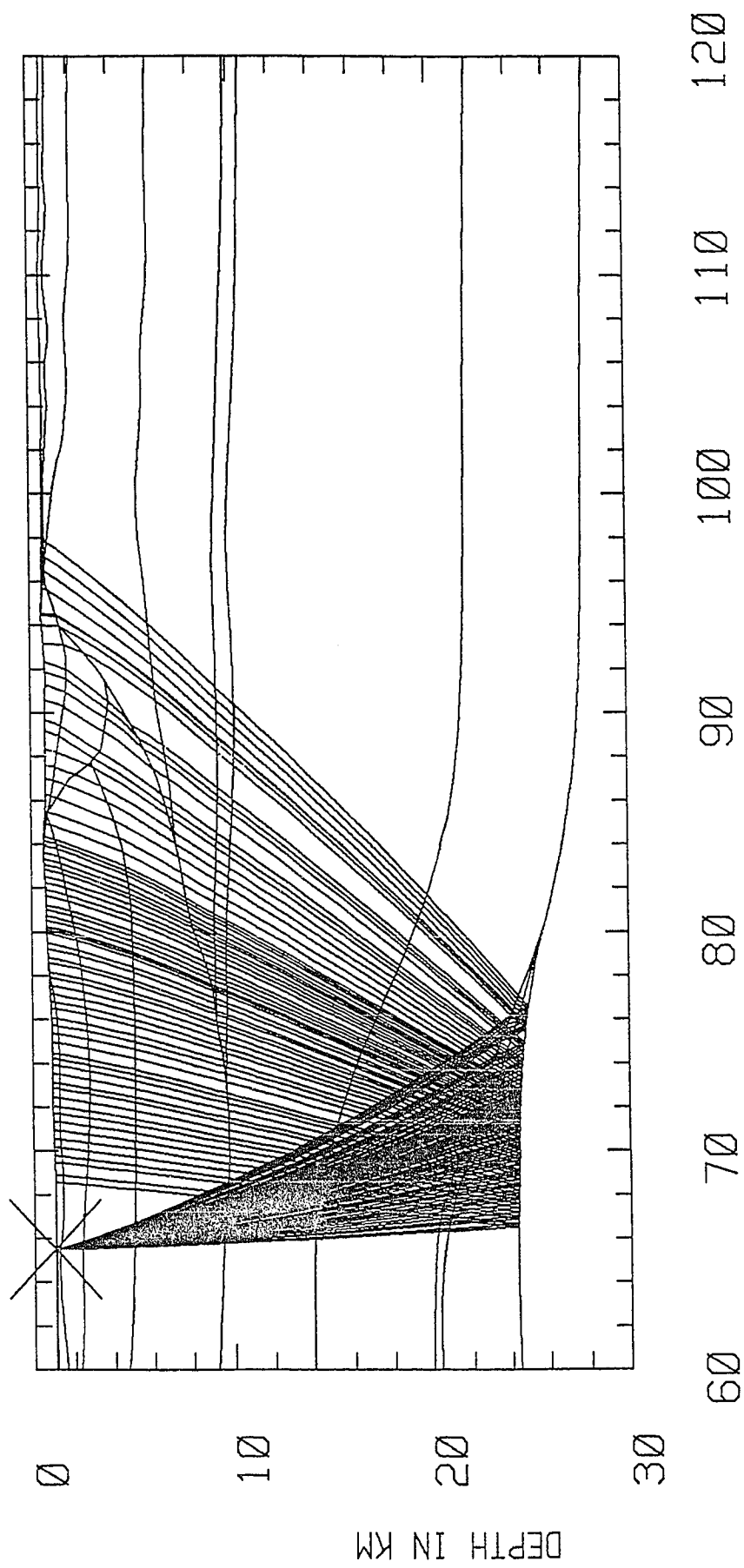


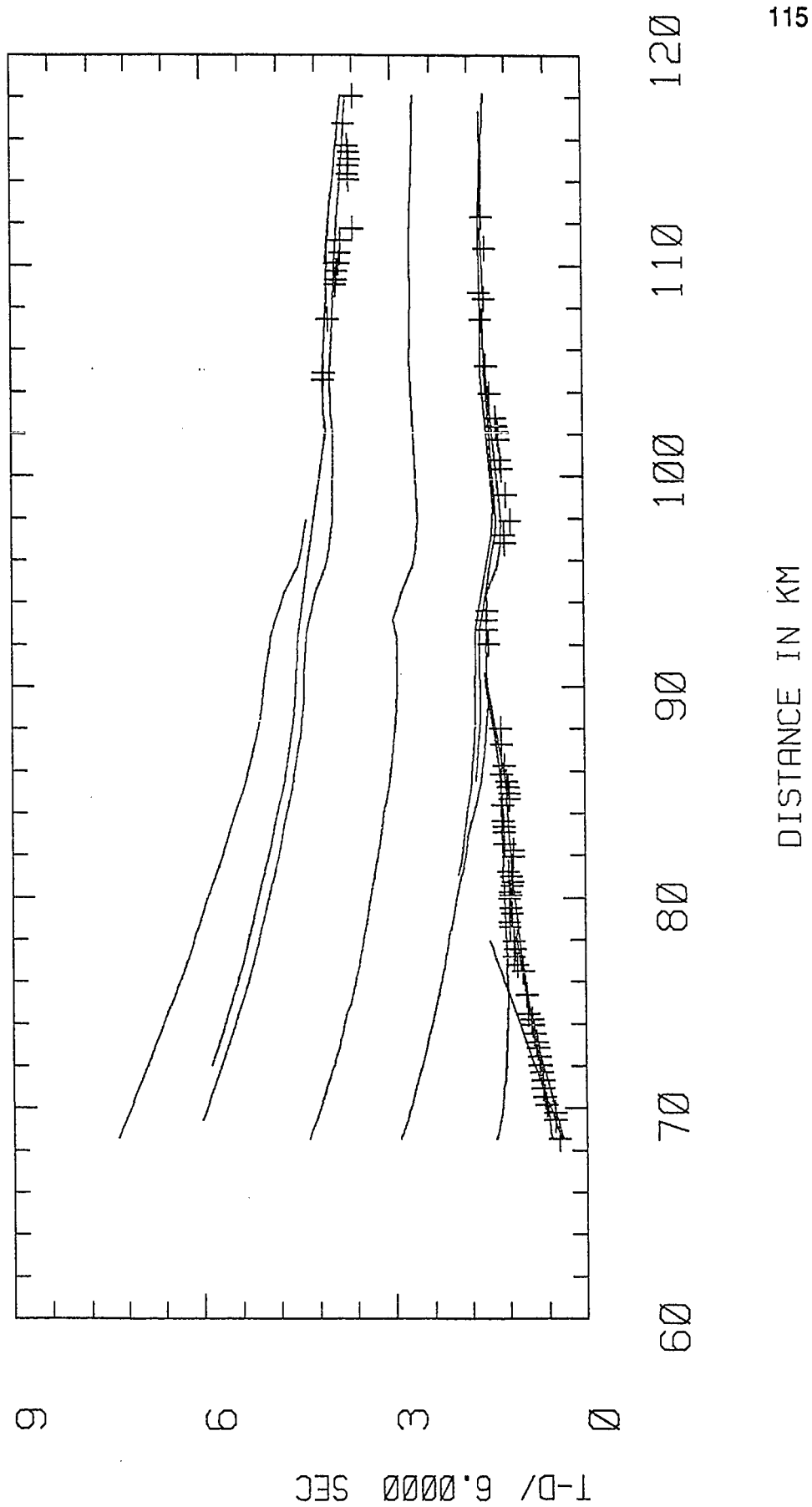












Appendix B

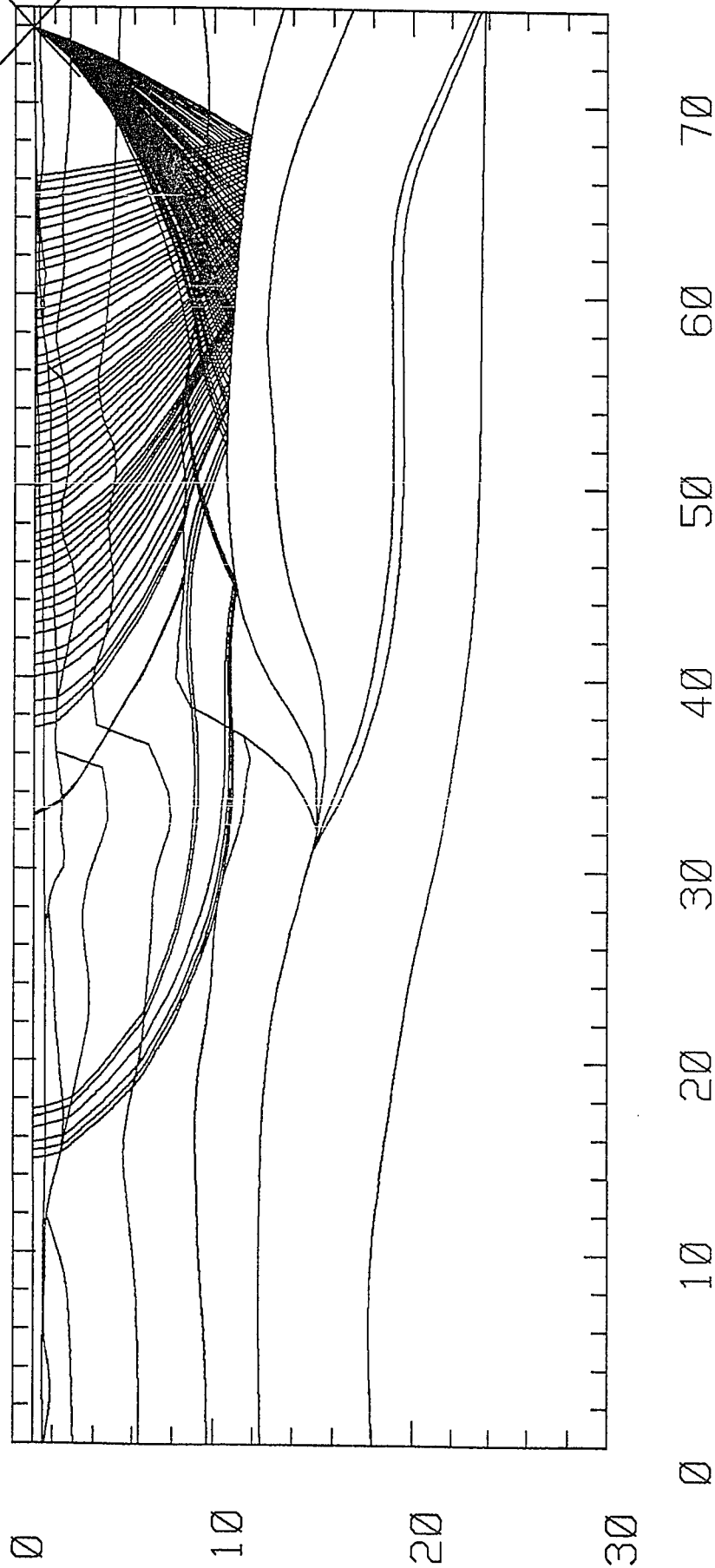
Ray diagrams for Velocity Model 2 (Figure 14) from:

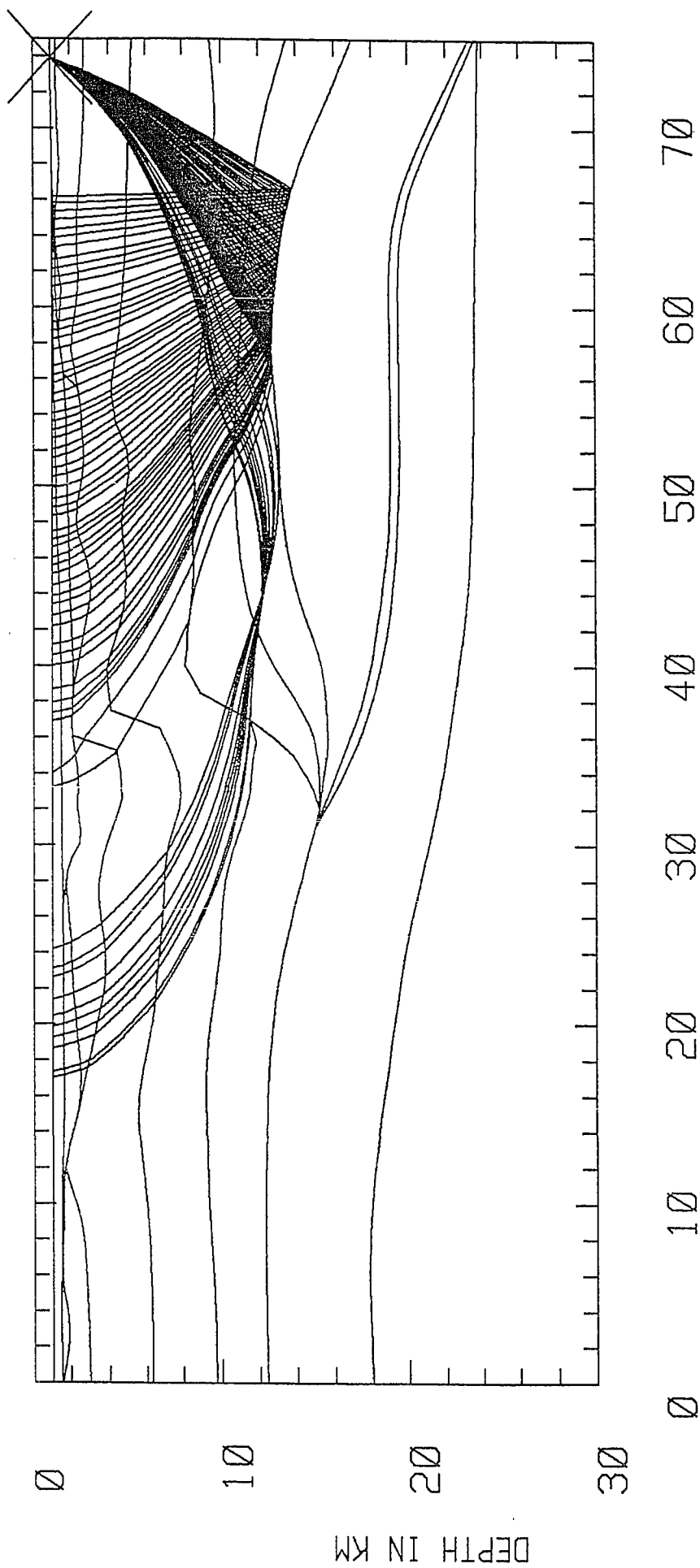
- A) Receiver 15
- B) Land Shot 1
- C) Land Shot 2
- D) Airgun Shot 6

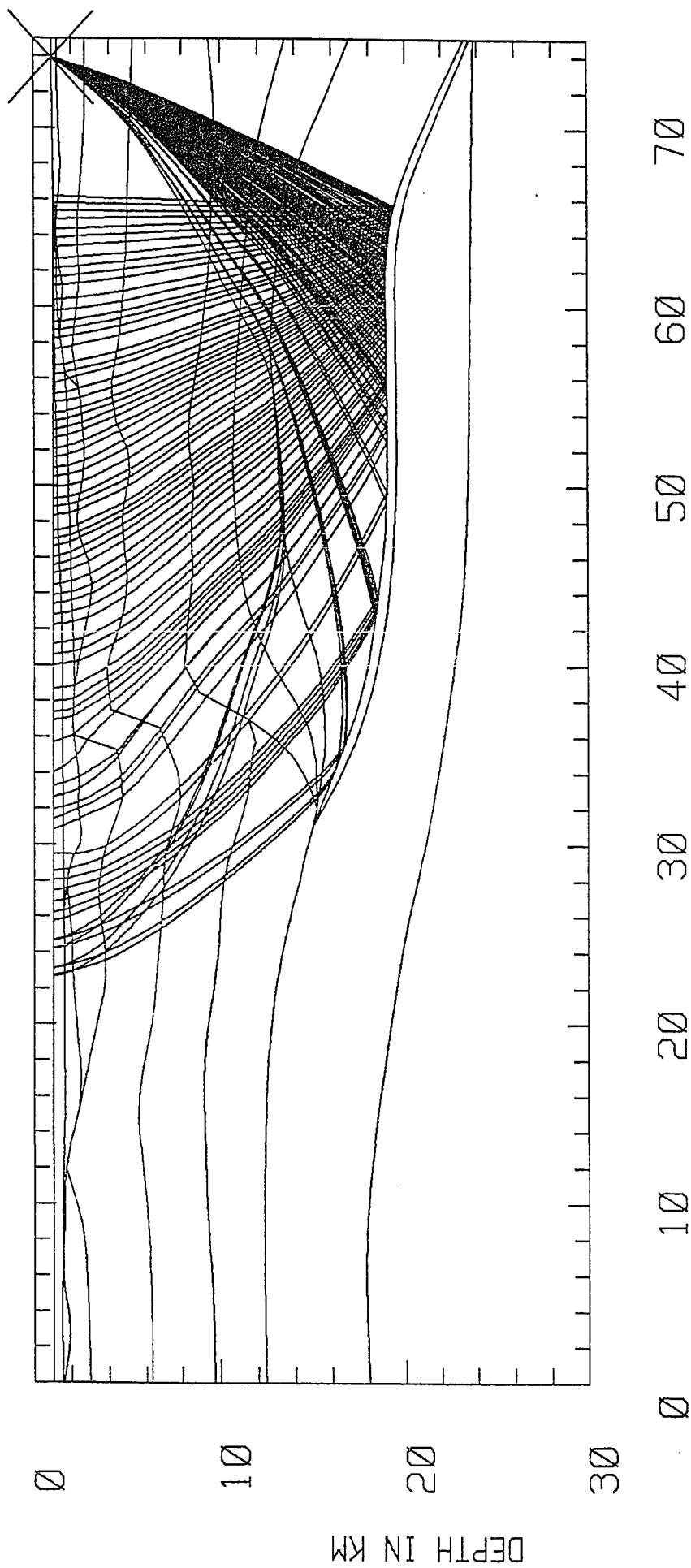
Travel time curves are included at the end of each section of ray diagrams, along with first break picks from the gathers.

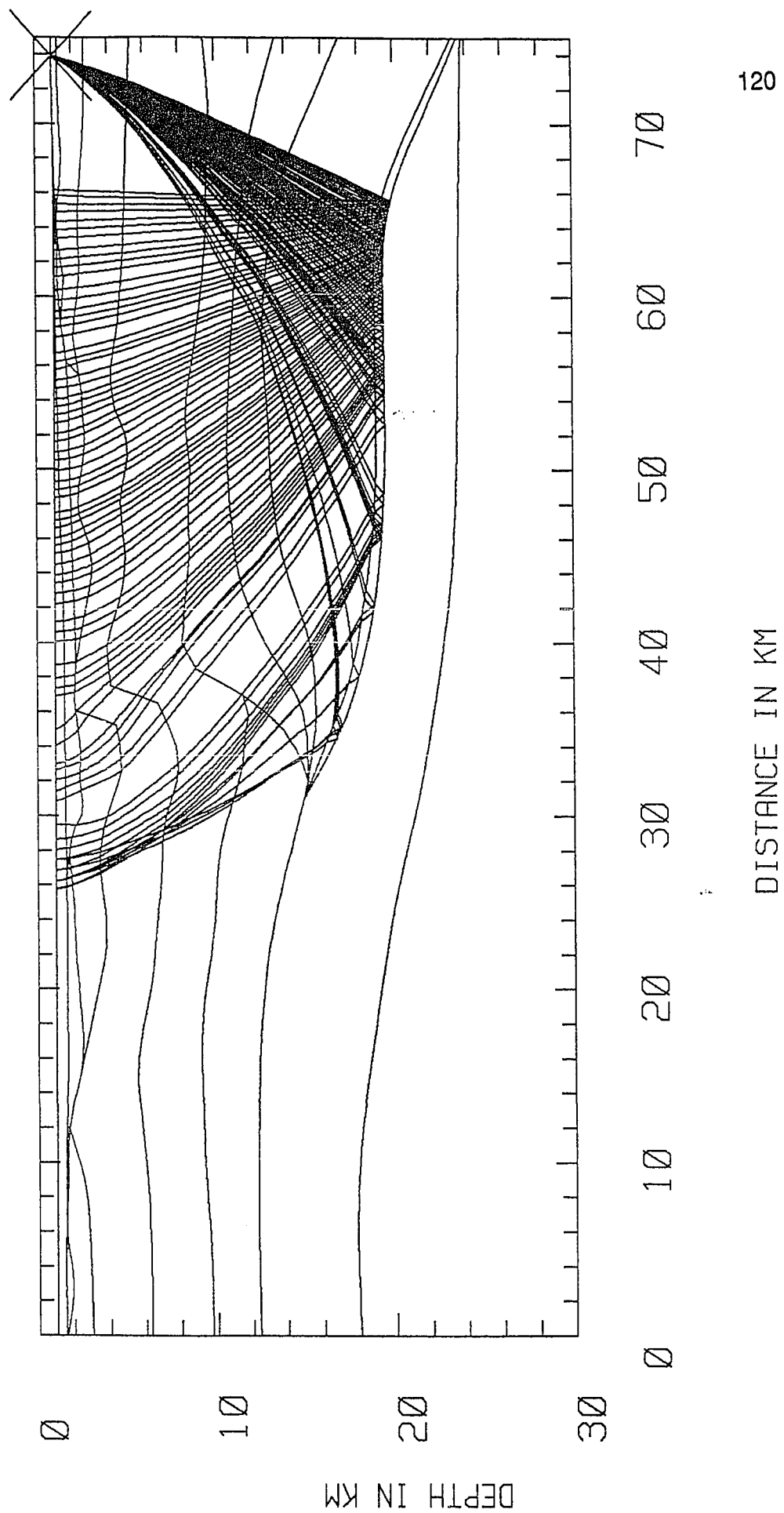
Only the rays through the lower crust are shown. Upper crustal rays are the same as for Velocity Model 1 (Appendix A) since the layering is the same. Rays through Velocity Model 1 from Receiver 15 are shown in Figure 17.

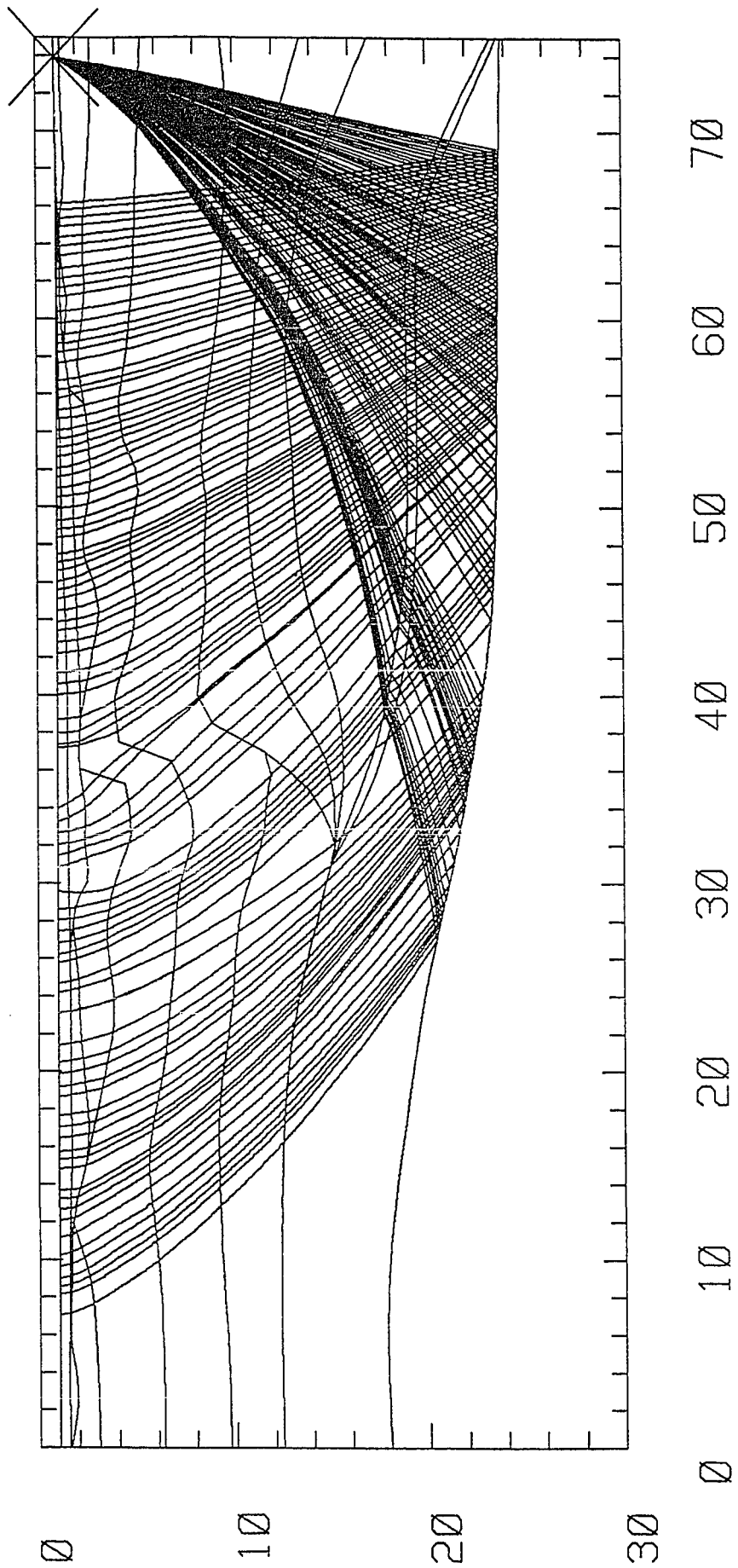
Rcvr 15

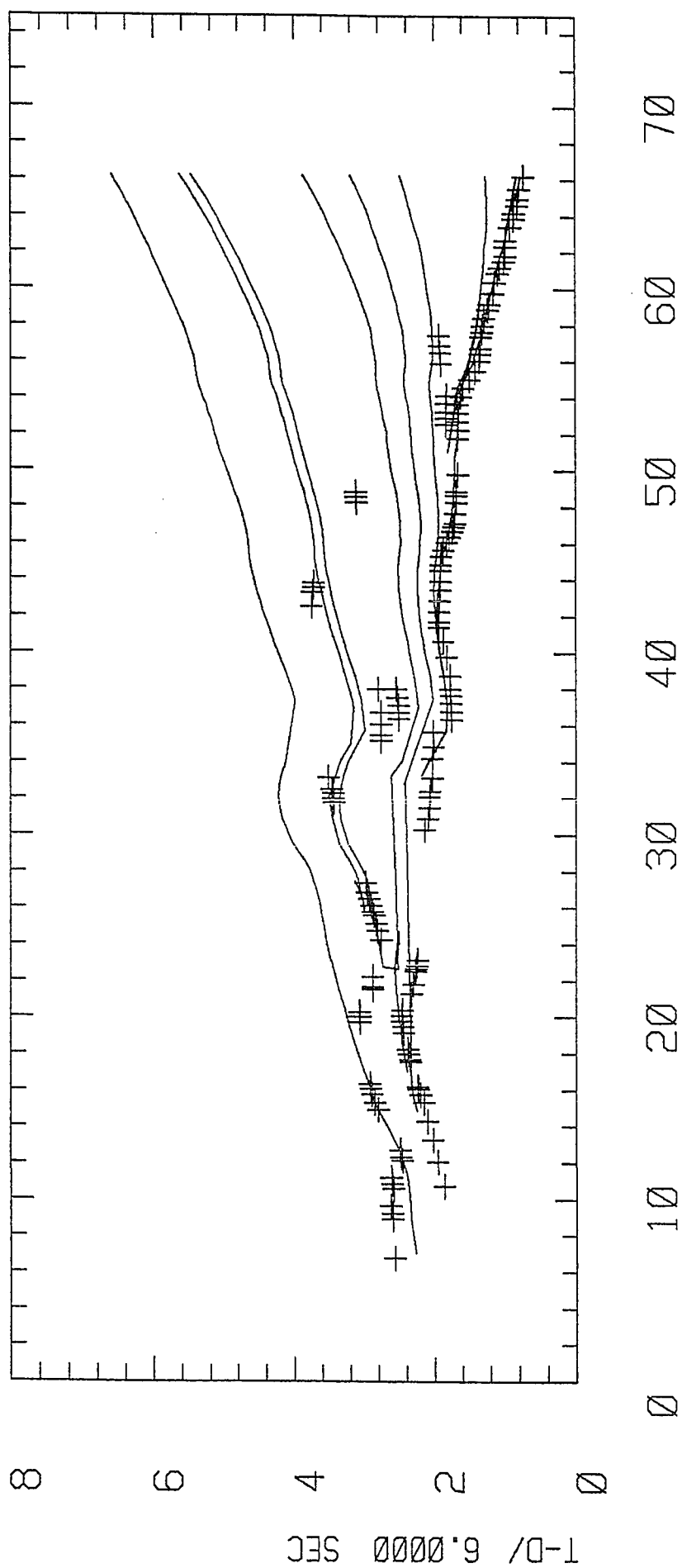


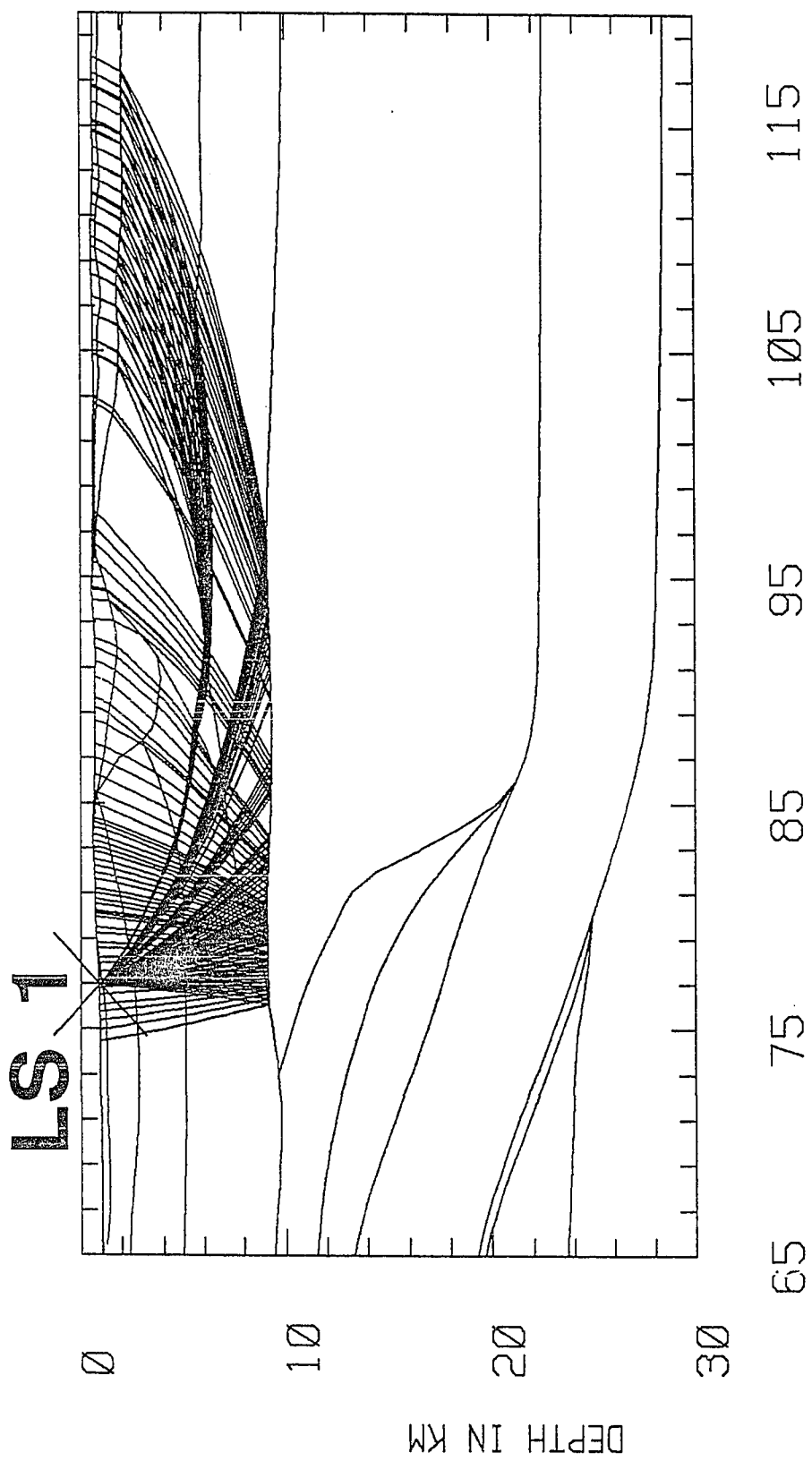




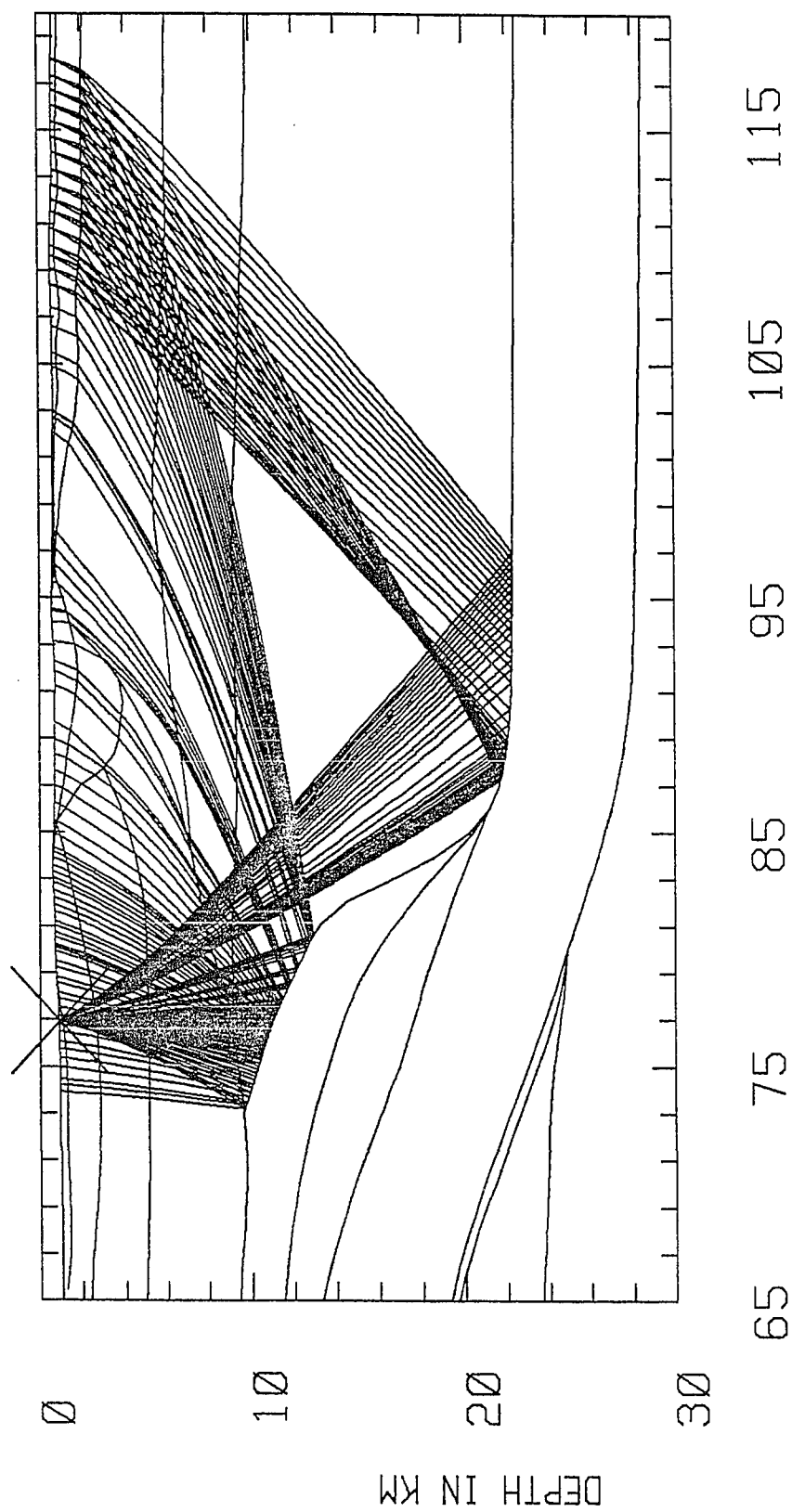


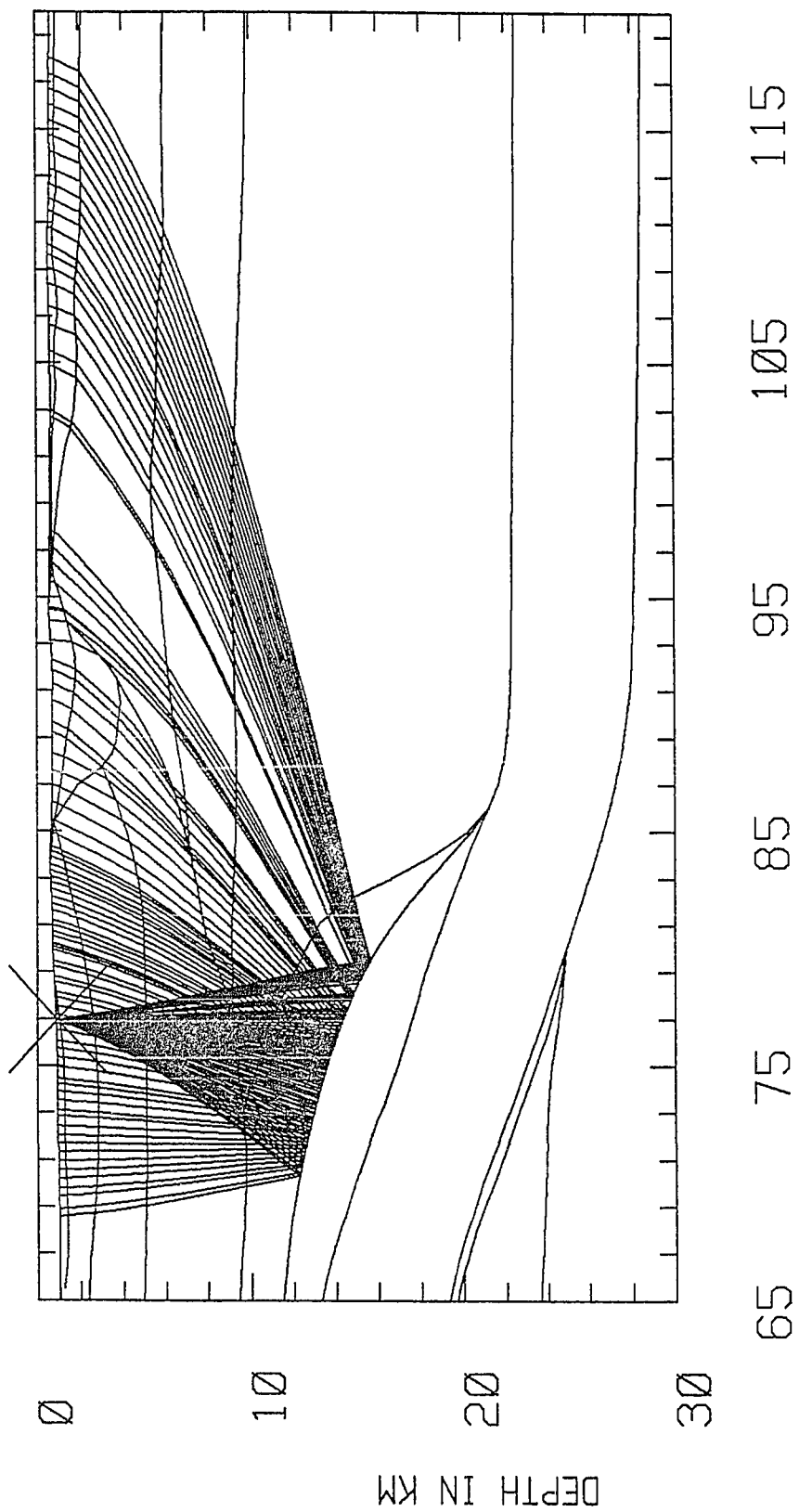


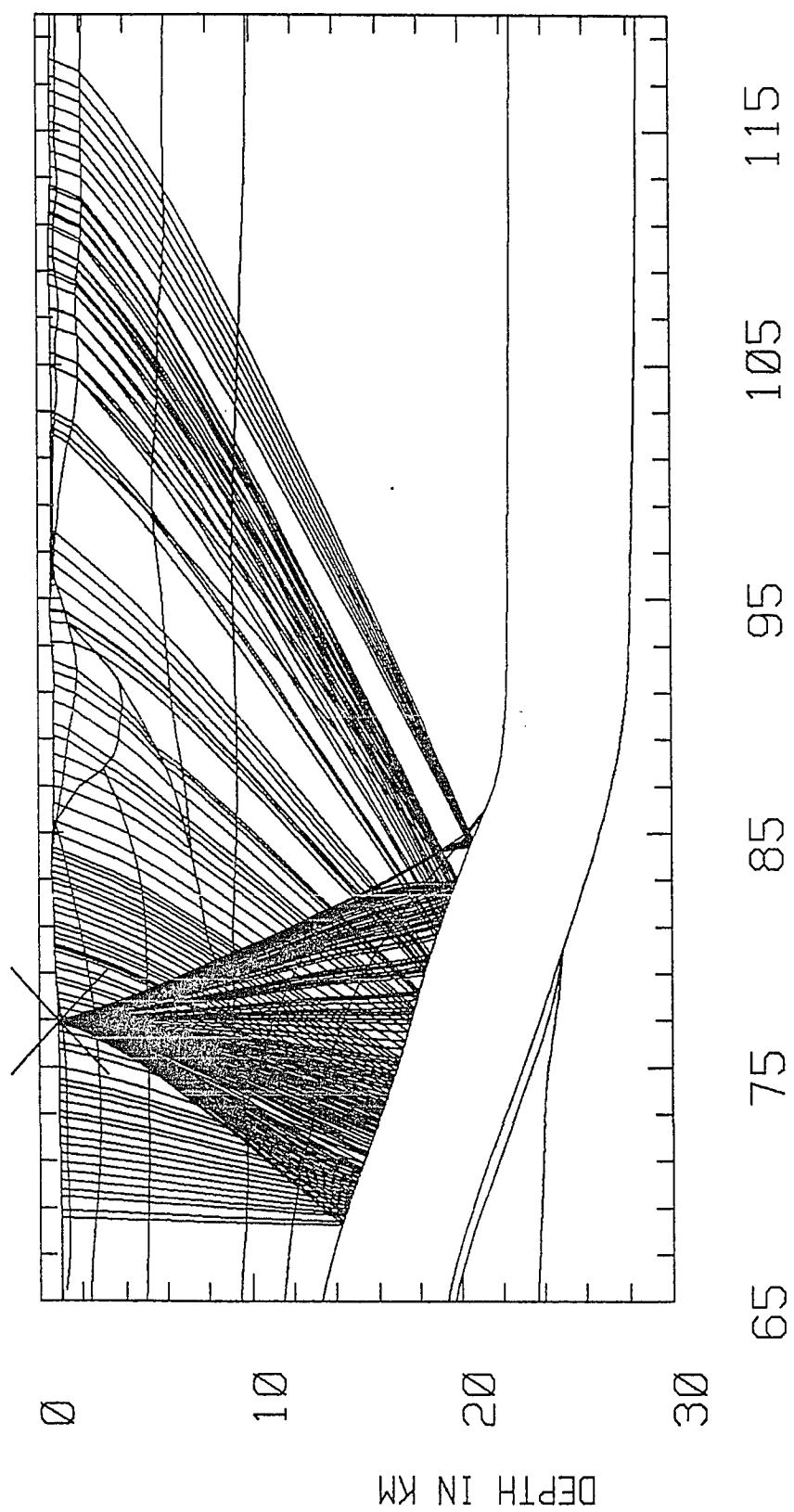


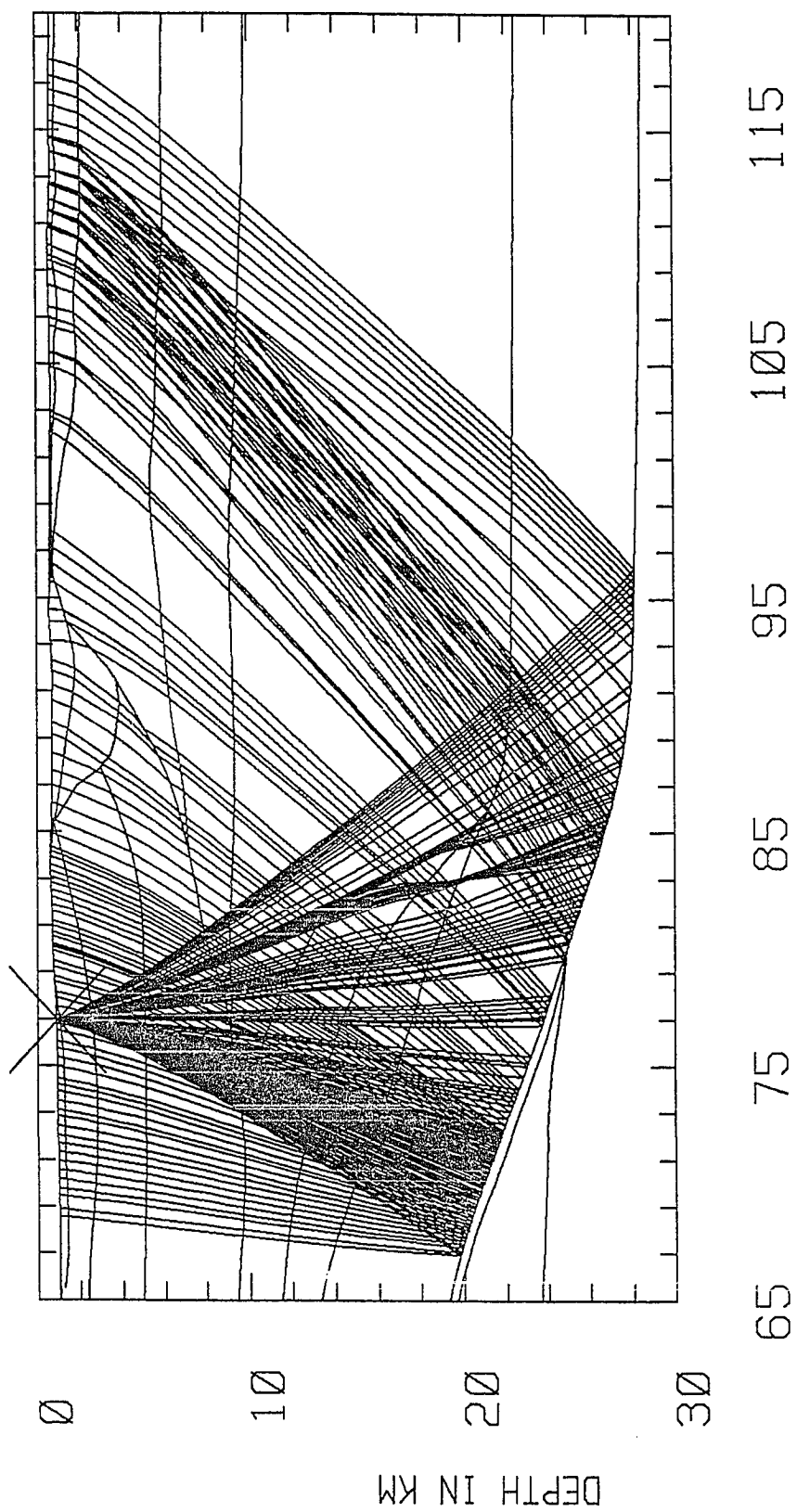


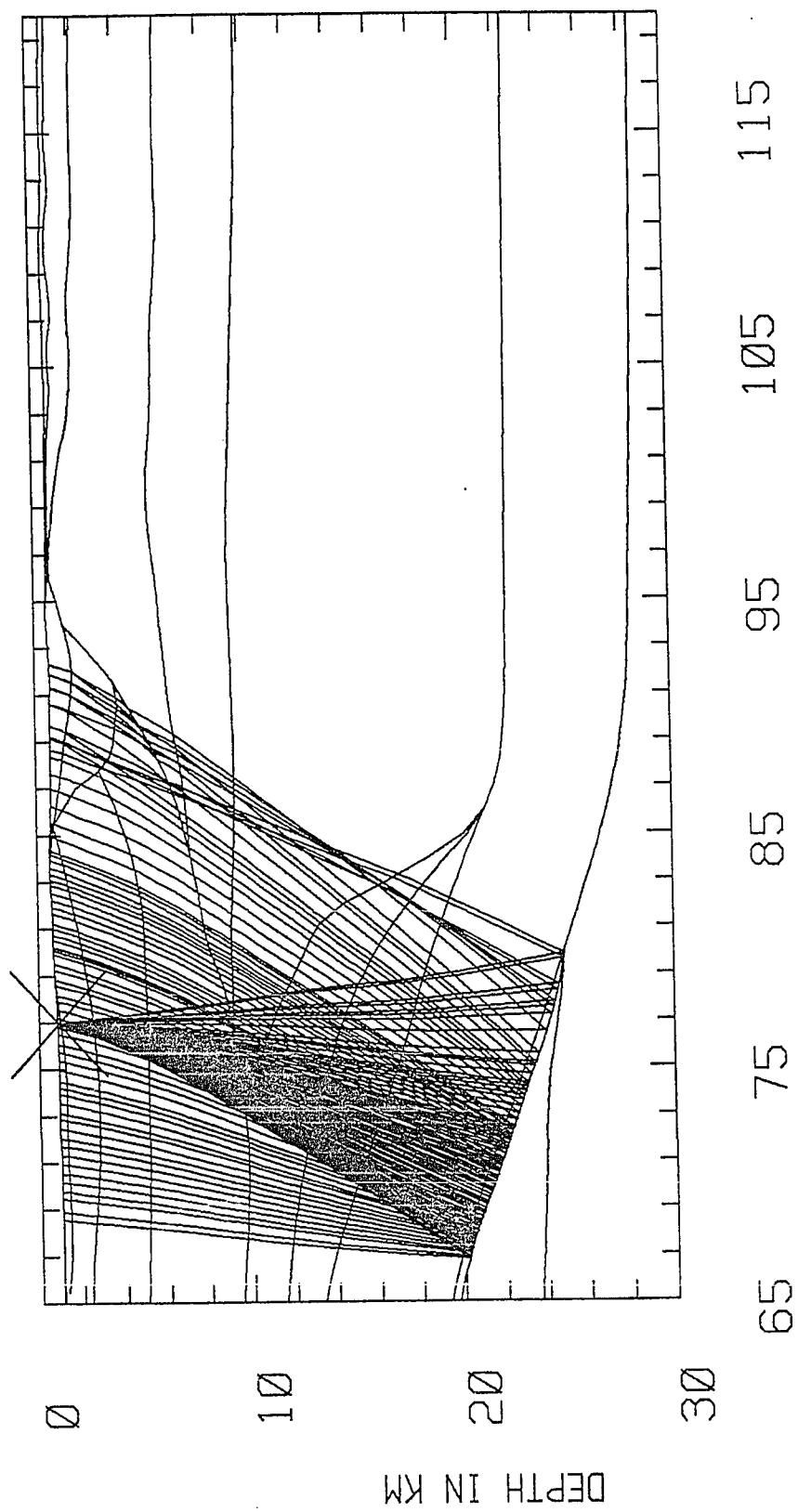
DISTANCE IN KM

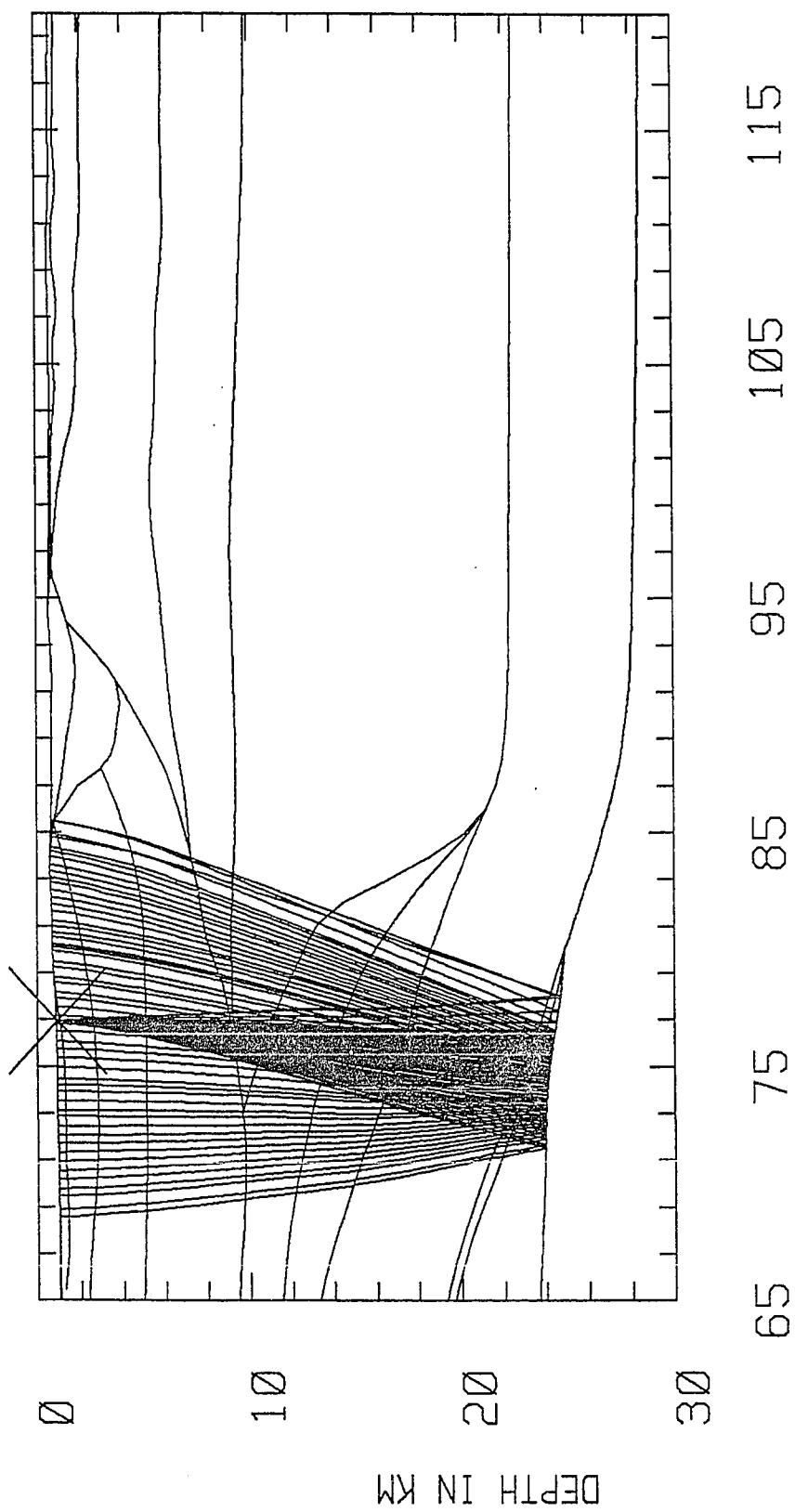


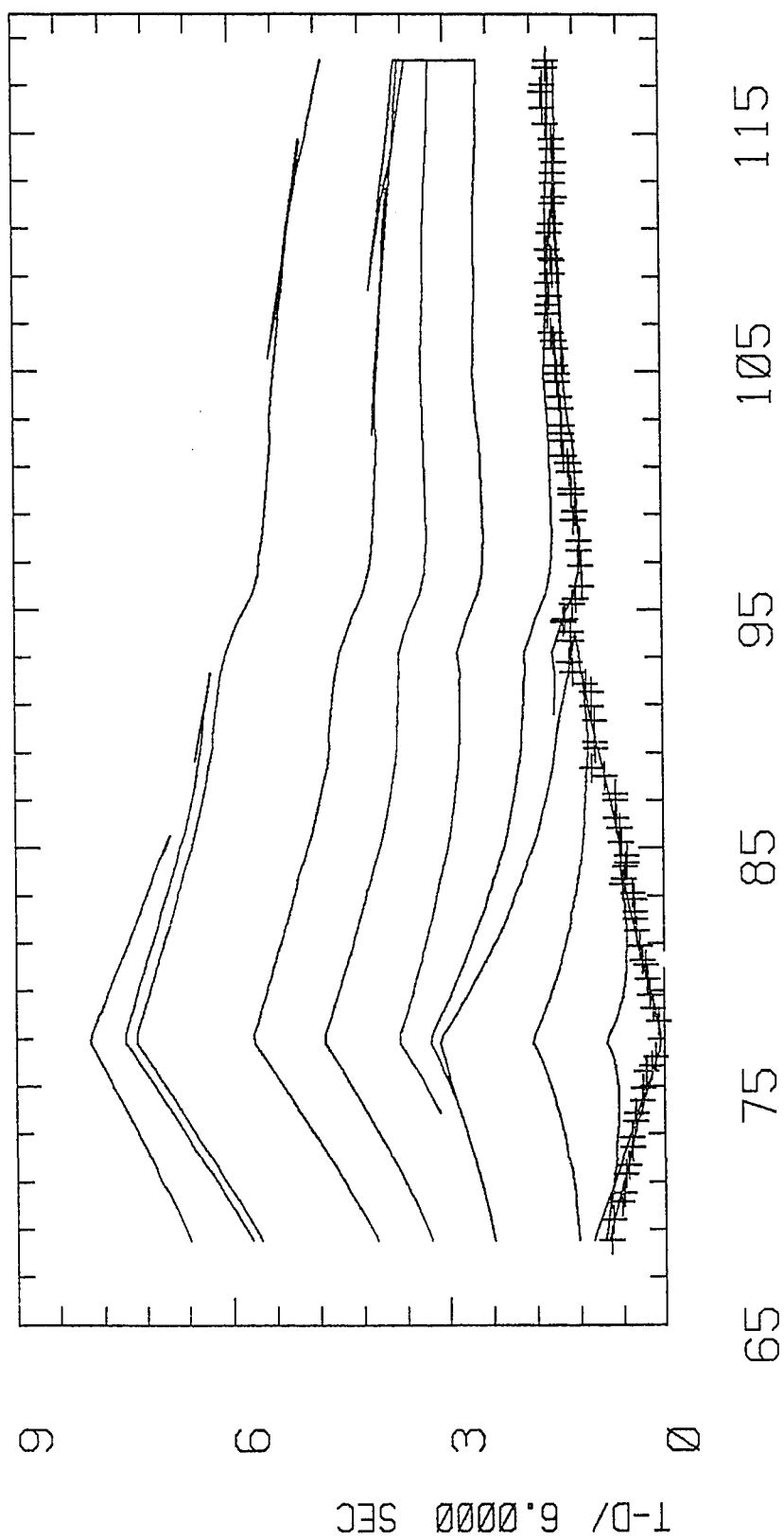




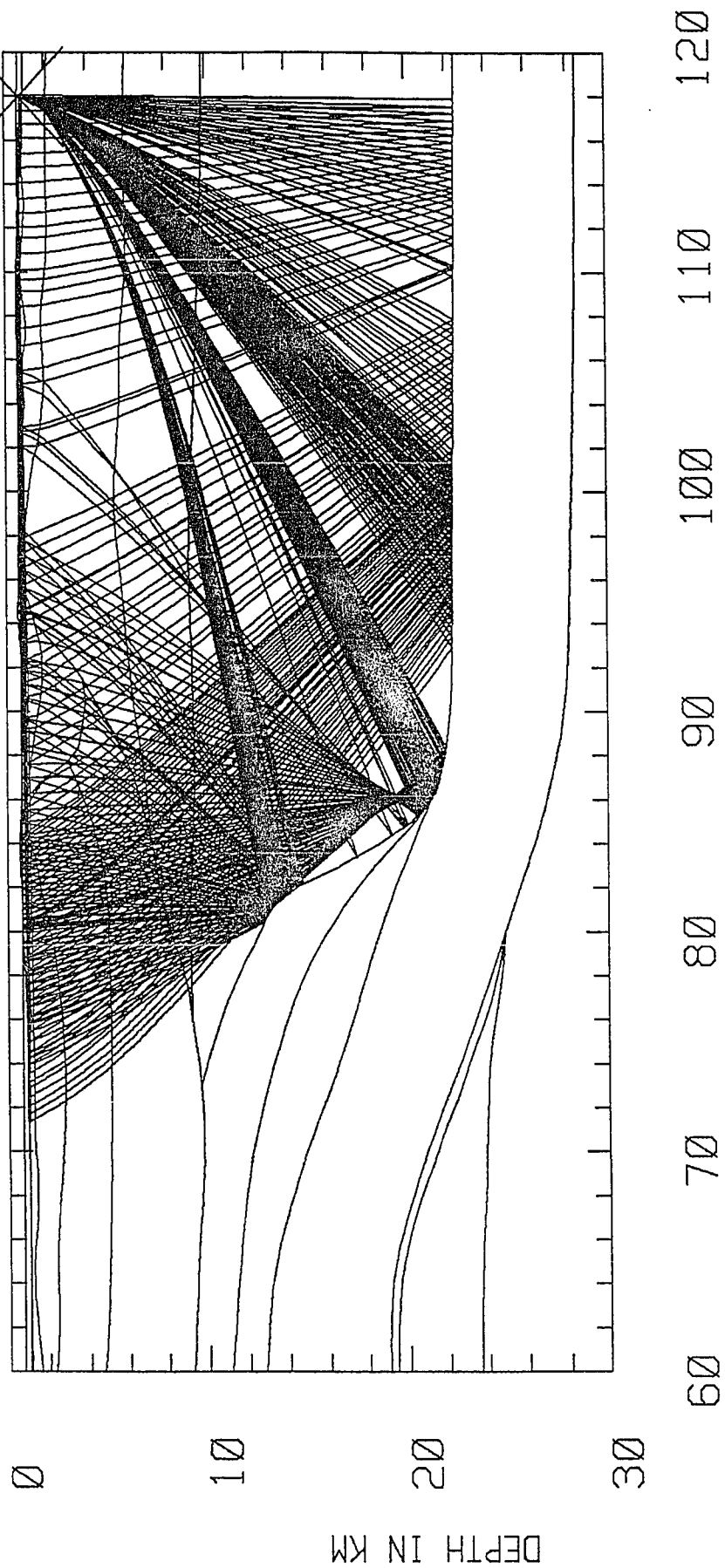


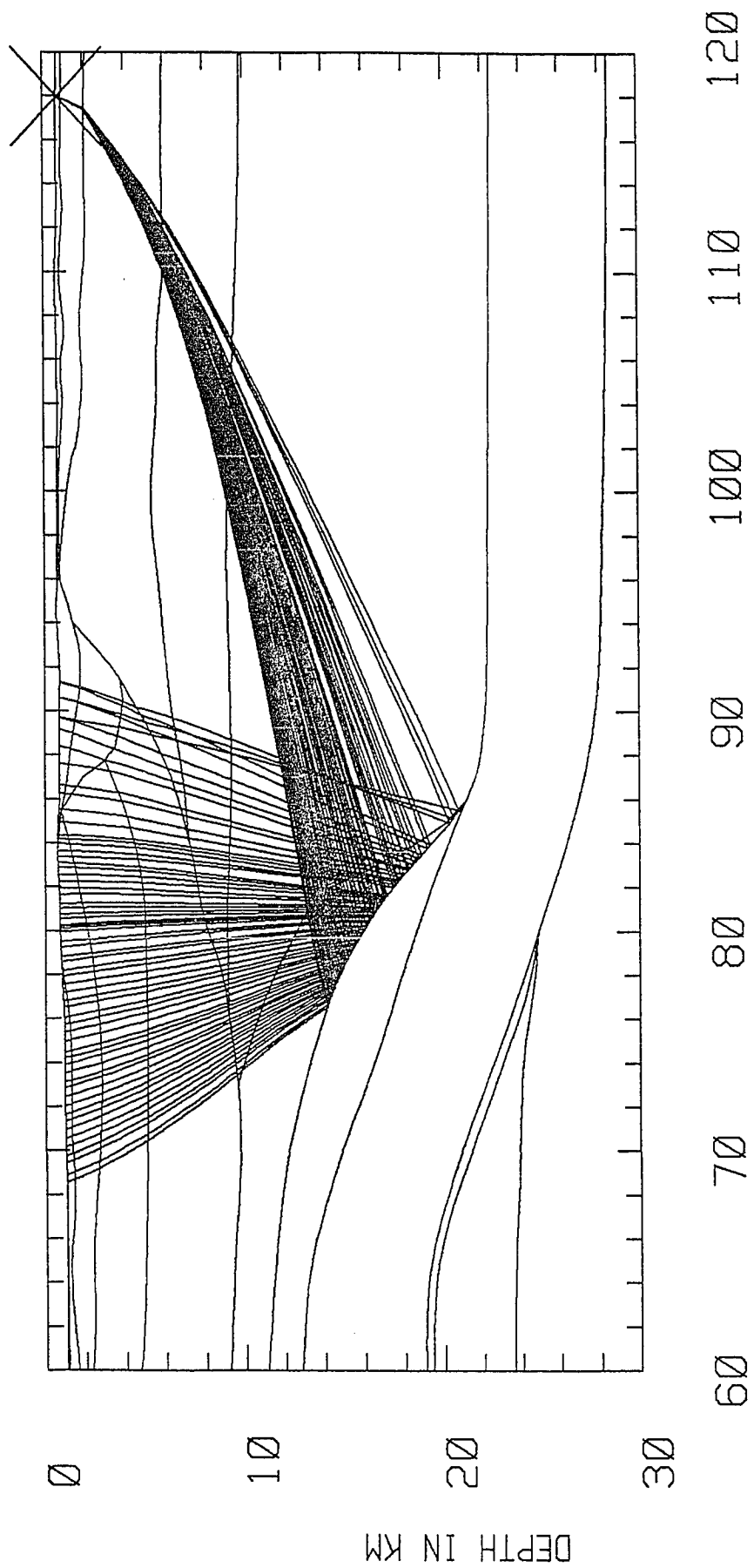


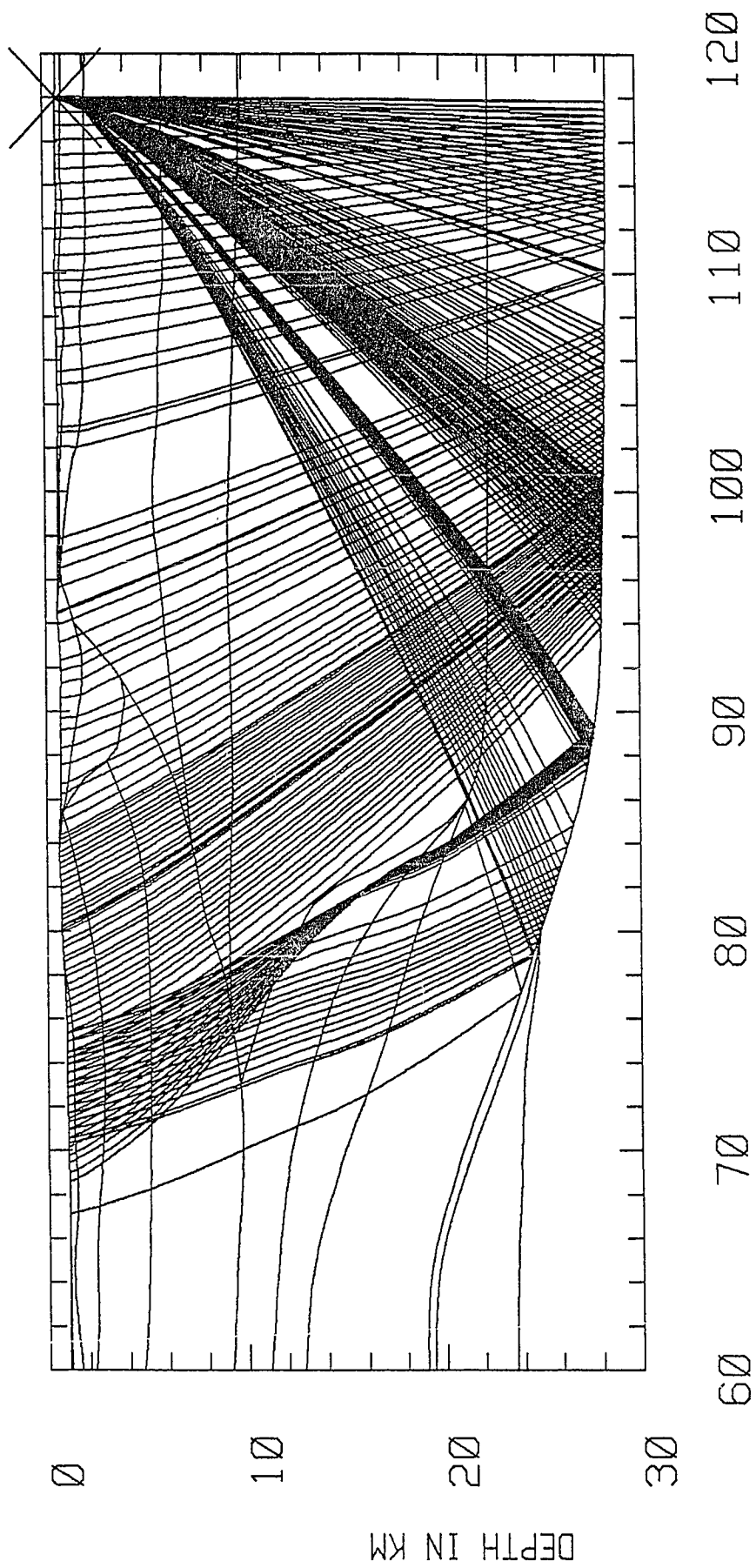




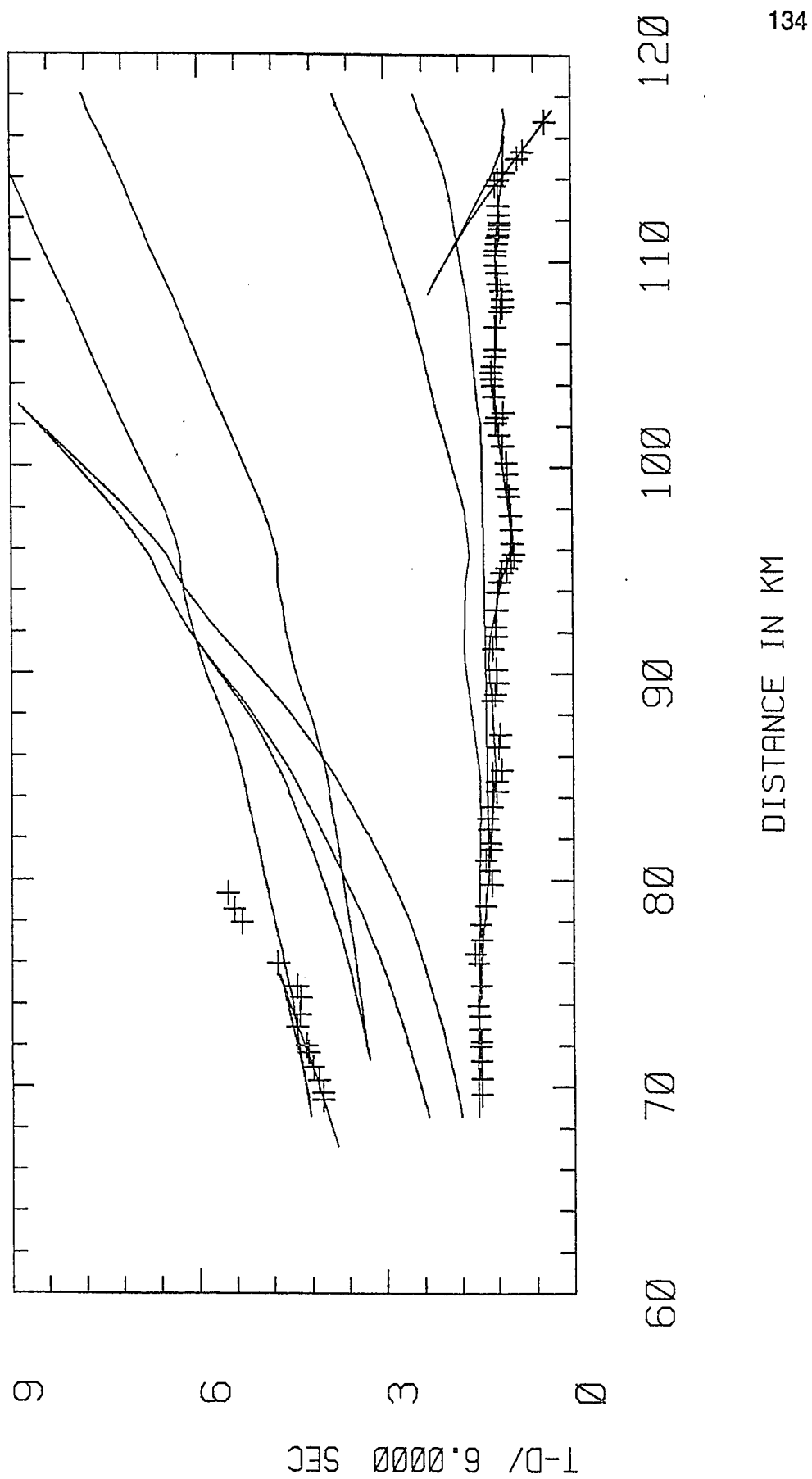
LS 2



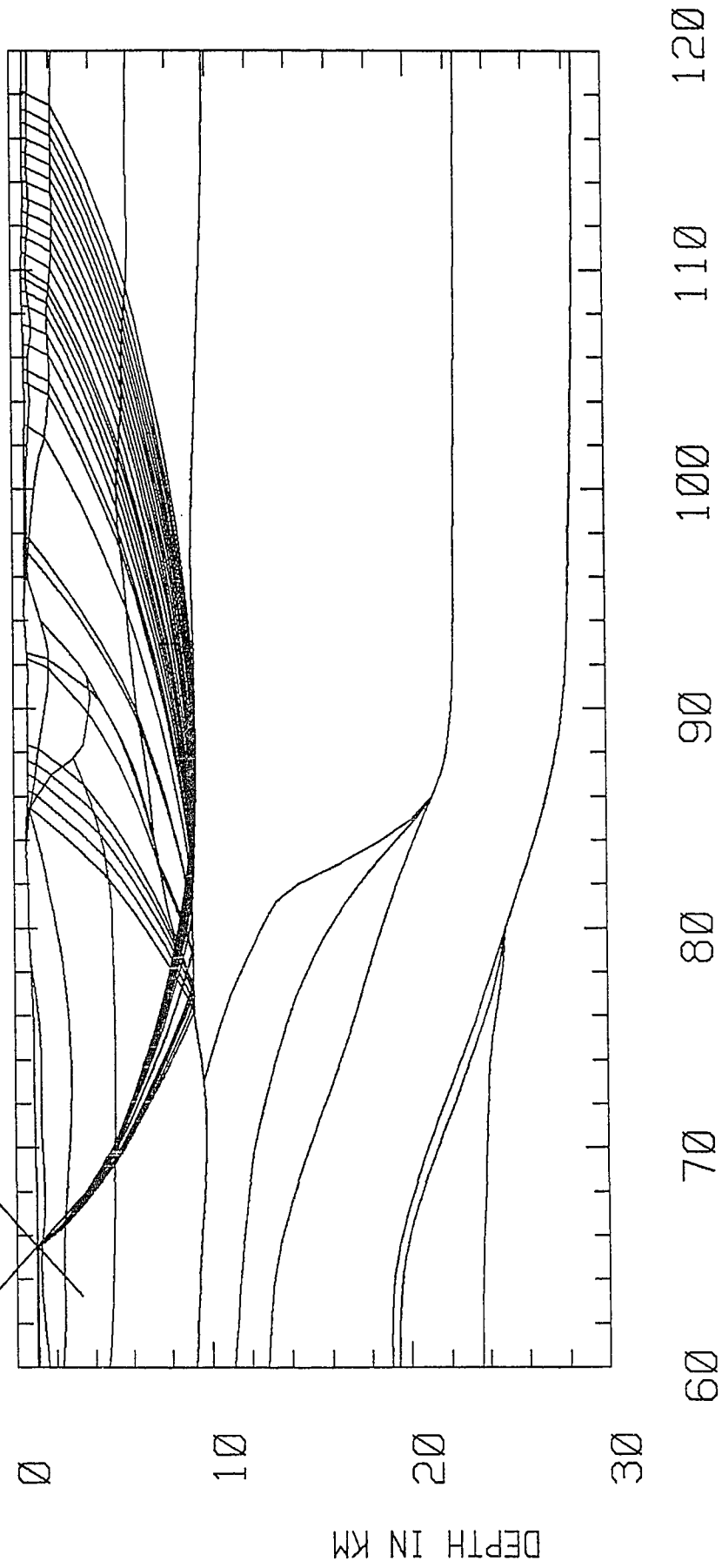




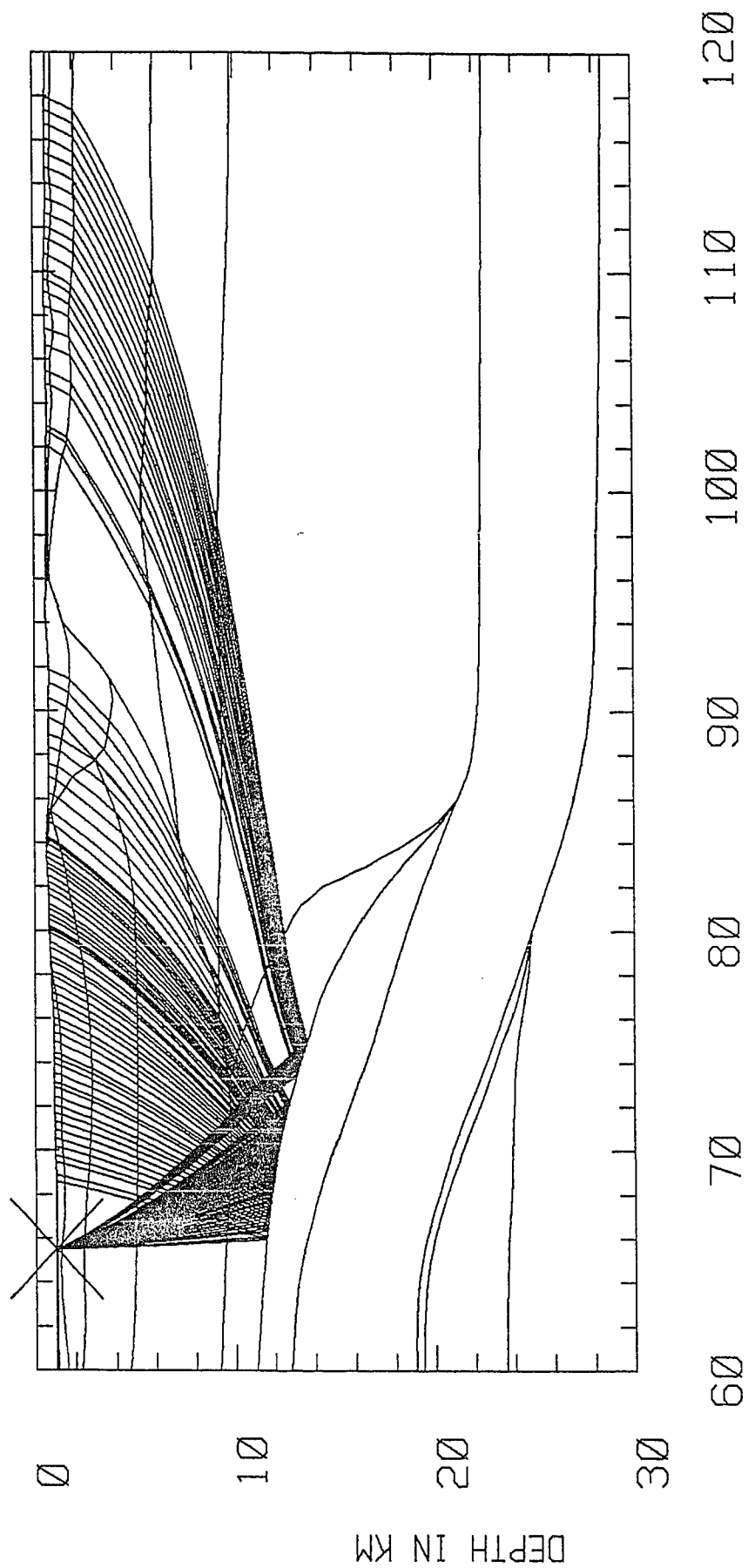
DISTANCE IN KM

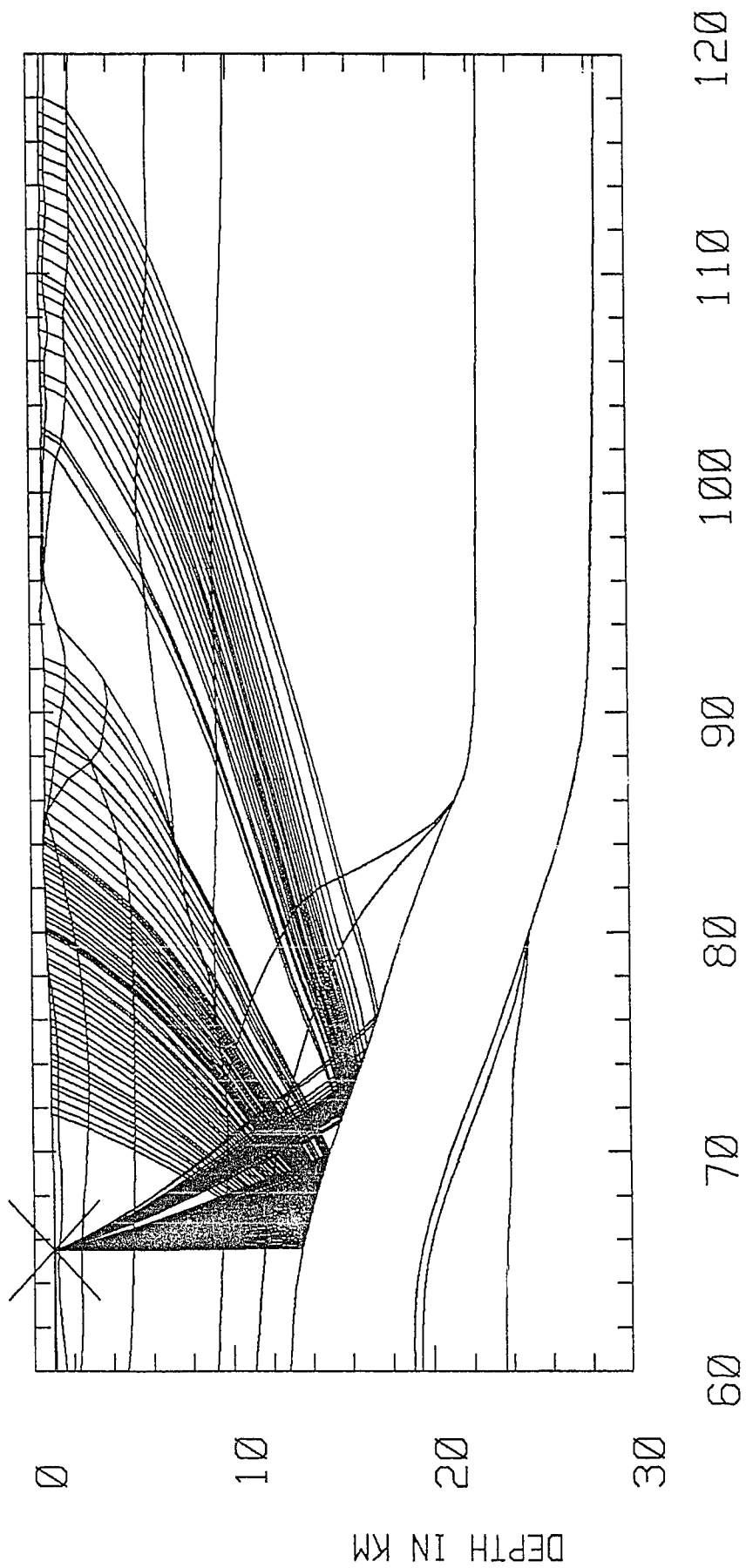


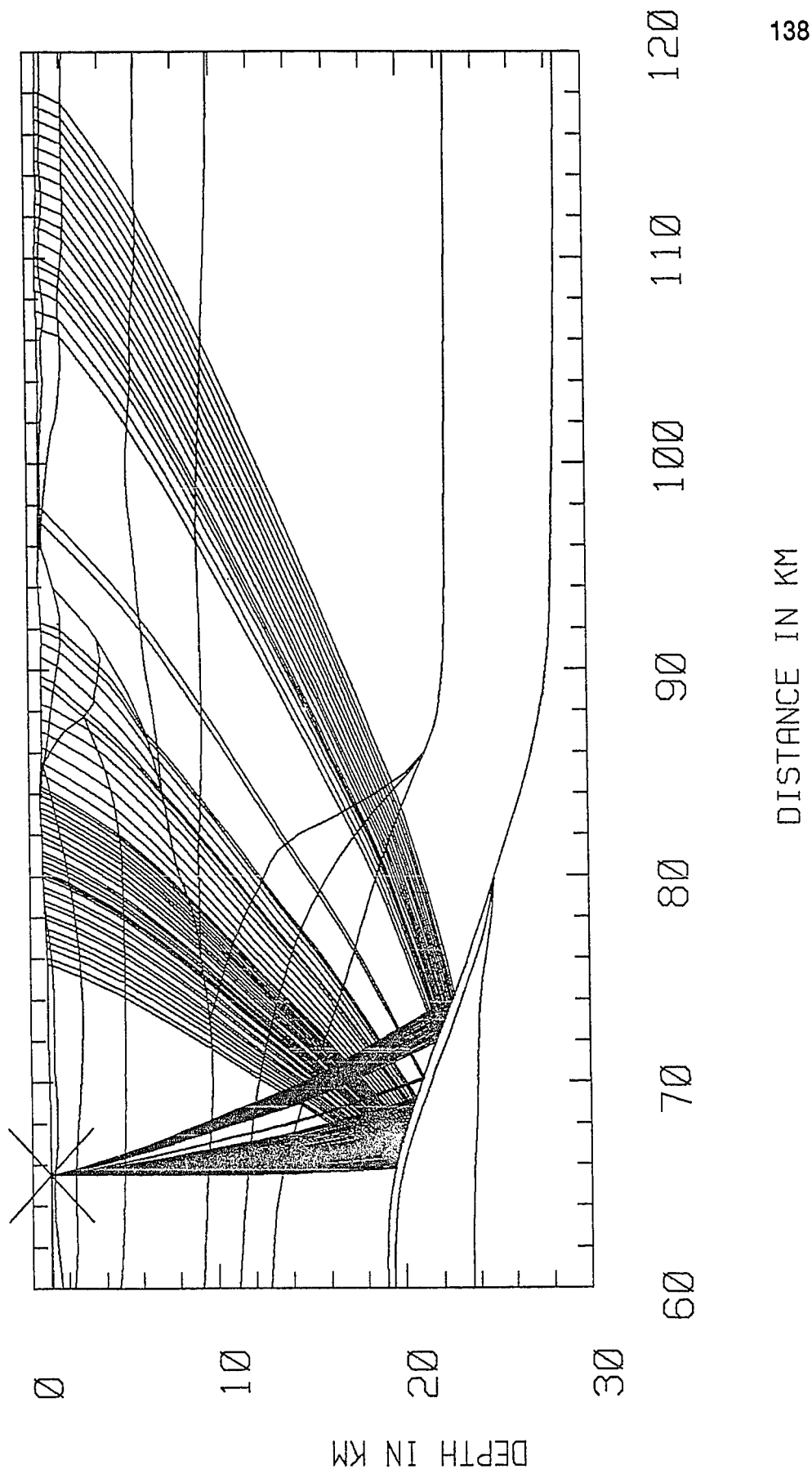
AG 6

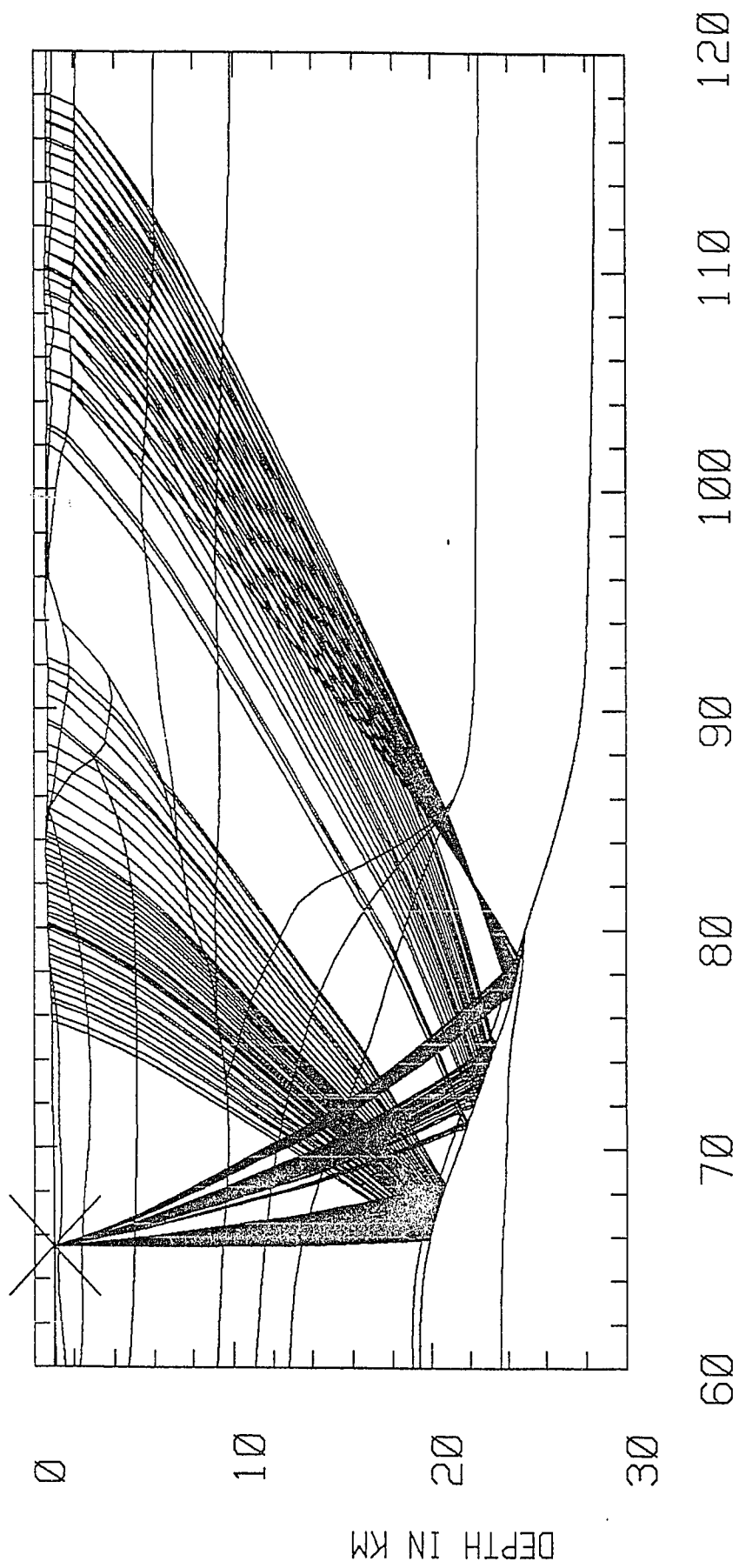


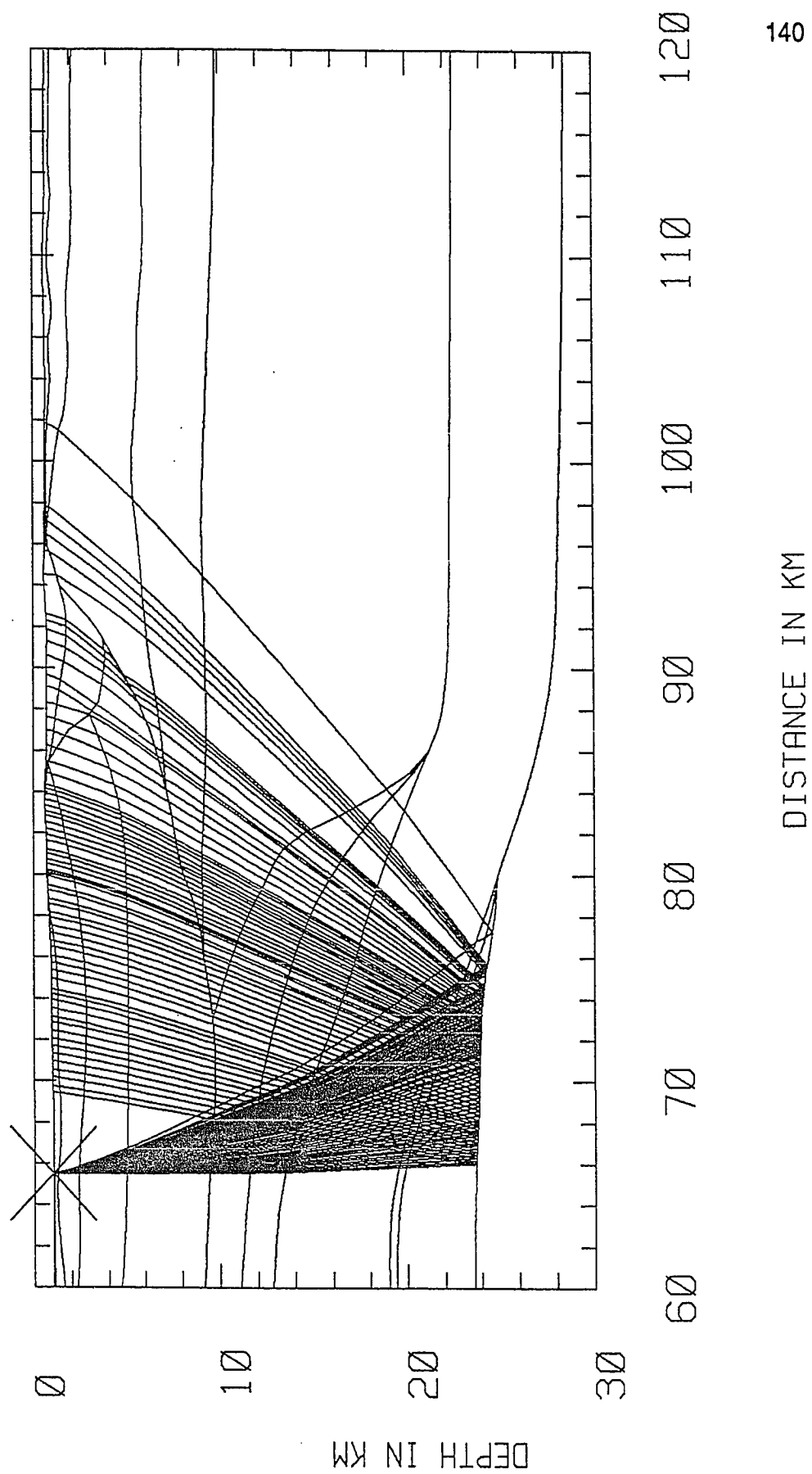
DISTANCE IN KM

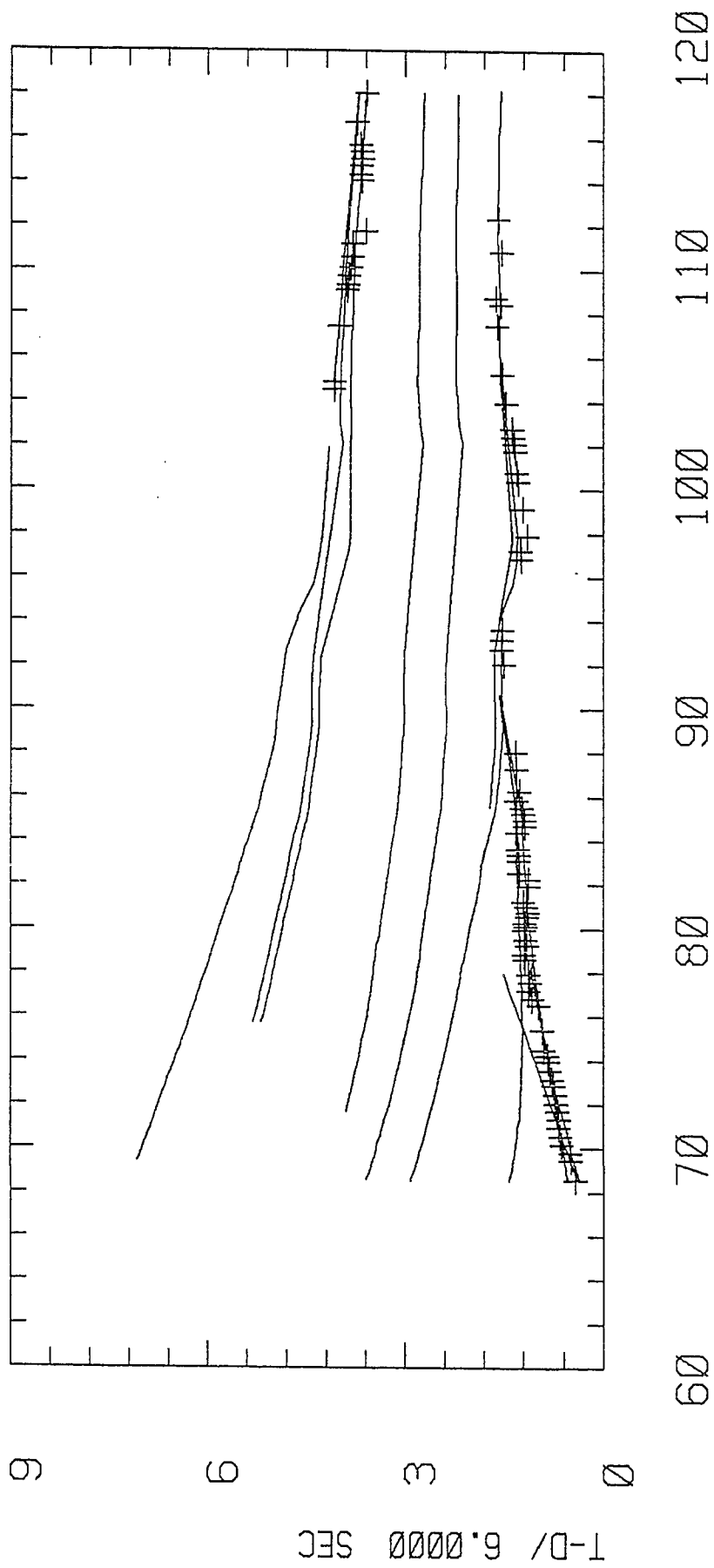












INFORMATION TO USERS

This reproduction was made from a copy of a document sent to us for microfilming. While the most advanced technology has been used to photograph and reproduce this document, the quality of the reproduction is heavily dependent upon the quality of the material submitted.

The following explanation of techniques is provided to help clarify markings or notations which may appear on this reproduction.

1. The sign or "target" for pages apparently lacking from the document photographed is "Missing Page(s)". If it was possible to obtain the missing page(s) or section, they are spliced into the film along with adjacent pages. This may have necessitated cutting through an image and duplicating adjacent pages to assure complete continuity.
2. When an image on the film is obliterated with a round black mark, it is an indication of either blurred copy because of movement during exposure, duplicate copy, or copyrighted materials that should not have been filmed. For blurred pages, a good image of the page can be found in the adjacent frame. If copyrighted materials were deleted, a target note will appear listing the pages in the adjacent frame.
3. When a map, drawing or chart, etc., is part of the material being photographed, a definite method of "sectioning" the material has been followed. It is customary to begin filming at the upper left hand corner of a large sheet and to continue from left to right in equal sections with small overlaps. If necessary, sectioning is continued again—beginning below the first row and continuing on until complete.
4. For illustrations that cannot be satisfactorily reproduced by xerographic means, photographic prints can be purchased at additional cost and inserted into your xerographic copy. These prints are available upon request from the Dissertations Customer Services Department.
5. Some pages in any document may have indistinct print. In all cases the best available copy has been filmed.

**University
Microfilms
International**

300 N. Zeeb Road
Ann Arbor, MI 48106

Order Number 1334873

**Modeling wide-angle seismic data from the central California
margin**

Putzig, Nathaniel Edward, M.A.

Rice University, 1988

U·M·I
300 N. Zeeb Rd.
Ann Arbor, MI 48106